Mineralogical Magazine (2019), **83**, 3–55
doi:10.1180/mgm.2018.152

CAMBRIDGE UNIVERSITY PRESS

Special category: Foundations in mineralogy and crystallography

A structure hierarchy for silicate minerals: sheet silicates

Frank C. Hawthorne[1]*, Yulia A. Uvarova[2] and Elena Sokolova[1]

[1]Department of Geological Sciences, University of Manitoba, Winnipeg, Manitoba R3T 2N2 Canada; and [2]CSIRO Mineral Resources, ARRC, 29 Dick Perry Avenue, Kensington, Western Australia 6151 Australia

Abstract

The structure hierarchy hypothesis states that *structures may be ordered hierarchically according to the polymerisation of coordination polyhedra of higher bond-valence*. A hierarchical structural classification is developed for sheet-silicate minerals based on the connectedness of the two-dimensional polymerisations of (TO_4) tetrahedra, where T = Si^{4+} plus As^{5+}, Al^{3+}, Fe^{3+}, B^{3+}, Be^{2+}, Zn^{2+} and Mg^{2+}. Two-dimensional nets and oikodoméic operations are used to generate the silicate (*sensu lato*) structural units of single-layer, double-layer and higher-layer sheet-silicate minerals, and the interstitial complexes (cation identity, coordination number and ligancy, and the types and amounts of interstitial (H_2O) groups) are recorded. Key aspects of the silicate structural unit include: (1) the type of plane net on which the sheet (or parent sheet) is based; (2) the u (up) and d (down) directions of the constituent tetrahedra relative to the plane of the sheet; (3) the planar or folded nature of the sheet; (4) the layer multiplicity of the sheet (single, double or higher); and (5) the details of the oikodoméic operations for multiple-layer sheets. Simple 3-connected plane nets (such as 6^3, 4.8^2 and 4.6.12) have the stoichiometry $(T_2O_5)_n$ (Si:O = 1:2.5) and are the basis of most of the common rock-forming sheet-silicate minerals as well as many less-common species. Oikodoméic operations, e.g. insertion of 2- or 4-connected vertices into 3-connected plane nets, formation of double-layer sheet-structures by (topological) reflection or rotation operations, affect the connectedness of the resulting sheets and lead to both positive and negative deviations from Si:O = 1:2.5 stoichiometry. Following description of the structural units in all sheet-silicate minerals, the minerals are arranged into decreasing Si:O ratio from 3.0 to 2.0, an arrangement that reflects their increasing structural connectivity. Considering the silicate component of minerals, the range of composition of the sheet silicates completely overlaps the compositional ranges of framework silicates and most of the chain-ribbon-tube silicates.

Keywords: structure hierarchy, sheet-silicate minerals, structural connectivity, stoichiometry, plane nets, oikodoméic operations

(Received 10 April 2018; accepted 15 August 2018)

Introduction

In recent years, there has been extensive work on the hierarchical classification of many groups of minerals, and we now have a reasonable idea of the principal factors that should be involved in such classifications. Hawthorne (2014) formalised the idea of a *Structure Hierarchy*, briefly reviewed several groups of minerals that have been so organised, and showed how such structure hierarchies (1) form a basis for understanding the factors affecting the chemical composition and bond topology of minerals, and (2) provide insight into mechanisms of crystallisation. Structure hierarchies have been developed for the following groups of minerals: phosphates, arsenates and vanadates (Kostov and Breskovska, 1989), phosphates (Hawthorne, 1998; Huminicki and Hawthorne, 2002*a*), arsenates (Majzlan *et al.*, 2014), vanadium bronzes (Evans and Hughes, 1990), sulfates (Sabelli and Trosti-Ferroni, 1985; Hawthorne *et al.*, 2000), tellurium oxy-compounds (Christy *et al.*, 2016), uranyl oxysalts (Burns, 1999, 2005, Burns *et al.*, 1996), borates (Burns *et al.*, 1995; Hawthorne *et al.*, 1996; Grice *et al.*, 1999), aluminofluoride minerals (Hawthorne, 1984), and structures based on anion-centred polyhedra (Filatov *et al.*, 1992; Krivovichev, 2008, 2009; Krivovichev and Filatov, 1999*a*,*b*; Krivovichev *et al.*, 1998, 2013). The surprising omission from this list of mineral groups is the silicate group (*sensu lato*), as these minerals are central to petrological processes in the crust and mantle of the Earth.

The basis of a structure hierarchy for common silicate minerals was developed by Matchatski (1928) and Bragg (1930), the classification that we still use today: *neso* (ortho-), *soro-*, *cyclo-* (ring-), *ino-* (chain-), *phyllo-* (sheet-) and *tecto-* (framework) *silicates*. The other major development was that of Belov (1958, 1961) who introduced the 'Second Chapter' of silicate crystal-chemistry that organises silicates of large alkali and alkaline-earth cations (e.g. Ca^{2+}, Ba^{2+} and Sr^{2+}) and focuses on the linkage between different coordination polyhedra in a wide variety of minerals in terms of 'mixed frameworks' (Voronkov *et al.*, 1974, 1975; Sandomirskii and Belov, 1984). Zoltai (1960) included other tetrahedrally coordinated oxyanions into the Bragg classification, focusing attention on the factors that affect the relative linkage of silicate, beryllate and borate groups in extended polymerisations. Several other classification criteria, based on the topological and geometrical characteristics of the silicate and aluminosilicate linkages, were introduced by Liebau (1985). The number of silicate minerals make the development of a coherent and detailed structure hierarchy for silicates a rather intimidating task.

*Author for correspondence: Frank Hawthorne, Email: frank_hawthorne@umanitoba.ca
Associate Editor: Sergey V Krivovichev
Cite this article: Hawthorne F.C., Uvarova Y.A., Sokolova E. (2019) A structure hierarchy for silicate minerals: sheet silicates. *Mineralogical Magazine*, **83**, 3–55. https://doi.org/10.1180/mgm.2018.152

However, it is time that this was done; an important topic should not be ignored just because it is a lot of work.

We will deal with the large number of minerals by dividing the silicate minerals into four categories and addressing these categories separately: (1) **Cluster silicates**: these are silicates that do not have any infinitely extended spatial polymerisation of tetrahedra (i.e. neso-, soro- and cyclosilicates); (2) **chain-ribbon silicates**: silicates with one direction of infinite polymerisation of tetrahedra (inosilicates); (3) **sheet silicates**: silicates with two directions of infinite polymerisation of tetrahedra (phyllosilicates); and (4) **framework silicates**: silicates with three directions of infinite polymerisation of tetrahedra (tectosilicates). Here, we examine the structure hierarchy of sheet-silicate minerals. Hawthorne (2015*a*) discussed the structures of sheet silicates in terms of *n*-connected plane nets ($2 < n \leq 4$), showed how such nets can be combined with various oikodoméic operations (topological building operations) to generate sheet-silicate (*sensu lato*) structures, and went on to develop *formula-generating and structure-generating functions* for such nets and their associated oikodoméic operations. Here, we examine observed sheet-silicate structures, see how their chemical compositions and structures may be generated from *n*-connected plane nets and associated building operations, and arrange them into a hierarchy based on increasing degree of connectivity of their silicate structural-unit.

Where we refer to a 'silicate sheet', that sheet must contain Si^{4+} but also may contain any other tetrahedrally coordinated cation such as Ti^{4+}, Al^{3+}, Fe^{3+}, B^{3+}, P^{5+}, As^{5+}, V^{5+}, Mg^{2+}, Fe^{2+}, Mn^{2+}, Zn^{2+} and possibly S^{6+}, Cr^{6+} and Li^{+}. We will refer to a tetrahedron by its central cation: thus 'Si^{4+} tetrahedron' represents an $(Si^{4+}O_4^{2-})^{4-}$ tetrahedron, and 'T tetrahedron' represents a $(TO_4)^{n-}$ tetrahedron, where T is one or more unspecified tetrahedrally coordinated cations. With such a wide compositional range of minerals and large number of structures, the colour scheme for the various polyhedra and nets is somewhat complicated; this is listed in Table 1, and we will not refer to this scheme in each figure caption. In some cases, other aspects of a structure need to be emphasised by using the colours of Table 1 to indicate other features (e.g. 2-connected vertices in a net); where this is done, the colour scheme will be noted in the figure caption. Also, mineral names are written in bold font to facilitate comparison of different structures throughout the text. Bond valences were calculated with the parameters of Gagné and Hawthorne (2015). In the tables listing mineral species, we have attempted where possible to write each mineral as the principal end-member formula (Hawthorne, 2002) as this simplifies the connections between mineral composition and bond topology, and also facilitates comparison of different minerals. Here, we follow the idea of *Binary Structural Representation* (Hawthorne and Schindler, 2008) whereby structures are partitioned into a strongly bonded *structural unit* and a weakly bonded '*interstitial complex*'. In the tables that follow, the *structural unit* (i.e. the silicate part of the structure) is written in square brackets and bold font, except where there is some question as to the formula of the structural unit (which may be the case where there is significant disorder of the constituents of that structural unit), and the interstitial complex (the weakly bonded constituents that link the structural unit into a complete crystal structure) is shown in normal font. References to specific minerals are made in the tables (not the text) except where dealing with more general topics.

Table 1. Legend for Figures.

	Polyhedron	Vertex
Si	Orange	Red
Al	Pale blue	Blue
Be	Yellow	Yellow
B	Violet	Violet
Zn	Pale green	Green
As	Red	Black
Fe	Mauve	Mauve

Nets and sheet-silicate structures

Nets are used widely to describe crystal structures, and have been particularly important to the description and theoretical analysis of silicate structures (e.g. Wells, 1962, 1977; Smith, 1977, 1978, 1988; Hawthorne and Smith, 1986*a*,*b*, 1988; Krivovichev, 2008, 2009). Hawthorne (2015*a*) described how nets may be used to theoretically derive possible atomic arrangements of the silicate components of minerals. With regard to the present work on sheet-silicate minerals, the salient issues are dealt with in the following sections.

Nets as representations of sheets of tetrahedra

Planar 3-connected nets may be used as compact representations of the connectivity of silicate sheets that have the stoichiometry $[T_{2n}O_{5n}]$ where $n = 1$–24; an example is shown in Fig. 1. In the sheet of corner-linked tetrahedra (Fig. 1*a*), all tetrahedra link to three other tetrahedra, i.e. they are 3-connected. In Fig. 1*b*, the vertices of the net represent the tetrahedra and the edges of the net represent the linkage between the tetrahedra. All tetrahedra in Fig. 1*a* have their apical vertices pointing in the same direction (up in terms of the viewer), and the tetrahedra of the six-membered rings are designated as being in the u^6 arrangement (Hawthorne, 2015*a*); note that such an arrangement is not inherent in Fig. 1*b* unless we specifically colour the vertices to indicate u and d behaviour of the analogous tetrahedra. Also emphasised in Fig. 1*b* is the three-connected nature of the net vertices and the unit cell of the net (which contains two vertices and five edges: $[Si_2O_5]$). Common 3-connected nets are listed in Table 2 and illustrated in Fig. 2. Nearly all of these nets correspond to known structures of silicate minerals. There are an infinite number of

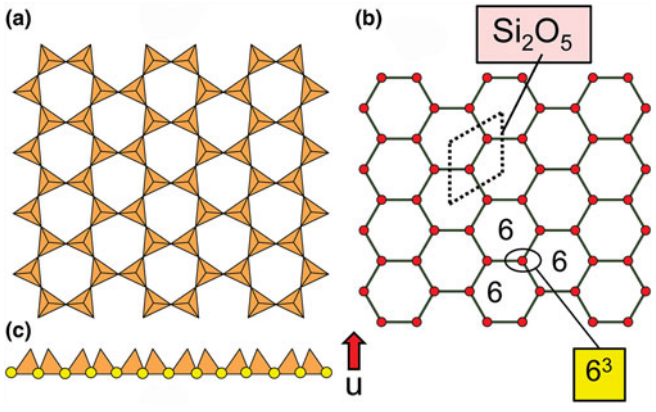

Fig. 1. (*a*) The mica sheet of tetrahedra; (*b*) the 6^3 net with its unit cell shown by dotted black lines; and (*c*) the mica sheet showing that the tetrahedra all point in the same direction, and that the O(br) anions (shown as yellow circles) are planar. Net vertices: red circles; net edges: green lines. Modified from Hawthorne (2015*a*).

https://doi.org/10.1180/mgm.2018.152 Published online by Cambridge University Press

Table 2. Simple 3-connected plane nets.

Number	Symbol	Unit-cell content	Figure
1	6^3	Si_2O_5	1*b*, 2*a*
2	4.8^2	Si_4O_{10}	2*b*
3	3.12^2	Si_6O_{15}	2*c*
4	$(4.6.8)_2(6.8^2)_1$	Si_6O_{15}	2*e*
5	$(5^2.8)_1(5.8^2)_1$	Si_6O_{15}	2*f*
6	$(4.6.10)_4(6^2.10)_1$	$Si_{10}O_{25}$	2*g*
7	4.6.12	$Si_{12}O_{30}$	2*d*
8	$(3.8^2)_1(6.8^2)_1$	$Si_{12}O_{30}$	2*h*
9	$(5^2.8)_1(5.6^2)_1(5.6.8)_2(6^2.8)_1$	$Si_{20}O_{50}$	2*i*
10	$(5.6.7)_4(5.7^2)_1(6^2.7)_1$	$Si_{24}O_{60}$	2*i*

other 3-connected plane nets, but these need not be considered until structural analogues are discovered or suspected. There are certain geometrical variations in single-layer sheets of tetrahedra that do not change the linkage of the corresponding net, and hence stoichiometry is conserved by these variations (Hawthorne, 2015*a*). However, these variations play an important role in the formation of more complicated sheets, and also are key features in linkage between the sheet and the interstitial complex.

Planar and folded sheets of tetrahedra

In Figs 1 and 3, all O(bridging) [= O(br)] anions are shown as yellow circles; note that in Fig. 1, the O(br)] anions lie in the plane of the net. Figure 3*a* shows the sheet in **sanbornite** with tetrahedra at the vertices of a 6^3 net; the view from one direction shows that the O(br) anions are very non-planar whereas the view from the orthogonal direction shows that the O(br) anions are quasi-planar. The arrangement of tetrahedra in **cuprorivaite** (Fig. 3*b*) shows a sheet with tetrahedra at the vertices of a 4.8^2 net. The view of the sheet from both horizontal directions shows that the O(br) anions are very non-planar in each direction, and the sheet in Fig. 3*b* is repetitively folded about (fold) axes parallel to both viewing directions orthogonal to the sheet. Here, we will not consider linkage between sheets and extra-sheet species, but note that geometrically-planar sheets *tend* to link to units involving edge-sharing octahedra coordinating medium-sized di- and trivalent cations whereas folded sheets *tend* to link to polymerisations of more highly coordinated cation polyhedra.

The relative orientation of tetrahedra in sheets of tetrahedra

In the net of Fig. 1*b*, each vertex represents a tetrahedron. However, a vertex has no orientation relative to the plane of the net, which is not the case for a tetrahedron. The apical ([1]-coordinated) anion of a 3-connected tetrahedron may lie on one side of the sheet or the other. Thus tetrahedra in a sheet may all point in the same direction or the tetrahedra may point in different directions. In Fig. 1, the tetrahedra all point in one direction (see Fig. 1*c*) which we designate as u (up towards the reader). Figures 4*a*,*b* show tetrahedra at the vertices of the 6^3 net, and both Figs 4*a* and 4*b* show that the tetrahedra point in both directions, u and d (down), relative to the plane of the sheet. There are two distinct six-membered rings in Fig. 4*a*; in

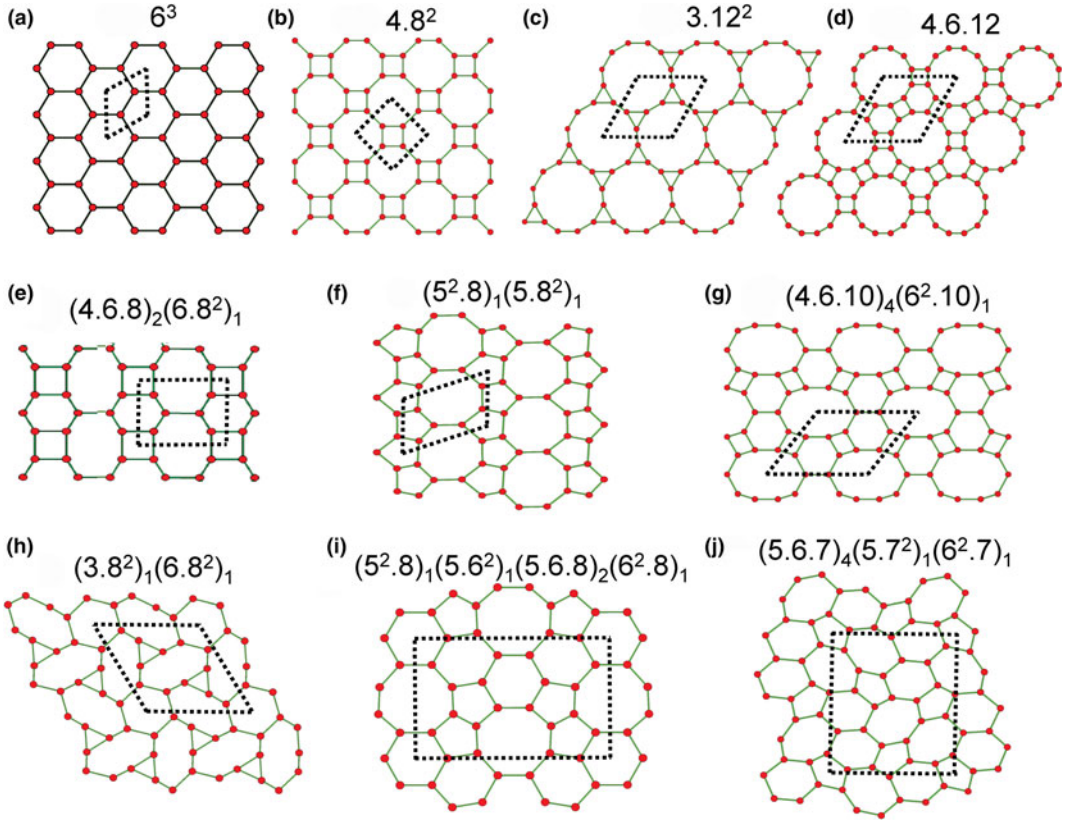

Fig. 2. The simpler 3-connected plane nets: (*a*) the 6^3 net; (*b*) the 4.8^2 net; (*c*) the 3.12^2 net; (*d*) the 4.6.12 net; (*e*) the $(4.6.8)_2(6.8^2)_1$ net; (*f*) the $(5^2.8)_1(5.8^2)_1$ net; (*g*) the $(4.6.10)_4(6^2.10)_1$ net; (*h*) the $(3.8^2)_1(6.8^2)_1$ net; (*i*) $(5^2.8)_1(5.6^2)_1(5.6.8)_2(6^2.8)_1$ net; and (*j*) the $(5.6.7)_4(5.7^2)_1(6^2.7)_1$ net; the unit cell of each net is shown by dotted lines.

https://doi.org/10.1180/mgm.2018.152 Published online by Cambridge University Press

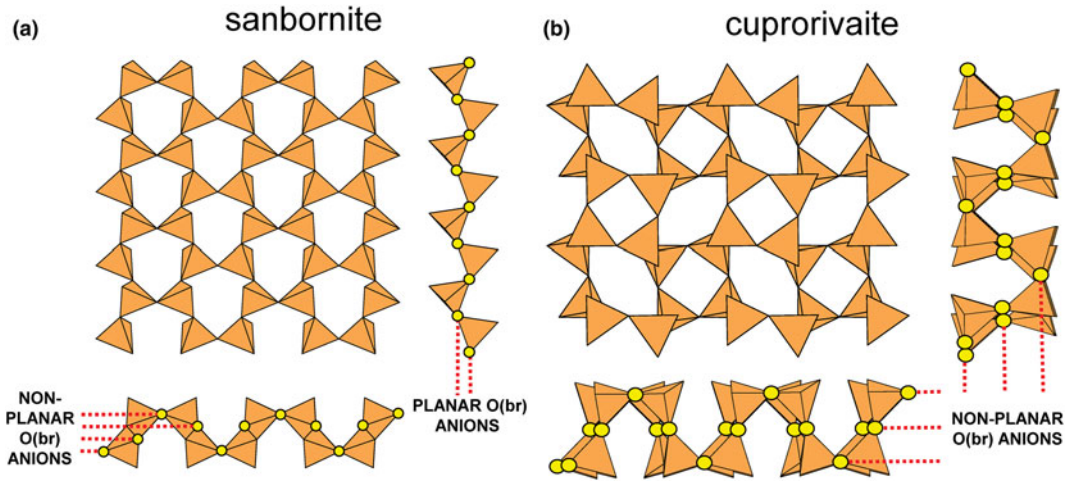

Fig. 3. Folded sheets of tetrahedra; (*a*) **sanbornite**: the 6^3 silicate sheet and views in the plane of the sheet, showing folding in one direction; and (*b*) **cuprorivaite**: 4.8^2 silicate sheet and views in the plane of the sheet, showing folding in two directions. Yellow circles represent O(br) anions.

one ring, all tetrahedra point in the same direction: (u^6); in the other ring, tetrahedra point in different directions: four point up (in the same direction as the tetrahedra in the first ring) and two point down (in the opposite direction to the tetrahedra of the first ring), and the sequence around the ring gives the symbol (u^2du^2d) (Fig. 4*a*). Thus the attitude of the tetrahedra in a sheet may be represented by these (u–d) strings. For a single-layer sheet, the designation of a specific tetrahedron as u (or d) is arbitrary. In single-layer sheets, we adopt the convention whereby the direction of the larger number of tetrahedra is defined as u. For a double-layer sheet, tetrahedra of the upper parent-layer sheet that point away from the plane containing the oikodoméic operation are defined as u.

The apical anions of the u and d tetrahedra of Fig. 4 lie out of the plane of the T–O–T linkages. However, this is not necessarily the case. Figure 5*a* shows the sheet of tetrahedra in **ferronordite-(Ce)**. As is apparent in the cross-section of a narrow slice of the sheet (Fig. 5*b*), the presence of tetrahedra with their edges in the upper and lower surfaces of the sheet allows the u and d tetrahedra not to project above or below the sheet itself, and produces a new type of tetrahedron which we will denote as o. Although this type of arrangement is more common in sheets involving 4-connected tetrahedra, as in **ferronordite-(Ce)**, it does occur in sheets with only 3-connected tetrahedra (as in the minerals of the **gadolinite supergroup** (Bačík, 2017), see below).

We also need to define the directions u and d relative to the rest of the structure. As noted below, silicate sheets may have more than one layer of tetrahedra (Liebau, 1985; Hawthorne, 2015*a*). In double-layer silicate structures, we will define d tetrahedra of the upper layer as linking to tetrahedra in the lower layer, and hence u tetrahedra link to the rest of the structure. In

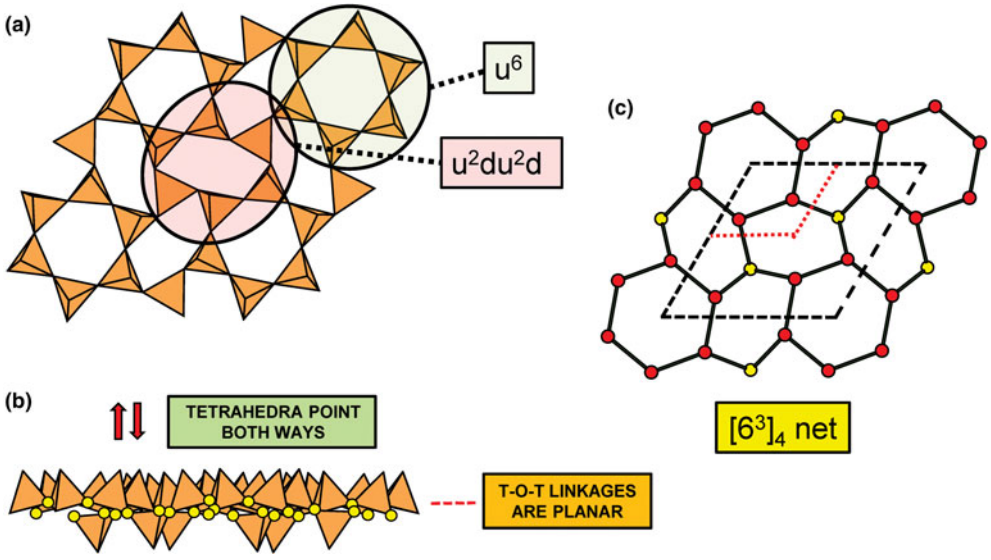

Fig. 4. The occurrence of u–d tetrahedra in the structure of **gyrolite**; (*a*) shows the tetrahedra at the vertices of a 6^3 net with u and d tetrahedra indicated; (*b*) shows a cross-sectional view of the sheet, showing the tetrahedra pointing both ways and the planar nature of the O(br) anions (shown as yellow circles); and (*c*) the net of vertices in which red circles represent u tetrahedra and the yellow circles represent d tetrahedra; the unit cell is shown by heavy broken lines and the unit cell of the parent 63 net (cf. Fig. 2a) is shown by dotted red lines.

https://doi.org/10.1180/mgm.2018.152 Published online by Cambridge University Press

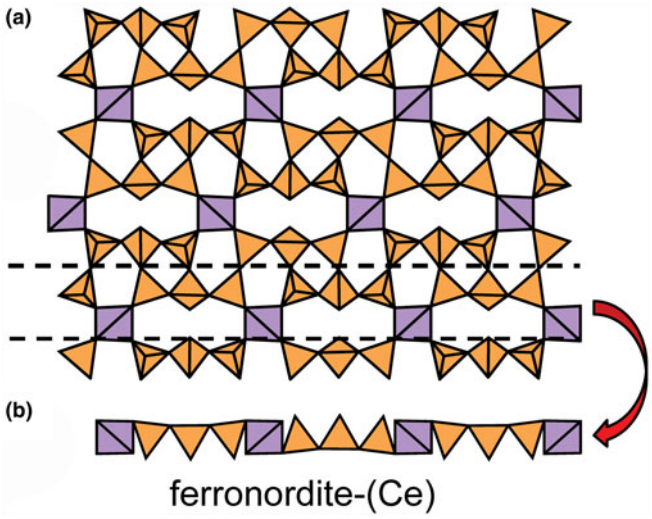

Fig. 5. The sheet of 3-connected (orange) and 4-connected (violet) tetrahedra in **ferronordite-(Ce)**: (*a*) plan view of the sheet; and (*b*) view of a thin ribbon (between the dashed lines of Fig. 5a) of the sheet in the plane of the sheet.

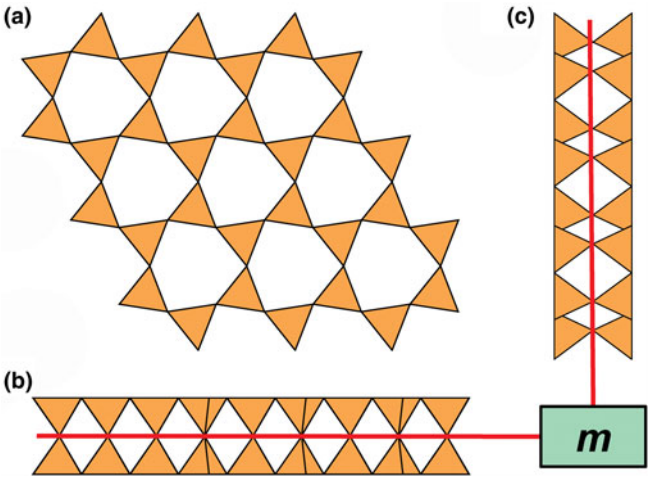

Fig. 6. A double-layer silicate sheet; (*a*) d tetrahedra at the vertices of a 6^3 net; (*b*) and (*c*) views of the sheet parallel to the plane of the sheet, showing that the double sheet has a lower-layer component in which u tetrahedra occur at the vertices of a 6^3 net; the upper and lower payers are related by a mirror (or pseudo-mirror) plane shown by the red line and labelled ***m***.

single-layer silicates, we do not have this internal definition of direction. In this case, we generally define the majority of tetrahedra as u and the minority as d, and hence the designation of u and d in these cases is more arbitrary.

In order to represent the information of the u and d directions of tetrahedra, it is necessary to use a slightly more complicated net nomenclature. The nets in Fig. 2 show the unit cells in dotted lines. Consider the net 6^3 (Fig. 2*a*) and its associated silicate sheet (Fig. 1*a*); these have a unit cell that contains two vertices/tetrahedra. Consider the silicate sheet in Fig. 4*a*; the topology of this sheet is based on the 6^3 net but the unit cell has to be larger in order to represent the u and d nature of the tetrahedra; this is equivalent to colouring the vertices of the net different colours according to the u or d nature of the tetrahedron corresponding to that vertex. It is obvious from Fig. 4*a* that the unit cell of the 6^3 net in Fig. 2 is not adequate to do this. The net corresponding to the sheet in Fig. 4*a* is shown in Fig. 4*c* with the u tetrahedra shown as red vertices and the d tetrahedra shown as yellow vertices. The corresponding unit-cell in Fig. 4*c* is shown as heavy broken lines, and part of the unit cell of the parent 6^3 net is shown as dotted red lines. It is apparent that the true unit-cell is four times the size of the parent unit-cell. We wish to retain the number of constituent vertices in the net symbol, and hence this number will need to be contained in the net. We may do this by enclosing the reduced net symbol. i.e. the set of vertices with any common factor removed from the stoichiometric coefficients and placed outside a pair of square brackets. Thus the nets in Figs 2*a–d* are expressed as $[6^3]_2$, $[4.8^2]_4$, $[3.12^2]_6$ and $[4.6.12]_{12}$. For the net in Fig. 2*e*, there are six vertices in the unit cell and there are two distinct vertices, (4.6.8) and (6.8^2) in the ratio 2:1; hence the net symbol is $[(4.6.8)_2(6.8^2)_1]_2$ such that the product of the sum of the stoichiometric coefficients within the square brackets and the subscript outside the square brackets is equal to the number of vertices in the unit cell of the net: (2 + 1) x 2 = 6 (Fig. 2*e*). We note that this approach is only a notation for the recording the u and d directions of tetrahedra. A more rigorous method of describing u and d tetrahedra based on orientational matrices was developed by Krivovichev and Burns (2003) and amplified by Krivovichev (2009). The former has the advantage of simplicity whereas the latter has potential for combining with structure-generating functions (Hawthorne, 2015*a*) to rigorously derive all possible sheet arrangements.

Multi-layer tetrahedron-sheets and oikodoméic operations

Liebau (1985) divided sheet silicates into two types: *single-layer sheets* and *double-layer sheets*. In Fig. 6*a*, tetrahedra lie at the vertices of a 6^3 net, and all tetrahedra have their apical vertices concealed below the plane of the figure. However, viewing perpendicular to the sheet (Figs. 6*b*,*c*) shows that there is another single-layer of tetrahedra directly underlying the upper net, and

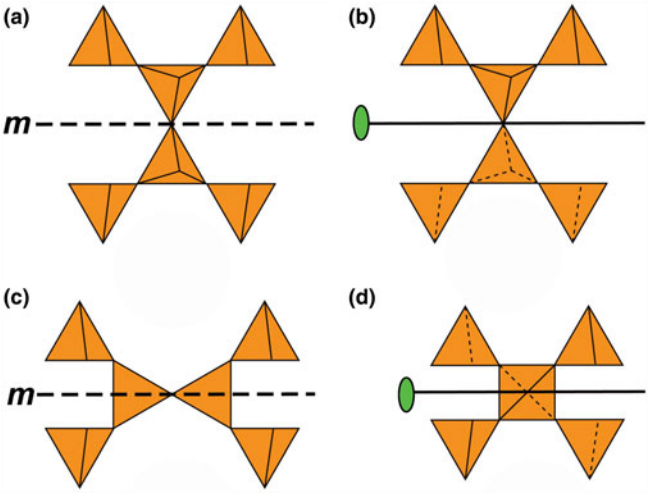

Fig. 7. Oikodoméic operations replicating and reorienting the upper single-layer tetrahedra from above the plane of the operation to below the plane of the operation; (*a*) the mirror operation acting though apical anions of the upper single-layer parent sheet; (*b*) the two-fold rotation operation acting though apical anions of the upper single-layer parent sheet; (*c*) the mirror operation though the central T cations of tetrahedra shared between the upper and lower single-layer sheets; and (*d*) the two-fold rotation operation acting though the central T cations of tetrahedra shared between the upper and lower single-layer sheets.

https://doi.org/10.1180/mgm.2018.152 Published online by Cambridge University Press

the lower tetrahedra have their apical vertices pointing upward. The sheet of Fig. 6 is a double-layer sheet with a mirror (or pseudo-mirror) plane relating the upper and lower layers of the sheet.

Hawthorne (2015*a*) introduced a series of topological operations that change the bond topology of a parent net. Stoichiometry is not conserved but changes systematically in accord with the particular operation, giving rise to more complicated nets that can represent more complicated sheet structures. These operations are designated as *oikodoméic operations* as they involve the act of building new structural arrangements (from the Greek word oikodomé: the act of building). There are three classes of oikodoméic operations that can affect nets or sheets of connected tetrahedra: [1] *insertion*, whereby vertices of different connectedness are inserted into the edges of a parent net; [2,3] *replication operations*, whereby a single-layer sheet is replicated, reoriented and linked to the original single-layer sheet to produce a double-layer sheet of tetrahedra. Class-2 oikodoméic operations replicate the parent layer about apical anions of d tetrahedra (Figs 7*a*,*b*), whereas class-3 operations replicate the parent layer about the central cations of d tetrahedra (Figs 7*c*,*d*). How do these oikodoméic operations differ from symmetry operators? A symmetry element is part of the symmetry of an already existing arrangement, and the corresponding symmetry operation describes the transformation of part of the arrangement to geometrical congruence with another part of the arrangement, whereas oikodoméic operations generate arrangements with the corresponding (topological) symmetry from a simpler parent arrangement of tetrahedra.

Recently, three silicate minerals have been described as triple-layer: **günterblassite**, $(K,Ca)_{3-x}Fe[(Si,Al)_{13}O_{25}(OH,O)_4](H_2O)_7$ (Chukanov *et al.*, 2012*a*); **umbrianite**, $K_7Na_2Ca_2[Al_3Si_{10}O_{29}]F_2Cl_2$ (Sharygin *et al.*, 2013); and **hillesheimite**, $(K,Ca,\square)_2(Mg,Fe,Ca,\square)_2[(Si,Al)_{13}O_{23}(OH)_6](OH)(H_2O)_8$ (Chukanov *et al.*, 2013). These also may be generated from parent sheets by oikodoméic replication operations.

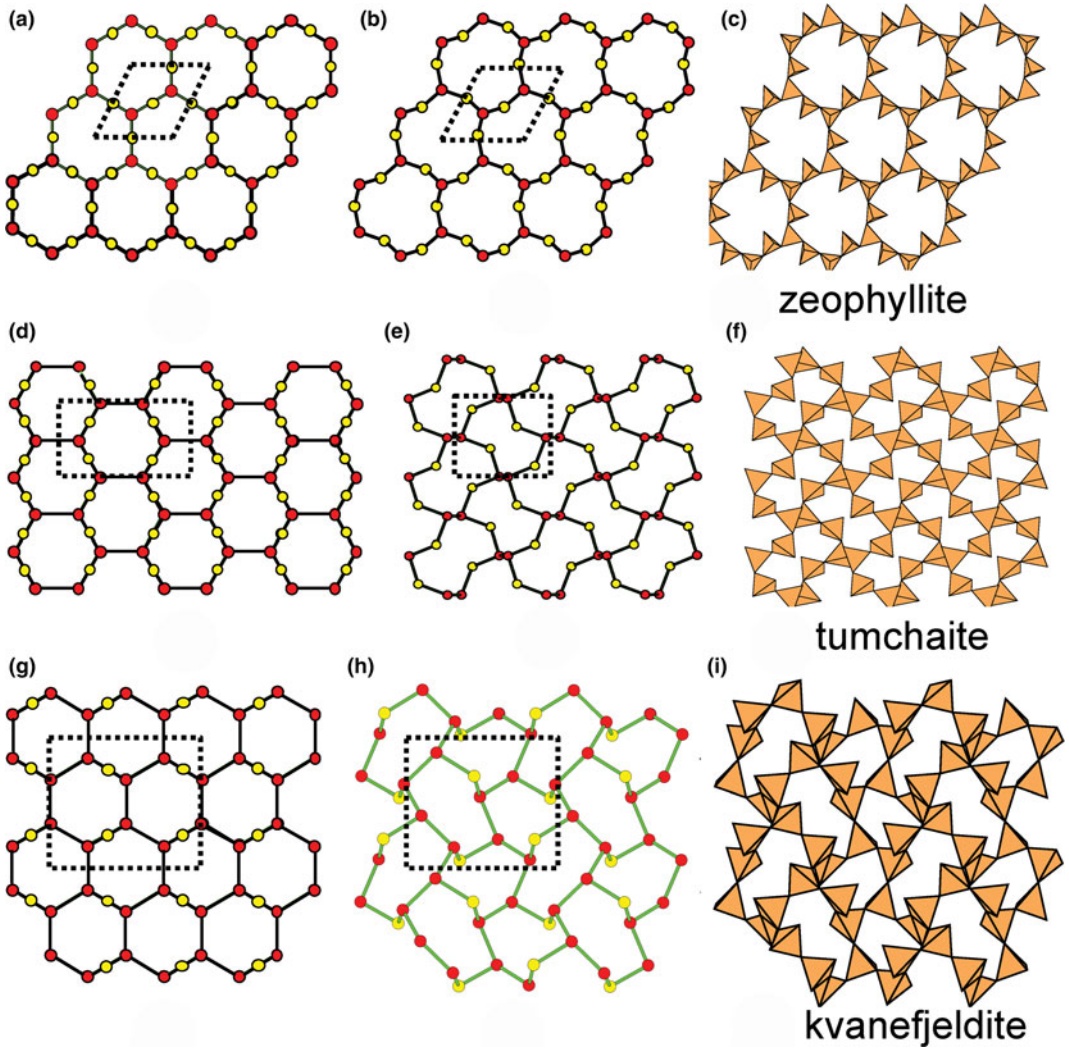

Fig. 8. Nets and corresponding structures derived from the 3-connected plane net 6^3 by insertion of 2-connected vertices between 3-connected vertices; (*a*) the $(12^2)_3(12^3)_2$ net; (*b*) the $[(12^2)_3(12^3)_2]_1$ net in the structure of **zeophyllite**; (*c*) the sheet of tetrahedra in **zeophyllite**; (*d*) the $(10^2)_4(10^3)_4$ net; (*e*) the $[(10^2)_4(10^3)_4]_1$ net in the structure of **tumchaite**; (*f*) the sheet of tetrahedra in **tumchaite**; (*g*) the $(8^2)_4(8^3)_8$ net; (h) the $[(8^2)_4(8^3)_8]_1$ net in the structure of **kvanefjeldite**; and (i) the sheet of tetrahedra in **kvanefjeldite**. Yellow circles: two-connected vertices.

https://doi.org/10.1180/mgm.2018.152 Published online by Cambridge University Press

Table 3. Single-layer sheet-silicates based on 3-connected nets with inserted 2-connected vertices.

Mineral	Net	u–d arrangement*	P/F**	Formula	T:O ratio	Fig. No.	Ref.
Zeophyllite	$[12^2_3 12^3_2]_1$	(ududud)	P	Ca_{13}**[Si_5O_{14}]$_2$**$F_{10}(H_2O)_6$	1:2.80	8*a*,*b*,*c*; 47*a*	(1)
Britvinite	$[12^2_3 12^3_2]_2$	(u^6)	P	$Pb_{15}Mg_9$**[$Si_{10}O_{28}$]**$(BO_3)_4(CO_3)_2(OH)_{12}O_2$	1:2.80	---	(2)
Molybdophyllite	$[12^2_3 12^3_2]_2$	(u^6)	P	Pb_8Mg_9**[$Si_{10}O_{28}$]**$(OH)_8\|O_2\|(CO_3)_3(H_2O)$	1:2.80	---	(3)
Tumchaite	$[10^2_4 10^3_4]_1$	(u^3d^3)	1F	$Na_2(Zr,Sn)$**[Si_4O_{11}]**$(H_2O)_2$	1:2.75	8*d*,*e*,*f*	(4)
Kvanefjeldite	$[8^3_8.8^2_4]_1$	(u^4d^2)(u^2d^4)	1F	$Na_4(Ca,Mn)$**[Si_6O_{16}]**	1:2.67	8*g*,*h*,*i*	(5)
Hyttsjöite	$[(14^2)_6(14^3)_2]_1$	------	P	$Pb_{18}Ba_2Ca_5Mn^{2+}_2Fe^{3+}_2$**[$Si_{30}O_{90}$]**$Cl(H_2O)_6$	1:3.00	9	(6)

References: (1) Merlino (1972); (2) Chukanov *et al.* (2008), Yakubovich *et al.* (2008); (3) Kolitsch *et al.* (2012); (4) Subbotin *et al.* (2000); (5) Johnsen *et al.* (1983), Petersen *et al.* (1984); and (6) Grew *et al.* (1996).
*The u–d arrangement refers to the parent 6^3 net.
**P = planar; 1F = folded in one direction.

Interstitial constituents

The idea of *Binary Structure Representation* (e.g. Hawthorne and Schindler, 2008) considers structures as being partitioned into two parts, a strongly bonded (usually anionic) *Structural Unit* and a (usually cationic) *Interstitial Complex* that binds the structural units into a continuous structure. The development of structure hierarchies focuses on the structural units, but the interstitial complex is also of great interest as the *Principle of Correspondence of Lewis-acidity – Lewis-basicity* (Hawthorne, 2012*a*, 2015*b*) allows analysis of the factors that control the chemical compositions and aspects of the structural arrangements of both the structural unit and the interstitial complex (e.g. Hawthorne and Schindler, 2008, Schindler and Hawthorne, 2001*a*,*b*,*c*, 2004, 2008; Schindler *et al.*, 2000, 2006). As we plan to do this as part of our future work on sheet-silicate minerals, we shall describe the stereochemistry of the interstitial complex, i.e. the coordination of the cation constituents and (H_2O), in particular the role of (H_2O) as *Transformer* $(H_2O)^t$, *Non-Transformer* $(H_2O)^n$, *Inverse-Transformer* $(H_2O)^i$ and solely hydrogen-bonded $(H_2O)^z$ groups (Hawthorne, 1992; Hawthorne and Schindler, 2008; Hawthorne and Sokolova, 2012) unless the details are obscured by positional disorder.

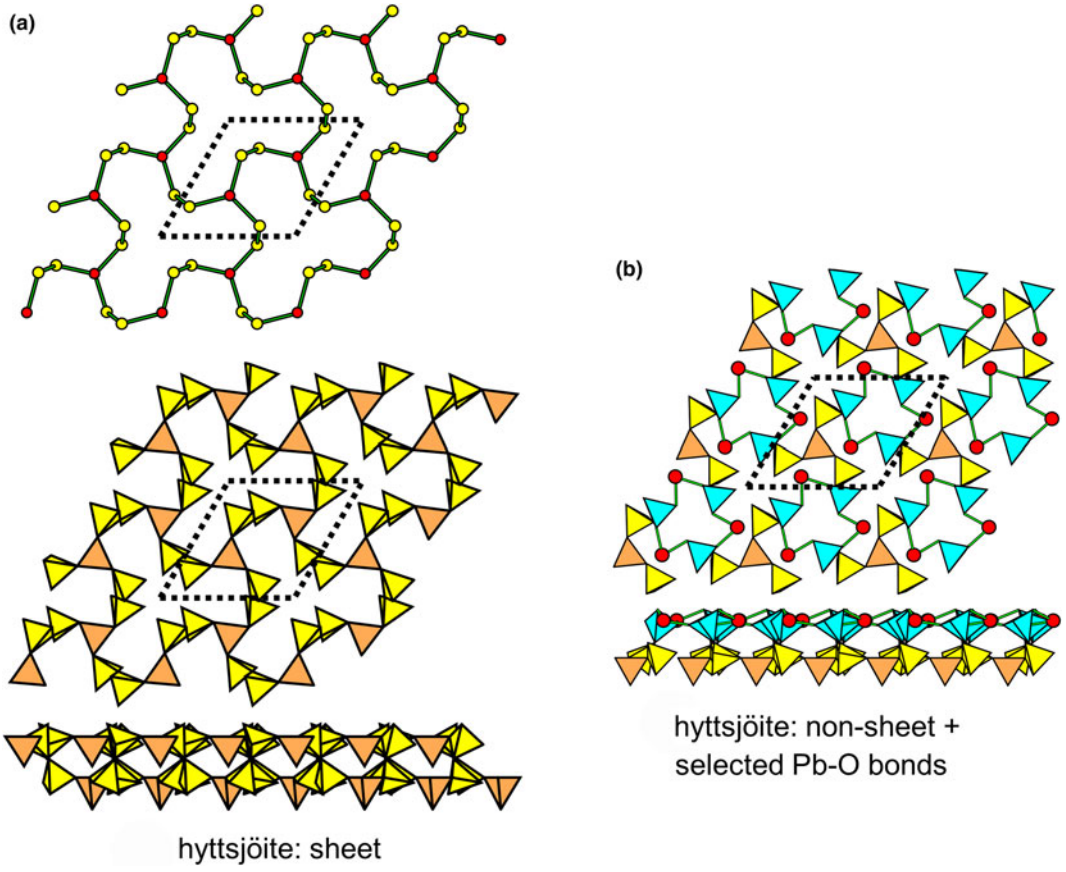

Fig. 9. Net and corresponding structure derived from the 3-connected plane net 6^3 by insertion of pairs of 2-connected vertices between all 3-connected vertices; (*a*) the $(14^2)_6(14^3)_2$ net and the sheet of tetrahedra in **hyttsjöite**; and (*b*) the partly disconnected layer of tetrahedra in **hyttsjöite,** showing short Pb^{2+}–O bonds that link it into a sheet. Yellow circles: two-connected vertices; yellow tetrahedra: two-connected tetrahedra; large red circles: lone-pair-stereoactive Pb^{2+}; and blue tetrahedra: one-connected tetrahedra.

https://doi.org/10.1180/mgm.2018.152 Published online by Cambridge University Press

Table 4. Single-layer sheet-silicates based on the 6^3 net with mixed u–d arrangements.

Mineral	Net	u–d configuration	P/F*	Formula	T:O ratio	Fig. No.	Ref.
			Planar sheets of u tetrahedra				
Chlorite group	$[6^3]_2$	(u^6)	P	M_6**[T_4O_{10}]**$(OH)_8$	1:2.50	1*a*	(1)
Kaolinite subgroup	$[6^3]_2$	(u^6)	P	M_3**[T_2O_5]**$(OH)_4$	1:2.50	1*a*	(1)
Mica supergroup	$[6^3]_2$	(u^6)	P	AM_3**[T_4O_{10}]**$(OH)_2$	1:2.50	1*a*	(2)
Serpentine subgroup	$[6^3]_2$	(u^6)	P	M_3**[T_2O_5]**$(OH)_4$	1:2.50	1*a*	(1)
Talc group	$[6^3]_2$	(u^6)	P	M_3**[T_4O_{10}]**$(OH)_2$	1:2.50	1*a*	(1)
Clay minerals	$[6^3]_2$	(u^6)	P	----------	1:2.50	1*a*	--
Smectite group	$[6^3]_2$	---	P	----------	-----	1a	--
Hanjiangite	$[6^3]_2$	(u^6)	P	$Ba_2Ca(V^{3+}Al)$**[$Si_3AlO_{10}(OH)_2$]**$F(CO_3)_2$	1:2.50	1*a*	(3)
			Planar sheets of u–d tetrahedra				
Gyrolite	$[6^3]_8$	$(u^6)_1(u^2d^1u^2d^1)_3$	P	$NaCa_{16}$**[$(Si_{23}Al)O_{60}$]** $(OH)_8(H_2O)_{14}$	1:2.50	11*a*	(4)
Martinite	$[6^3]_8$	$(u^6)_1(u^2d^1u^2d^1)_3$	P	$(Na,\square)_{13}Ca_4$**[$Si_{14}B_2O_{38}(OH)_2$]**$F_2(H_2O)_4$	1:2.50	11*b*	(5)
Cairncrossite	$[6^3]_8$	$(u^6)_1(u^2d^1u^2d^1)_3$	P	Sr_2Ca_7**[$Si_{16}O_{40}$]**$(OH)_2(H_2O)_{15}$	1:2.50	11*b*	(6)
Ellingsenite	$[6^3]_8$	$(u^6)_1(u^2d^1u^2d^1)_3$	P	See Appendix	1:2.50	11*c*	(7)
Natrosilite	$[6^3]_4$	(ududud)	P	Na_2**[Si_2O_5]**	1:2.50	11*d*	(8)
			Folded sheets of u–d tetrahedra				
Kanemite	$[6^3]_4$	ud^2ud^2-$u^2d^1u^2d^1$	1F	HNa**[Si_2O_5]**$(H_2O)_3$	1:2.50	12*a*	(9)
Sanbornite	$[6^3]_4$	ud^2ud^2-u^2du^2d	1F	Ba**[Si_2O_5]**	1:2.50	12*a*	(10)
Makatite	$[6^3]_4$	u^4d^2	1F	Na_2**[$Si_4O_8(OH)_2$]**$(H_2O)_4$	1:2.50	12*b*	(11)
			Modulated sheets of u–d tetrahedra				
Pentagonite	$[6^3]_8$	u^4d^2-d^4u^2	P	$CaV^{4+}O$**[Si_4O_{10}]**$(H_2O)_4$	1:2.50	13*a*	(12)
Silinaite	$[6^3]_4$	u^3d^3	P	$NaLi$**[Si_2O_5]**$(H_2O)_2$	1:2.50	13*b*	(13)
Plumbophyllite	$[6^3]_8$	u^4d^2-d^4u^2	P	Pb_2**[Si_4O_{10}]**(H_2O)	1:2.50	13*c*	(14)
Palygorskite	$[6^3]_8$	u^6-u^3d^3-d^6-d^3u^3	P	$MgAl$**[Si_4O_{10}]**$(OH)(H_2O)_4$	1:2.50	14*a*	(15)
Tuperssuatsiaite	$[6^3]_8$	u^6-u^3d^3-d^6-d^3u^3	P	$Na_{(2-x)}(Fe^{3+},Mn)_3$**[Si_8O_{20}]**$(OH)_2(H_2O)_4$	1:2.50	"	(16)
Windhoekite	$[6^3]_8$	u^6-u^3d^3-d^6-d^3u^3	P	$Ca_2Fe^{3+}_{(3-x)}$**[$(Si,Al)_8O_{20}$]**$(OH)_4(H_2O)_{10}$	1:2.50	"	(17)
Yofortierite	$[6^3]_8$	u^6-u^3d^3-d^6-d^3u^3	P	$(Mn^{2+},Mg,Fe^{3+},\square)_5$**[$Si_8O_{20}$]**$(OH)_2(H_2O)_9$	1:2.50	"	(18)
Raite	$[6^3]_8$	u^6-u^3d^3-d^6-d^3u^3	P	$Na_3Mn_3Ti_{0.25}$**[Si_2O_5]**$_4(OH)_2(H_2O)_{10}$	1:2.50	14*b*	(19)
Kalifersite	$[6^3]_{10}$	u^6-u^6-u^3d^3-d^6-d^3u^3	P	$(K,Na)_5Fe^{3+}_7$**[$Si_{20}O_{50}$]**$(OH)_6(H_2O)_{12}$	1:2.50	15*a*	(20)
Sepiolite	$[6^3]_{12}$	u^6-u^6-u^3d^3-d^6-d^6-d^3u^3	P	$(Mg,Fe,Al)_4$**[Si_6O_{15}]**$(O,OH)_2(H_2O)_6$	1:2.50	15*b*	(21)
Loughlinite	$[6^3]_{12}$	Iso sepiolite	P	Na_2Mg_3**[Si_6O_{15}]**$(H_2O)_8$	1:2.50	15*b*	(22)
Antigorite	$[6^3]_{28}$	u^6-u^6-u^4d^2-d^6-d^6-d^6-d^2u^4-u^6…	P	Mg_3**[Si_2O_5]**$(OH)_4$	1:2.50	15c	(23)

References: (1) Bailey (1988); (2) Brigatti and Poppi (1993), Brigatti *et al.* (2003), Brigatti and Guggenheim (2002); (3) Liu *et al.* (2012), Merlino (2014); (4) Merlino (1988*a*); (5) McDonald and Chao (2007); (6) Giester *et al.* (2016); (7) Yakovenchuk *et al.* (2011); (8) Pant (1968); (9) Garvie *et al.* (1999), Vortmann *et al.* (1999); (10) Hesse and Liebau (1980); (11) Annehed *et al.* (1982); (12) Evans (1973); (13) Grice (1991); (14) Kampf *et al.* (2009); (15) Artioli and Galli (1994), Chiari *et al.* (2003), Giustetto and Chiari (2004), Post and Heaney (2008); (16) Cámara *et al.* (2002); (17) Chukanov *et al.* (2012*b*); (18) Hawthorne *et al.* (2013); (19) Pluth *et al.* (1997); (20) Ferraris *et al.* (1998); (21) Post *et al.* (2007); (22) Fahey *et al.* (1960), Biedl and Preisinger (1962); and (23) Capitani and Mellini (2006), Dódony *et al.* (2002).
*P = planar; 1F = folded in one direction; M = octahedrally coordinated cations, T = tetrahedrally coordinated cations, A = interstitial cations.

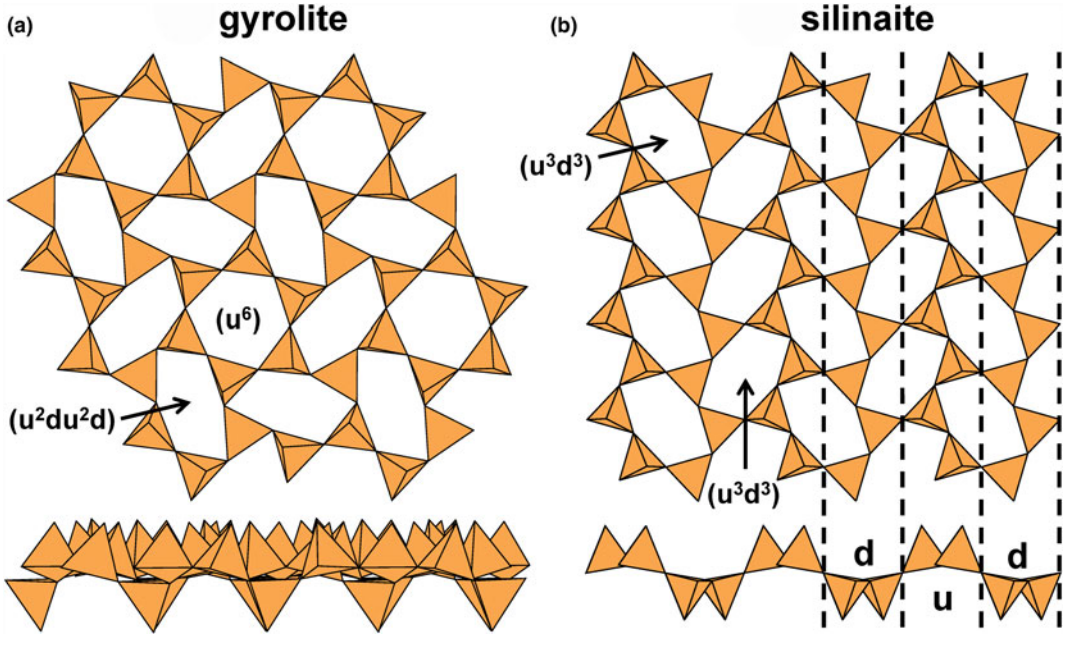

Fig. 10. The 6^3 sheets of tetrahedra in (*a*) **gyrolite** and (*b*) **silinaite**. In **gyrolite**, the (u^6) ring links only to d tetrahedra, and hence ribbons of like-pointing tetrahedra cannot form; in **silinaite**, (u^3d^3) rings link such that chains of tetrahedra form in one direction, allowing modulation of the sheet.

https://doi.org/10.1180/mgm.2018.152 Published online by Cambridge University Press

Structure hierarchy

In a hierarchical classification, it is general practice to arrange the structural units in terms of increasing connectivity. Connectivity is inversely correlated with T:O ratio, and planar 3-connected nets have the stoichiometry $[T_{2n}O_{5n}]$. Insertion of 2-connected vertices will increase the T:O ratio, whereas insertion of 4-connected vertices and generation of double-layer sheets *via* oikodoméic replication operations will decrease the T:O ratio (i.e. they increase the connectivity of the tetrahedra). For those structures with the same T:O ratio, we will arrange the structures in order of increasing complication of the nets on which they are based. We will start with single-layer 3-connected nets with inserted 2-connected vertices, as these structures have T:O ratios greater $n = 2.5$ (and the lowest connectivity of the sheet-silicate structures).

Single-layer sheets: 3-connected nets with inserted 2-connected vertices

Single 2-connected vertices

Figure 8 shows three inserted plane nets derived from the 6^3 net. In Fig. 8*a*, 2-connected vertices have been inserted into all edges of the 6^3 net (a class-1 oikodoméic operation), maintaining the original translational symmetry. The original six-membered rings have the u–d sequence (ududud) and become twelve-membered rings on insertion of the 2-connected tetrahedra; the resulting net is $(12^2)_3(12^3)_2$. Figure 8*b* shows the net of the silicate sheet in **zeophyllite** (Table 3) and Fig. 8*c* shows the corresponding silicate sheet in **zeophyllite**. The geometrical symmetry of the archetype 6^3 net is preserved and the unit cell is the same in both nets (cf. Figs 1*b* and 8*b*). The interstitial complex consists of three distinct Ca^{2+} ions with coordination numbers [6] (= six O^{2-}), [8] (= four O^{2-} and four F^-) and [8] (= four O^{2-}, three F^- and one $(H_2O)^t$ group). The O(1) anion is bonded to Si(1) and accepts three hydrogen bonds from the $(H_2O)^t$ group, and one F^- ion accepts a hydrogen bond from the (H_2O) group.

The sheets in **britvinite** and **molybdophyllite** (Table 3) are also based on the $(12^2)_3(12^3)_2$ net, but the u–d sequence in the parent 6^3 sheet is (u^6) for both minerals. The interstitial complex in **britvinite** consists of twenty distinct Pb^{2+} ions with coordination numbers from [6] to [10] and coordinating anions O^{2-}, $(OH)^-$, F^- and Cl^-. The interstitial complex in **molybdophyllite** consists of four distinct Pb^{2+} ions with coordination numbers from [6] to [9] and six distinct Mg^{2+} ions each of which is coordinated by six O^{2-} ions.

In Fig. 8*d*, 2-connected vertices have been inserted into two-thirds of the edges of the 6^3 net, again maintaining the original translational symmetry. The original six-membered rings become ten-membered rings and the resulting net is $(10^2)_4(10^3)_4$. Figure 8*e* shows the net of the silicate sheet in **tumchaite** (Table 3) and Fig. 8*f* shows the corresponding silicate sheet. The net corresponding to the sheet of tetrahedra is strongly geometrically distorted (Fig. 8*e*), but is $[(10^2)_4(10^3)_4]_1$ and topologically identical to the ideal inserted net in Fig. 8*d*. This geometrical distortion causes a doubling in the size of the unit cell (Fig. 8*e*) relative to that of the parent net (Fig. 1*b*). The interstitial complex in **tumchaite** consists of one distinct Zr^{4+} ion with coordination number [6] and one distinct Na^+ ion which is coordinated by five O^{2-} ions and two (H_2O) groups.

In Fig. 8*g*, 2-connected vertices are inserted into one-third of the edges of the 6^3 net, maintaining the original translational symmetry. As noted by Hawthorne (2015*a*), the resulting arrangement is very different from those of the nets in Figs 8*a* and 8*d*. The six-membered ring in Fig. 8*g* does not have *trans* symmetry and hence the unit cell must span more than one single six-membered ring. As a result, the unit cell must be larger than that of the parent net, and a further doubling is caused by the geometrical distortion of the sheet. Figure 8*h* shows the net of the silicate sheet in **kvanefjeldite** (Table 3) and Fig. 8*i* shows the corresponding silicate sheet. The interstitial complex in **kvanefjeldite** consists of one distinct Ca^{2+} ion with coordination number [6] and two distinct Na^+ ions both of which are coordinated by seven O^{2-} ions.

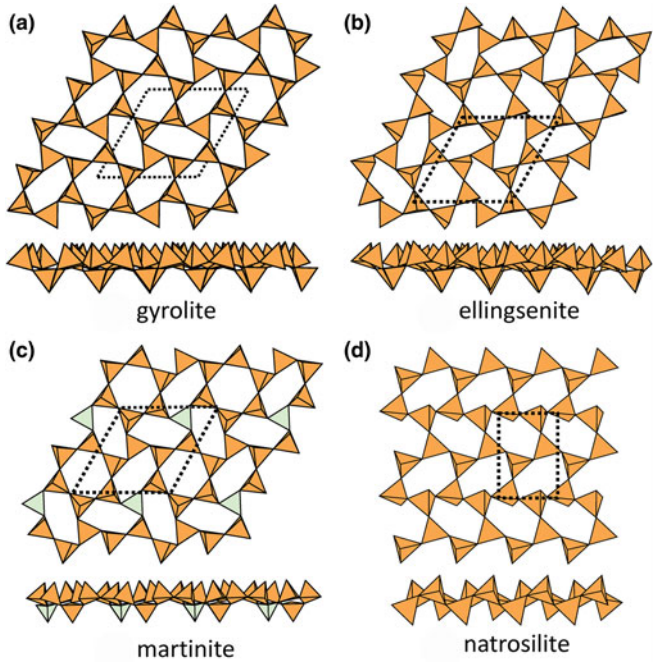

Fig. 11. Planar 6^3 sheets of u–d tetrahedra in (*a*) **gyrolite**, (*b*) **ellingsenite**, (*c*) **martinite** and **cairncrossite**, and (*d*) **natrosilite**.

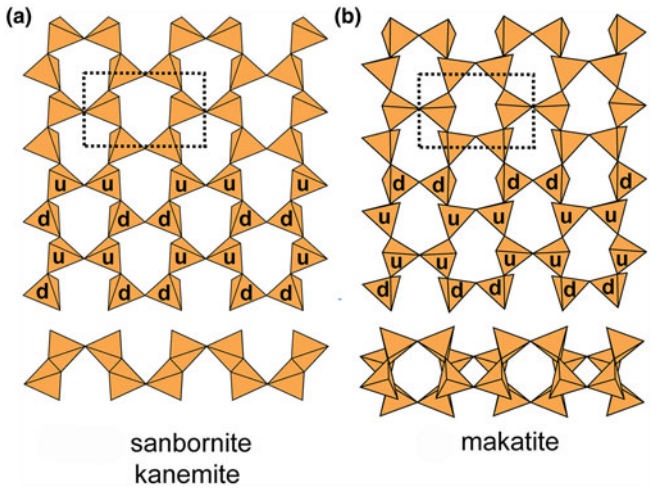

Fig. 12. Folded 6^3 sheets of u–d tetrahedra in (*a*) **sanbornite** and **kanemite** and (*b*) **makatite**; cross-sections of each sheet show the folding in one direction, and the u–d symbols indicate the different u–d arrangements in each type of sheet.

https://doi.org/10.1180/mgm.2018.152 Published online by Cambridge University Press

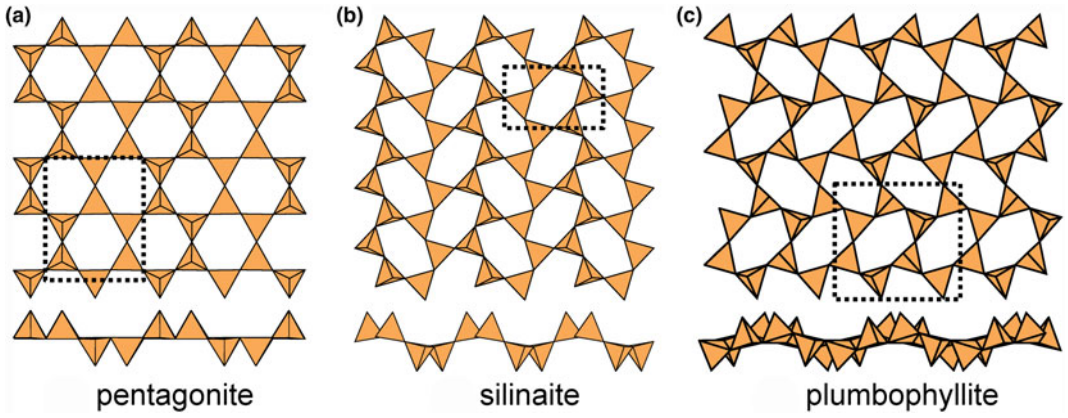

Fig. 13. Modulated 6^3 sheets (ribbon width = 2u2d tetrahedra) of u–d tetrahedra in (*a*) **pentagonite**, (*b*) **silinaite** and (*c*) **plumbophyllite**.

Pairs of 2-connected vertices

In Fig. 9, pairs of 2-connected vertices have been inserted into one-third of the edges of the 6^3 net, maintaining the original translational symmetry. The resultant net is $(14^2)_6(14^3)_2$, and in the corresponding sheet of tetrahedra in **hyttsjöite** (Fig. 9*a*; Table 3), the 2-connected tetrahedra are coloured yellow. The sheet is quite corrugated and also shows considerable geometrical distortion from a geometrically holosymmetric 6^3 net. The structure of **hyttsjöite** also contains a discontinuous layer of tetrahedra (Fig. 9*b*) which is linked into a continuous layer by pairs of short bonds involving lone-pair-stereoactive Pb^{2+}, and this arrangement accounts for the very high Si:O ratio: 1:3.00 (Table 3). The interstitial complex in **hyttsjöite** is quite complicated. It consists of three distinct Pb^{2+} ions coordinated solely by O^{2-} with coordination numbers [8], [8] and [6], respectively, one Ba^{2+} coordinated by twelve O^{2-} ions, three distinct Ca^{2+} ions with coordination numbers [6] (= six O^{2-}) and [9] (= eight O^{2-} ions and one (H_2O) group, and nine O^{2-} ions, respectively), one Fe^{3+} and one Mn^{2+} each coordinated by six O^{2-} ions.

Single-layer sheets: 3-connected nets

The 6^3 net

The most common single-layer sheet-silicate minerals are based on this net (Fig. 1*b*; Table 4); note that all tetrahedra are in the u configuration (hence the nets have the (u^6) arrangement) and are planar (i.e. not folded). Table 4 also lists the single-layer sheet-silicate minerals based on the 6^3 net which have tetrahedra of their six-membered rings in arrangements other than (u^6). These minerals are dominated by planar (P) sheets of tetrahedra. We will not discuss the common silicate-mineral groups here as their crystal structures and crystal chemistry have been dealt with in detail elsewhere (e.g. Brigatti and Guggenheim, 2002; Brigatti *et al.*, 2003). The structures of the smectites are not well-known; some are T–O–T structures and others are double-layer structures that we will deal with later in the paper. **Hanjiangite** has a large interlayer component and is probably related to the **surite–ferrisurite** series (Hayase *et al.*, 1978; Uehara *et al.*, 1997; Kampf *et al.*, 1992) and **niksergievite** (Saburov *et al.*, 2005), with complex polytypism (Merlino, 2014) possibly giving rise to several structural variants.

Let us examine the sheet in **gyrolite** (Fig. 10*a*). Some of the six-membered rings are reasonably close to showing 6-fold rotational symmetry, whereas others are strongly distorted from this arrangement. If we examine the configurations of the apical vertices of the tetrahedra in the different rings (Fig. 10*a*), we see that the less-distorted rings have a (u^6) arrangement of their apical vertices, whereas the more-distorted rings have a (u^2du^2d) arrangement where some apical vertices lie above the plane of the sheet and others lie below the plane of the sheet. Despite vertices pointing in different directions, the T–O–T linkages within the sheet are planar (or nearly so).

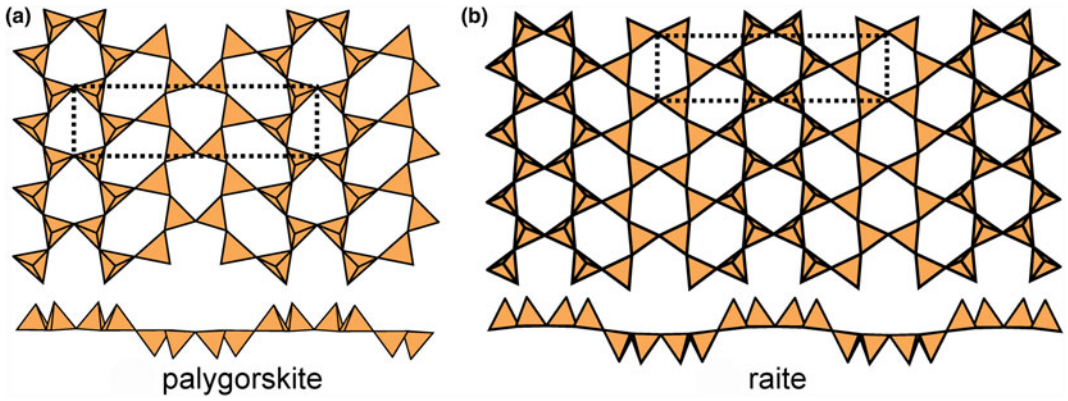

Fig. 14. Modulated 6^3 sheets (ribbon width = 4u4d tetrahedra) of u–d tetrahedra in (*a*) **palygorskite** and (*b*) **raite**.

https://doi.org/10.1180/mgm.2018.152 Published online by Cambridge University Press

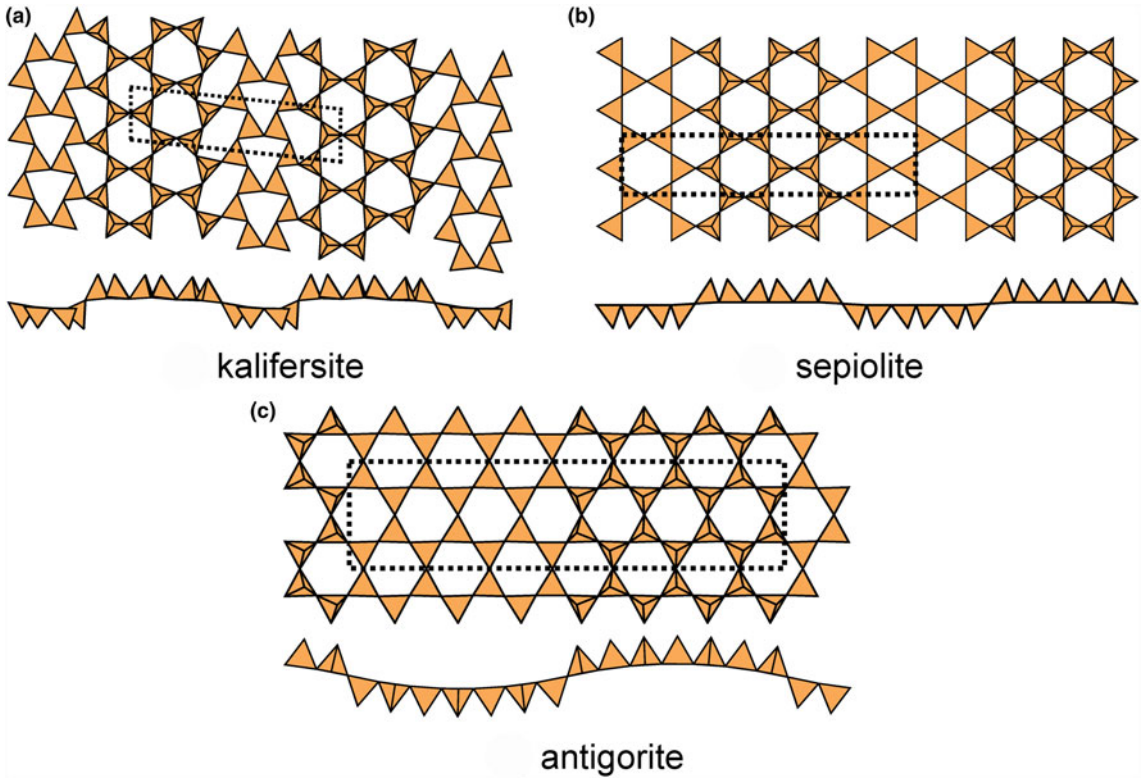

Fig. 15. Modulated 6^3 sheets of u–d tetrahedra in (*a*) **kalifersite** (ribbon width = 6u4d), (*b*) **sepiolite** (ribbon width = 6u6d) and (*c*) **antigorite** (ribbon width = 7u7d).

Compare the sheet in **gyrolite** (Fig. 10*a*) with the sheet in **silinaite** (Fig. 10*b*). In **silinaite**, there is only one type of six-membered ring: (u^3d^3). Inspection of the cross-sections of gyrolite (Fig. 10*a*) and **silinaite** (Fig. 10*b*) shows that the bridging anions within the sheets behave somewhat differently; although they are topologically equivalent, there are significant geometrical differences. In **gyrolite**, the bridging anions are planar (or their deviations from planarity are not spatially modulated) whereas in **silinaite**, the bridging anions are topologically planar but their deviations from planarity are spatially modulated in one direction (Fig. 10*b*). In **silinaite**, the u tetrahedra are arranged in ribbons, interspersed with ribbons of d tetrahedra, and the parallel arrangement of these ribbons allows the sheet to modulate in a direction orthogonal to these ribbons. In **gyrolite**, the (u^6) ring links only to d tetrahedra (Fig. 10*a*) and hence ribbons of u tetrahedra do not occur (as the definition of the direction of u is arbitrary, similarly ribbons of d tetrahedra are not present). Thus in **gyrolite**, the lack of ribbons of u (and d) tetrahedra inhibits modulation. Hence we expect two types of single-sheet arrangements: (1) planar arrangements, and (2) modulated (or potentially modulated) arrangements.

Planar sheets of u–d tetrahedra

Gyrolite (Fig. 11*a*), **ellingsenite** (Fig. 11b), **martinite** (Fig. 11*c*) and **natrosilite** (Fig. 11*d*) contain planar sheets. **Gyrolite, ellingsenite** and **martinite** contain topologically identical sheets: there are two types of six-membered rings, a (u^6) ring and a (u^2du^2d) ring, and the (u^6) ring is completely surrounded by (u^2du^2d) rings, whereas each (u^2du^2d) ring is surrounded by two (u^6) rings and four (u^2du^2d) rings, and the planar unit-cell contains one (u^6) ring and three (u^2du^2d) rings. In **martinite**, one third of the d tetrahedra are occupied by B^{3+}. The interstitial complex in **gyrolite** consists of eight distinct Ca^{2+} ions and one distinct Na^+ ion. There are three [7]-coordinated Ca^{2+} ions, each of which is bonded to 5 O^{2-} ions and two $(OH)^-$ groups, and five [6]-coordinated Ca^{2+} ions, with coordinations $O_5^{2-}OH)^-$ (×3), $O_3^{2-}(OH)_3^-$ (×1) and $O_2^{2-}(H_2O)_4^t$ (×1). There is also one [6]-coordinated Na^+ ion bonded to 6 $(H_2O)^t$ groups. The interstitial complex in **ellingsenite** consists of two distinct Ca^{2+} ions, two distinct Na^+ ions, and one site that is occupied by 50% Ca^{2+} and 50% Na^+. The Ca^{2+} ions are [6]-coordinated, one by six O^{2-} ions and the other by five O^{2-} ions and one $(OH)^-$ group. Both Na^+ ions are [8]-coordinated, one by six O^{2-} ions and two $(OH)^-$ groups, and the other by five O^{2-} ions, two $(OH)^-$ groups and one $(H_2O)^t$ group. The site containing $Ca_{0.50} + Na_{0.50}$ is [6]-coordinated by five O^{2-} ions and one $(OH)^-$ group. The formula given for **ellingsenite** is not compatible with the refined structure; this issue is discussed in the Appendix and a revised formula is suggested. The interstitial complex in **martinite** consists of two sites occupied by Ca^{2+} ions and seven sites occupied by Na^+ ions. There are two Ca^{2+} ions bonded to O_6^{2-} F and O_6^{2-} ions, respectively, and seven distinct Na^+ ions, four of which are [8]-coordinated by $O_6^{2-}F_2^-$, $O_5^{2-}(OH)_2^-(H_2O)^n$, $O_6^{2-}(H_2O)_2^n$ and O_6^- $F^-(H_2O)^n$, one of which is [7]-coordinated by O_6^{2-} F^-, and two of which are positionally disordered such that both sites cannot be locally occupied, with coordinations $O_5^{2-}(OH)^-(H_2O)^n$ and $O_3^{2-}(OH)^-(H_2O)^n$, respectively.

In **natrosilite**, there is only one type of six-membered ring, a (ududud) ring, and thus each (ududud) ring is surrounded by other (ududud) rings. It should be noted that neither (ududud)

https://doi.org/10.1180/mgm.2018.152 Published online by Cambridge University Press

Table 5. Single-layer sheet-silicates based on the 4.8^2, 4.6.12, $(4.6.8)_2(6.8^2)_1$, $(5^2.8)_2(5.8^2)_1$, (4.6.12), $(4.6.10)_4(6^2.10)_1$, $(5.6.7)_4(5.7^2)_1(6^2.7)_1$ and $(4^2.14)_{12}(4.6.14)_8(6.14^2)_4$ nets with mixed u–d arrangements.

Mineral	Net	u–d configuration	P/F*	Formula	T:O ratio	Fig. No.	Ref.
		4.8^2					
		Planar sheets					
		Gadolinite supergroup					
Datolite	$[4.8^2]_8$	$(u^2d^2)(u^4d^4)_2$	P	$Ca[\mathbf{BSiO_4(OH)}]$	1:2.50	16	(1)
Gadolinite-(Ce)	$[4.8^2]_8$	$(u^2d^2)(u^4d^4)_2$	P	$Ce_2Fe^{2+}[\mathbf{Be_2Si_2O_{10}}]$	1:2.50	"	(2)
Gadolinite-(Y)	$[4.8^2]_8$	$(u^2d^2)(u^4d^4)_2$	P	$Y_2Fe^{2+}[\mathbf{Be_2Si_2O_{10}}]$	1:2.50	"	(3)
Hingganite-(Ce)	$[4.8^2]_8$	$(u^2d^2)(u^4d^4)_2$	P	$Ce_2\square[\mathbf{Be_2Si_2O_8(OH)_2}]$	1:2.50	"	(4)
Hingganite-(Y)	$[4.8^2]_8$	$(u^2d^2)(u^4d^4)_2$	P	$Yb_2\square[\mathbf{Be_2Si_2O_8(OH)_2}]$	1:2.50	"	(5)
'Hingganite-(Yb)'	$[4.8^2]_8$	$(u^2d^2)(u^4d^4)_2$	P	$Y_2\square[\mathbf{Be_2Si_2O_8(OH)_2}]$	1:2.50	"	(6)
'Calcybeborosilite'	$[4.8^2]_8$	$(u^2d^2)(u^4d^4)_2$	P	$CaY\square[\mathbf{BeBSi_2O_8(OH)_2}]$	1:2.50	"	(7)
Homilite	$[4.8^2]_8$	$(u^2d^2)(u^4d^4)_2$	P	$Ca_2Fe^{2+}[\mathbf{B_2Si_2O_{10}}]$	1:2.50	"	(8)
Minasgeraisite-(Y)	$[4.8^2]_8$	$(u^2d^2)(u^4d^4)_2$	P	$CaY_2[\mathbf{Be_2Si_2O_{10}}]$	1:2.50	"	(9)
		Apophyllite group					
Fluorapophyllite-(K)	$[4.8^2]_8$	$(u^4)_1(d^4)_1(u^2d^2u^2d^2)_2$	P	$KCa_4[\mathbf{Si_4O_{10}}]_2F(H_2O)_8$	1:2.50	17*a*	(10)
Hydroxyapophyllite-(K)	$[4.8^2]_8$	$(u^4)_1(d^4)_1(u^2d^2u^2d^2)_2$	P	$KCa_4[\mathbf{Si_4O_{10}}]_2(OH)(H_2O)_8$	1:2.50	"	(11)
Fluorapophyllite-(Na)	$[4.8^2]_8$	$(u^4)_1(d^4)_1(u^2d^2u^2d^2)_2$	P	$NaCa_4[\mathbf{Si_4O_{10}}]_2F(H_2O)_8$	1:2.50	"	(12)
		Miscellaneous					
Cavansite	$[4.8^2]_4$	$(u^2d^2)_1(u^4d^4)_2$	P	$CaV[\mathbf{Si_4O_{10}}]O(H_2O)_4$	1:2.50	17*b*	(13)
Cryptophyllite	$[4.8^2]_4$	$(u^4)_1(d^4)_1(u^2d^2u^2d^2)$	P	$K_2Ca[\mathbf{Si_4O_{10}}](H_2O)_5$	1:2.50	18*a*	(14)
Shlykovite	$[4.8^2]_4$	$(u^3d^1)(u^4d^1u^2d^1)$	P	$KCa[\mathbf{Si_4O_9(OH)}](H_2O)_3$	1:2.50	18*b*	(15)
Mountainite	$[4.8^2]_4$	$(u^3d^1)(u^3d^1u^3d^1)$	P	$KNa_2Ca_2[\mathbf{Si_8O_{19}(OH)}](H_2O)_6$	1:2.50	18*c*	(16)
		Folded sheets					
		Gillespite group					
Cuprorivaite	$[4.8^2]_8$	$(u^4)_1(d^4)_1(u^2d^2u^2d^2)_2$	2F	$CaCu[\mathbf{Si_4O_{10}}]$	1:2.50	19*a*	(17)
Effenbergerite	$[4.8^2]_8$	$(u^4)_1(d^4)_1(u^2d^2u^2d^2)_2$	2F	$BaCu[\mathbf{Si_4O_{10}}]$	1:2.50	"	(18)
Gillespite	$[4.8^2]_8$	$(u^4)_1(d^4)_1(u^2d^2u^2d^2)_2$	2F	$BaFe[\mathbf{Si_4O_{10}}]$	1:2.50	"	(19)
Wesselsite	$[4.8^2]_8$	$(u^4)_1(d^4)_1(u^2d^2u^2d^2)_2$	2F	$SrCu[\mathbf{Si_4O_{10}}]$	1:2.50	"	(20)
		Ekanite group					
Arapovite	$[4.8^2]_8$	$(u^4)_1(d^4)_1(u^2d^2u^2d^2)_2$	2F	$U^{4+}(CaNa)K[\mathbf{Si_4O_{10}}]_2$	1:2.50	19*b*	(21)
Ekanite	$[4.8^2]_8$	$(u^4)_1(d^4)_1(u^2d^2u^2d^2)_2$	2F	$ThCa_2[\mathbf{Si_4O_{10}}]_2$	1:2.50	19*b*	(22)
Iraqite-(La)	$[4.8^2]_8$	$(u^4)_1(d^4)_1(u^2d^2u^2d^2)_2$	2F	$LaCa_2K[\mathbf{Si_4O_{10}}]_2$	1:2.50	"	(23)
Steacyite	$[4.8^2]_8$	$(u^4)_1(d^4)_1(u^2d^2u^2d^2)_2$	2F	$Th(CaNa)K[\mathbf{Si_4O_{10}}]_2$	1:2.50	"	(24)
Turkestanite	$[4.8^2]_8$	$(u^4)_1(d^4)_1(u^2d^2u^2d^2)_2$	2F	$Th(CaNa)K[\mathbf{Si_4O_{10}}]_2$	1:2.50	"	(25)
		4.6.12					
Pyrosmalite-(Fe)	$[4.6.12]_{12}$	$(u^2d^2)_3(u^6)(d^6)(u^2d^2u^2d^2u^2d^2)$	P	$Fe_8^{2+}[\mathbf{Si_6O_{15}}](OH,Cl)_{10}$	1:2.50	20	(26)
Pyrosmalite-(Mn)	$[4.6.12]_{12}$	$(u^2d^2)_3(u^6)(d^6)(u^2d^2u^2d^2u^2d^2)$	P	$Mn_8^{2+}[\mathbf{Si_6O_{15}}](OH,Cl)_{10}$	1:2.50	"	(27)
Schallerite	$[4.6.12]_{12}$	$(u^2d^2)_3(u^6)(d^6)(u^2d^2u^2d^2u^2d^2)$	P	$Mn_{16}^{2+}As_3^{3+}O_6[\mathbf{Si_{12}O_{30}}](OH)_{17}$	1:2.50	"	(28)
Friedelite	$[4.6.12]_{12}$	$(u^2d^2)_3(u^6)(d^6)(u^2d^2u^2d^2u^2d^2)$	P	$Mn_8[\mathbf{Si_6O_{15}}](OH)_{10}$	1:2.50	"	(29)
Mcgillite	$[4.6.12]_{12}$	$(u^2d^2)_3(u^6)(d^6)(u^2d^2u^2d^2u^2d^2)$	P	$Mn_8[\mathbf{Si_6O_{15}}](OH)_8Cl_2$	1:2.50	"	(30)
Nelenite	$[4.6.12]_{12}$	$(u^2d^2)_3(u^6)(d^6)(u^2d^2u^2d^2u^2d^2)$	P	$Mn_{16}As_3^{3+}O_6[\mathbf{Si_{12}O_{30}}](OH)_{17}$	1:2.50	"	(31)
		$(4.6.8)_2(6.8^2)_1$					
Armstrongite	$[(4.6.8)_2(6.8^2)_1]_2$	$(u^2d^2)(ududud)(u^4d^4)$	1F	$CaZr[\mathbf{Si_6O_{15}}](H_2O)_{2.5}$	1:2.50	21*a*	(32)
Dalyite	$[(4.6.8)_2(6.8^2)_1]_2$	$(u^2d^2)(ududud)(u^4d^4)$	1F	$K_2Zr[\mathbf{Si_6O_{15}}]$	1:2.50	21*b*	(33)
Davanite	$[(4.6.8)_2(6.8^2)_1]_2$	$(u^2d^2)(ududud)(u^4d^4)$	1F	$K_2Ti[\mathbf{Si_6O_{15}}]$	1:2.50	"	(34)
Sazhinite-(Ce)	$[(4.6.8)_2(6.8^2)_1]_4$	$(u^4)(d^4)(u^2du^2d)(ud^2ud^2)(u^2dud^2ud)$	1F	$HNa_2Ce[\mathbf{Si_6O_{15}}](H_2O)_n$	1:2.50	21*c*	(35)
Sazhinite-(La)	$[(4.6.8)_2(6.8^2)_1]_4$	$(u^4)(d^4)(u^2du^2d)(ud^2ud^2)(u^2dud^2ud)$	1F	$HNa_2La[\mathbf{Si_6O_{15}}](H_2O)_n$	1:2.50	"	(36)
		$(5^2.8)_2(5.8^2)_1$					
Nekoite	$[(5^2.8)_2(5.8^2)_1]_2$	$(u^3d^2)(u^2dud)(u^6d^2)$	P	$Ca_3[\mathbf{Si_6O_{15}}](H_2O)_7$	1:2.50	22*a*	(37)
Okenite	$[(5^2.8)_2(5.8^2)_1]_2$	$(u^4d)\ (u^7d)$	P	$Ca_{10}[(\mathbf{Si_6O_{16}})(\mathbf{Si_6O_{15}})_2](H_2O)_{18}$	1:2.56	22*b*,*c*	(38)
Zeravshanite	$[(5^2.8)_2(5.8^2)_1]_6$	$(u^3d^2)(u^2d^3)(u^4d^4)$	1F	$Cs_4Na_2Zr_3[\mathbf{Si_{18}O_{45}}](H_2O)_2$	1:2.50	22*d*	(39)
		$(4.6.10)_4(6^2.10)_1$					
Varennesite	$[(4.6.10)_4(6^2.10)_1]_4$	$(u^2d^2)_4(u^6)_2(d^6)_2(u^3d^2u^3d^2)(d^3u^2d^3u^2)$	P	$Na_8Mn_2^{2+}[\mathbf{Si_{10}O_{25}}](OH)_2(H_2O)_{12}$	1:2.50	23*a*	(40)
		$(5.6.7)_4(5.7^2)_1(6^2.7)_1$					
Bementite	$[(5.6.7)_4(5.7^2)_1(6^2.7)_1]_4$	$(u^3d^2)(u^2d^3)(u^6)(d^6)(u^5d)(u^2d^5)$	P	$Mn_7^{2+}[\mathbf{Si_6O_{15}}](OH)_8$	1:2.50	23*b*	(41)
		$(5^2.8)_1(5.6^2)_1(5.6.8)_2(6^2.8)_1$					
Intersilite	$[(5^2.8)_1(5.6^2)_1(5.6.8)_2(6^2.8)_1]_4$	$(u^2dud)_2(udud^2)_2(u^6)(u^3d^3)_2(d^6)(u^4du^2d)$ (d^4ud^2u)	P	$Na_6Mn^{2+}Ti[\mathbf{Si_{10}O_{25}}]$ $(OH)_2(H_2O)_4$	1:2.50	23*c*	(42)
		$(4^2.14)_{12}(4.6.14)_8(6.14^2)_4$					
Yakovenchukite-(Y)	$[(4^2.14)_{12}(4.6.14)_8(6.14^2)_4]_1$	$(u^2d^2)_3(u^2du^2d)(ud^2ud^2)(ud^2ud^2udu^2du^2d)$	2F	$K_3NaCaY_2[\mathbf{Si_{12}O_{30}}](H_2O)_4$	1:2.50	24	(43)

References: (1) Foit *et al.* (1973), Rinaldi *et al.* (2010); (2) Segalstad and Larsen (1978), Demartin *et al.* (1993); (3) Cámara *et al.* (2008); (4) Ximen and Peng (1985), Miyawaki *et al.* (2007); (5) Demartin *et al.* (2001), Miyawaki *et al.* (2007); (6) Yakubovich *et al.* (1983); (7) Rastsvetaeva *et al.* (1996); (8) Miyawaki *et al.* (1985); (9) Foord *et al.* (1986); Cooper and Hawthorne (2017); (10) Bartl and Pfeifer (1976), Ståhl (1993); (11) Dunn *et al.* (1978); (12) Matsueda *et al.* (1981); (13) Evans (1973); (14) Zubkova *et al.* (2010); (15) Zubkova *et al.* (2010); (16) Zubkova *et al.* (2009); (17) Chakoumakos *et al.* (1993), Bensch and Schur (1995); (18) Lin *et al.* (1992), Giester and Rieck (1994), Knight *et al.* (2010); (19) Pabst (1943), Hazen and Finger (1983); (20) Giester and Rieck (1996); (21) Uvarova *et al.* (2004*a*); (22) Szymański *et al.* (1982); (23) Livingstone *et al.* (1976); (24) Perrault and Szymański (1982); (25) Kabalov *et al.* (1998); (26) Yang *et al.* (2011); (27) Takeuchi *et al.* (1969), Kato and Takéuchi (1983); (28) Kato and Watanabe (1992); (29) Ozawa *et al.* (1983); (30) Ozawa *et al.* (1983); (31) Dunn and Peacor (1984); (32) Kasahev and Sapozhnikov (1978); (33) Fleet (1965); (34) Gebert *et al.* (1983), Lazebnik *et al.* (1984); (35) Es'kova *et al.* (1974), Shumyatsaya *et al.* (1980); (36) Cámara *et al.* (2006); (37) Alberti and Galli (1983); (38) Merlino (1983); (39) Uvarova *et al.* (2004*b*); (40) Grice and Gault (1995); (41) Heinrich *et al.* (1994); (42) Yamnova *et al.* (1996); and (43) Krivovichev *et al.* (2007).
*P = planar; 1F = folded in one direction.

https://doi.org/10.1180/mgm.2018.152 Published online by Cambridge University Press

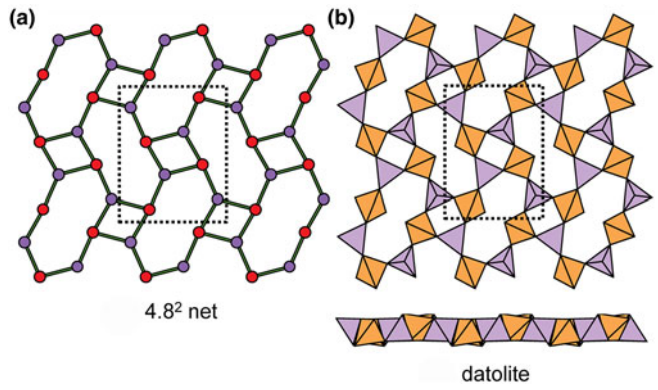

Fig. 16. The 4.8^2 net and sheet in **datolite**; (*a*) the geometrically distorted 4.8^2 net; and (*b*) the sheet of tetrahedra.

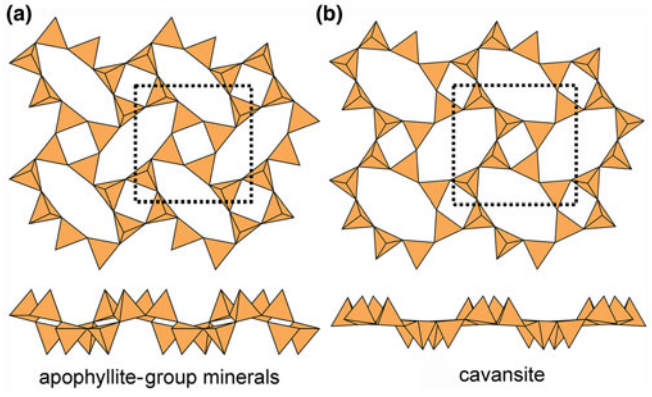

Fig. 17. Kinked planar 4.8^2 sheets of u–d tetrahedra in (*a*) **apophyllite** and (*b*) **cavansite**.

rings nor combinations of (u^6) and (u^2du^2d) rings can produce modulated sheets. The interstitial complex in **natrosilite** consists of two sites occupied by Na^+ ions with coordinations O_5^{2-} and O_6^{2-}, respectively.

Folded sheets of u–d tetrahedra

Sanbornite and **kanemite** (Fig. 12*a*) and **makatite** (Fig. 12*b*) contain folded sheets (cf. Fig. 3) of six-membered rings of tetrahedra. The sheets differ in their arrangements of u–d tetrahedra; in **sanbornite** and **kanemite**, there are two types of rings, (ud^2ud^2) and ($u^2d^1u^2d^1$), whereas in **makatite** there is only one type of ring, (u^4d^2). As is apparent from Fig. 12, the sheets are folded strongly: in one direction, cf. Fig. 3, leading to a very non-planar arrangement of O(br) anions; in the other direction, adjacent tetrahedra point u and d and the O(br) anions are only slightly non-planar. In **sanbornite** and **kanemite**, the folding is in phase in that the topological repeat in the sheet along the fold axis is one pair of tetrahedra, whereas in makatite, the topological repeat along the fold axis is two pairs of tetrahedra, giving a different appearance to the sheet in the direction of the fold axes (Fig. 12). In **kanemite**, there is one interstitial Na^+ ion coordinated by $(H_2O)_6^n$. In **sanbornite**, there is one interstitial Ba^{2+} ion coordinated by O_9^{2-}. In **makatite**, there are three interstitial Na^+ ions coordinated by $(H_2O)_6^n$ (×2) and $O_3^{2-}(H_2O)_2^n$, respectively.

Modulated sheets of u–d tetrahedra

Above, we saw that in order for sheets to be modulated in a particular direction, the sheets must contain parallel ribbons of u tetrahedra and ribbons of d tetrahedra (Fig. 10*b*). A convenient way of classifying such modulated sheets is by the width (i.e. the number of tetrahedra) across the ribbon. The minimum width of these ribbons is two tetrahedra, and those structures thus formed are shown in Fig. 13. In **pentagonite** (Fig. 13*a*), there are two types of six-membered rings, (u^2d^4) and (u^4d^2), that share two adjacent similarly pointing tetrahedra to form ribbons of similarly pointing tetrahedra. Inspection of Fig. 13*a* shows no perceptible sign of modulation of the sheet, but the possibility of modulation exists in terms of the linkage of tetrahedra. In **pentagonite**, there are two interstitial cations, one V^{4+} coordinated by O_5^{2-} and one Ca^{2+} coordinated by $O_6^{2-}(H_2O)^t$, plus an $(H_2O)^z$ group. In **silinaite**, there is only one type of six-membered ring, (u^3d^3), that shares vertices with adjacent rings such that like-pointing tetrahedra form fairly extended ribbons (Fig. 13*b*), and there is a pronounced modulation with a wavelength of four tetrahedra orthogonal to these ribbons. There are two interstitial

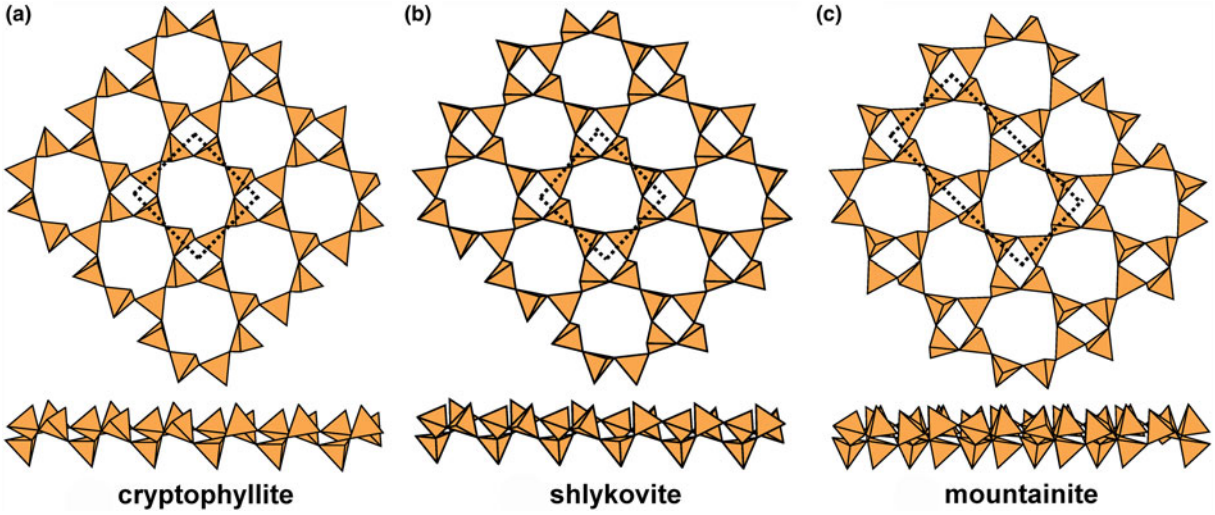

Fig. 18. Planar 4.8^2 sheets of u–d tetrahedra in (*a*) **cryptophyllite**, (*b*) **shlykovite** and (*c*) **mountainite**.

https://doi.org/10.1180/mgm.2018.152 Published online by Cambridge University Press

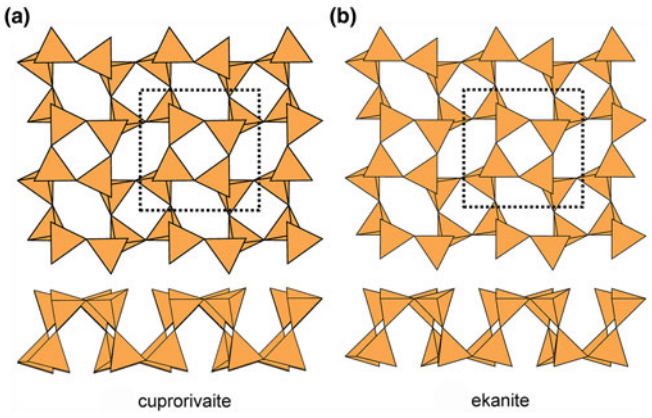

Fig. 19. Folded 4.8^2 sheets of u–d tetrahedra in (*a*) **cuprorivaite** and (*b*) **ekanite**.

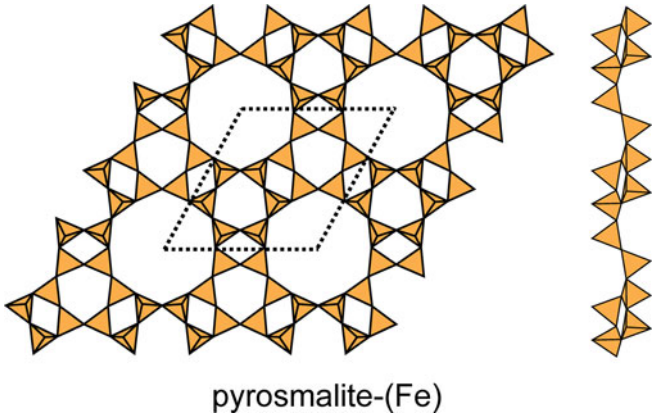

Fig. 20. The 4.6.12 sheet in the structures of **pyrosmalite-(Fe), pyrosmalite-(Mn)** and **schallerite**. Note the slight modulation in the sheet.

cations, Li^+ coordinated by O_4^{2-} and Na^+ coordinated by $O_2^{2-}(H_2O)_4^n$.

In **plumbophyllite**, there are two types of six-membered rings, (u^4d^2) and (u^2d^4), that share vertices with adjacent rings such that like-pointing tetrahedra form fairly extended ribbons (Fig. 13*c*), and there is a pronounced modulation with a wavelength of four tetrahedra orthogonal to these ribbons; however, note that the sheet is more folded than is the case in **silinaite** (Fig. 13*b*), and hence the modulation tends to appear blurred where viewed parallel to the ribbons (Fig. 13*c*). There is one interstitial lone-pair stereoactive Pb^{2+} cation coordinated by $O_6^{2-}(H_2O)^t$ where the site containing (H_2O) is only half-occupied.

Sheets with a ribbon width of four tetrahedra are shown in Fig. 14. In **palygorskite** (Fig. 14*a*) and **raite** (Fig. 14*b*), there are two types of six-membered rings, (u^6) and (u^3d^3), that share three adjacent similarly pointing tetrahedra to form ribbons of similarly pointing tetrahedra four tetrahedra wide. There is only a very slight modulation of this sheet in **palygorskite** and a more prominent modulation in **raite**; the magnitude of the modulation is more a function of the strip of octahedra to which the sheet is attached than a characteristic of the sheet itself (Guggenheim and Eggleton, 1998). In **palygorskite**, the interstitial cations are all [6]-coordinated; there are two sites each half-occupied by Mg^{2+} and Al^{3+} (Giustetto and Chiari, 2004), plus interstitial (H_2O) groups. In **raite**, there are two interstitial Mn^{2+} cations coordinated by $O_4^{2-}(OH)_2$, two Na^+ cations coordinated by O_6^{2-} and $(H_2O)_6$, respectively, and one quarter-occupied site containing Ti^{4+} coordinated by $O_2^{2-}(H_2O)_4$.

In **kalifersite** (Fig. 15*a*), there are two types of six-membered rings, (u^6) and (d^6), in the ratio 2:1. The (u^6) rings link to form an upward-pointing ribbon six-tetrahedra wide, and these ribbons are linked laterally by a ribbon of (d^6) rings that form a downward-pointing ribbon four-tetrahedra wide, forming a modulation in which the widths of the ribbons with like-pointing tetrahedra are different. The interstitial cations are five [6]-coordinated Fe^{2+} ions with coordinations O_6^{2-} (×2) and $O_4^{2-}(OH)_2$ (×3), and three K^+ ions (+ minor Na^+) with coordinations $O_2^{2-}(H_2O)_4$ (×2) and $(H_2O)_6$. In **sepiolite** (Fig. 15*b*), there are two types of six-membered rings, (u^6) and (d^6), in the ratio 1:1. The (u^6) rings link to form an upward-pointing ribbon six-tetrahedra wide, and the (d^6) rings link to form a downward-pointing ribbon six-tetrahedra wide. Interstitial cations are four distinct Mg^{2+} ions with coordinations $O_4^{2-}(OH)_2^-$ (×3) and $O_4^{2-}(H_2O)_2^t$ plus four interstitial $(H_2O)^z$ sites that may show partial occupancy and positional disorder. In **antigorite** (Fig. 15*c*), there are four types of six-membered rings, (u^6), (u^4d^2), (u^2d^4) and (d^6), in the ratio 2:1:1:2. The (u^6) and (u^4d^2) rings link to form an upward-pointing ribbon seven-tetrahedra wide, the (u^2d4^2) and (d^6) rings link to form a downward-pointing ribbon seven-tetrahedra wide, and **antigorite** shows the most prominent modulation of these modulated sheet-silicates.

Inspection of Figs 13–15 indicates that (u^6) rings are generally much less distorted away from planar hexagonal symmetry than six-membered rings containing both u and d tetrahedra. It is obvious that commensurate modulation and folding are connected to linkage requirements between the sheets and the non-tetrahedrally coordinated parts of the structures, but the diversity of the latter, involving variations in stoichiometry, coordination number and ligancy of non-tetrahedrally coordinated cations, differing amounts of H and the ensuing hydrogen bond networks, are beyond the scope of the present work.

The 4.8^2 net

Details of the 4.8^2 net are shown in Fig. 2*b*. There are both four-membered and eight-membered rings but only one type of vertex: one four-membered ring and two eight-membered rings meet at each vertex, and the unit cell contains $[Si_4O_{10}]$. Table 5 lists the single-layer sheet-silicate minerals based on this net.

The minerals of the **gadolinite supergroup** (Table 5) show the simplest type of 4.8^2 net (Fig. 16*a*). The B^{3+} tetrahedra point both up and down in **datolite**, but do not project above or below the plane of the sheet. Instead, they link to Si^{4+} tetrahedra which have edges in the top and bottom surfaces of the sheet (Fig. 16*b*) and hence occur entirely within the body of the sheet. In general, the ordering of cations in this structure type is very strong, with Si^{4+} and (Be^{2+}, B^{3+} and Al^{3+}) occupying discrete tetrahedra (Fig. 16). Bačík *et al.* (2014) wrote the general formula of the minerals of this group as $W_2XZ_2T_2O_8V_2$ where W = Ca^{2+}, *REE*$^{3+}$ (Y^{3+} + lanthanoids), Bi^{3+}; X = Fe^{2+}, □ (vacancy), Mg^{2+}, Mn^{2+}, Zn^{2+}, Cu^{2+}, Al^{3+}, Fe^{3+}; Z = B^{3+}, Be^{2+}, Li^+; T = Si^{4+}, B^{3+}, Be^{2+}, S^{6+}, P^{5+}; V = O^{2-}, OH^-, F^-, and divided the minerals into two subgroups on the basis of the *Z*-site occupancy: the **datolite subgroup** where Z = B^{3+}, and the **gadolinite subgroup** where Z = Be^{2+}. The interstitial cations occupy the *W*, *X* and *Z* sites. In the datolite-subgroup minerals, the *W* site is [8]-coordinated and

https://doi.org/10.1180/mgm.2018.152 Published online by Cambridge University Press

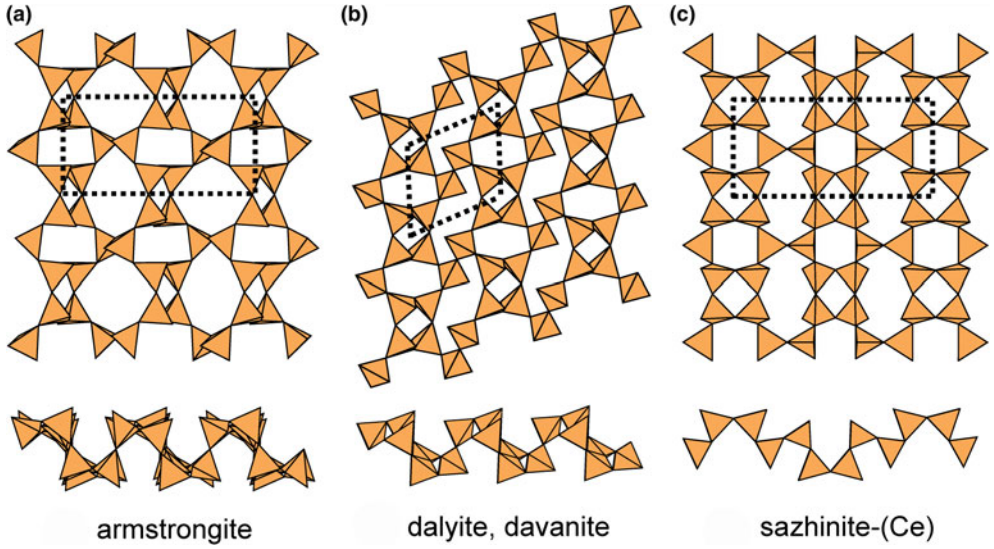

Fig. 21. Folded 4.6.8 sheets in the structures of (*a*) **armstrongite**, (*b*) **dalyite** and **davanite**, and (*c*) **sazhinite-(Ce)** and **sazhinite-(La)**.

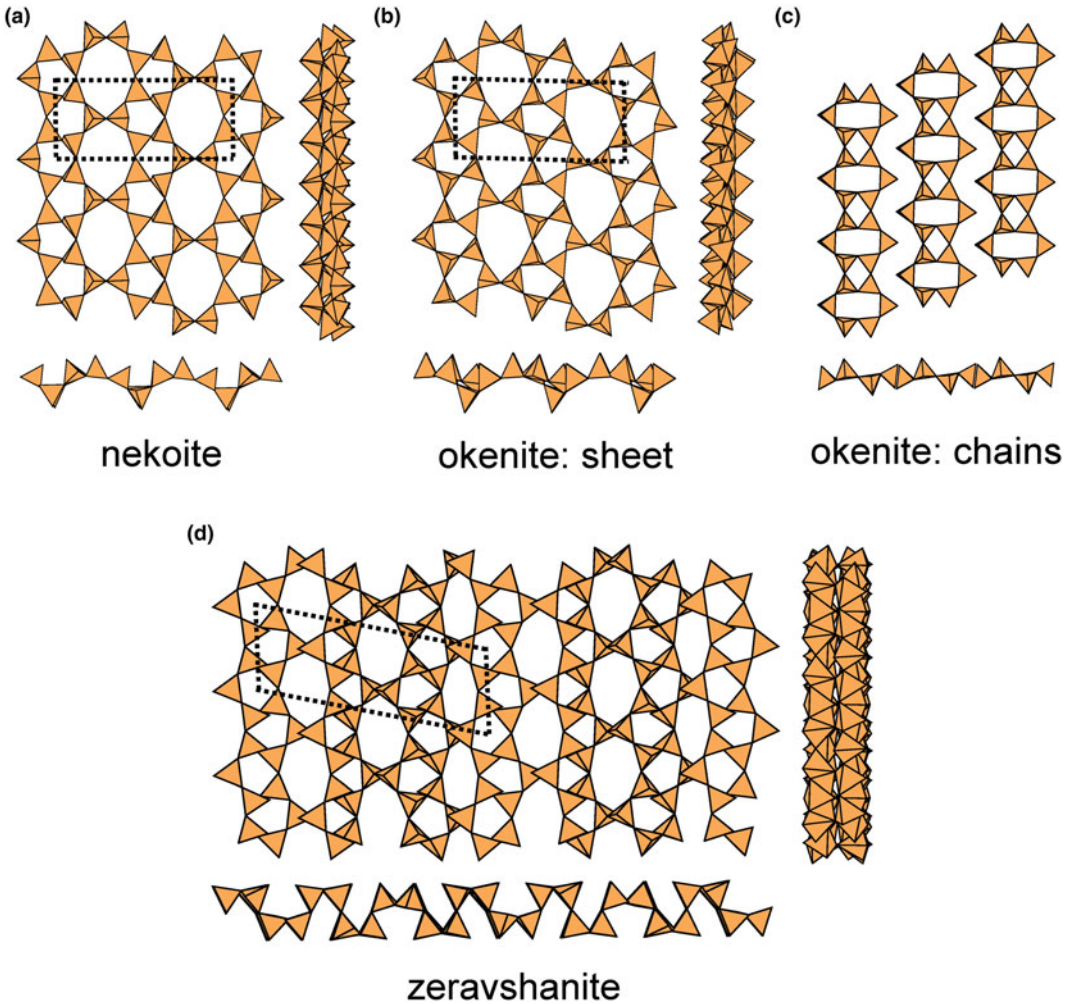

Fig. 22. Planar $(5^2.8)_2(5.8^2)_1$ sheets in the structures of (*a*) **nekoite**; (*b*) **okenite**; (*c*) chains of tetrahedra in okenite; and (*d*) z**eravshanite**; note the one-dimensional folding of the silicate sheet in **zeravshanite**. Legend as in Fig. 1.

https://doi.org/10.1180/mgm.2018.152 Published online by Cambridge University Press

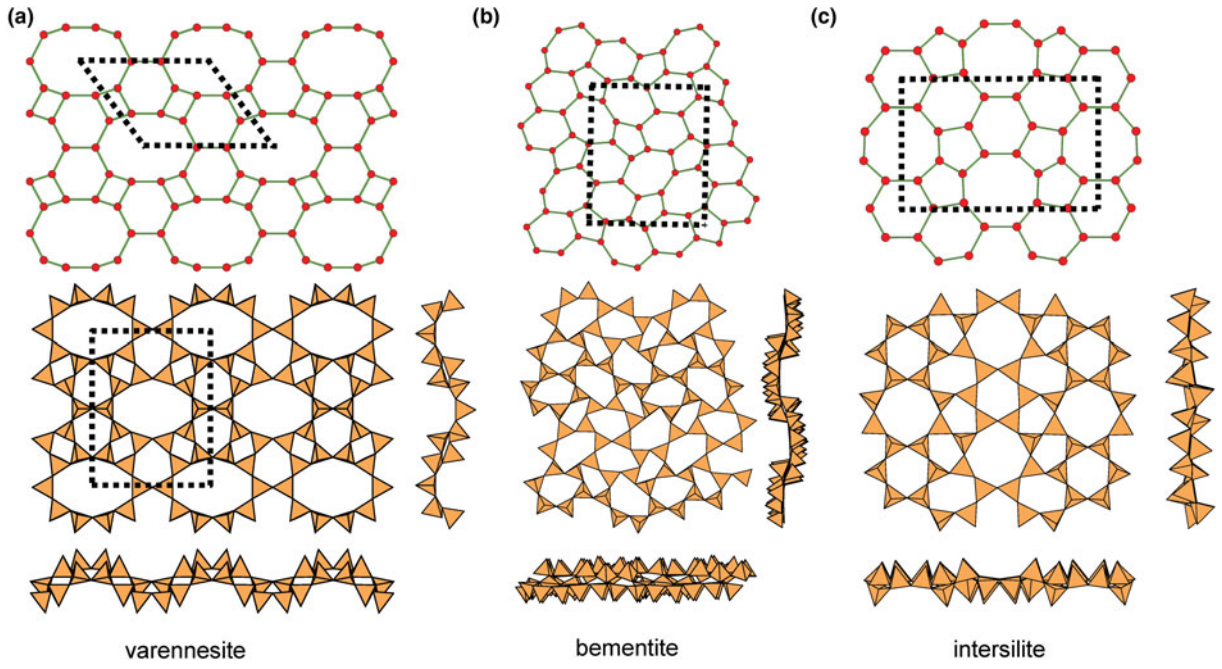

Fig. 23. Miscellaneous 3-connected plane nets and their corresponding structures; (*a*) the $(4.6.10)_4(6^2.10)_1$ net and sheet in **varennesite**; (*b*) the $(5.6.7)_4(5.7^2)_1(6^2.7)_1$ net and sheet in **bementite**; and (*c*) the $(5^2.8)_1(5.6^2)_1(5.6.8)_2(6^2.8)_1$ net and sheet in **intersilite**.

is occupied by Ca^{2+} coordinated by $O_6^{2-}(OH)_2^-$; the *X* site is vacant in datolite, and is occupied by Fe^{2+} in homilite (Table 5) where it is [6]-coordinated by $O_4^{2-}(OH)_2^-$. In the gadolinite-subgroup minerals, the *W* site is [8]-coordinated and is occupied by REE^{3+} coordinated by $O_6^{2-}(OH)_2^-$; the *X* site is vacant in hingganite minerals, and is occupied by Fe^{2+} in gadolinite minerals (Table 5) where it is [6]-coordinated by $O_4^{2-}(OH)_2^-$. Minasgeraisite-(Y) is more complicated as it has triclinic *P*1 (rather than monoclinic $P2_1/a$) symmetry; there is prominent order of Ca^{2+}, Bi^{3+} and REE^{3+} over four symmetrically distinct *W* sites and the two X sites are vacant (occupied by minor Mn^{2+}). Moreover, preliminary results suggest that (at least) some hingganite minerals have similar symmetry and cation order as minasgeraisite-(Y) (Cooper and Hawthorne, 2017).

The **apophyllite-group minerals** (Fig. 17*a*) and **cavansite** (Fig. 17*b*) have planar sheets. Both minerals have u and d tetrahedra in both four-membered and eight-membered rings. However, the patterns of u and d tetrahedra are different in both types of ring. In the **apophyllite** structure, there are (u^4) and (d^4) four-membered rings that combine to give $(u^2d^2u^2d^2)$ eight-membered rings (Fig. 17*a*), whereas in **cavansite**, there is only one type of four-membered ring, (u^2d^2), that combines to give (u^4d^4) eight-membered rings (Fig. 17*b*). The interstitial complex in the **apophyllite** structure consists of one distinct Ca^{2+} ion that is [7]-coordinated by $O_4^{2-}(F^-,OH^-)(H_2O)_2$, and one K^+ ion that is [8]-coordinated by $(H_2O)_8$. The interstitial complex in **cavansite** consists of one distinct Ca^{2+} ion that is [8]-coordinated by $O_4^{2-}(H_2O)_4$, and one V^{4+} ion that is [5]-coordinated by $O_4^{2-}(OH)^-$.

The 4.8^2 sheets in **cryptophyllite, mountainite** and **shlykovite** are shown in Fig. 18, and give us some insight into the coupling of u and d tetrahedra in the different rings. In all three structures, the four-membered rings have the configuration (u^3d^1). However, in **cryptophyllite** (Fig. 18*a*) and **shlykovite** (Fig. 18*b*), the eight-membered ring has the configuration $(u^4d^1u^2d^1)$ whereas in **mountainite** (Fig. 18*c*), the eight-membered ring has the configuration $(u^3d^1u^3d^1)$. Inspection of Fig. 18 shows how this difference arises. Each four-membered ring links to four other four-membered rings. In **cryptophyllite** and **shlykovite**, all adjacent four-membered rings have the same orientation, whereas in **mountainite** this is not the case. In mountainite (Fig. 18*c*), two adjacent four-membered rings have the same orientation and the other two four-membered rings have a different orientation (rotated by ~180°); the result is a different combination of u and d tetrahedra in the eight-membered rings formed by linkage of the four-membered rings. It is apparent that these differences in u–d arrangements of tetrahedra play a major role in the diversity of linkage to the non-tetrahedrally coordinated constituents of these structures, and this will be examined more rigorously in a later paper. The interstitial complex in **cryptophyllite** consists of one Ca^{2+} ion that is [6]-coordinated by $O_5(H_2O)$, and two K^+ ions [8]-coordinated by $O_6(H_2O)_2$ and $O_3(H_2O)_5$, respectively. The interstitial complex in **shlykovite** consists of one Ca^{2+} ion that is [6]-coordinated by $O_5^{2-}(H_2O)$, and one K^+ ion that is [8]-coordinated by $O_6^{2-}(H_2O)_2$. The interstitial complex in **mountainite** consists of one Ca^{2+} ion that is [6]-coordinated by $O_5(H_2O)$, one K^+ ion [8]-coordinated by $O_6(H_2O)_2$, and one Na^+ ion coordinated by $O_2^{2-}(OH)^-(H_2O)_5$.

Cuprorivaite (Fig. 19*a*) and **ekanite** (Fig. 19*b*) have doubly folded sheets with u and d tetrahedra in both four-membered and eight-membered rings. Unlike apophyllite (Fig. 17*a*) and **cavansite** (Fig. 17*b*), **cuprorivaite** and **ekanite** have the same pattern of u and d tetrahedra in their four-membered and eight-membered rings: (u^4), (d^4) and $(u^2d^2u^2d^2)$. Thus the sheets in apophyllite and **cavansite** (Fig. 17), although based on the same type of 3-connected net, are significantly different, whereas the sheets in **cuprorivaite** and **ekanite** (Fig. 19) are topologically identical. There are four minerals with the **cuprorivaite** structure in the so-called 'gillespite group' (Table 5). The interstitial

https://doi.org/10.1180/mgm.2018.152 Published online by Cambridge University Press

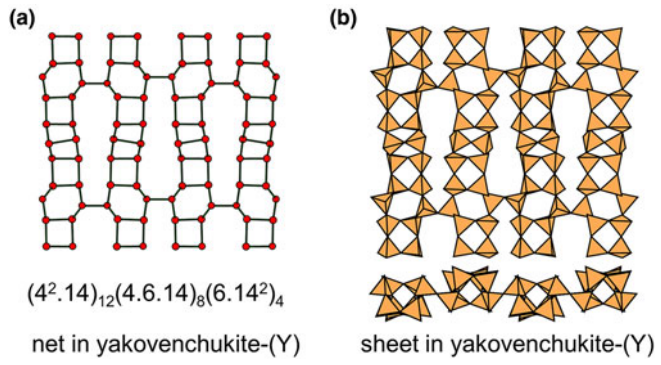

Fig. 24. Miscellaneous 3-connected plane nets and their corresponding structures; (*a*) the $(4^2.14)_{12}(4.6.14)_8(6.14^2)_4$ net, and (*b*) the sheet in **yakovenchukite-(Y)**.

complex in these minerals consists of one distinct M^{2+} ion (M^{2+} = Ca^{2+}, Ba^{2+} or Sr^{2+}) that is [8]-coordinated by O_8^{2-}, and one Cu^{2+} (or Fe^{2+}) ion that is [4]-coordinated by O_4^{2-}. There are five minerals in the **ekanite** group (Table 5). The interstitial complex in **ekanite** consists of one distinct Ca^{2+} ion that is [8]-coordinated by O_8^{2-}, and one Th^{4+} ion that is [8]-coordinated by O_8^{2-}.

The 3.12² net

As far as we are aware, there are no sheet-silicate minerals based on this 3-connected net, despite its simplicity. Three-membered rings are unusual in silicates but do occur, e.g. the benitoite-group minerals (Hawthorne, 1987). Possibly this is connected with the association of large and small rings in a sheet (Fig. 2*c*), although there are structures based on the 4.6.12 net. Perhaps the occurrence of an intermediate-sized ring relieves strain in the sheet.

The 4.6.12 net

This net contains three four-membered rings, two six-membered rings and one twelve-membered ring in the unit cell (Fig. 2*d*) in the ratio 3:2:1, and there is only one type of vertex: (4.6.12) with 12 vertices per unit cell. There are six structures with sheets based on this net: **pyrosmalite-(Fe), pyrosmalite-(Mn), schallerite, friedelite, mcgillite** and **nelenite** (Table 5). The sheets are

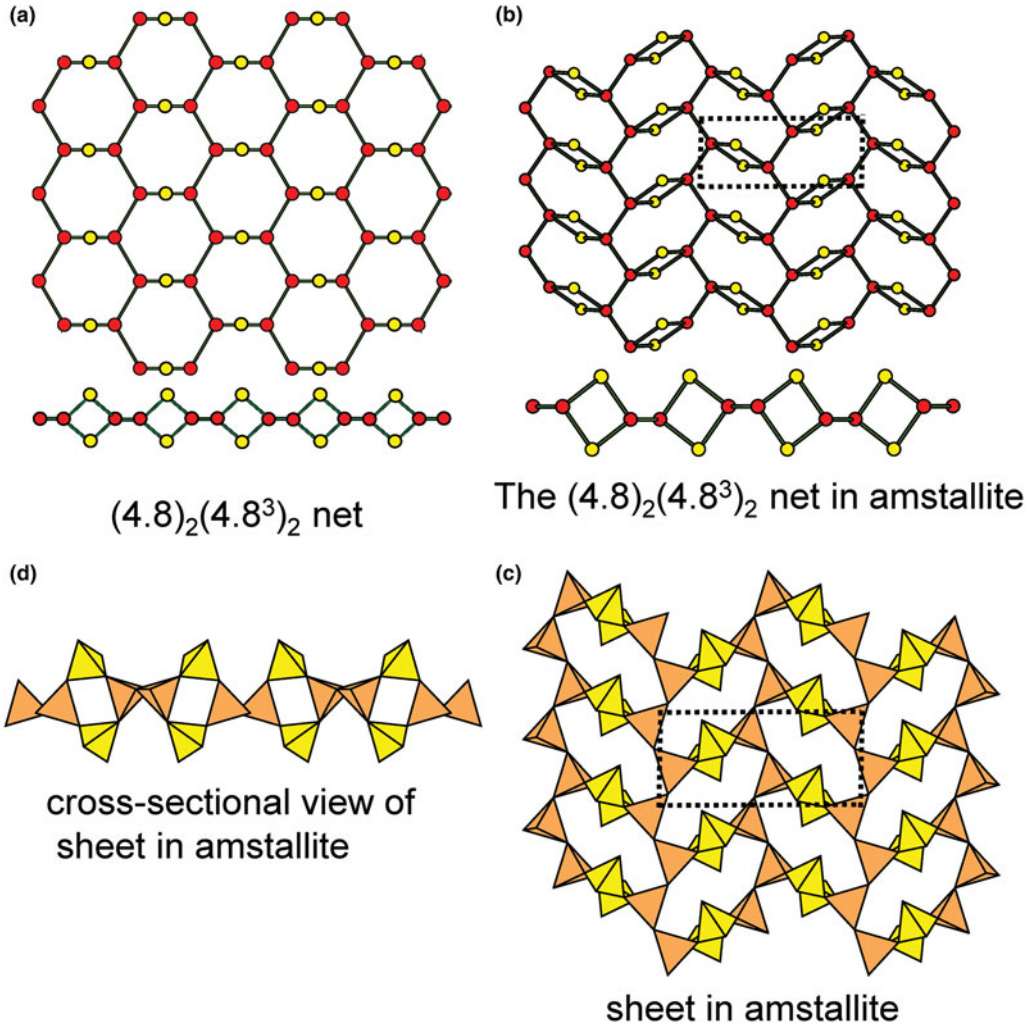

Fig. 25. Insertion of pairs of 2-connected vertices into the 6^3 net; (*a*) view and cross-section of the inserted 6^3 net; (*b*) the net of the sheet of tetrahedra in **amstallite**; (*c*) the sheet of tetrahedra in **amstallite**; and (*d*) horizontal view of the sheet of tetrahedra in **amstallite**. Legend as in Fig. 1, yellow vertices and tetrahedra are 2-connected.

https://doi.org/10.1180/mgm.2018.152 Published online by Cambridge University Press

topologically identical in these minerals, but link to sheets of octahedra in different ways to form polytypes (Takéuchi *et al.*, 1983). In the sheets of **schallerite** and **nelenite**, an oxygen anion bridging two (SiO_4) tetrahedra also links to an As^{3+} cation, thereby violating the valence-sum rule, and hence there must be significant disorder involving vacancies, Si^{4+} and As^{3+} that is not resolved in the current refined structure. The four-membered rings in the As^{3+}-free minerals have the sequence (u^2d^2), there are two six-membered rings with the sequences (u^6) and (d^6), and one twelve-membered ring with the sequence ($u^2d^2u^2d^2u^2d^2$) (Fig. 20). Note that there is significant modulation of this sheet. The interstitial complex in the **pyrosmalite-group minerals** consists of four distinct M^{2+} ions ($M^{2+} = Fe^{2+}$ or Mn^{2+}) that are [6]-coordinated by Cl_6^-, $O_4^{2-}Cl_2^-$, O_6^{2-} and $O_5^{2-}Cl^-$, respectively.

The $(4.6.8)_2(6.8^2)_1$ net

Details of the $(4.6.8)_2(6.8^2)_1$ net are shown in Fig. 2*e*. This net contains four-, six- and eight-membered rings and there are two types of vertex: (4.6.8) and (6.8^2) in the ratio 2:1; the unit cell contains $[Si_6O_{15}]$. Table 5 lists the single-layer sheet-silicate minerals based on this net, and their structures are shown in Fig. 21. Despite the differing appearance of these sheets, they do show the linkage of this net, but differ in their patterns of u

Table 6. Single-layer sheet-silicates based on nets with 3- and 4-connected vertices.

Mineral	Net	u–d configuration	P/F*	Formula	T:O ratio	Fig. No.	Ref.
Amstallite	$[(4.8)_2(4.8^3)_2]_2$	-----	P	$CaAl(OH)_2$**$[AlSi_3O_8(OH)_2]$**(H_2O)	1:2.50	25	(1)
Prehnite	$[(6^2)_2(6^4)_2]_1$	(udo^3)	P	Ca_2Al**$[Si_3AlO_{10}]$**$(OH)_2$	1:2.50	26	(2)
Searlesite	$[(5^2)_2(5^4)_4]_1$	$(uo^4)(do^4)$	P	Na**$[BSi_2O_5(OH)_2]$**	1:2.33	27	(3)
		Melilite Group					
Åkermanite	$[(5^3)_2(5^4)_1]_2$	$(u^2odo)(uod^2o)$	P	Ca_2**$[Mg(Si_2O_7)]$**	1:2.33	29*a*	(4)
Alumoåkermanite	$[(5^3)_2(5^4)_1]_2$	$(u^2odo)(uod^2o)$	P	$(CaNa)$**$[Al(Si_2O_7)]$**	1:2.33	"	(5)
'Ferri-gehlenite'	$[(5^3)_2(5^4)_1]_2$	$(u^2odo)(uod^2o)$	P	Ca_2**$[Fe^{3+}(AlSiO_7)]$**	1:2.33	"	(6)
Gehlenite	$[(5^3)_2(5^4)_1]_2$	$(u^2odo)(uod^2o)$	P	Ca_2**$[Al(AlSiO_7)]$**	1:2.33	"	(7)
Gugiaite	$[(5^3)_2(5^4)_1]_2$	$(u^2odo)(uod^2o)$	P	Ca_2**$[Be(Si_2O_7)]$**	1:2.33	"	(8)
Hardystonite	$[(5^3)_2(5^4)_1]_2$	$(u^2odo)(uod^2o)$	P	Ca_2**$[Zn(Si_2O_7)]$**	1:2.33	"	(9)
Okayamalite	$[(5^3)_2(5^4)_1]_2$	$(u^2odo)(uod^2o)$	P	Ca_2**$[B(BSiO_7)]$**	1:2.33	"	(10)
		Melilite-Group Superstructures					
Leucophanite	$[(5^3)_2(5^4)_1]_2$	$(u^2odo)(uod^2o)$	P	$(NaCa)$**$[Be(Si_2O_6F)]$**	1:2.33	29*b*	(11)
Meliphanite	$[(5^3)_2(5^4)_1]_4$	$(u^2odo)(uod^2o)$	P	$(Na,Ca)_4Ca_4$**$[Be_4AlSi_7O_{24}(F,O)_4]$**	1:2.33	29*c*	(12)
Jeffreyite	$[(5^3)_2(5^4)_1]_n$	-----	P	$(Ca,Na)_2$**$[(Be,Al)Si_2O,OH)_7]$**	1:2.33	–--	(13)
		Hellandite Group					
Ciprianiite	$[(4.5.8)_2(4.5^2.8)_2(5^3)_2(5^2.8)_4]_1$	$(uodo)(u^3do)(ud^3o)(u^2d^2o)$ (u^3od^3o)	P	$Ca_4(Th,U,Ca)Al(Be_{0.5}\square_{1.5})$ **$[Si_4B_4O_{22}(OH)_2]$**	1:2.40	30*a*	(14)
Hellandite-(Ce)	$[(4.5.8)_2(4.5^2.8)_2(5^3)_2(5^2.8)_4]_1$	$(uodo)(u^3do)(ud^3o)(u^2d^2o)$ (u^3od^3o)	P	$Ca_4(REE)Ce_2Al$**$[\square_2Si_4B_4O_{22}(OH)_2]$**	1:2.40	"	(15)
Hellandite-(Y)	$[(4.5.8)_2(4.5^2.8)_2(5^3)_2(5^2.8)_4]_1$	$(uodo)(u^3do)(ud^3o)(u^2d^2o)$ (u^3od^3o)	P	$Ca_4(REE)Y_2Al$**$[\square_2Si_4B_4O_{22}(OH)_2]$**	1:2.40	"	(16)
Mottanaite-(Ce)	$[(4.5.8)_2(4.5^2.8)_2(5^3)_2(5^2.8)_4]_1$	$(uodo)(u^3do)(ud^3o)(u^2d^2o)$ (u^3od^3o)	P	$Ca_4Ce_2Al(Be_{1.5}\square_{0.5})$**$[Si_4B_4O_{22}O_2]$**	1:2.40	"	(14)
Tadzhikite-(Ce)	$[(4.5.8)_2(4.5^2.8)_2(5^3)_2(5^2.8)_4]_1$	$(uodo)(u^3do)(ud^3o)(u^2d^2o)$ (u^3od^3o)	P	$Ca_4Ce_2Ti^{4+}$**$[\square_2Si_4B_4O_{22}(OH)_2]$**	1:2.40	"	(17)
Piergorite-(Ce)	$[(4.5.8)_2(4.5^2.8)_2(5^3)_6(5^2.8)_4(5^4)_2]_1$	$(u^2odo)(uod^2o)(u^3od^3o)$	P	$Ca_8Ce_2(Al,Fe^{3+})$**$[(\square,Li,Be)_2[Si_6B_8O_{36}(OH)_2]$**	1:2.38	30*b*	(18)
		Nordite Group					
Ferronordite-(Ce)	$[(4.5.8)_8(5^2.8)_4(5.8.5.8)_2]_2$	$(u^2d^2)(u^3do)(ud^3o)(u^3od^3o)$	P	Na_3SrCe**$[Fe^{2+}Si_6O_{17}]$**	1:2.43	31	(19)
Ferronordite-(La)	$[(4.5.8)_8(5^2.8)_4(5.8.5.8)_2]_2$	$(u^2d^2)(u^3do)(ud^3o)(u^3od^3o)$	P	Na_3SrLa**$[Fe^{2+}Si_6O_{17}]$**	1:2.43	"	(19)
Manganonordite-(Ce)	$[(4.5.8)_8(5^2.8)_4(5.8.5.8)_2]_2$	$(u^2d^2)(u^3do)(ud^3o)(u^3od^3o)$	P	Na_3SrCe**$[Mn^{2+}Si_6O_{17}]$**	1:2.43	"	(20)
		Semenovite Group					
Semenovite-(Ce)	$[(4.5^2)_1(4.5.8.5)_1(5^2.8)_3]_4$	$(uodo)(u^3do)(ud^3o)(u^3od^3o)$	P	$(Ca,Na)_8Na_{0-2}REE_2(Fe,Ti)$**$[(Si,Be)_{10}(O,F)_{24}]_2$**	1:2.40	32*a*	(21)
Harstigite	$[(4.5^2)_1(4.5.8.5)_1(5^2.8)_3]_4$	$(uodo)(u^3do)(ud^3o)$ (u^3od^3o)	P	Ca_6Mn^{2+}**$[Be_4Si_6O_{22}(OH)_2]$**	1:2.40	32*b*	(22)
Perettiite-(Y)	$[(4.5^2)_1(4.5.8.5)_1(5^2.8)_3]_4$	$(uodo)(u^3do)(ud^3o)(u^3od^3o)$	P	$Y_2Mn_4^{2+}Fe^{2+}$**$[Si_2B_8O_{24}]$**	1:2.40	32*c*	(23)
		Miscellaneous Nets					
Aminoffite	$[(6^4)_1(4.6^2)_4]_1$	$(u^4)(d^4)(u^2od^2o)$	P	Ca_2**$[Be_2Si_3O_{10}(OH)_2]$**	1:2.40	33*a*	(24)
Bussyite-(Ce)	$[(4.5.8)_8(5.8.5.8)_2(5^2.8)_4]_1$	$(u^2d^2)(u^3od)(uod^3)(u^3od^3o)$	P	$(Ce,Ca)_3(Na,H_2O)_6Mn$**$[Si_9Be_5(O,OH)_{30}(F,OH)_4]$**	1:2.43	33*b*	(25)
Vladykinite	$[(5^3)_4(5^2.8)_4(4.5.8)_8(5^3.8)_4]_1$	$(u^2d^2)(u^3do)(ud^3o)(u^2odo)$ $(uod^2o)(u^3od^3o)$	P	Na_3Sr_4**$[(Fe^{2+}Fe^{3+})Si_8O_{24}]$**	1:2.40	34*a*	(26)
Samfowlerite	$[(4.5^2)_8(4.8^2)_4(4.5.8)_{12}(5^2.8)_{20}$ $(5^2.8^2)_4]_1$	$(u^3d)(ud^3)(u^4d)(ud^4)(u^2odo)$ $(uod^2o)(u^3od^3o)$	P	$Ca_{14}Mn_{23}$**$[(Be_7Zn)Zn_2Si_{14}O_{52}(OH)_6]$**	1:2.42	34*b*	(27)
		Decorated nets					
Magadiite	$[(5^4)_8(5^2.6^2)_4]_1$	–-------	1F	Na_2**$[Si_{14}O_{29}]$**$(H_2O)_{11}$	1:2.07	35	(28)

References: (1) Quint (1987); (2) Papike and Zoltai (1967), Baur *et al.* (1990); (3) Ghose and Wan (1976); (4) Kimata (1981); (5) Louisnathan (1970), Wiedenmann *et al.* (2009); (6) Dondi *et al.* (1999); (7) Louisnathan (1971), Kimata and Li (1982); (8) Kimata and Ohashi (1982), Yang *et al.* (2001); (9) Louisnathan (1969), Bindi *et al.* (2001); (10) Matsubara *et al.* (1998); (11) Cannillo *et al.* (1967, 1992), Grice and Hawthorne (1989); (12) Dal Negro *et al.* (1967), Grice and Hawthorne (2002); (13) Grice and Robinson (1984); (14) Della Ventura *et al.* (2002), Oberti *et al.* (2018); (15) Oberti *et al.* (1999), Oberti *et al.* (2018); (16) Mellini and Merlino (1977), Miyawaki *et al.* (2015); (17) Hawthorne *et al.* (1998); (18) Boiocchi *et al.* (2006); (19) Bakakin *et al.* (1970), Pekov *et al.* (1998, 2001), Pushcharovskii *et al.* (1999); (20) Pekov *et al.* (1998), Pushcharovskii *et al.* (1999); (21) Mazzi *et al.* (1979); (22) Hesse and Stümpel (1986); (23) Danisi *et al.* (2015); (24) Huminicki and Hawthorne (2002*b*); (25) Grice *et al.* (2009); (26) Chakhmouradian *et al.* (2014); (27) Rouse *et al.* (1994); and (28) Garcés *et al.* (1988).
*P = planar; 1F = folded in one direction.

https://doi.org/10.1180/mgm.2018.152 Published online by Cambridge University Press

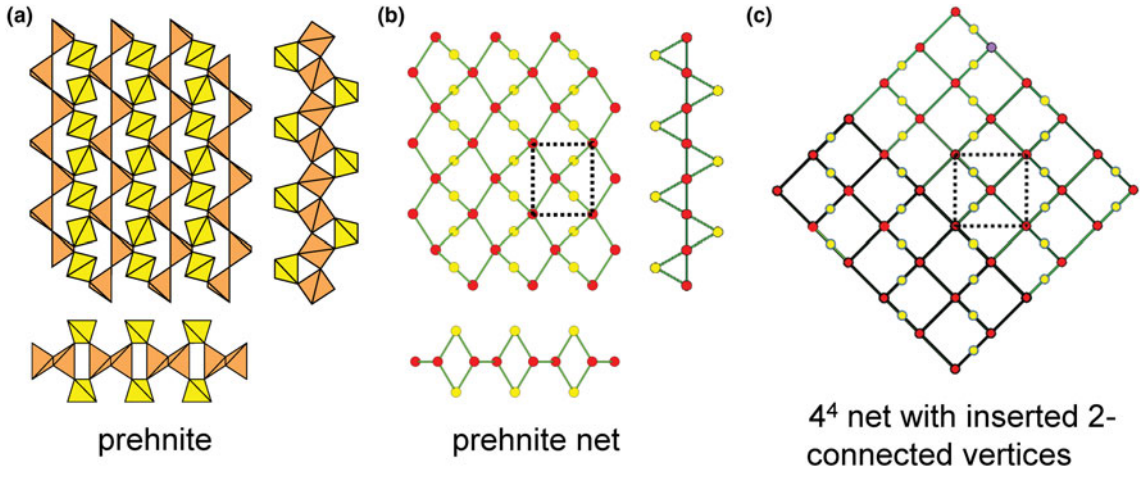

Fig. 26. Insertion of 3-connected vertices into the 4^4 net; (*a*) the sheet of 2- and 4-connected tetrahedra in **prehnite**; (*b*) the corresponding net in the aluminosilicate sheet in **prehnite**; and (*c*) the sheet of 2- and 4-connected tetrahedra in **prehnite**. Red circles: 4-connected vertices; yellow circles: 2-connected vertices.

and d tetrahedron vertices (Table 5). In **armstrongite** (Fig. 21*a*), the four-membered and six-membered rings have the sequences (u^2d^2) and (ud^3ud), and they link such that the eight-membered rings have the sequence (u^4d^4). In **dalyite** (Fig. 21*b*), all rings show the same u–d sequence as in **armstrongite** but the sheet is strongly sheared relative to that of **armstrongite**. The interstitial complex in **armstrongite** consists of one distinct Ca^{2+} ion that is [7]-coordinated by $O_5^{2-}(H_2O)_2$, and one Zr^{4+} that is coordinated by O_6^{2-}; there are two distinct interstitial transformer (H_2O) groups. The interstitial complex in **dalyite** consists of one Na^+ ion that is [8]-coordinated by O_8^{2-}, and one Zr^{4+} ion that is [6]-coordinated by O_6^{2-}.

In **sazhinite-(Ce)** and **sazhinite-(La)** (Fig. 21*c*), four-membered rings have the sequences (u^4) and (d^4), six-membered rings have the sequences (u^2du^2d) and (ud^2ud^2), and they link such that the eight-membered rings have the sequence (u^2dud^2ud). These structures show an interesting contrast with the structures of the 4.8^2 net (Figs 4*b*, 10; Table 5); they are each folded, as is apparent in Fig. 21, but unlike the 4.8^2 structure of Fig. 5*b*, they are folded only in one direction. The interstitial complex in **sazhinite-(Ce)** and **sazhinite-(La)** consists of one distinct M^{3+} ion that is [7]-coordinated by O_7^{2-}, and two Na^+ ions, the coordination of which is somewhat ambiguous: there is one Na^+ ion with a coordination of either O_5^{2-} or $O_5^{2-}(H_2O)$, and one Na^+ ion with a coordination of either $O_3^{2-}(H_2O)_2$ or $O_3^{2-}(H_2O)_5$; one (H_2O) group is either a hydrogen-bonded group or an inverse transformer group, depending on the coordinations chosen for the Na^+ cations, and the other (H_2O) group is a hydrogen-bonded group.

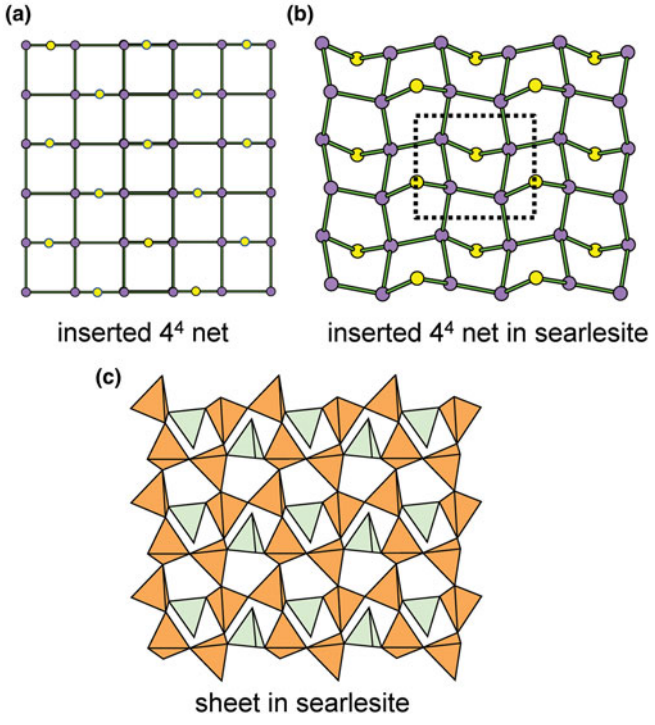

Fig. 27. (*a*) A parent 4-connected net with a 2-connected vertex inserted on one edge of each four-membered ring such that each vertex in the parent net is adjacent to only one 2-connected vertex; (*b*) the analogous net in **searlesite**; and (*c*) the corresponding sheet of tetrahedra in **searlesite**. All borate tetrahedra are 2-connected and all silicate tetrahedra are 4-connected. The net corresponds to 5^4 and is crinkled in three dimensions in order to allow four 5-membered rings to be incident at a single vertex; yellow circles: 2-connected vertices.

The $(5^2.8)_2(5.8^2)_1$ net

This net contains 5- and 8-membered rings (Fig. 2*f*) and there are two types of vertex: ($5^2.8$) and (5.8^2) in the ratio 2:1; the unit cell contains [Si_6O_{15}], and this net topology occurs in the structures of **nekoite, okenite** and **zeravshanite** (Table 5). **Nekoite** (Fig. 22*a*), has two distinct five-membered rings with u–d arrangements (u^3d^2) and (u^2dud) and one eight-membered ring with the arrangement (u^6d^2), and the sheet is planar. **Okenite** (Fig. 22*b*) has one distinct five-membered ring with the u–d arrangement (u^4d) and one eight-membered ring with the arrangement (u^7d), and the sheet is also planar. Thus the sheets in **nekoite** and **okenite** are geometrical isomers, they have the same topology (connectivity of chemical bonds) but the geometrical details are distinct in that the u–d arrangements of tetrahedra are different in each mineral. In **okenite**, the sheets alternate with layers of [Si_6O_{16}] chains (Fig. 22*c*) which has the stoichiometric effect of decreasing the connectivity of the silicate part of the structure (Table 5).

Zeravshanite (Fig. 22*d*) is significantly different. It has two distinct five-membered rings with u–d arrangements (u^3d^2) and

https://doi.org/10.1180/mgm.2018.152 Published online by Cambridge University Press

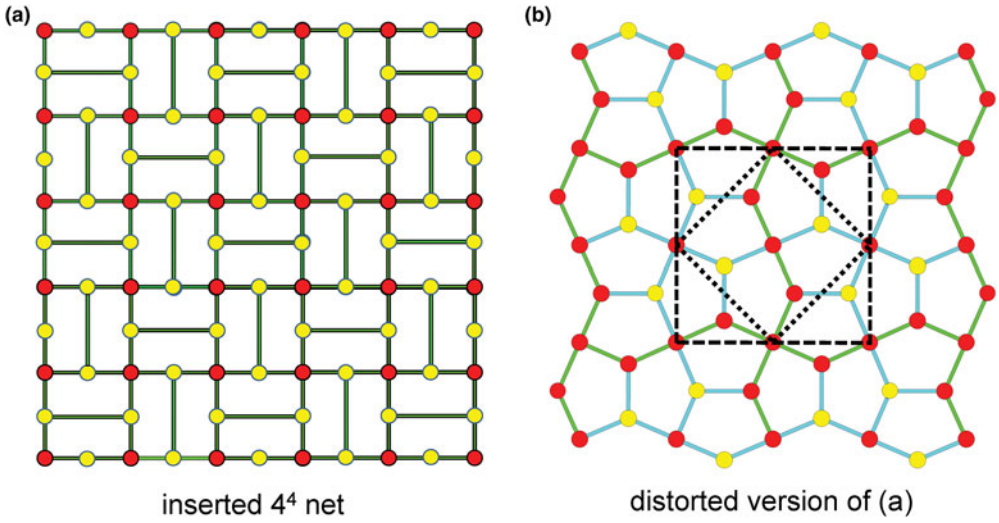

Fig. 28. Insertion of 3-connected vertices into the 4^4 net; (*a*) the 4^4 net with 3-connected vertices inserted into *trans* edges of the net; and (*b*) geometrically distorted version of the net in Fig. 25a; the unit cell of the nets in **åkermanite, leucophanite** and **meliphanite** are marked by dotted, dotted and dashed lines, respectively.

(u^2d^3) and one eight-membered ring with the arrangement (u^4d^4). Moreover, unlike **nekoite** and **okenite**, the sheet in **zeravshanite** is folded in one direction. The interstitial complex in **nekoite** consists of three distinct Ca^{2+} ions that are all [6]-coordinated by $O_4^{2-}(H_2O)_2$; there are seven distinct (H_2O) groups, four are transformer, one is non-transformer and two are hydrogen bonded only. The interstitial complex in **okenite** consists of six distinct sites occupied by Ca^{2+} ions; four of these sites are fully occupied and are [6]-coordinated by $O_5^{2-}(H_2O)$ (×3) and O_6^{2-}, and two are half-occupied and coordinated by $O_2^{2-}(H_2O)_5$ and $(H_2O)_6$, respectively. There are thirteen distinct (H_2O) sites, not all of which are fully occupied; four (H_2O) groups are transformer, seven are non-transformer and two are hydrogen-bonded only. The interstitial complex in **zeravshanite** consists of two Cs^+ ions coordinated by O_9^{2-} and O_8^{2-}, respectively, one Na^+ ion coordinated by $O_6^{2-}(H_2O)_2$, and two Zr^{4+} ions each of which are coordinated by O_6^{2-}. There is one interstitial transformer (H_2O) group.

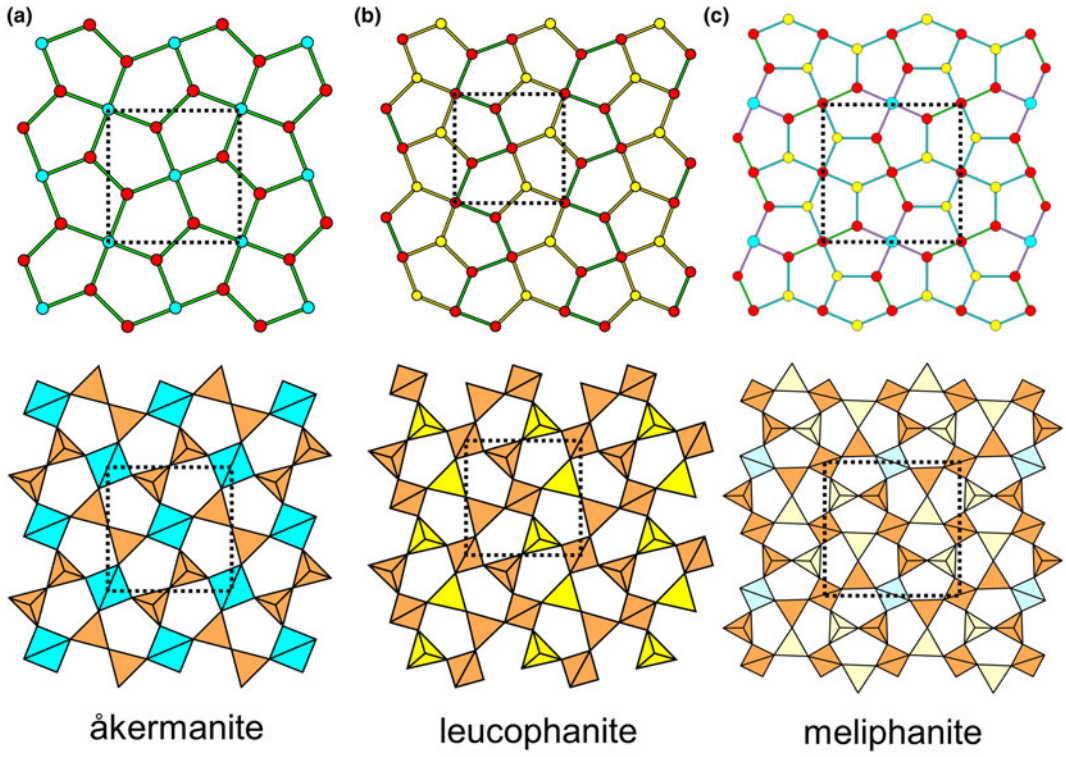

Fig. 29. Structures based on the $5_2^35_1^4$ net; (*a*) **åkermanite**; (*b*) **leucophanite**; and (*c*) **meliphanite**.

https://doi.org/10.1180/mgm.2018.152 Published online by Cambridge University Press

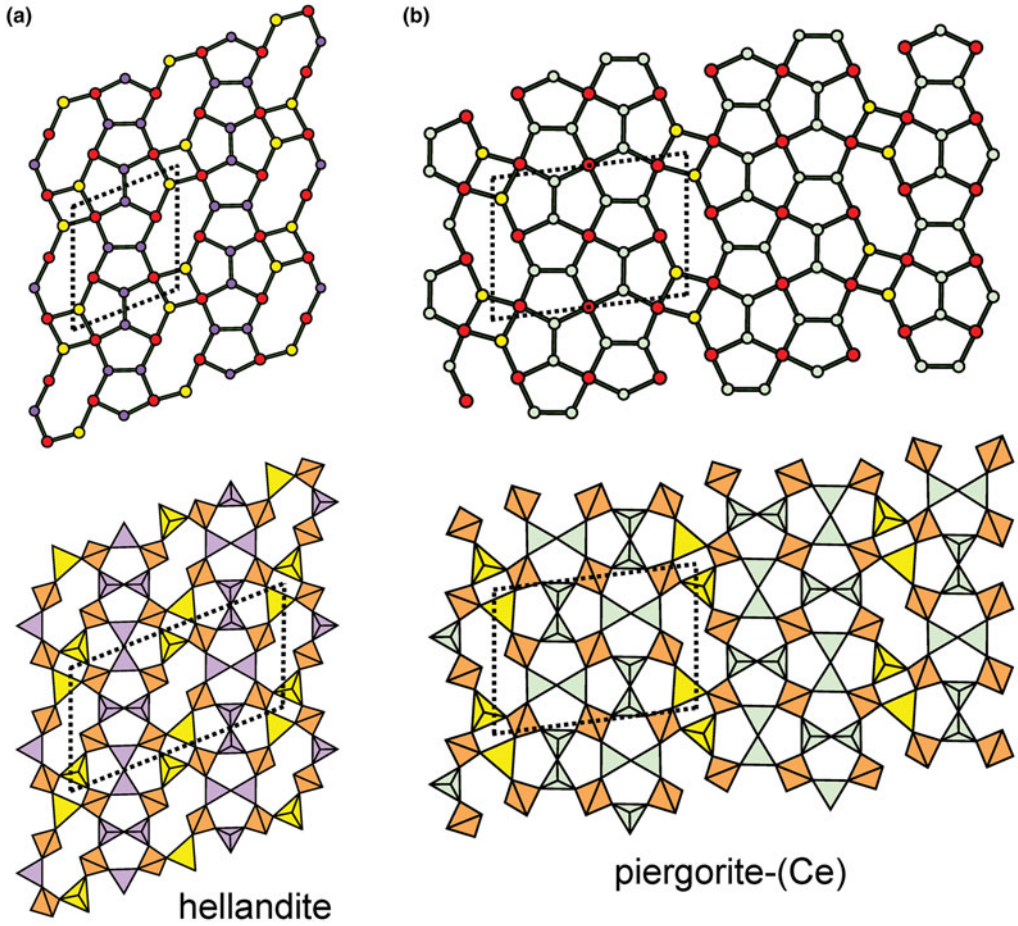

Fig. 30. (*a*) The $(4.5.8)_2(4.5^2.8)_2(5^3)_2(5^2.8)_4$ net and sheet in the **hellandite structure**; and (*b*) the $(4.5.8)_2(4.5^2.8)_2(5^3)_6(5^2.8)_4(5^4)_2$ net and sheet in **piergorite-(Ce)**.

Miscellaneous nets

There are several nets (Table 5) that just have just one example each of a sheet-silicate unit.

The $(4.6.10)_4(6^2.10)_1$ net has four-membered, six-membered and ten-membered rings in the ratio 2:2:1 (Fig. 23*a*). In the structure of **varennesite** (Table 5), all four-membered rings have the u–d arrangement (u^2d^2), the six-membered rings have the arrangements (u^6) and (d^6), and the two types of ten-membered ring have the arrangements ($u^3d^2u^3d^2$) and ($d^3u^2d^3u^2$). The sheet is planar but with a strong modulation in both directions (Fig. 23*a*). The interstitial complex in **varennesite** consists of three Na^+ ions coordinated by $O_4^{2-}(OH)^-(H_2O)$, $O_3^{2-}(H_2O)_3$, and $O_2^{2-}(H_2O)_4$, and one Mn^{2+} ion coordinated by $O_4^{2-}(OH)_2^-$; there are six interstitial (H_2O) groups, five of which are non-transformer and one of which is hydrogen-bonded only.

The $(5.6.7)_4(5.7^2)_1(6^2.7)_1$ net has five-membered, six-membered and seven-membered rings in the ratio 1:1:1 (Fig. 23*b*). In the structure of **bementite** (Table 5), there are two types of five-membered rings with u–d arrangements (u^3d^2) and (u^2d^3), two types of six-membered rings with the arrangements (u^6) and (d^6), and the two types of seven-membered rings with the arrangements (u^5d) and (u^2d^5). The sheet is planar but with a modulation in one direction (Fig. 23*b*). The interstitial complex in **bementite** consists of fifteen distinct Mn^{2+} ions all of which are [6]-coordinated by $O_2^{2-}(OH)_4^-$ (×6), $O_3^{2-}(OH)_3^-$ (×7) and $O_4^{2-}(OH)_2^-$ (×2).

The $(5^2.8)_1(5.6^2)_1(5.6.8)_2(6^2.8)_1$ net has five-membered, six-membered and eight-membered rings in the ratio 2:2:1 (Fig. 23*c*). In the structure of **intersilite** (Table 5), there are two types of five-membered rings with u–d arrangements (u^2dud) and ($udud^2$), three types of six-membered rings with the arrangements (u^6), (u^3d^3) and (d^6), and two types of eight-membered rings with the arrangements (u^4du^2d) and (d^4ud^2u). The sheet is planar (Fig. 23*c*) with no significant modulation. The interstitial cations in **intersilite** consists of Mn^{2+}, Ti^{4+} and Na^+, but the interatomic distances and coordinations are not compatible with these cations, suggesting considerable positional disorder between the sheets.

The $(4^2.14)_{12}(4.6.14)_8(6.14^2)_4$ net has four-membered, six-membered and fourteen-membered rings in the ratio 3:2:1 (Fig. 24*a*). In the structure of **yakovenchukite-(Y)** (Fig. 24*b*; Table 5), there is one type of four-membered ring with the arrangement (u^2d^2), two types of six-membered ring with the arrangements (u^2du^2d) and (ud^2ud^2), and one type of fourteen-membered ring with the arrangement ($ud^2ud^2udu^2du^2d$). The sheet is folded in one direction (Fig. 24*b*). The interstitial complex in **yakovenchukite-(Y)** consists of two K^+ (+ some Na^+) ions coordinated by $O_7^{2-}(H_2O)_2$ and $O_7^{2-}(H_2O)$, two Ca^{2+} ions coordinated by $O_6^{2-}(H_2O)_2$ and $O_5^{2-}(H_2O)$, and two Y^{3+} ions each of which is coordinated by O_6^{2-}; there are three interstitial (H_2O) groups, two of which are non-transformer and one of which is hydrogen-bonded only.

https://doi.org/10.1180/mgm.2018.152 Published online by Cambridge University Press

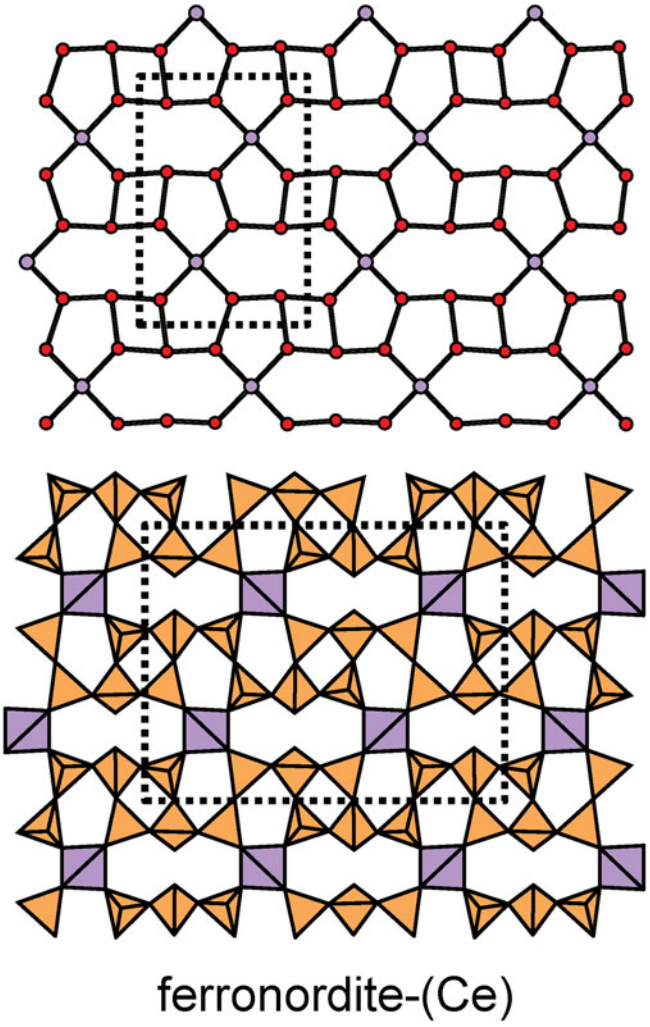

Fig. 31. The $(4.5.8)_8(5^2.8)_4(5.8.5.8)_2$ net and corresponding sheet of tetrahedra in **ferronordite-(Ce)**.

Single-layer sheets: 3- and 4-connected nets with inserted 2- and 3-connected vertices

Many single-sheet silicate minerals contain 4-connected tetrahedra in addition to tetrahedra of lower connectivity. Hawthorne (2015*a*) showed how suitable planar nets may be derived for these minerals by insertion of lower-connectivity vertices into planar 3- and 4-connected nets. It is not straightforward to insert vertices into a 3-connected net to produce a net of 3- and 4-connected vertices that forms a suitable basis for a sheet of tetrahedra, although it is feasible. Figure 25*a* shows the 6^3 net with pairs of 2-connected vertices inserted on one pair of *trans* edges of each six-membered ring; examination of the plan and horizontal views shows that the original 3-connected vertices are converted to 4-connected vertices. The result is a $(4.8)_2(4.8^3)_2$ net with only 2- and 4-connected vertices. Figure 25*b* shows the corresponding net for the sheet of tetrahedra in **amstallite** (Table 6); the unit cell is doubled, $(4.8)_4(4.8^3)_4$, due to geometrical distortion. The plan and horizontal views of the sheet in **amstallite** are shown in Figs 25*c*,*d*. Alternatively, the tetrahedra in **amstallite** could be considered as a double-layer sheet in which a pair of 2-connected vertices are inserted into *trans* edges of the 6^3 net with the 2-connected vertices out of the geometric plane of the 6^3 net; an oikodoméic ***m*** operation then repeats the 2-connected vertices below the geometric plane to produce a sheet with the cross-sectional aspect shown in Fig. 25*d*. The interstitial complex in **amstallite** consists of one Ca^{2+} ion coordinated by $O_2^{2-}(OH)_4^-$ $(H_2O)_2$ and one Al^{3+} ion coordinated by $O_2^{2-}(OH)_4^-$; there is one interstitial transformer (H_2O) group.

It is much more straightforward to generate nets of 3- and 4-connected vertices by inserting 2- or 3-connected vertices into a 4-connected net. Consider the structure of **prehnite** (Table 6) in which the sheet of tetrahedra are 2-connected (yellow) and 4-connected (orange) (Fig. 26*a*). The net representation (Fig. 26*b*) consists of a plane 4-connected net 4^4 shown in which two 2-connected vertices are inserted on adjacent edges of each four-membered ring to form a $(6^2)_2(6^4)_2$ net with a u–d arrangement (udo^3); this net is topologically identical to the

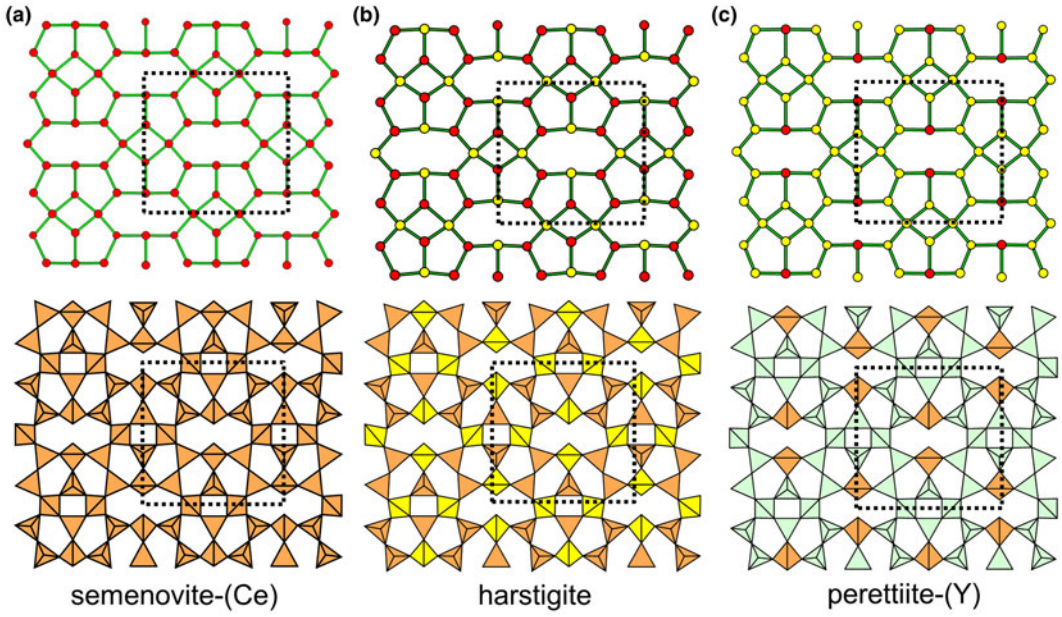

Fig. 32. The $[(4.5^2)_1(4.5.8.5)_1(5^2.8)_3]_4$ net and corresponding sheet of tetrahedra in (*a*) **semenovite-(Ce)**; (*b*) **harstigite**; and (*c*) **perettiite-(Y)**.

https://doi.org/10.1180/mgm.2018.152 Published online by Cambridge University Press

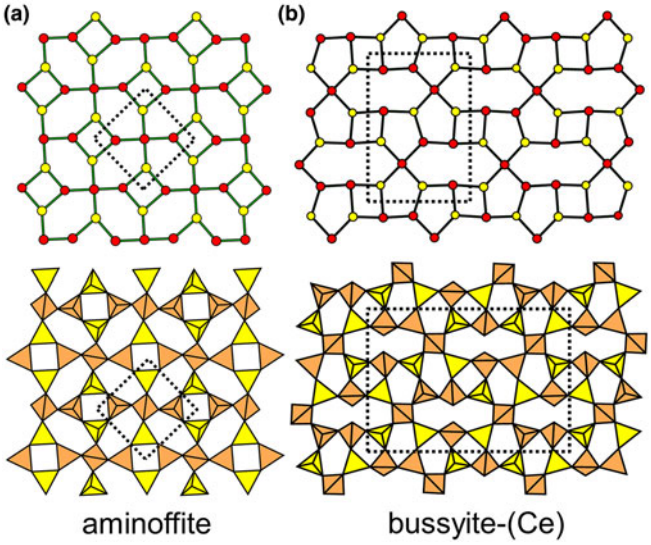

Fig. 33. (*a*) the $[(6^4)_2(4.6^2)_8]$ net and corresponding sheet of tetrahedra in **aminoffite**; and (*b*) the $[(4.5.8)_{16}(5.8.5.8)_4(5^2.8)_8]$ net and corresponding sheet of tetrahedra in **bussyite-(Ce)**.

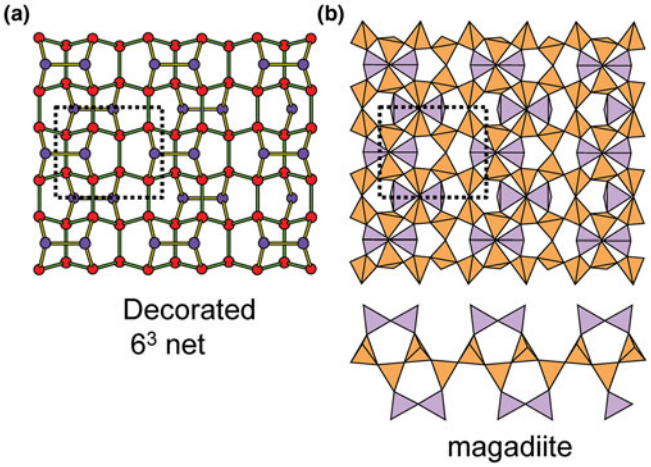

Fig. 35. (*a*) the 6^3 net decorated above and below by dimers of 3-connected vertices; and (*b*) the corresponding sheet in **magadiite**. Violet circles: added pairs of edge-linked vertices; mauve polyhedra: added dimers.

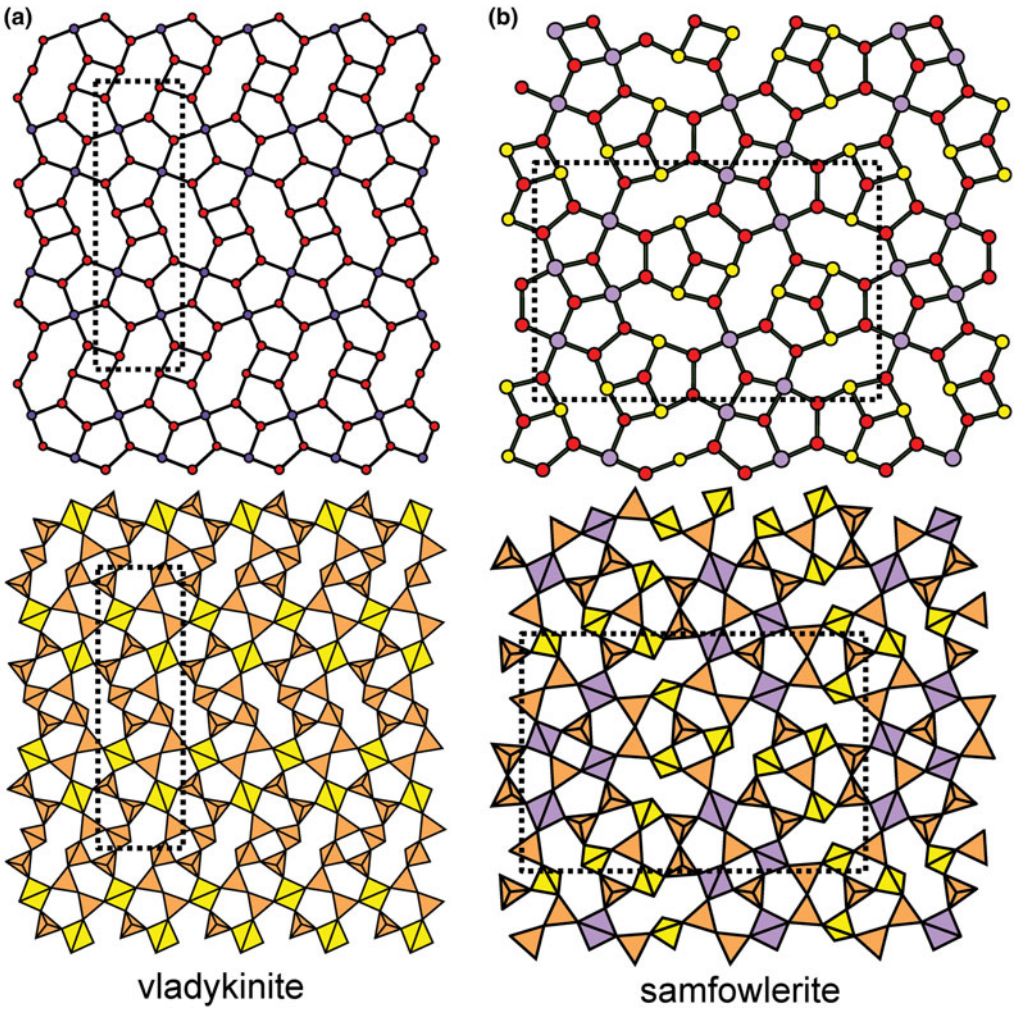

Fig. 34. (*a*) the $(5^3)_4(5^2.8)_4(4.5.8)_8(5^3.8)_4$ net and corresponding sheet of tetrahedra in **vladykinite**; and (*b*) the $(4.5.8.5)_2(5^2.8^2)_2(4.5.8)_6(5^2.8)_4(4.5^2)_6(4.8^2)_2(5^2.8)_{12}$ net and corresponding sheet of tetrahedra in **samfowlerite**.

https://doi.org/10.1180/mgm.2018.152 Published online by Cambridge University Press

Table 7. Double-layer sheet-silicates based on 6^3 and 4.8^2 nets.

Mineral	Parent net	u–d configuration in upper parent sheet	Formula	T:O ratio	Fig. No.	Ref.
			6^3			
Burckhardtite	$[6^3]_2$	(d^6)	$Pb_2(Fe^{3+}Te^{6+})$**$[AlSi_3O_8]$**O_6	1:2.00	36*b*	(1)
Cymrite	$[6^3]_2$	(d^6)	Ba**$[Al_2Si_2O_8]$**(H_2O)	1:2.00	36*a*	(2)
Dmisteinbergite	$[6^3]_2$	(d^6)	Ca**$[Al_2Si_2O_8]$**	1:2.00	36*b*	(3)
Fedorite	$[6^3]_8$	$(d^6)_1(d^2ud^2u)_3$	$Na_3(Ca_4Na_3)$**$[Si_{16}O_{38}]$**$F_2(H_2O)_{3.5}$	1:2.38	37*a*	(4)
Hexacelsian	$[6^3]_2$	(d^6)	Ba**$[Al_2Si_2O_8]$**	1:2.00	36*a*	(5)
Kampfite	$[6^3]_4$	(d^6)	See Appendix	1:2.00	36*c*	(6)
Lalondeite	$[6^3]_8$	$(d^6)(d^2ud^2u)$	$(Na,Ca)_6(Ca,Na)_3$**$[Si_{16}O_{38}]$**$F_2(H_2O)$	1:2.38	37*a*	(7)
Naujakasite	$[6^3]_{12}$	$(u^2d^4)_2(ud^2ud^2)_1$	Na_6Fe^{2+}**$[Al_4Si_8O_{26}]$**	1:2.17	37*b*	(8)
Manganonaujakasite	$[6^3]_{12}$	$(u^2d^4)_2(ud^2ud^2)_1$	Na_6Mn^{2+}**$[Al_4Si_8O_{26}]$**	1:2.17	37*b*	(9)
			4.8^2			
Macdonaldite	$[4.8^2]_4$	$(u^3d)_1(u^4du^2d)_2$	$BaCa_4$**$[Si_{16}O_{36}(OH)_2]$**$(H_2O)_{10}$	1:2.38	38*a*	(10)
Monteregianite-(Y)	$[4.8^2]_4$	$(u^3d)_1(u^4du^2d)_2$	KNa_2Y**$[Si_8O_{19}]$**$(H_2O)_5$	1:2.38	38*a*	(11)
Rhodesite	$[4.8^2]_4$	$(u^3d)_1(u^4du^2d)_2$	$HKCa_2$**$[Si_8O_{19}]$**$(H_2O)_5$	1:2.38	38*a*	(12)
Delhayelite	$[4.8^2]_4$	$(u^3d)_1(u^4du^2d)_2$	K_4Ca_2**$[AlSi_7O_{17}(OH)_2]$**$(OH)_2Cl$	1:2.38	38*b*	(13)
Fivegite	$[4.8^2]_4$	$(u^3d)_1(u^4du^2d)_2$	K_4Ca_2**$[AlSi_7O_{17}O_2]$**$(H_2O)_2Cl$	1:2.38	38*b*	(14)
Carletonite	$[4.8^2]_{16}$	$(u^2d^2)_4(ududud)_4$	KNa_4Ca_4**$[Si_8O_{18}]$**$(CO_3)_4(OH,F)(H_2O)$	1:2.25	38*c*	(15)
Seidite-(Ce)	$[4.8^2]_8$	$(udud)_1(u^2d^2u^2d^2)_2$	Na_4Ce_2Ti**$[Si_8O_{22}]$**$(OH)(H_2O)_5$	1:2.75	39	(16)

References: (1) Christy *et al.* (2014); (2) Drits *et al.* (1975), Bolotina *et al.* (2010); (3) Chesnokov *et al.* (1990), Takéuchi and Donnay (1959); (4) Mitchell and Burns (2001); (5) Galuskina *et al.* (2017); (6) Basciano and Groat (2007); (7) McDonald and Chao (2009); (8) Basso *et al.* (1975); (9) Khomyakov *et al.* (2000); (10) Cannillo *et al.* (1968); (11) Ghose *et al.* (1987); (12) Hesse *et al.* (1992); (13) Sahama and Kai Hytönen (1959); (14) Pekov *et al.* (2011); (15) Chao (1972); and (16) Khomyakov *et al.* (1998), Ferraris *et al.* (2003).

Table 8. Double-layer sheet-silicates based on miscellaneous nets.

Mineral	Parent net	u–d configuration	Formula	T:O ratio	Fig. No.	Ref.
Chiappinoite-(Y)	$[(4.6.8)_8(6^2.8)_8]_1$	$(d^4)_2(d^2o^4)_4(d^2o^2d^2o^2)_2$	Y_2Mn**$[Si_3O_7]_4$**	1:2.33	40	(1)
Ajoite	$[(5.6^2)_4(5.6.7)_4(5.7^2)_2(6^2.7)_6]_1$	$(u^6)_3(u^4d^3)_2(u^3d^2)_2(u^2du^2d)_1$	$K_3Cu_{20}^{2+}$**$[Al_5Si_{29}O_{76}]$**$(OH)_{16}(H_2O)_8$	1:2.38	41*a*,*b*,c	(2)
Armbrusterite	$[(5^2.7)_8(5.6.7)_8(6.7^2)_4(5.6.8)_8(5.7.8)_8]_1$	$(u^5)_4(u^4d)_4(u_6)_4(u^5d^2)_4(u^4du^2d)_2$	$Na_6K_5Mn^{3+}Mn_4^{2+}$**$[(Si_9O_{22})_4]$**$(OH)_{10}(H_2O)_4$	1:2.44	41*d*,*e*	(3)
Stilpnomelane	$[(5.6^2)_6(6^3)_6(5.6.8)_{24}]_1$	$(u^3d^2)_6(u^6)_6(d^6)_2(u^2d^2u^2d^2)_3$	$(K,Ca,Na)(Fe,Mg,Al)_8$**$[(Si,Al)_{12}O_{28}]$**$(OH)_8(H_2O)_n$	1:2.33	42*a*	(4)
Franklinphilite	Iso stilpnomelane	Iso stilpnomelane	$(K,Na)_x(Mn^{2+},Mg,Zn)_8$**$[(Si,Al)_{12}O_{28}]$**$(OH)_8(H_2O)$	1:2.33	42*a*	(5)
Lennilenapeite	Iso stilpnomelane	Iso stilpnomelane	$K_x(Mg,Mn^{2+},Fe^{2+},Zn)_8$**$[(Si,Al)_{12}O_{28}]$**$(OH)_8(H_2O)_{2.7}$	1:2.33	42*a*	(6)
Bannisterite	$[(5.6^2)_8(5.6.7)_8(5.7^2)_4(6^2.7)_{12}]_1$	$(u^3d^2)_4(u^6)_6(u^2du^2d)_2(u^5d^2)_2(u^3d^4)_2$	$(K,Ca)Mn_{10}$**$[(Si,Al)_{16}O_{38}]$**$(OH)_8(H_2O)_4$	1:2.38	42*b*	(7)
Parsettensite	$[(4.5.12)_{24}(5.6^2)_{12}(6^3)_{12}(5.6.12)_{24}]_1$	$(u^4)_6(u^3d^2)_{12}(u^6)_{14}(u^2d^2u^2d^2u^2d^2)_4$	$K_{7.5}Mn_{49}$**$[(Si,Al)_{82}O_{168}]$**$(OH)_{50}$	1:2.05	42c	(8)
			Ganophyllite group			
Ganophyllite	-----	-----	$[Ca_x(K,Na)_y(Mn_{6-z}Al_z)]_{\Sigma10}[Si_8(Al_{2x+y+z}Si_{2-2x-y-z})]$ $O_{24}(OH)_4(H_2O)_n$	1:~2.67	---	(9)
Eggletonite	Iso ganophyllite	-----	$(Na,K,Ca)_{1.61}(Mn,Fe,Mg,Al)_8(Si,Al)_{12}O_{29}(OH)_7(H_2O)_{8-9}$	1:~2.67	---	(10)
Tamaite-O	$[(5.6^2)_6(5.6.7)_4(6^2.7)_{10}]_1$	$(u^3d^2)_2(u^6)_4(u^2du^2d)_2(u^5d^2)_2$	KMn_6**$[Si_9AlO_{24}]$**$(OH)_4(H_2O)_n$	1:2.67	43	(11)
Zussmanite	$[(3.8^2)_6(6.8^2)_6]_1$	$(d^3)(u^6)(u^2d^2u^2d^2)_3$	KFe_{13}^{2+}**$[AlSi_{17}O_{42}]$**$(OH)_{14}$	1:2.33	44	(12)
Coombsite	Iso zussmanite	Iso zussmanite	KMn_{13}^{2+}**$[AlSi_{17}O_{42}]$**$(OH)_{14}$	1:2.33	44	(13)
Esquireite	$[(8^2)_2(8^3)_4]_1$	$(ud^2ududd^2)_2$	Ba**$[Si_6O_{13}]$**$(H_2O)_7$	1:2.17	45	(14)
Tuscanite	$[(8^2)_1(6^2.8)_2(6.8^2)_2]_1$	$(d^6)(d^3ud^3u)$	$KCa_{5.5}$**$[(Si_6Al_4)O_{22}]$**$(SO_4)_2(H_2O)$	1:2.20	46*a*	(15)
Latiumite	$[(8^2)_1(6^2.8)_2(6.8^2)_2]_1$	$(d^6)(d^3ud^3u)$	KCa_3**$[Si_2Al_3)O_{11}]$**$(SO_4)/(CO_3)$	1:2.20	46*b*	(16)
Synthetic $LaAlSiO_5$	$[(8^2)_1(6^2.8)_2(6.8^2)_2]_1$	$(d^6)(d^3ud^3u)$	La**$[AlSiO_5]$**	1:2.50	46c	(17)
Asbecasite	$[(12^2)_3(12^3)_2]_1$	(dodododododo)	Ca_3Ti^{4+}**$[Be_2Si_2As_6^{3+}O_{20}]$**	1:2.00	47*b*	(18)
Leucosphenite	$[(14^2)_8(14^3)_4]_1$	(d^{14})	$BaNa_4Ti_2$**$[B_2Si_{10}O_{30}]$**	1:2.50	48	(19)
Altisite	$[(14^2)_8(14^3)_4]_1$	-----	$Na_3K_6Ti_2$**$[Al_2Si_8O_{26}]$**Cl_3	1:2.60	49*a*,c	(20)
Lemoynite	$[(14^2)_8(14^3)_4]_1$	-----	$(Na,K)CaZr_2$**$[Si_{10}O_{26}]$**$(H_2O)_{5-6}$	1:2.60	49*b*	(21)
Natrolemoynite	$[(14^2)_8(14^3)_4]_1$	-----	Na_4Zr_2**$[Si_{10}O_{26}]$**$(H_2O)_9$	1:2.60	49*b*	(22)
Sørensenite	-----	-----	Na_4Sn^{4+}**$[Be_2Si_6O_{18}]$**$(H_2O)_2$	1:2.25	50	(23)
Diegogattaite	$[(6.14)_2(6.14^2)_4(14^2)_2]_1$	$(d^4ud^2ud^2ud^2u)$	Na_2CaCu_2**$[Si_8O_{20}]$**(H_2O)	1:2.50	51	(24)
Wickenburgite	$[6^3]_6$	$(u^3dud)_3$	Pb_3CaAl**$[AlSi_{10}O_{27}]$**$(H_2O)_4$	1:2.46	52	(25)

References: (1) Kampf and Housley (2014); (2) Pluth and Smith (2002); (3) Yakovenchuk *et al.* (2007); (4) Eggleton (1972), Eggleton and Chappell (1978), Guggenheim and Eggleton (1994); (5) Dunn *et al.* (1992); (6) Dunn *et al.* (1984); (7) Heaney and Post (1992); (8) Eggleton and Guggenheim (1986), Guggenheim and Eggleton (1994); (9) Noe and Veblen (1999); (10) Peacor *et al.* (1984); (11) Hughes *et al.* (2003); (12) Lopes-Vieira and Zussman (1969); (13) Sameshima and Kawachi (1991); (14) Kampf *et al.* (2015); (15) Mellini *et al.* (1977); (16) Cannillo *et al.* (1973); (17) Kahlenberg and Krueger (2004); (18) Cannillo *et al.* (1969), Sacerdoti *et al.* (1993); (19) Shumyatsaya *et al.* (1971), Malinovskii *et al.* (1981); (20) Khomyakov *et al.* (1994), Ferraris *et al.* (1995); (21) Blinov *et al.* (1975), Le Page and Perrault (1976); (22) McDonald and Chao (2001); (23) Maksimova *et al.* (1974), Metcalf-Johansen and Hazell (1976); (24) Rumsey *et al.* (2013), Welch and Rumsey (2013); and (25) Lam *et al.* (1994).

https://doi.org/10.1180/mgm.2018.152 Published online by Cambridge University Press

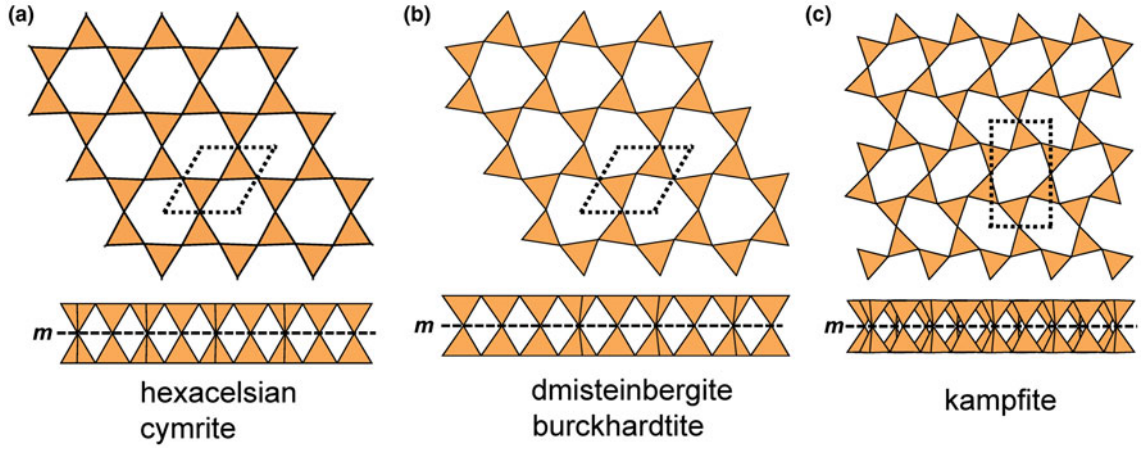

Fig. 36. Double-layer sheets of tetrahedra based on the 3-connected plane net 6^3 plus an oikodoméic operation: (*a*) the (d^6) arrangement in **hexacelsian** and **cymrite**; (*b*) the (d^6) arrangement in **dmisteinbergite** and **burckhardtite**; and (*c*) the (d^6) arrangement in **kampfite**.

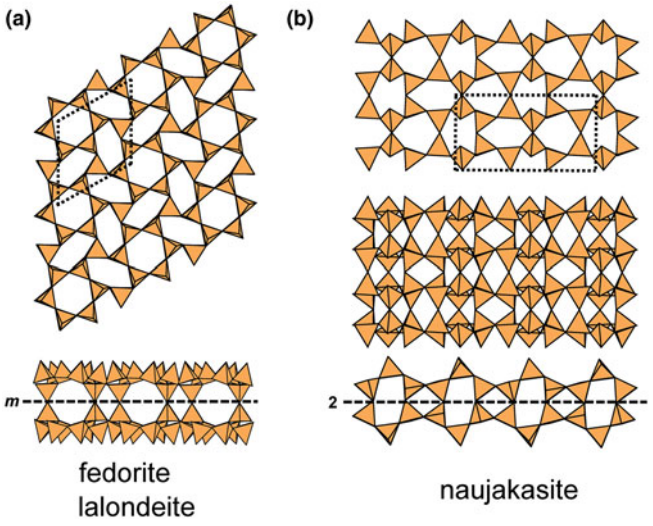

Fig. 37. (*a*) The (u^6) and (u^2du^2d) arrangement in **fedorite** and **lalondeite**; and (*b*) the (u^2d^4) and (ud^2ud^2) arrangement in **naujakasite**.

ideal inserted 4^4 net (Fig. 26*c*). The interstitial complex in **prehnite** consists of one Ca^{2+} ion coordinated by O_7^{2-} and one Al^{3+} ion coordinated by O_6^{2-}.

Figure 27*a* shows a parent 4-connected net with a 2-connected vertex inserted on one edge of each four-membered ring such that each vertex in the parent net is adjacent to only one 2-connected vertex. Figure 27*b* shows the analogous net in **searlesite** (Table 6) and Fig. 27*c* shows the corresponding sheet of tetrahedra in **searlesite**. All borate tetrahedra are 2-connected and all silicate tetrahedra are 4-connected, and the u–d arrangement is (uo^4) (do^4) in the ratio 1:1. The net corresponds to (5^4) and is crinkled in three dimensions in order to allow four five-membered rings to be incident at a single vertex. The interstitial complex in **searlesite** consists of one Na^+ ion [6]-coordinated by $O_2^{2-}(OH)_4^-$.

In Fig. 28*a*, we see a parent $(4^4)_1$ net completely inserted with 3-connected vertices with the edges between the 3-connected vertices parallel and perpendicular to the edges of the parent net. The 3-connected vertices occupying *trans* edges of the original $(4^4)_1$ net link across the original four-membered ring, and the transitivity requirements of translational symmetry require

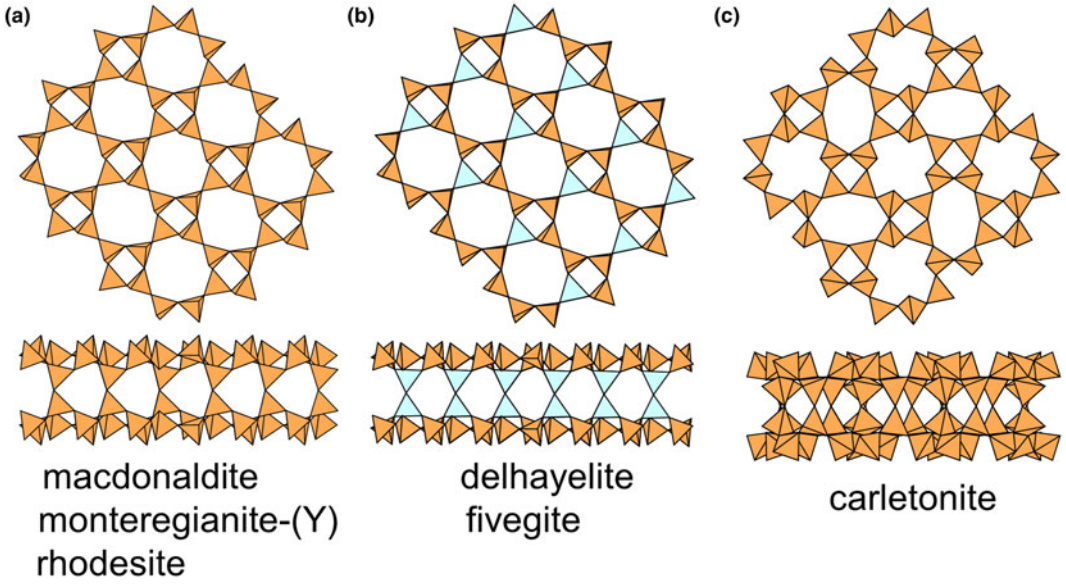

Fig. 38. Double-sheets of tetrahedra based on the 3-connected plane net 4.8^2 plus an oikodoméic operation: (*a*) the $(u^3d)_1(u^4du^2d)_1$ arrangement in **macdonaldite, monteregianite-(Y)** and **rhodesite**; (*b*) the $(u^3d)_1(u^4du^2d)_1$ arrangement in **delhayelite** and **fivegite**, note how all d tetrahedra are occupied by Al^{3+}; and (*c*) the $(u^2d^2)_4(u^2d^2u^2d^2)_2(udududud)_2$ arrangement in **carletonite**.

https://doi.org/10.1180/mgm.2018.152 Published online by Cambridge University Press

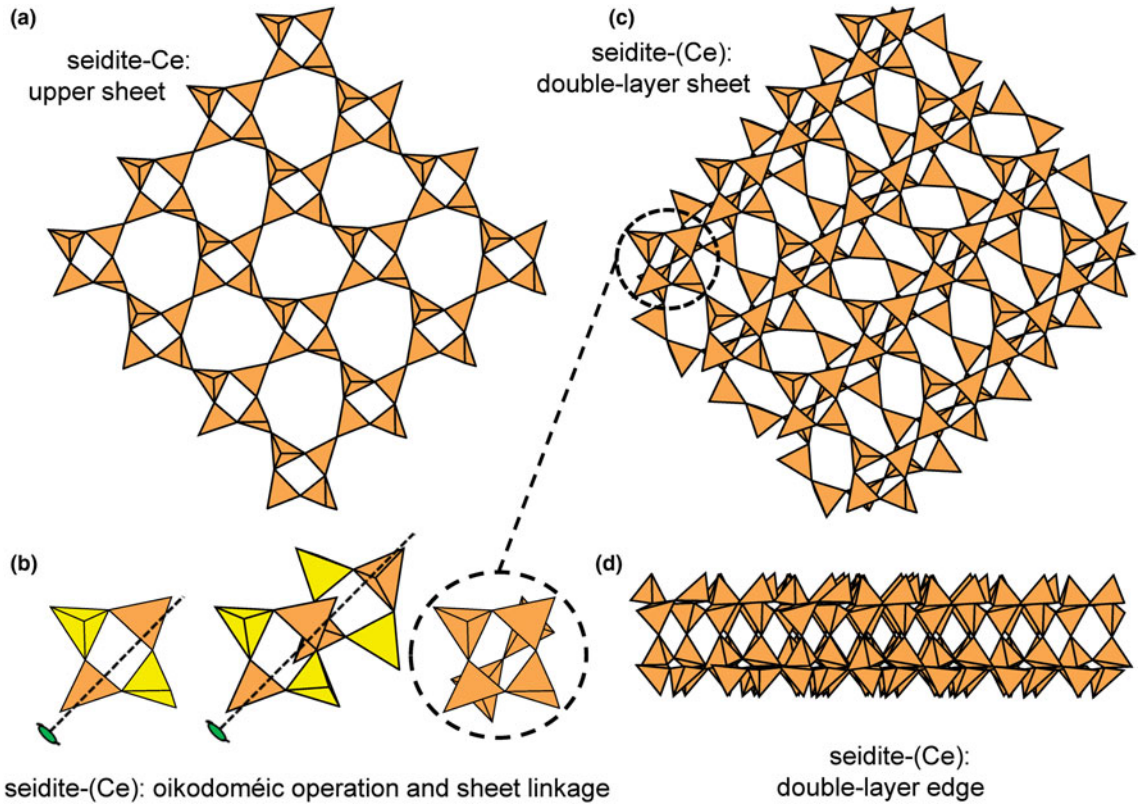

Fig. 39. Double-sheets of tetrahedra based on the 3-connected plane net 4.8^2 plus an oikodoméic operation in **seidite-(Ce)**: (*a*) the upper-layer parent sheet; (*b*) sketch of the linkage of four-membered rings in the upper- and lower-layer sheets; and (*c*,*d*) the double-layer sheet in plan and cross-section.

edge-adjacent squares to be oriented differently (i.e. rotated by 90°). The result is a net with both 3- and 4-connected vertices: $(5^3)_2(5^4)_1$. Figure 28*b* shows a geometrically distorted version of this net, with the unit cells of the **melilite-group minerals** and **leucophanite** shown as the dotted lines, and the unit cell of **meliphanite** shown by the dashed lines. The $(5^3)_2(5^4)_1$ net contains only five-membered rings (Fig. 28*a*) with one 4-connected vertex and two 3-connected vertices. The assignment of u and d tetrahedra is now complicated by the presence of 4-connected tetrahedra that point neither up nor down (cf. Fig. 5*b*); we denote these tetrahedra as o. Thus there are two distinct five-membered rings in this net: (u^2odo) and (uod^2o). The 4-connected tetrahedron (corresponding to the red vertex in Fig. 28*a*) can accept a wide range of cations (Mg^{2+}, Be^{2+}, Zn^{2+}, B^{3+}, Al^{3+} and Fe^{3+}) in minerals (Table 6) and other compositions with this structure type that have been synthesised (Kimata, 1983, 1985, 1988). The 3-connected tetrahedron can incorporate B^{3+}, Al^{3+} and Si^{4+} in minerals (Table 6). As is typical for 4-connected tetrahedra in sheets, the tetrahedra are arranged such that two of their edges lie on the surfaces of the sheet, and the anions at the terminations of these edges can be ligands for 3-connected tetrahedra that point accordingly both u and d in the sheet (e.g. Fig. 29*a*). Many structures based on this net show incommensurate behaviour (see Armbruster *et al.*, 1990). The interstitial complex in the **melilite-group minerals** consists of a single *M* site occupied by Ca^{2+} (except in alumoåkermanite, Table 6) that is [8]-coordinated by O^{2-} anions. In **leucophanite** and **meliphanite**, the topological unit cells and the u–d–o arrangements are the same but the ordering of cations over the net-vertices/tetrahedra is different. In **leucophanite**, (Fig. 29*b*), the 4-connected tetrahedron is occupied by Si^{4+} and half of the 3-connected tetrahedra are occupied by Be^{2+}. In **meliphanite**, (Fig. 29*c*), half of the 4-connected tetrahedra are occupied by Al^{3+} and half of the 3-connected tetrahedra are occupied by Be^{2+}. The structure of **jeffreyite** is not yet known. The

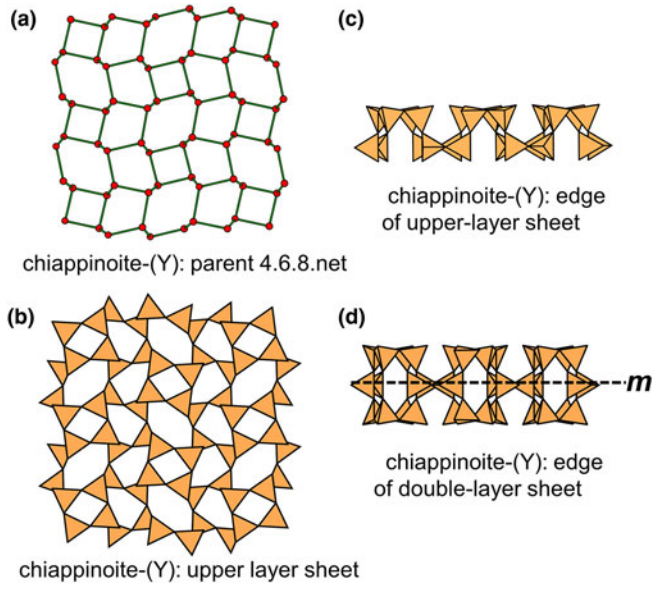

Fig. 40. Double-sheet of tetrahedra based on the 3-connected plane net 4.6.8 plus a class-3 oikodoméic ***m*** operation in **chiappinoite-(Y)**: (*a*) the upper-layer parent net; (*b*) the upper-layer parent sheet in plan and (*c*) in cross-section; and (*d*) the double-layer sheet in plan showing the class-3 oikodoméic operation ***m***.

https://doi.org/10.1180/mgm.2018.152 Published online by Cambridge University Press

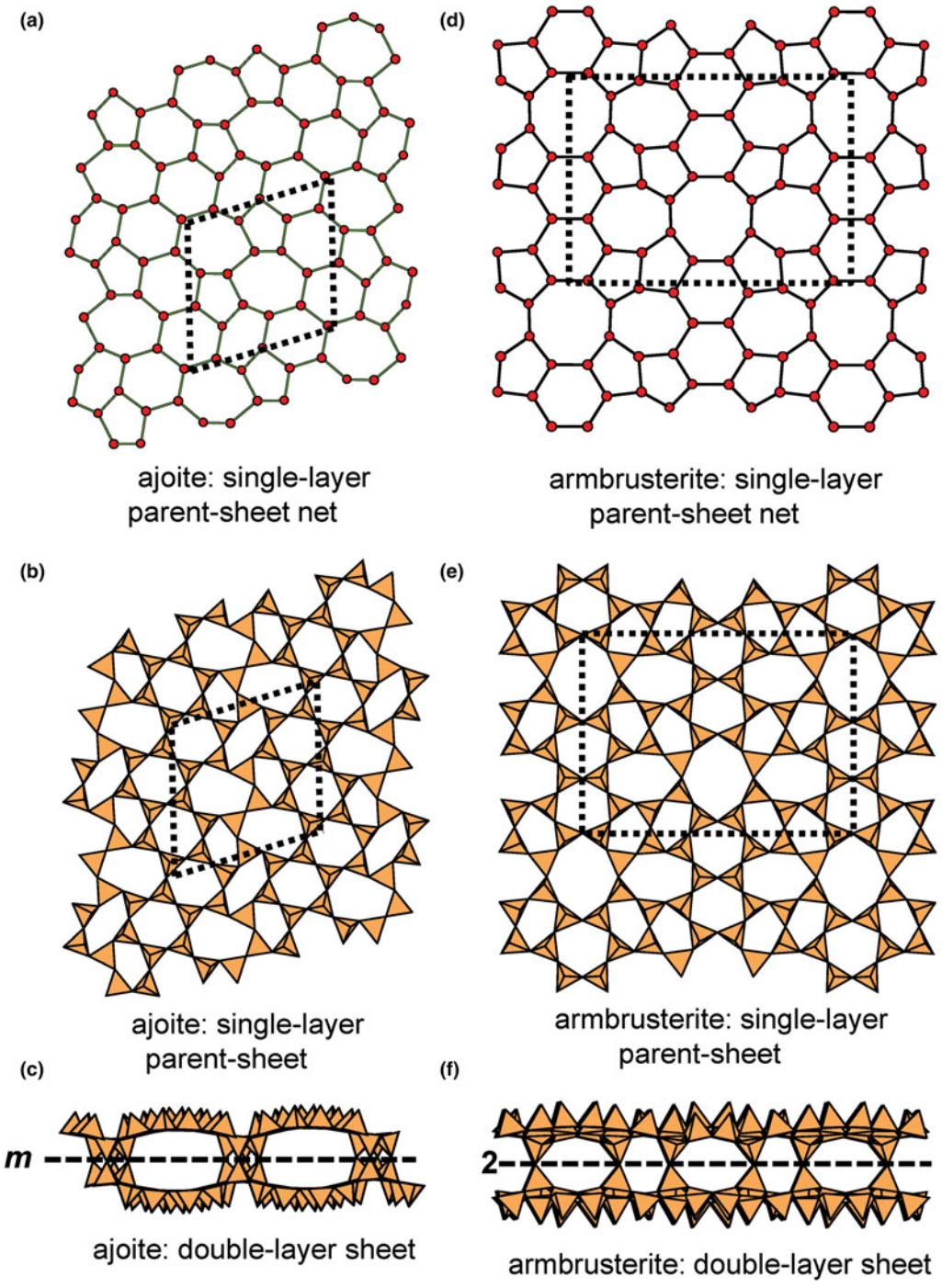

Fig. 41. Double-layer sheets of tetrahedra based on miscellaneous complex 3-connected plane nets plus an oikodoméic operation: (*a*) the parent $(5.6^2)_2(5.6.7)_4(5.7^2)_2(6^2.7)_6$ net in **ajoite**; (*b*) the parent upper single-layer sheet in **ajoite**; (*c*) the double-layer sheet in **ajoite;** (*d*) the parent $(5^2.7)_8(5.6.7)_8(6.7^2)_4(5.6.8)_8(5.7.8)_8$ net in **armbrusterite**; (*e*) the parent upper single-layer sheet in **armbrusterite**; and (*f*) the double-layer sheet in **armbrusterite**.

interstitial complex in **leucophanite** consists of one Ca^{2+} ion and one Na^+ ion each of which is coordinated by O_8^{2-}; the interstitial complex in **meliphanite** consists of one Ca^{2+} ion and one Na^+ ion with coordinations $O_7^{2-}F^-$ and $O_6^{2-}F_2^-$, respectively.

Figure 30 shows the related nets $(4.5.8)_2(4.5^2.8)_2(5^3)_2(5^2.8)_4$ and $(4.5.8)_2(4.5^2.8)_2(5^3)_6(5^2.8)_4(5^4)_2$. The $(4.5.8)_2(4.5^2.8)_2(5^3)_2(5^2.8)_4$ net corresponds to the sheet in the structures of the **hellandite-group minerals** (Fig. 30*a*; Table 6) with a rather complicated u–d–o arrangement: (uodo)(u^3do)(ud^{3}o)(u^2d^2o)(u^3od^{3}o), and the net $(4.5.8)_2(4.5^2.8)_2(5^3)_6(5^2.8)_4(5^4)_2$ corresponds to the sheet in the structure of **piergorite-(Ce)** with the same u-d-o arrangement (Fig. 30*b*; Table 6). Oberti *et al.* (2002) discussed the crystal chemistry of the hellandite-group minerals and wrote their general formula as $X_4Y_2ZT_2[B_2Si_4O_{22}]W_2$ where X = Na^+, Ca^{2+}, Y^{3+}, *LREE*$^{3+}$ at the *M*3 and *M*4 sites with coordinations O_8^{2-} and O_7^{2-}(OH^-,F^-), respectively [except

https://doi.org/10.1180/mgm.2018.152 Published online by Cambridge University Press

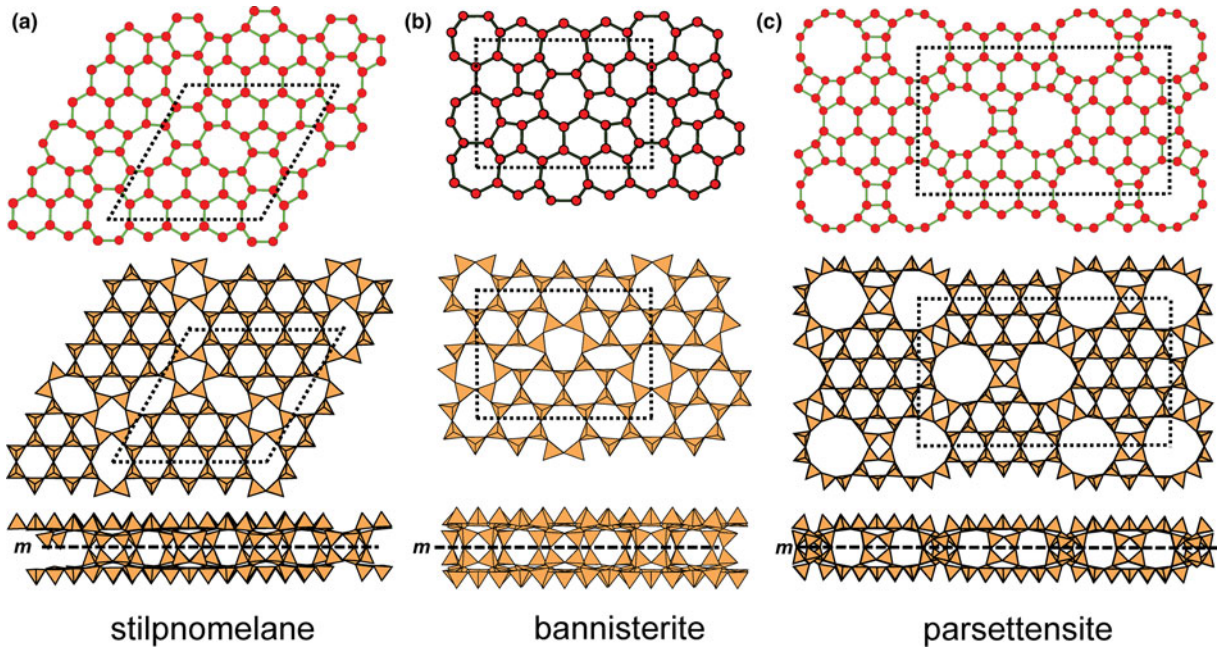

Fig. 42. Double-layer sheets of tetrahedra based on miscellaneous complex 3-connected plane nets plus an oikodoméic operation: (*a*) the $(5.6^2)_6(6^3)_6(5.6.8)_{24}$ net and sheet in **stilpnomelane**; (*b*) the $(5.6^2)_8(5.7^2)_4(5.6.7)_8(6^2.7)_{12}$ net and sheet in **bannisterite**; and (*c*) the $(4.5.12)_{24}(5.6^2)_{12}(6^3)_{12}$ $(5.6.12)_{24}$ net and sheet in **parsettensite.**

in ciprianiite and mottanaite-(Ce) where it is O_8^{2-} (×2)]; Y = Ca^{2+}, Y^{3+}, *HREE*$^{3+}$, Th^{4+}, U^{4+} at the *M*2 site which is coordinated by $O_7^{2-}(OH)^-$ [except in ciprianiite and mottanaite-(Ce) where it is O_8^{2-} (×2)]; Z = Al^{3+}, Mn^{3+}, Fe^{3+} and Ti^{4+} at the *M*1 site which is coordinated by $O_4^{2-}(OH^-)_2$; T = □ (vacancy), Li^+ or Be^{2+} at a new tetrahedrally coordinated site; and W = $(OH)^-$, F^-, O^{2-} at the O5 site. The interstitial complex in **piergorite-(Ce)** consists of four Ca^{2+} ions coordinated by O_8^{2-} (×3) and $O_7^{2-}(OH)^-$, one Ce^{3+} ion coordinated by $O_7^{2-}(OH)^-$, and Al^{3+} coordinated by $O_4^{2-}(OH)_2^-$.

The $(4.5.8)_8(5^2.8)_4(5.8.5.8)_2$ net has four-membered, five-membered and eight-membered rings in the ratio 4:2:1 (Fig. 31). There is one type of four-membered ring with the arrangement (u^2d^2), two types of five-membered rings with the arrangements (u^3do) and (ud^3o), and one type of eight-membered ring with the arrangement (u^3od^3o). This sheet occurs in the minerals of the nordite group: **ferronordite-(Ce)** and **manganonordite-(Ce)** (Table 6). Note that the unit cell of the net is half that of the sheet; this is the case because vertices of the net do not represent the u–d nature of the corresponding tetrahedra (unless we label them as such) whereas the u–d nature of tetrahedra is a property of the sheet. For **ferronordite-(Ce)**, tetrahedra corresponding to translationally equivalent vertices point in different directions, causing a doubling of the unit cell in that direction (Fig. 31). The interstitial complex in **ferronordite-(Ce), ferronordite-(La)** and **manganonordite-(Ce)** consists of two Na^+ ions each coordinated by O_6^{2-}, one Sr^{2+} ion coordinated by O_8^{2-}, and one *REE*$^{3+}$ ion coordinated by O_8^{2-}.

The $[(4.5^2)_1(4.5.8.5)_1(5^2.8)_3]_4$ net has four-membered, five-membered and eight-membered rings in the ratio 1:1:3 (Fig. 32). There is one type of four-membered ring with the arrangement (uodo), two types of five-membered rings with the arrangements (u^3do) and (ud^3o), and one type of eight-membered ring with the arrangement (u^3od^3o). This sheet occurs in the structures of **semenovite-(Ce), harstigite** and **perettiite-(Y)** (Table 6). In **semenovite-(Ce)** (Fig. 32*a*), the tetrahedra are completely occupied by Si^{4+}. In **harstigite** (Fig. 32*b*), the 4-connected tetrahedron and one 3-connected tetrahedron are occupied by Be^{2+} and the remaining 3-connected tetrahedra are occupied by Si^{4+}. In **perettiite-(Y)** (Fig. 32*c*), one 3-connected tetrahedron is occupied by Si^{4+} and the remaining 3- and 4-connected tetrahedra are occupied by B^{3+}; one 3-connected tetrahedron is partly occupied by Be^{2+}, and this tetrahedron corresponds to that 3-connected tetrahedron occupied by Be^{2+} in **harstigite** (Fig. 32*b*). The interstitial complex in **semenovite-(Ce)** consists of two Ce^{3+} ions each coordinated by O_8^{2-}, two Fe^{2+} ions each coordinated by O_6^{2-}, and two Ca^{2+} ions (with minor Na^+ substitution) coordinated by O_8^{2-} and $O_7^{2-}F^-$, respectively. The interstitial complex in **harstigite** consists of three Ca^{2+} ions coordinated by $O_7^{2-}(OH)^-$, O_7^{2-} and $O_6^{2-}(OH)^-$, respectively, and one Mn^{2+} ion coordinated by O_6^{2-}. The interstitial complex in **perettiite-(Y)** consists of one Y^{3+} ion coordinated by O_8^{2-}, one Mn^{2+} ion coordinated by O_8^{2-}, and one Fe^{2+} ion coordinated by O_6^{2-}.

The $[(6^4)_2(4.6^2)_8]$ net has four-membered and six-membered rings in the ratio 1:2. In the structure of **aminoffite** (Fig. 33*a*; Table 6), there are two four-membered rings with the arrangements (u^4) and (d^4), and one six-membered ring with the arrangement (u^2od^2o). Be^{2+} occupies half the 3-connected tetrahedra and Si^{4+} occupies half the 3-connected tetrahedra and all 4-connected tetrahedra. The interstitial complex in **aminoffite** consists of two Ca^{2+} ions coordinated by $O_6^{2-}(OH)^-$ and $O_6^{2-}(OH)_2^-$.

The $[(4.5.8)_{16}(5.8.5.8)_4(5^2.8)_8]$ net (Fig. 33*b*) has four-membered, five-membered and eight-membered rings in the ratio 1:2:1. In the structure of **bussyite-(Ce)** (Fig. 33*b*; Table 6), the (topological) unit cell is doubled relative to that of the parent net because of the u–d nature of the tetrahedra (cf. **ferronordite-(Ce)**, Fig. 31). There is one four-membered ring with the arrangement (u^2d^2), two five-membered rings with the arrangements (u^3od) and (uod^3), and one eight-membered ring

https://doi.org/10.1180/mgm.2018.152 Published online by Cambridge University Press

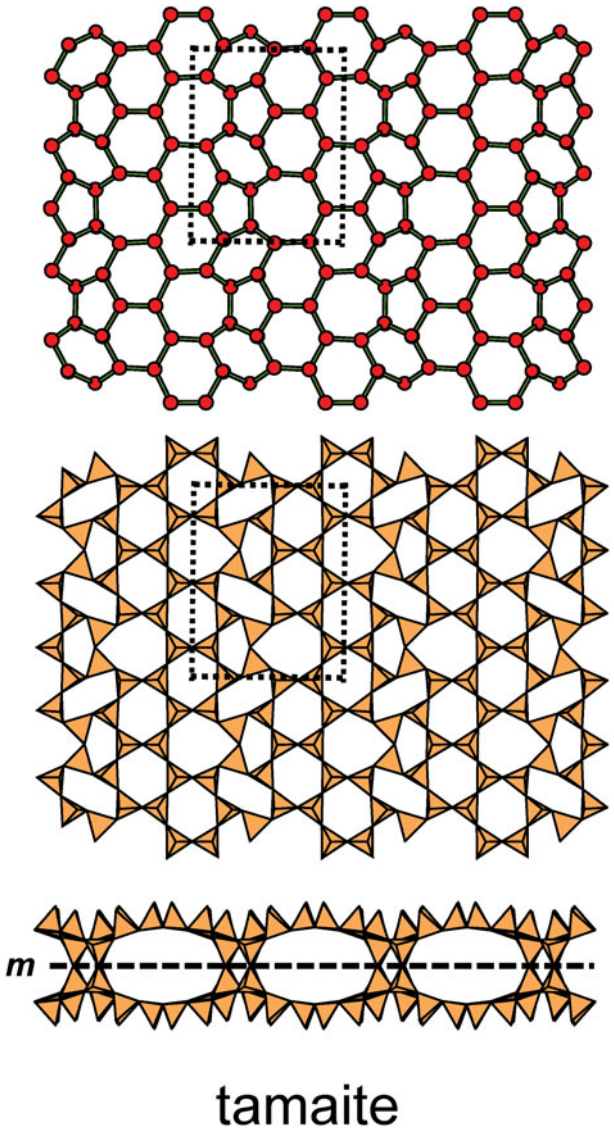

Fig. 43. Double-layer sheets of tetrahedra based on miscellaneous complex 3-connected plane nets plus an oikodoméic operation: the $(5.6^2)_6(5.6.7)_4(6^2.7)_{10}$ net and sheet in **tamaite**.

with the arrangement (u^3od^3o) in the topological unit-cell. As with **aminoffite** (Fig. 33*a*), Be^{2+} occupies half the 3-connected tetrahedra and Si^{4+} occupies half the 3-connected tetrahedra and all 4-connected tetrahedra. The interstitial complex in **bussyite-(Ce)** consists of one Ce^{3+} ion coordinated by $O_7^{2-}(OH)^-$, one Ca^{2+} ion coordinated by $O_6^{2-}F_2^-$, four Na^+ ions coordinated by $O_6^{2-}F_2^-$ (×2), $O_5^{2-}(OH)^-F^-$ and $O_5^{2-}F_2^-$, and Mn^{2+} coordinated by $O_6^{2-}F_2^-$.

The $(5^3)_4(5^2.8)_4(4.5.8)_8(5^3.8)_4$ net has four-membered, five-membered and eight-membered rings in the ratio 1:2:1. In the structure of **vladykinite** (Fig. 34*a*; Table 6), there is one four-membered ring with the arrangement (u^2d^2), four five-membered rings with the arrangements (u^3do), (ud^3o), (u^2odo) and (uod^2o), and one eight-membered ring with the arrangement (u^3od^3o) in the topological unit-cell. Be^{2+} occupies the 4-connected tetrahedra and Si^{4+} occupies the 3-connected tetrahedra. The interstitial complex in **vladykinite** consists of two Na^+ ions coordinated by O_6^{2-}, and two Sr^{2+} ions coordinated by O_8^{2-} (×2).

The $(4.5.8.5)_2(5^2.8^2)_2(4.5.8)_6(5^2.8)_4(4.5^2)_6(4.8^2)_2(5^2.8)_{12}$ net has four-membered, five-membered and eight-membered rings in the ratio 2:8:2 (Fig. 34*b*). In the structure of **samfowlerite** (Fig. 34*b*; Table 6), there are two four-membered rings with the arrangements (u^3d) and (ud^3), four five-membered rings with the arrangements (u^4d), (ud^4), (u^2odo) and (d^2ouo), and one eight-membered ring with the arrangement (u^3od^3o) in the topological unit-cell. Zn^{2+} occupies the 4-connected tetrahedra, and Si^{4+} and Al^{3+} occupy the 3-connected tetrahedra. The interstitial complex in **samfowlerite** consists of seven Ca^{2+} ions coordinated by $O_7^{2-}(OH)^-$ (×4), $O_6^{2-}(OH)^-$, O_7^{2-} and O_8^{2-}, and two Mn^{2+} ions coordinated by O_6^{2-} (×2).

The structure of **magadiite** (Table 6) is based on a 6^3 net which is decorated by dimers of 3-connected vertices; in Fig. 35*a*, the 6^3 net is shown by the red vertices and green edges, and the decorating vertices and edges are violet and yellow, respectively. The resulting sheet at first seems to be a double-layer sheet (Fig. 35*b*), but this is not the case as there is no parent sheet, only 'parent ribbons'. However, the stoichiometry of the sheet is not compatible with the IMA-accepted formula and the interstitial complex in **magadiite** was not located.

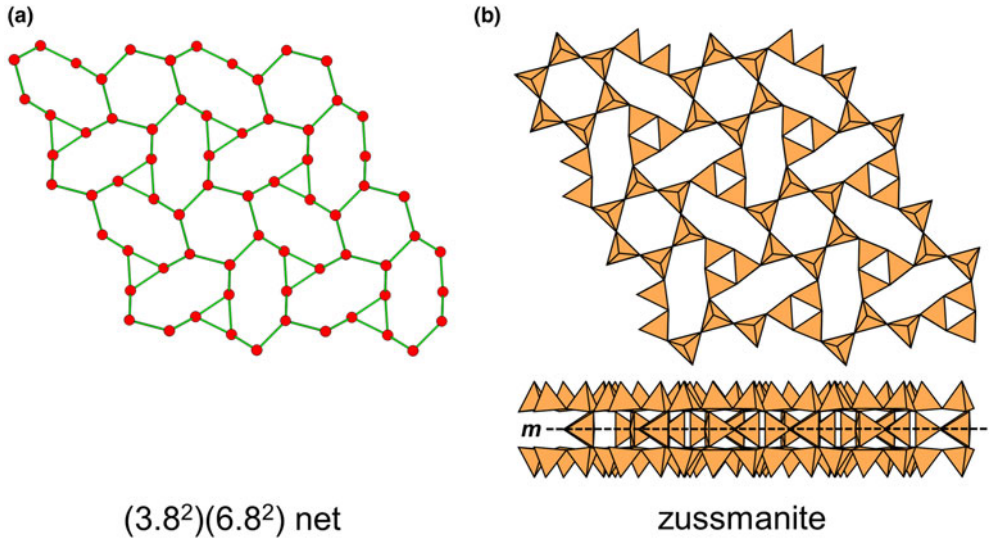

Fig. 44. Double-layer sheets derived by class-3 oikodoméic operations: (*a*) the $(3.8^2)(6.8^2)$ net; and (*b*) the corresponding arrangements of tetrahedra in **zussmanite**, showing the class-3 oikodoméic operation ***m***.

https://doi.org/10.1180/mgm.2018.152 Published online by Cambridge University Press

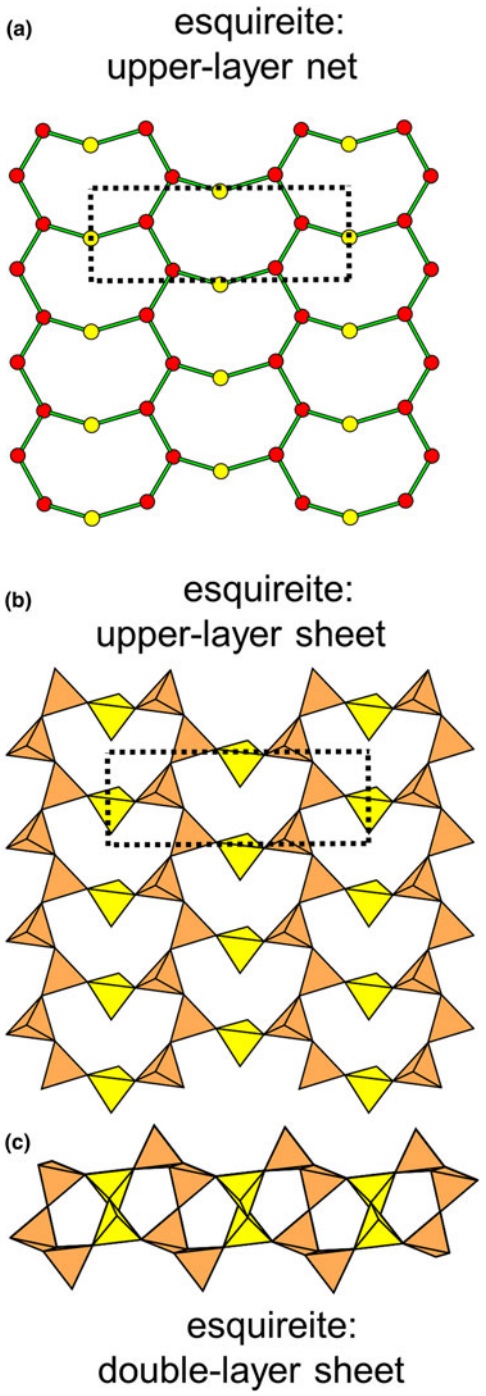

Fig. 45. Double-layer sheets derived from the 3-connected plane net 6^3 by insertion of 2-connected vertices between 3-connected vertices: **esquireite**. (*a*) the parent upper-layer $(8^2)_2(8^3)_4$ net; (*b*) the parent upper-layer sheet; and (*c*) the double-layer sheet. Yellow vertices and tetrahedra are 2-connected.

Double-layer sheets: 3-connected nets

Double-layer sheet structures and their corresponding nets are listed in Tables 7 and 8.

The 6^3 net

The most common double-layer sheet-silicate minerals are based on this net (Table 7). **Hexacelsian** (Fig. 36*a*), **cymrite** (Fig. 36*a*), **dmisteinbergite** (Fig. 36*b*) and **burckhardtite** (Fig. 36*b*) have a simple (d^6) arrangement that is repeated by the oikodoméic operation ***m*** (class-2) to give a sheet of the form $[TO_2]_n$, and the sheet in **burckhardtite** shows slight geometrical distortion relative to the sheets in **hexacelsian** and **cymrite**. This double-layer sheet is not restricted to silicate minerals; for example, it occurs in **minjiangite**, $Ba[Be_2(PO_4)_2]$ (Rao *et al.*, 2015). In **kampfite** (Fig. 36*c*), the six-membered rings are all quite distorted from geometrical hexagonal symmetry, a feature that is presumably imposed on the sheet by the interstitial linkage between the double-layer sheets. Note that the formula given for **kampfite** is not compatible with the crystal structure: the structure shows that all anions bonded to tetrahedrally coordinated Si^{4+} and Al^{3+} are each linked to two *T* cations and hence the formula must contain $[T_{16}O_{32}]$, not $[T_{16}O_{31}]$; this issue is discussed in the Appendix and a revised formula is suggested.

The interstitial complex in h**exacelsian** consists of one Ba^{2+} ion coordinated by O^{2-}_{12} anions. The interstitial complex in **cymrite** consists of four Ba^{2+} ions [11]-coordinated by $O^{2-}_{10}(H_2O)$ (×3) and O^{2-}_{11} [see Gagné and Hawthorne (2016) for minimum and maximum bondlengths observed in alkaline-earth–O^{2-} bonds]. The interstitial complex in **dmisteinbergite** consists of one Ca^{2+} ion coordinated by O^{2-}_6 anions. The interstitial complex in **burckhardtite** consists of one Pb^{2+} ion coordinated by O^{2-}_9 anions and showing lone-pair-stereoactive behaviour, and one site occupied by Fe^{2+} and Fe^{3+} ions and coordinated by O^{2-}_6 anions. The interstitial complex in **kampfite** consists of three Ba^{2+} ions coordinated by $O^{2-}_{10}Cl^-$, $O^{2-}_{10}Cl^-_4$ and $O^{2-}_6Cl^-_6$, together with (CO_3) groups.

In **fedorite** and **lalondeite** (Fig. 37*a*), the upper 6^3 sheet has the u–d arrangements (u^6) and (u^2du^2d) in the ratio 1:3. In **naujakasite** (Fig. 37*b*, the 6^3 nature of the double sheet is not immediately apparent (centre figure) as the class-2 oikodoméic operation does not correspond to rigorous reflection symmetry; however, when the upper sheet only is illustrated (top figure), the 6^3 nature of the parent single sheet, with its (u^2d^4) arrangement, becomes apparent. The interstitial complexes in **fedorite** and **lalondeite** consist of four octahedrally coordinated sites containing different amounts of Ca^{2+} and Na^+ with coordinations O^{2-}_6, $O^{2-}_5F^-$ (×2) and $O^{2-}_4F^-_2$, and three sites with strong positional disorder occupied by Na^+ and K^+ and coordinated by partly disordered O^{2-} and (H_2O). The interstitial complexes in **naujakasite** and **manganonaujakasite** consist of one octahedrally coordinated Fe^{2+} (Mn^{2+}) ion coordinated by O^{2-}_6, and by three Na^+ ions the coordinations of which are very irregular, but are O^{2-}_5 or O^{2-}_7, O^{2-}_4 or O^{2-}_5 and O^{2-}_5 or O^{2-}_8, respectively.

The 4.8^2 net

The double-layer sheet-silicate minerals based on this net are listed in Table 7. **Macdonaldite, monteregianite-(Y)** and **rhodesite** (Fig. 38*a*) and **delhayelite** and **fivegite** (Fig. 38*b*) have u–d arrangements $(u^3d)_1(u^4du^2d)_1$ but differ in the occupancy of the vertices. In **macdonaldite, monteregianite-(Y)** and **rhodesite**, the sheets are silicate, whereas in **delhayelite** and **fivegite**, the sheet is an aluminosilicate and Al^{3+} occupies the tetrahedra that link the single sheets into a double sheet (i.e. all the d tetrahedra in the upper sheet). Note that there is an acid silicate-group in **macdonaldite. Carletonite** (Fig. 38*c*) has a more highly connected double-sheet with the u–d arrangement $(u^2d^2)_4(u^2d^2u^2d^2)_2$ $(udududud)_2$ in a completely silicate sheet. All double-layer arrangements are generated from the parent single-layer sheet by the

https://doi.org/10.1180/mgm.2018.152 Published online by Cambridge University Press

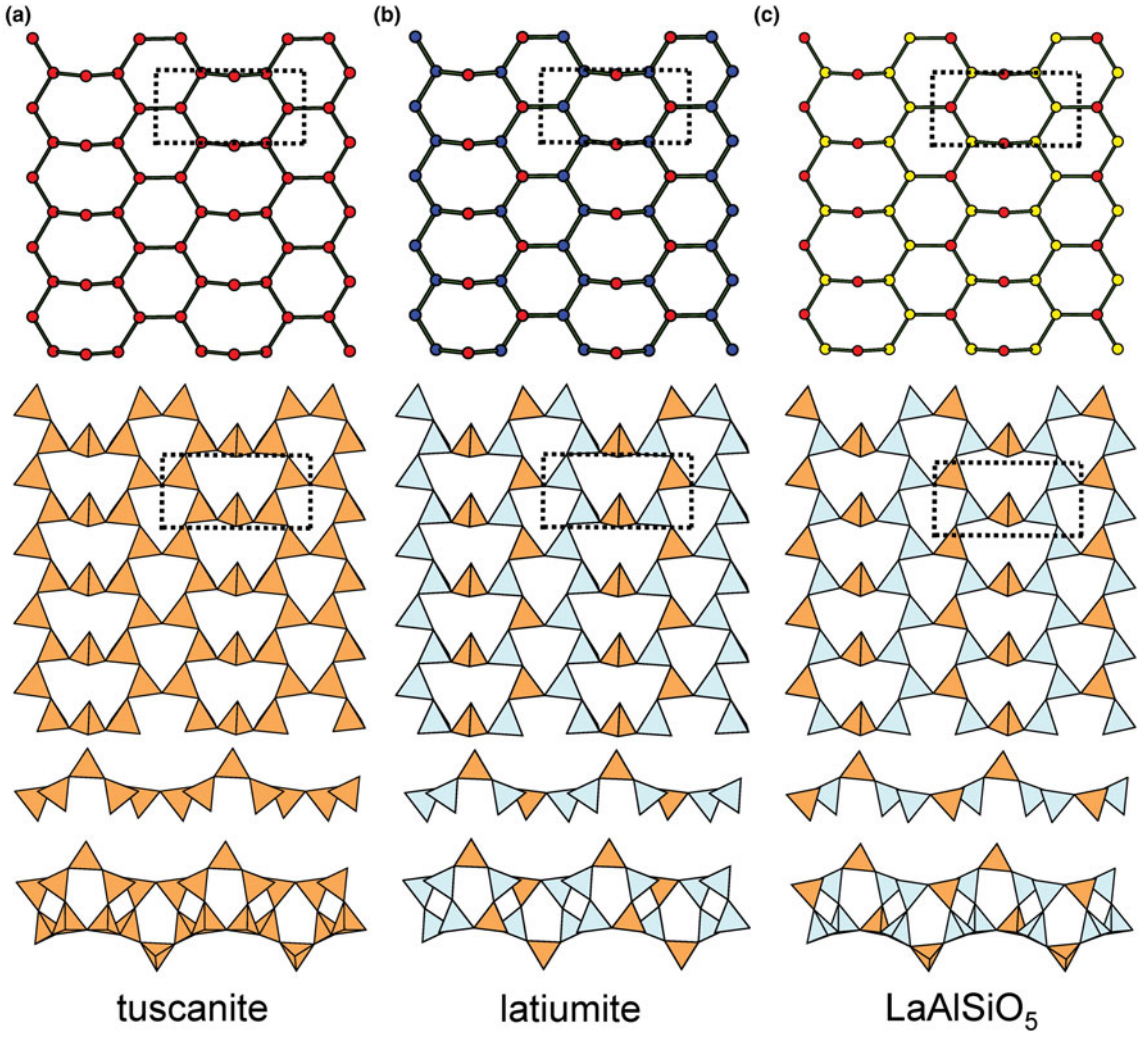

Fig. 46. Double-layer sheets derived from the 3-connected plane net 6^3 by insertion of 2-connected vertices between 3-connected vertices; (*a*) the $(8^2)_2(6^2.8)_4(6.8^2)_4$ net, the corresponding sheet in **tuscanite**, the single sheet viewed edge-on, and the double-layer sheet viewed edge-on; (*b*) the $(8^2)_2(6^2.8)_4(6.8^2)_4$ net, the corresponding sheet in **latiumite**, the single-layer sheet viewed edge-on, and the double-layer sheet viewed edge-on. Orange: Si; blue: Al^{3+}; and (*c*) the $(8^2)_2(6^2.8)_4(6.8^2)_4$ net, the corresponding sheet in **synthetic $LaAlSiO_5$**, the single-layer sheet viewed edge-on, and the double-layer sheet viewed edge-on.

class-2 oikodoméic operation ***m***. The interstitial complex in **macdonaldite** consists of one Ba^{2+} ion coordinated by $O_4^{2-}(H_2O)_6$, three Ca^{2+} ions coordinated by $O_4^{2-}(H_2O)_2$ (× 2) and $O_4^{2-}(OH)_2^-$, and seven distinct (H_2O) groups, five of which are transformer groups and two of which are non-bonded groups. The interstitial complex in **monteregianite-(Y)** consists of two K^+ ions coordinated by $O_6^{2-}(H_2O)_4$ (x 2), three Na^+ ions coordinated by $O_5^{2-}(H_2O)_2$ $O_4^{2-}(H_2O)_2$ (x 2), and one Y^{3+} ion coordinated by O_6^{2-}; in addition, there are six distinct non-transformer (H_2O) groups. The interstitial complex in **rhodesite** consists of one K^+ ion coordinated by $O_6^{2-}(H_2O)_4$, two Ca^{2+} ions coordinated by $O_4^{2-}(H_2O)_2$ and O_6^{2-}, respectively, with three distinct transformer (H_2O) groups. The interstitial complex in **delhayelite** consists of one Na^+ ion coordinated by $O_8^{2-}(H_2O)_2$, one K^+ ion coordinated by $O_6^{2-}(H_2O)_5$, and two Ca^{2+} ions coordinated by $O_5^{2-}(H_2O)$ (x 2) and O_6^{2-}, respectively, with four distinct (H_2O) groups. The interstitial complex in **fivegite** consists of three K^+ ions coordinated by $O_7^{2-}Cl^-$ (x 2) and $O_6^{2-}Cl_2^-$, and two Ca^{2+} ions, one coordinated by $O_5^{2-}(OH)^-$ and the other coordinated by $O_3^{2-}(OH)_2^-$ (although one of the Ca^{2+}–O^{2-} distances is unrealistically short, cf. Gagné and Hawthorne, 2016). The interstitial complex in **carletonite** consists of three Na^+ ions coordinated by $O_4^{2-}F^-(H_2O)$, $O_5^{2-}(H_2O)$ and O_8^{2-}, respectively, one K^+ ion coordinated by O_9^{2-}, and one Ca^{2+} ion coordinated by $O_7^{2-}F^-$; there are one transformer and one non-transformer (H_2O) groups.

The crystal structure of **seidite-(Ce)** was not determined by solution of the structure from single-crystal diffraction data; it is a proposed structure-model based on chemical composition, electron and X-ray powder-diffraction data, and proposed similarities with the structure of miserite (Scott, 1976). The parent upper-layer sheet in **seidite-(Ce)** (Fig. 39*a*) is a 4.8^2 net with one type of four-membered ring with the u–d arrangement (udud) and one type of eight-membered ring with the arrangement ($u^2d^2u^2d^2$). The topological unit-cell contains four tetrahedra but the crystallographic unit-cell is larger as is apparent from the fact that all nearest-neighbour four-membered rings are not geometrically equivalent. A fragment of the upper-layer sheet is shown in Fig. 39*b* (left) with the u tetrahedra shaded in yellow and the d tetrahedra shaded in brown to better illustrate the

https://doi.org/10.1180/mgm.2018.152 Published online by Cambridge University Press

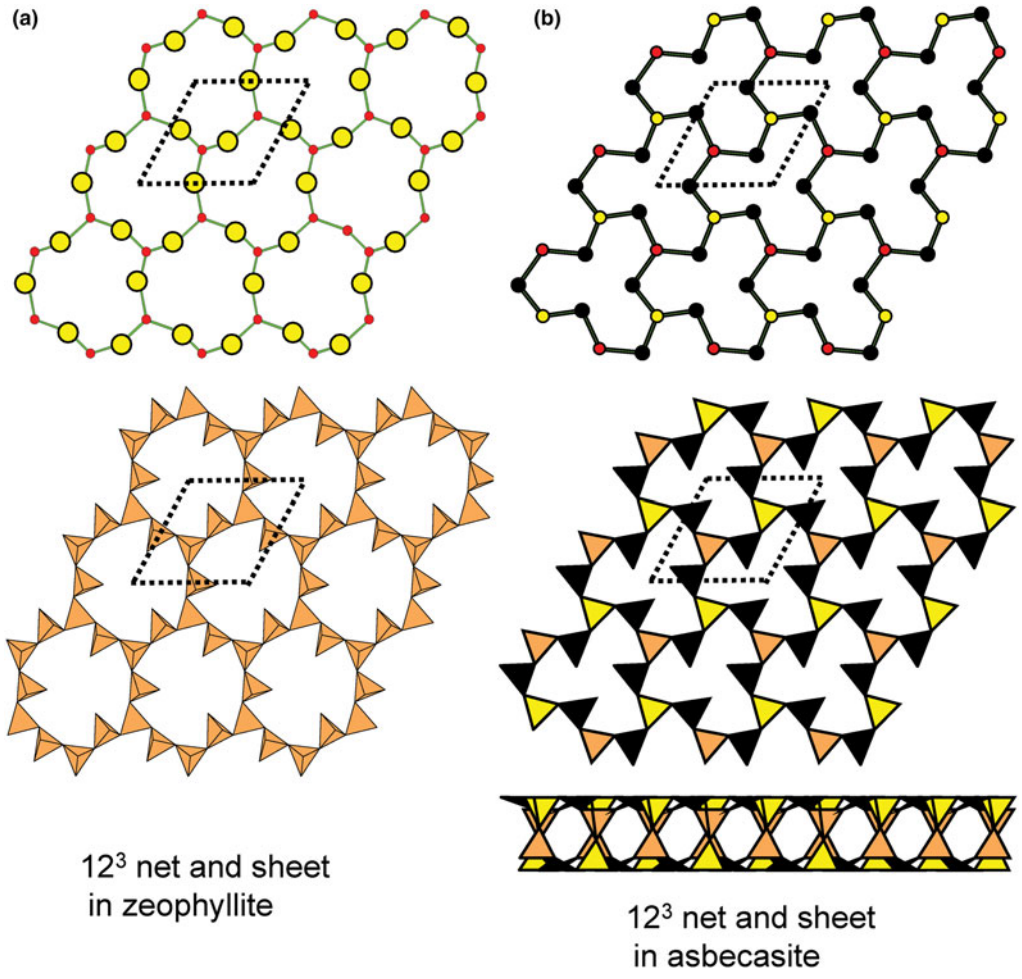

Fig. 47. Nets and corresponding structures derived from the 3-connected plane net 6^3 by insertion of six 2-connected vertices on edges between 3-connected vertices; (*a*) the $(12^2)_6(12^3)_6$ net and the single-layer sheet in **zeophyllite**; and (*b*) the $(12^2)_6(12^3)_6$ net and the parent upper-layer sheet in **asbecasite**. As^{3+}: black circles; As^{3+} polyhedra: black.

class-2 oikodoméic operation generating the lower-layer sheet from the parent upper-layer sheet. There is a 2_1 screw-rotation operation that generates the corresponding fragment from the lower-layer sheet (Fig. 39*b*, centre), producing the double-layer-sheet fragment in Fig. 39*b* (right). The resulting double-layer sheet is shown in Fig. 39*c* and its cross-section is shown in Fig. 39*d*. The interstitial complex in **seidite-(Ce)** consists of two Na^+ ions coordinated by $O_4^{2-}(H_2O)_3$ and $O_3^{2-}(H_2O)_4$, one Ce^{3+} ion coordinated by $O_3^{2-}(H_2O)_3$, and one Ti^{4+} ion coordinated by $O_4^{2-}(OH)_2^-$; there are five non-transformer (H_2O) groups.

Miscellaneous complex 3-connected nets

The simple nets are the basis of the more common groups of minerals, and also a single net can be the basis of several significantly different structures. This is not the case with the more complicated nets of Table 8. The parent single-layer of **chiappinoite-(Y)** is based on the 4.6.8 net (Fig. 40*a*); the four-membered ring has the arrangement (d^4), the six-membered ring has the arrangement (u^2d^4), and the eight-membered ring has the arrangement $(d^2u^2d^2u^2)$ (Fig. 40*b*). The sheet is folded (Fig. 40*c*) and a class-3 oikodoméic operation ***m*** gives rise to the double-layer sheet (Fig. 40*d*). The interstitial complex in **chiappinoite-(Y)** consists of one Y^{3+} ion coordinated by O_8^{2-} and one Mn^{2+} ion coordinated by O_8^{2-}.

The structure of **ajoite** has a parent $(5.6^2)_2(5.6.7)_4(5.7^2)_2(6^2.7)_6$ net (Fig. 41*a*) with 5-, 6- and 7-membered rings as the basis of its single-layer parent sheet. The upper-layer parent sheet has the following u–d structure: $(u^6)_3(u^4d^3)_2(u^3d^2)_2(u^2du^2d)_1$ (Fig. 41*b*) and the oikodoméic operation generating the double-layer structure is a class-2 ***m*** operation (Fig. 41*c*). The interstitial complex in **ajoite** consists of one positionally disordered K^+ ion coordinated by O_8^{2-}, and ten Cu^{2+} ions coordinated by $O_2^{2-}(OH)_4^-$, $O_3(OH)_3$ (×3), $O_4(OH)_2$ (×4) and $O_5(OH)$ (×2); there are two non-bonded interstitial (H_2O) groups.

The $(5.6.7)_4(5.6.8)_4(5.7.8)_4(5.7^2)_4(6^2.7)_2$ net (Fig. 41*d*) is the basis of the silicate sheet in **armbrusterite** (Fig. 41*e*) and has five-, six-, seven- and eight-membered rings. The u–d arrangements in the parent upper-layer sheet are as follows: $(u^5)_4(u^4d)_4(u_6)_4(u^5d^2)_4(u^4du^2d)_2$, and the oikodoméic operation generating the double-layer structure is a class-2 ***m*** operation (Fig. 41*f*). The interstitial complex in **armbrusterite** consists of two Na^+ ions coordinated by O_6^{2-} and $O_5^{2-}(OH)^-$, one Mn^{3+} ion coordinated by O_6^{2-}, five Mn^{2+} ions coordinated by $O_4^{2-}(OH)_2^-$ (×5), and eight disordered K^+ ions and disordered interstitial (H_2O) groups.

https://doi.org/10.1180/mgm.2018.152 Published online by Cambridge University Press

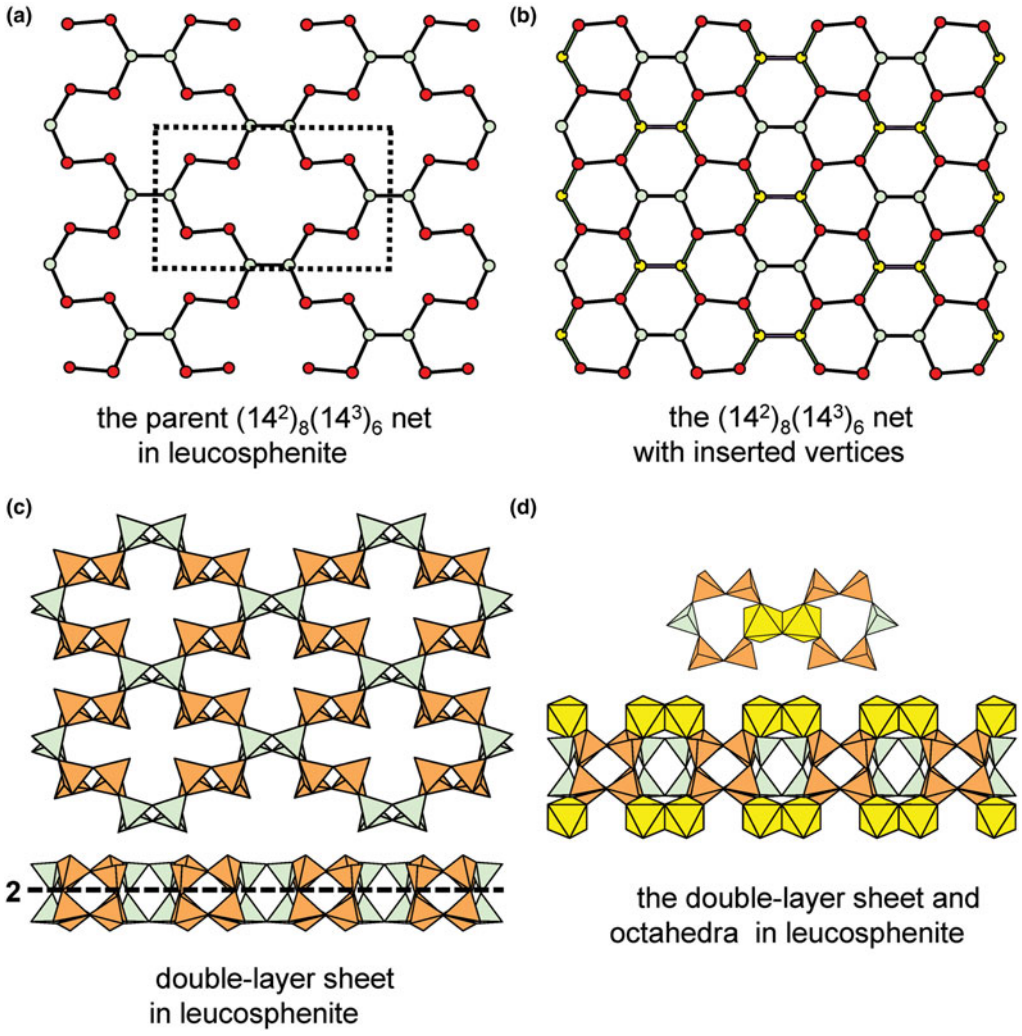

Fig. 48. Nets and corresponding structures derived from the 3-connected plane net 6^3 by insertion of pairs of 2-connected vertices on four edges between 3-connected vertices; (*a*) the $(14^2)_8(14^3)_6$ net in **leucosphenite**; (*b*) the $(14^2)_8(14^3)_6$ net with inserted 3-connected vertices; (*c*) the double-layer sheet in **leucosphenite**; and (*d*) cross-section of the double-layer sheet in **leucosphenite** with associated octahedra (shown in yellow).

The $(5.6^2)_6(6^3)_6(5.6.8)_{24}$ net that is the basis of the silicate sheet in **stilpnomelane** (Fig. 42*a*) (and presumably its Mg- and Mn-analogues **lennilenapeite** and **franklinphilite**) has five-, six- and eight-membered rings. In **stilpnomelane**, the u–d arrangements are as follows: (u^3d^2), (u^6), (d^6) and $(u^2d^2u^2d^2)$, and the oikodoméic operation is a class-2 ***m*** operation. The $(5.6^2)_8(5.7^2)_4(5.6.7)_8(6^2.7)_{12}$ net is the basis of the silicate sheet in **bannisterite** (Fig. 42*b*) and has five-, six- and seven-membered rings. In **bannisterite**, the u–d arrangements are as follows: (u^3d^2), (u^6), (u^2du^2d), (u^3d^4) and (u^5d^2), and the oikodoméic operation is ***m***. The $(4.5.12)_{24}(5.6^2)_{12}(6^3)_{12}(5.6.12)_{24}$ net is the basis of the silicate sheet in **parsettensite** (Fig. 42*c*) and has four-, five-, six- and twelve-membered rings. In **parsettensite**, the u–d arrangements are as follows: (d^4), (u^3d^2), (u^6) and $(u^2d^2u^2d^2u^2d^2)$, and the oikodoméic operation is a class-2 ***m*** operation. The interstitial complexes in **stilpnomelane, bannisterite** and **parsettensite** consist of sheets of octahedrally coordinated Fe^{2+} or Mn^{2+} with additional alkali- and alkaline-earth cations and (H_2O) groups that either have not been located or are strongly positionally disordered.

The structure of **ganophyllite** (Table 8) has been the object of much work since its description by Hamberg (1890). Noe and Veblen (1999) refined the **ganophyllite** structure in a subcell (a_{sub} x 3 = a) and presented high-resolution transmission electron microscopy evidence of incommensurate behaviour in some crystals (or parts of crystals). **Eggletonite** (Table 8) was described as the Na analogue of **ganophyllite**, and the structure was refined on a subcell (Peacor *et al.*, 1984). Hughes *et al.* (2003) solved the structure of an orthorhombic dimorph of **tamaite** (Table 8) and showed that the parent layer of the silicate double-layer sheet is based on the $(5.6^2)_6(5.6.7)_4(6^2.7)_{10}$ net (Fig. 43). This net has five-, six- and seven-membered rings with the following u–d arrangements in the parent single-layer: (u^3d^2), (u^6), (u^2du^2d) and (u^6d^2), and the oikodoméic operation is ***m***. The interstitial complexes in **ganophyllite, eggletonite** and **tamaite** consist of sheets of octahedrally coordinated Fe^{2+} or Mn^{2+} with additional alkali- and alkaline-earth cations and (H_2O) groups that either have not been located or are strongly positionally disordered.

The $(3.8^2)(6.8^2)$ net (Fig. 44*a*) consists of three-membered, six-membered and eight-membered rings in the ratio 2:1:3, and corresponds to the parent-layer silicate sheet in **zussmanite** (Fig. 44*b*) and presumably to the isostructural **coombsite** (Table 8). The u–d arrangements are (d^3), (u^6) and $(u^2d^2u^2d^2)$, and the oikodoméic operation is a class-3 ***m*** operation. The interstitial complex consists of two Fe^{2+} ions coordinated by

https://doi.org/10.1180/mgm.2018.152 Published online by Cambridge University Press

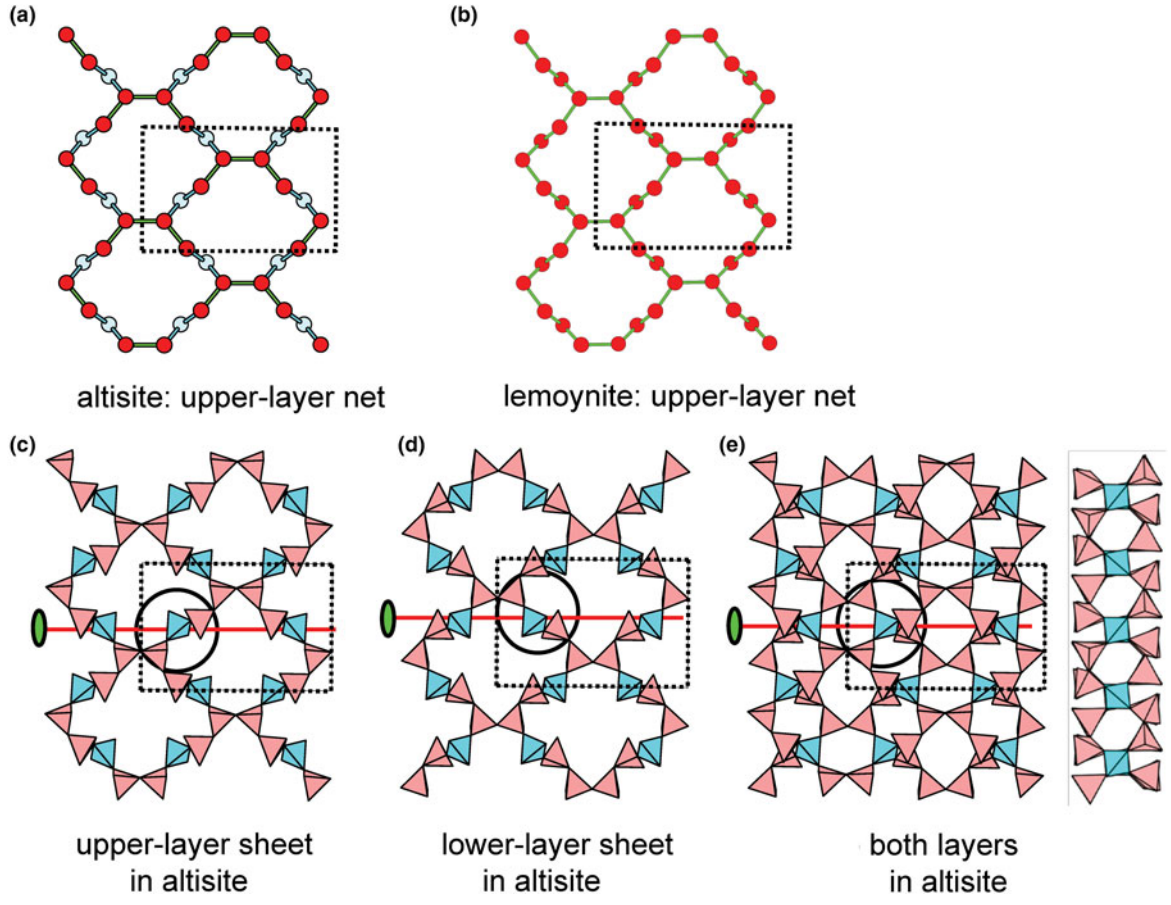

Fig. 49. Nets and corresponding structures derived from the 3-connected plane net 6^3 by insertion of pairs of 2-connected vertices on four edges between 3-connected vertices; (*a*) the $(14^2)_8(14^3)_6$ net in **altisite**; (*b*) the $(14^2)_8(14^3)_6$ net in **lemoynite**; (*c*) the upper-layer parent sheet in **altisite**; (*d*) the lower-layer parent sheet in **altisite**; and (*e*) the double-layer sheet **in altisite**. The class-3 oikodoméic operation is indicated.

$O_3^{2-}(OH)_3^-$ (×2), one site occupied by Fe^{2+} and smaller ions and coordinated by O_6^{2-}, and one K^+ ion coordinated by O_{12}^{2-}.

Double-layer sheets: 3-connected nets with inserted vertices

As with the single plane-nets, vertices may be inserted into parent 3-connected nets to form additional nets of different connectivities, and the 6^3 net seems to be dominant in this type of structure. Two-connected vertices may be inserted into a net in many different ways (e.g. Fig. 8). In double-layer minerals, there is (1) insertion on two *trans* edges, (2) insertion on three non-*trans* edges, (3) insertion on six edges, and (4) insertion of four pairs of 2-connected vertices on four *trans* edges.

The parent single-layer sheet in **esquireite** (Table 8) is based on the $(8^2)_2(8^3)_4$ net (Fig. 45*a*) in which 2-connected vertices (yellow circles) are inserted on one pair of *trans* edges of each parent six-membered ring. The parent single-layer sheet (Fig. 45*b*) has the u–d sequence (ud^2udud^2) with the inserted 2-connected vertices pointing down. A class-2 oikodoméic glide-operation generates the lower-layer sheet (Fig. 45*c*). The interstitial complex in **esquireite** consists of one Ba^{2+} ion but its coordination is uncertain because of partial occupancy of the sites coordinating the cation.

Figure 46 shows the 6^3 net with two 2-connected vertices inserted on two *trans* edges of alternate rows of six-membered rings to produce an $(8^2)_1(6^2.8)_2(6.8^2)_2$ net with the u–d sequence $(d^6)(d^3ud^3u)$. Where all vertices are occupied by Si^{4+}, this net is the basis of the upper single sheet in **tuscanite**; this sheet is replicated by an oikodoméic operation as shown in the lower part of Fig. 46*a*. This is a class-2 oikodoméic operation, a $\mathbf{2_1}$ screw axis; as this is a topological (as distinct from a geometrical) operation, the axis does not need to trace out a straight line, and it replicates the topology (linkage) of the tetrahedra, as is apparent from Fig. 46*a* (bottom). Chromatically different nets of the same topology (Figs 46*b*,*c*) are the bases of the double sheets in **latiumite** (Fig. 46*b*) and **synthetic $LaAlSiO_5$** (Fig. 46*c*). Ignoring the chromatic nature of the tetrahedra, the double-layer structure in **latiumite** is produced by a class-2 oikodoméic glide operation and the double-layer structure in **$LaAlSiO_5$** is produced by a class-2 2_1 screw axis operation, as is the case for **tuscanite**. The interstitial complex in **tuscanite** consists of three Ca^{2+} ions coordinated by O_8^{2-}, O_7^{2-} and O_6^{2-}, and one site partly occupied by both K^+ and (H_2O). The interstitial complex in **latiumite** consists of three Ca^{2+} ions coordinated by O_8^{2-} and O_7^{2-} (×2), one [10]-coordinated K^+, and one disordered $(SO_4)^{2-}$ / $(CO_3)^{2-}$ oxyanion group. The interstitial complex in **synthetic $LaAlSiO_5$** consists of three La^{3+} ions coordinated by O_8^{2-} and O_7^{2-} (×2), respectively.

In **zeophyllite** (Figs 8*b*,*c*, 47*a*), 2-connected vertices have been inserted in all edges of the 6^3 net. In **asbecasite** (Fig. 47*b*; Table 8), the parent net is topologically identical to that in **zeophyllite**,

https://doi.org/10.1180/mgm.2018.152 Published online by Cambridge University Press

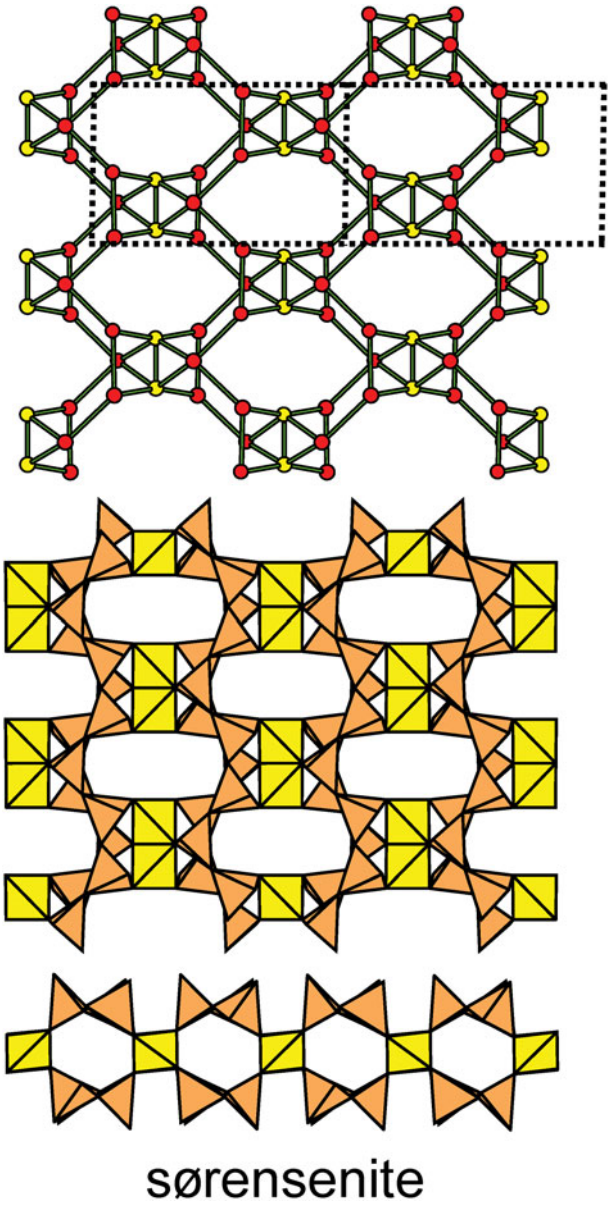

Fig. 50. Net and double-layer sheet with edge-sharing tetrahedra: the net and double-layer sheet in **sørensenite**; note the Be^{2+} tetrahedra that share edges to form $[Be_2O_6]$ dimers.

$(12^2)_3(12^3)_2$, albeit considerably geometrically distorted; Si^{4+} and Be^{2+} occupy the 3-connected vertices and As^{3+} occupies the 2-connected vertices. As is apparent in Fig. 46*b*, all Si^{4+} and Be^{2+} tetrahedra in the upper parent-layer point down, and hence are 4-connected in the double-layer sheet. The interstitial complex in **asbecasite** consists of one Ca^{2+} ion coordinated by O_8^{2-} and one Ti^{4+} ion coordinated by O_6^{2-}.

In **leucosphenite** (Fig. 48; Table 8), pairs of 2-connected vertices have been inserted into four edges of the 6^3 net to produce a $(14^2)_8(14^3)_6$ net; the 2-connected vertices are occupied by Si^{4+} and the 3-connected vertices are occupied by Al^{3+} (Fig. 48*a*). Substitution of pairs of vertices (pale blue in Fig. 48*b*) may be inserted to produce a 6^3 net. In the parent single-layer upper-sheet of Fig. 48*a*, all tetrahedra point down, (d^{14}), and the double-layer sheet is produced by a class-2 two-fold rotation oikodoméic operation (Fig. 48*c*). As is apparent in Fig. 48*d*, the substituted pairs of vertices correspond to octahedra that link adjacent double-layer sheets to form the complete structure. The interstitial complex in **leucosphenite** consists of two Na^+ ions coordinated by O_8^{2-} and O_7^{2-}, respectively, one Ba^{2+} ion coordinated by O_{10}^{2-}, and one Ti^{4+} ion coordinated by O_6^{2-}.

A topologically similar parent sheet occurs in the structures of **altisite, lemoynite** and **natrolemoynite** (Fig. 49; Table 8), but the colourings of the vertices are different. In **altisite** (Fig. 49; Table 8), all 2-connected vertices correspond to Al^{3+} tetrahedra (Fig. 49*a*), whereas in lemoynite, all vertices are occupied by Si^{4+} (Fig. 49*b*), and the ring sequence is $(u^2du^2du^4du^2d)$ (Fig. 49*c*). In Figs 49*c–e*, the 2-connected d tetrahedra are coloured blue, and their central cations are the centres of the class-3 oikodoméic two-fold rotation operation that repeats the upper parent single-sheet layer (Fig. 49*c*) to the lower single-layer sheet (Fig. 49*d*) to form the double-layer sheet (Fig. 49*e*). The interstitial complex in **altisite** consists of two K^+ ions, one of which is coordinated by O_8^{2-} and one of which shows positional disorder and is coordinated by O_6^{2-}, two Na^+ ions coordinated by O_6^{2-} (×2), and one Ti^{4+} ion coordinated by O_6^{2-}. The interstitial complex in **lemoynite** consists of one K^+ ion, coordinated by $O_5^{2-}(H_2O)$, one Ca^{2+} ion coordinated by $O_4^{2-}(H_2O)_3$, one half-occupied site containing Na^+ and coordinated by $O_3^{2-}(H_2O)_2$, and one Zr^{4+} ion coordinated by O_6^{2-}. The interstitial complex in **natrolemoynite** consists of disordered Na^+ ions, several (H_2O) groups, and one Zr^{4+} ion coordinated by O_6^{2-}.

Double-layer sheets: 3-connected nets with edge-sharing tetrahedra

Beryllium is an unusual tetrahedrally coordinated cation in that the (BeO_4) tetrahedron can share an edge with another (BeO_4) tetrahedron to form a $[Be_2O_6]$ group; these groups were first recognised by Belov (1958) and named *maple-tip groups*. Such a group occurs in the sheet structure of **sørensenite**, $Na_4Sn^{4+}[Be_2Si_6O_{18}](H_2O)_2$ (Fig. 50; Table 8), and the framework structures of **eudidymite** and **epididymite**, both $Na_2[Be_2Si_6O_{15}](H_2O)$ (Robinson and Fang, 1970; Fang *et al.*, 1972; Gatta *et al.*, 2008). In structure of **sørensenite**, the $[Be_2O_6]$ group links $[SiO_3]$ chains to form a thick sheet that resembles a double-layer arrangement, although it does not fit easily into the scheme used here because its description would involve a net with double edges. The structure of **sørensenite** has strong similarities to the structures of eudidymite and epididymite. The interstitial complex in **sørensenite** consists of two Na^+ ions, each coordinated by $O_6^{2-}(H_2O)$, one Sn^{4+} ion coordinated by O_6^{2-}, and one non-transformer (H_2O) group.

Double-layer sheets with omitted tetrahedra

Nets and sheets may also be generated by omission of vertices in simpler nets. For example, **diegogattaite** (Table 8) is a double-layer sheet-silicate mineral with a parent single-layer net (Fig. 51*a*) that at first sight seems rather complicated, with both 2-connected and 3-connected vertices and the net symbol $(6.14)_2(6.14^2)_4(14^2)_2$. We may derive this net by insertion of 2-connected vertices into edges of the 4.8^2 net (as outlined by Hawthorne, 2015*a*). However, this net may be derived in a much more simple fashion from the 6^3 net by deletion of one edge per hexagon (the dotted edges in Fig. 51*b*). The parent upper-layer sheet (Figs 51*c*,*d*) contains both u and d tetrahedra, and the double-layer sheet

https://doi.org/10.1180/mgm.2018.152 Published online by Cambridge University Press

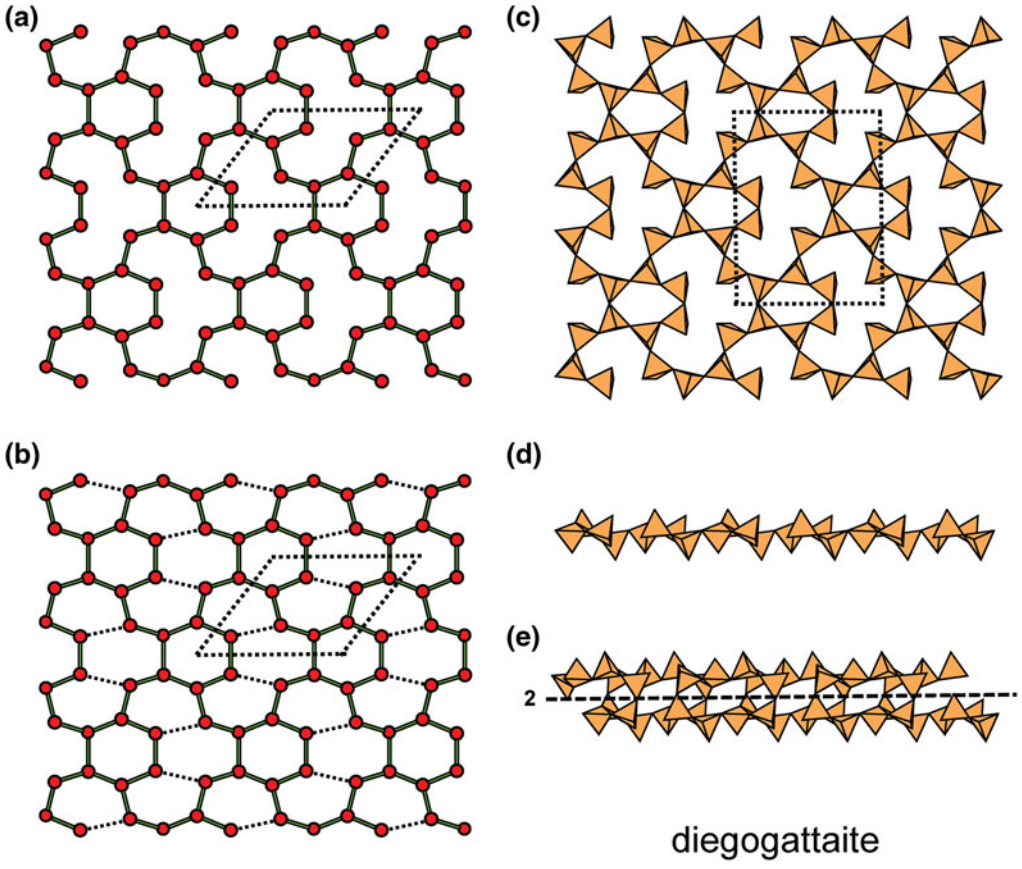

Fig. 51. Double-layer sheets with omitted tetrahedra: (*a*) the $(6.14)_2(6.14^2)_4(14^2)_2$ net in **diegogattaite**; (*b*) the 6^3 net with deleted edges (broken lines) that results in the $(6.14)_2(6.14^2)_4(14^2)_2$ net; (*c*,*d*) the upper-layer sheet of tetrahedra in **diegogattaite**; and (*e*) the double-layer sheet of tetrahedra in **diegogattaite** viewed in cross-section.

(Fig. 51*e*) is derived by the class-2 oikodoméic two-fold rotation operation. The interstitial complex in **diegogattaite** consists of three Na^+ ions coordinated by O_7^{2-}, O_8^{2-} and $O_6^{2-}(H_2O)$, one Ca^{2+} ion coordinated by O_6^{2-}, one Cu^{2+} ion coordinated by O_6^{2-}, and one inverse-transformer (H_2O) group.

Wickenburgite (Table 8) is a double-layer sheet-silicate mineral with a parent sheet based on the 6^3 net with the tetrahedra in the arrangement (u^3dud) (Fig. 52*a*). There is an incomplete class-2 oikodoméic operation (Hawthorne, 2015*a*) generating the lower-layer sheet: one tetrahedron in the upper parent single-layer sheet is not replicated by the oikodoméic operation; this 'missing' tetrahedron is shown in red in Figs 52*a*,*c* and is missing in the lower replicated single-layer sheet in Fig. 52*b*. The interstitial complex in **wickenburgite** consists of one Pb^{2+} ion coordinated by O_7^{2-}, one Ca^{2+} ion coordinated by $O_3^{2-}(H_2O)_3$, one Al^{3+} ion coordinated by O_6^{2-}, and one transformer (H_2O) group.

Mixed-layer sheets: Single-layer and double-layer sheets

A small number of minerals contain both one- and two-layer sheets. Although they fit into the hierarchy between one-layer and two-layer sheets (as their stoichiometry is, in principle, intermediate between these types of sheets), we will deal with them here because they incorporate aspects of both types of structure. All these minerals have both single-layer and double-layer sheets based on the 6^3 net and are listed in Table 9.

Reyerite has a single-layer sheet based on the 6^3 net with two types of six-membered rings with the u–d sequences (ududud) and (u^3d^3) in the ratio 1:3 (Fig. 53*a*). The parent upper single-layer net and sheet (Fig. 53*b*) are also based on the 6^3 net with two types of six-membered rings with the u–d sequences (u^6) and (u^2du^2d) in the ratio in the ratio 1:3 but where half of the d tetrahedra are occupied by Al^{3+} and half are occupied by Si^{4+}. The double-layer sheet is formed from a class-2 oikodoméic ***m*** operation.

Figure 54*a* shows the 6^3 sheet of tetrahedra that is the single-layer sheet in **minehillite**. It contains two types of six-membered rings with the following u–d arrangements: (ududud) and (u^3d^3) in the ratio 1:3, as in the single-layer sheet in **reyerite** (Fig. 53*a*). Figure 54*b* shows the idealised 6^3 net of the upper parent layer with two 2-connected vertices inserted on three non-*trans* edges of alternate rows of six-membered rings to produce a $(9^2)_3(6.9^2)_6$ net; the actual net in **minehillite** is shown in Fig. 54*c*. Where 2-connected vertices are occupied by Zn^{2+} and all 3-connected vertices are occupied by Si^{4+}, this net is the basis of the parent single-layer sheet in **minehillite** (Fig. 54*d*) which has the u–d arrangement (u^6) and ($u^2ou^2ou^2o$) in the ratio 1:2. This sheet is replicated by a class-3 two-fold rotation oikodoméic operation as shown in the lower part of Fig. 54*e*.

Jagoite has a single-layer sheet based on the $(12^2)_3(12^3)_2$ net (Fig. 55*a*) that also occurs in **zeophyllite** (Fig. 8*b*) and **asbecasite** (Fig. 47*b*). The sheet is further linked by Fe octahedra (Fig. 55*b*) that protrude above and below the plane of the constituent tetrahedra. The net of the parent single-layer sheet is also $(12^2)_3(12^3)_2$

https://doi.org/10.1180/mgm.2018.152 Published online by Cambridge University Press

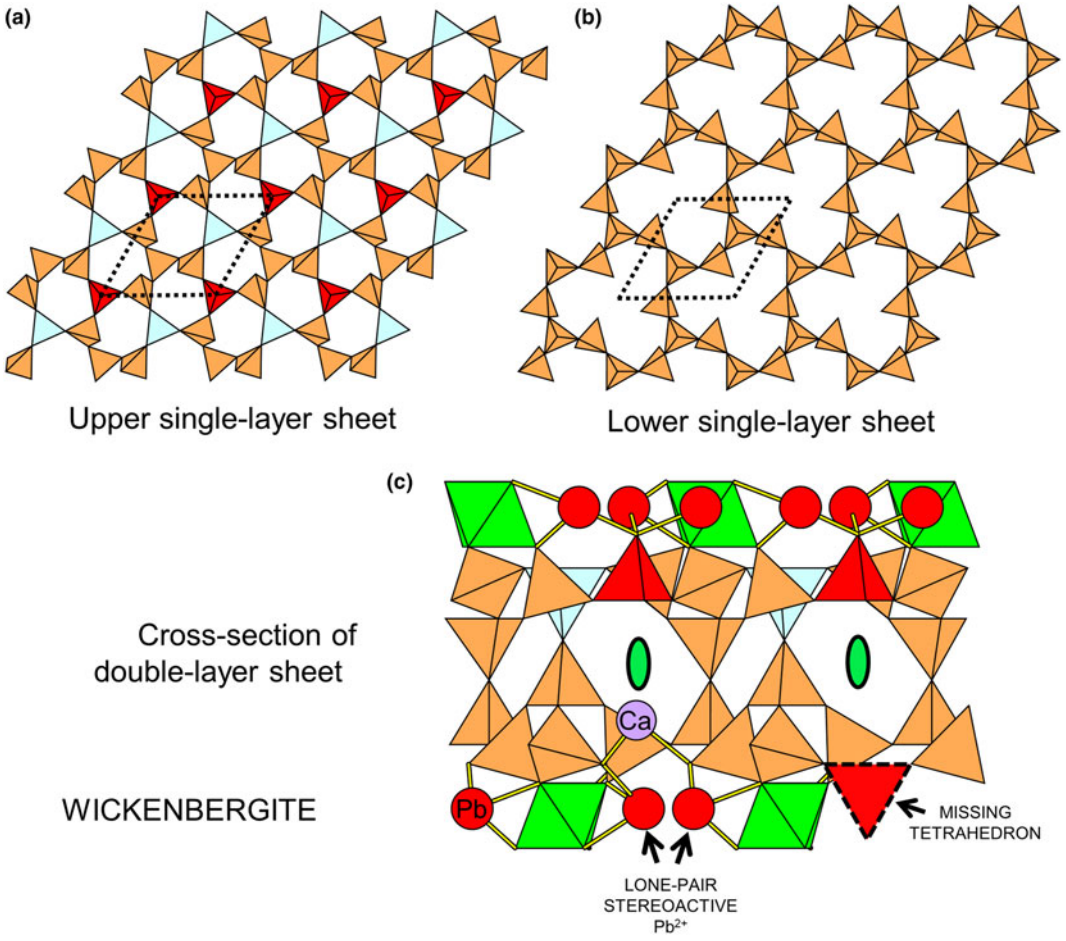

Fig. 52. Double-layer sheets with omitted tetrahedra: **wickenburgite**. (*a*) The parent upper-layer 6^3 sheet of tetrahedra; (*b*) the lower-layer single sheet of tetrahedra; and (*c*) cross-section of the double-layer sheet showing the class-2 oikodoméic 2-fold rotation operation orthogonal to the plane of the figure. Tetrahedra coloured red are present in the upper layer and are omitted in the lower layer; red circles: lone-pair stereoactive Pb^{2+}.

Table 9. Minerals with both single-layer and double-layer sheets.

Mineral	Nets	u–d configuration	Formula	T:O ratio	Fig. No.	Ref.
Reyerite	$[6^3]_8$ $[6^3]_8$	$(ududud)_1(u^3d^3)_3$ $(u^6)_1(u^2du^ud)_3$	$(Na,K)_2Ca_{14}$**$[Al_2Si_{22}O_{58}]$**$(OH)_8(H_2O)_6$	2.42	53, 56	(1)
Minehillite	$[6^3]_8$ $[(9^2)_3(6.9^2)_6]_1$	$(ududud)_1(u^3d^3)_3$ $(u^6)_1(u^2ou^2ou^2o)_2$	$K_2Ca_{28}Al_4$**$[Zn_5\square Si_{40}O_{112}]$**$(OH)_{16}$	2.49	54, 56	(2)
Jagoite	$[(12^2)_3(12^3)_2]_1$ $[(12^2)_3(12^3)_2]_1$	$(u^3du^3du^3d)$ $(u^3du^3du^3d)$	$Pb^{2+}_{22}Fe^{3+}_4$**$[Al_{10}Si_{26}O_{82}]$**Cl_6	2.28	55, 56	(3)

References: (1) Merlino (1988*b*); (2) Dai *et al*. (1995); (3) Mellini and Merlino (1981).

(Fig. 55*c*) but the twelve-membered rings are more open than is the case for the net of the single-layer sheet (Fig. 55*a*). The double-layer sheer (Fig. 55*d*) is formed by a class-2 oikodoméic ***m*** operation.

Cross-sectional views of these mixed-layer sheet-structures are shown in Fig. 56. In **reyerite** (Fig. 56*a*), the single- and double-layer sheets are linked through sheets of edge-sharing Ca^{2+} octahedra. In **minehillite** (Fig. 56*b*), the single- and double-layer sheets are also linked through sheets of edge-sharing Ca^{2+} octahedra. The single-layer sheets are similar in **reyerite** and **minehillite**, but the double sheets are quite different. As noted above, in **reyerite** the double-layer sheet is generated by a class-2 oikodoméic operation, whereas in **minehillite** the double-layer sheet is generated by a class-3 oikodoméic operation; moreover, the double-layer sheet in **minehillite** also incorporates octahedrally coordinated Al^{3+} (shown in red in Fig. 56*b*). In **jagoite** (Fig. 56*c*), the double-layer sheet is generated by a class-2 oikodoméic operation, and the single- and double-layer sheets are also linked through isolated Fe^{2+} octahedra (shown in green in Fig. 56*c*). The interstitial complex in **reyerite** consists of three Ca^{2+} ions coordinated by $O_3^{2-}(OH)_3^-$, $O_4^{2-}(OH)_2^-$ and $O_5^{2-}(OH)^-$, together with several disordered partly occupied sites containing Na^+ and (H_2O). The interstitial complex in **minehillite** consists of one K^+ ion coordinated by O_{12}^{2-}, three Ca^{2+} ions

https://doi.org/10.1180/mgm.2018.152 Published online by Cambridge University Press

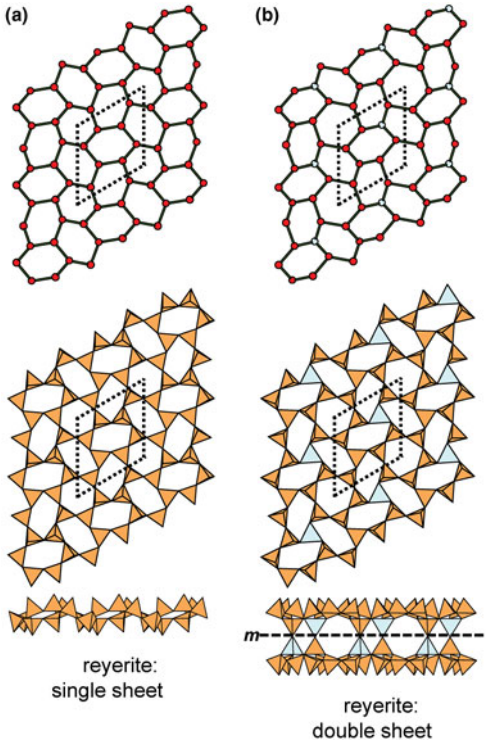

Fig. 53. Structures with both single-layer and double-layer sheets: **Reyerite**. (*a*) The 6^3 net and single-layer sheet; and (*b*) the parent upper-layer 6^3 net and double-layer sheet.

coordinated by $O_3^{2-}(OH)_3^-$, $O_4^{2-}(OH)_2^-$ and $O_5^{2-}(OH)^-$, and one Al^{3+} ion coordinated by O_6^{2-}. The interstitial complex in **jagoite** consists of two Pb^{2+} ions with strong lone-pair stereoactive behaviour, one Pb^{2+} ion with no lone-pair stereoactive behaviour, one [6]-coordinated Fe^{3+} ion coordinated by O_6^{2-}, and one Cl^- anion that bonds to the Pb^{2+} cations.

Multi-layer sheets

Three silicate minerals have been described as containing triple-layer sheets. An ideal triple-sheet structure is shown in Fig. 57. The parent sheet is based on a 6^3 net with an (ududud) arrangement (Figs 57*a*,*b*). An oikodoméic class-2 ***m*** operation produces a double-layer structure, and another oikodoméic class-2 ***m*** operation on the lower-layer sheet produces a third layer as shown in Fig. 57*c*. It must be borne in mind that oikodoméic operations are defined as acting on single parent sheets, and hence the second operation in Fig. 57 (the lower class-2 ***m*** operation) only acts on the single sheet generated by the first (the upper) class-2 ***m*** operation, not the double-layer structure produced by that operation. It is clear that such an arrangement has three layers, and no structure has yet been observed in minerals.

In **günterblassite, umbrianite** and **hillesheimite** (Table 10), the parent single-layer sheet is based on a 4.8^2 net (Fig. 58*a*) with a (u^3d) four-membered ring and a (u^4du^2d) eight-membered ring (Fig. 58*b*). The parent single-layer sheet (Fig. 58*c*) is repeated by a class-2 oikodoméic ***m*** operation to produce a (4.8^2) lower-layer sheet with the u–d arrangement (ud^3) and (ud^4ud^2) (Fig. 58*d*) that functions as a parent layer for a class-3 oikodoméic ***m*** operation. A third class-2 oikodoméic ***m*** operation produces the structure of **umbrianite** shown in Fig. 58*e*. The interstitial cations and anions in **günterblassite** are somewhat

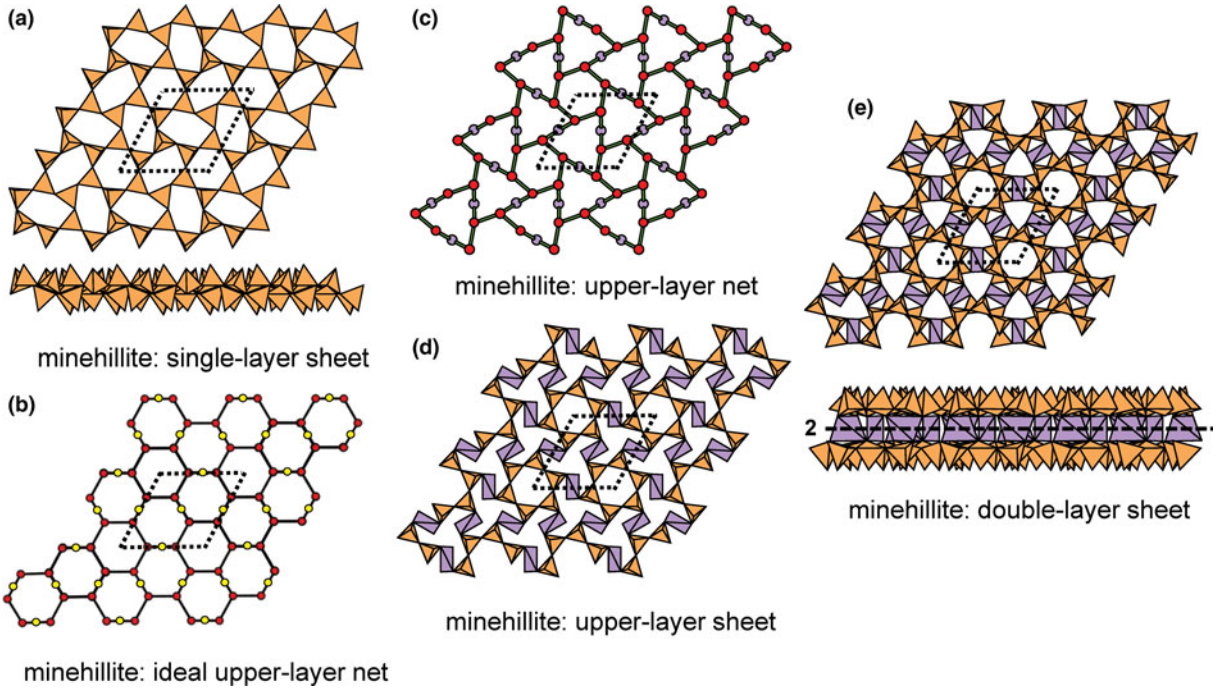

Fig. 54. Structures with both single-layer and double-layer sheets: **minehillite**. (*a*) The 6^3 net and single-layer sheet; (*b*) the parent upper-layer 6^3 net with inserted 2-connected vertices on three non-*trans* edges between 3-connected vertices in one-third of the six-membered rings; (*c*) the parent upper-layer $(9^2)_3(6.9^2)_6$ net in **minehillite**; (*d*) the parent upper-layer sheet in **minehillite**; and (*e*) the double-layer sheet in **minehillite**. Two-connected vertices: yellow circles, mauve circles; Zn tetrahedra: mauve.

https://doi.org/10.1180/mgm.2018.152 Published online by Cambridge University Press

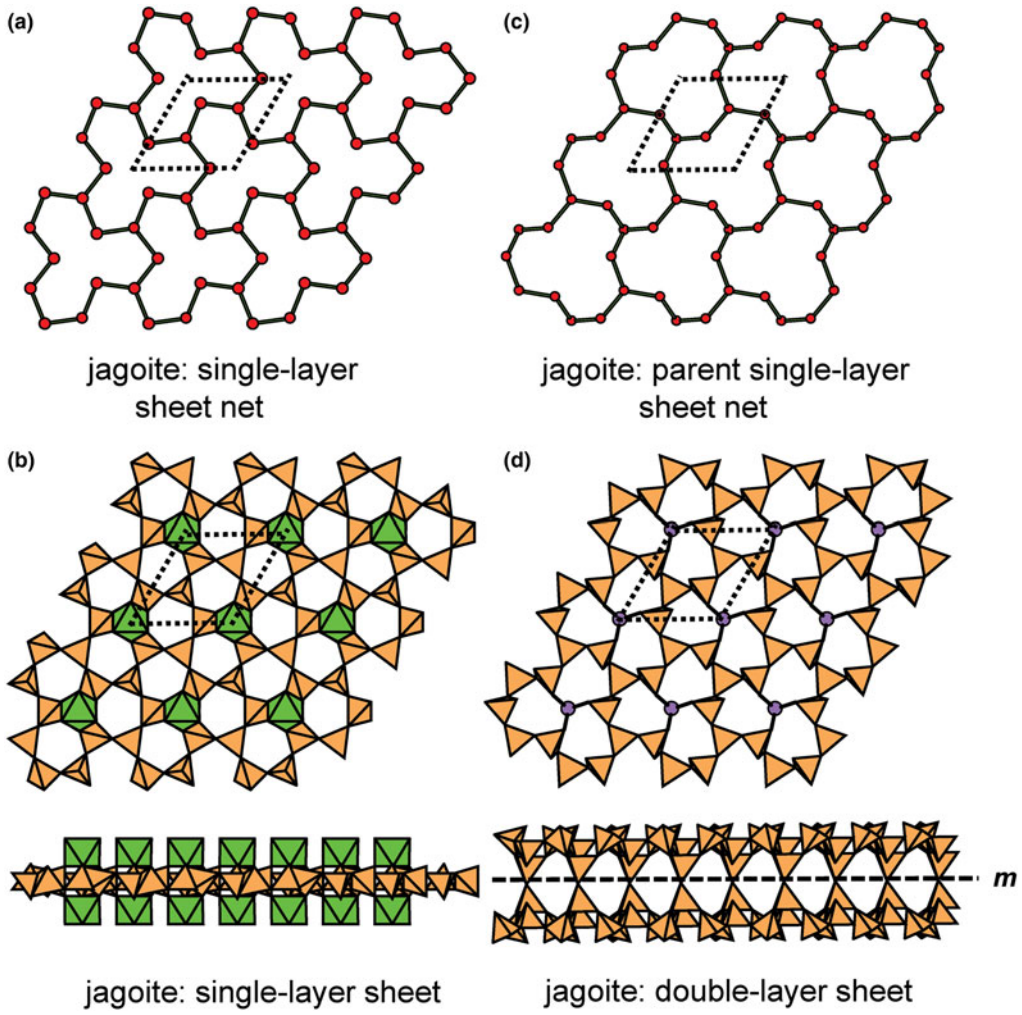

Fig. 55. Structures with both single-layer and double-layer sheets: **jagoite**. (*a*) The net of the single-layer sheet; (*b*) view and cross-section of the single-layer sheet; (*c*) the net of the parent single-layer sheet; and (*d*) the parent single-layer sheet with linking As trigonal pyramids and a cross-section view of the double-layer sheet. Green: Fe octahedra.

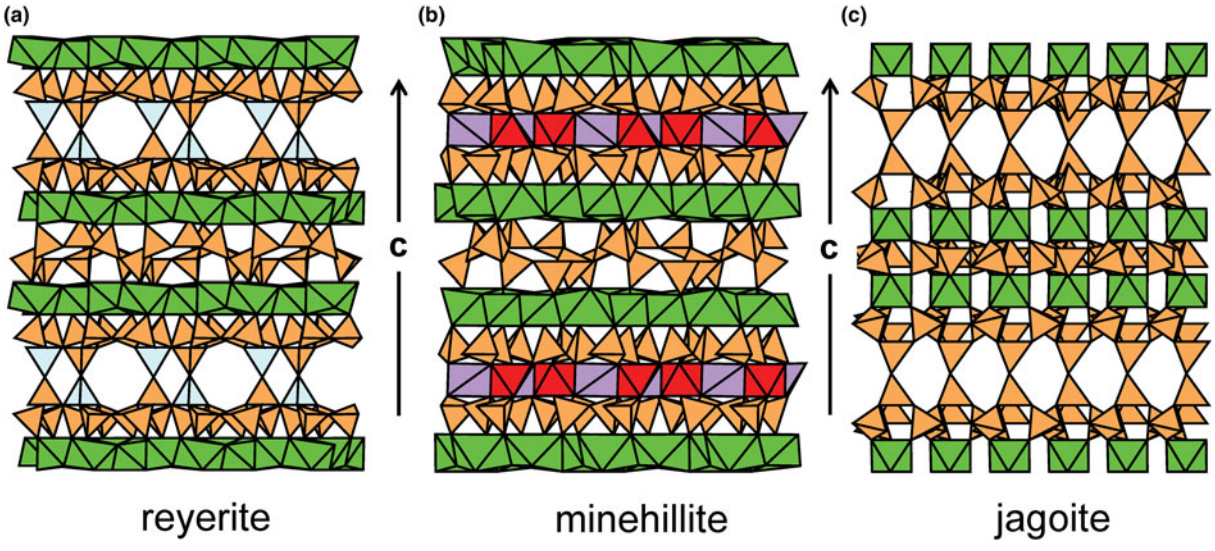

Fig. 56. Cross-sections of structures with both single-layer and double-layer sheets: (*a*) **reyerite**; (*b*) **minehillite**; and (*c*) **jagoite**.

https://doi.org/10.1180/mgm.2018.152 Published online by Cambridge University Press

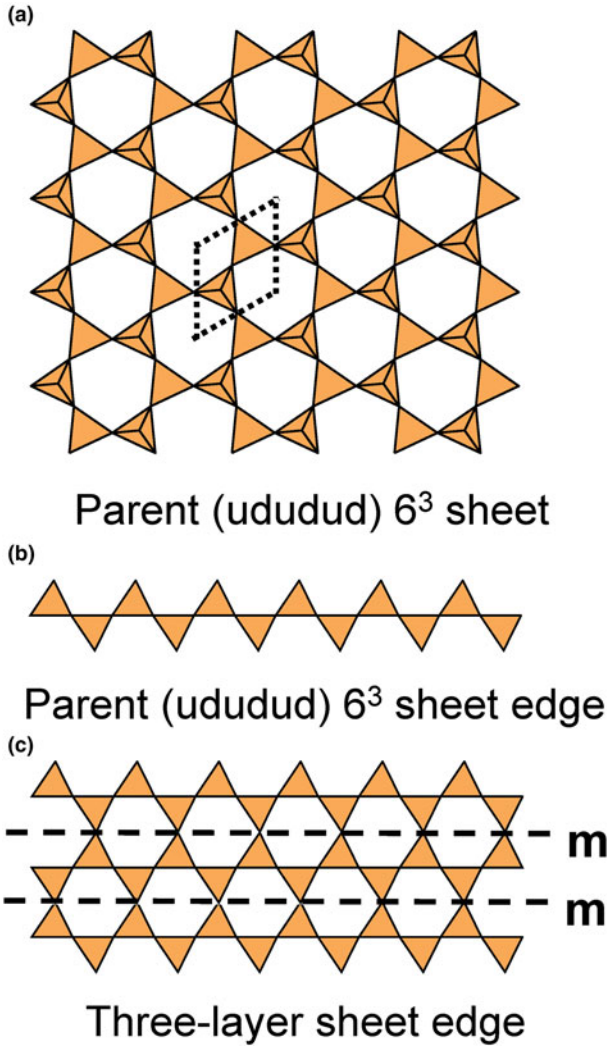

Fig. 57. A hypothetical structure with a triple-layer sheet: (*a*) the parent 6^3 sheet with (ududud) tetrahedra; (*b*) edge view of the parent 6^3 sheet with (ududud) tetrahedra; and (*c*) triple-layer sheet formed from two class-2 oikodoméic mirror operations.

disordered, making assignment of coordinations unreliable. However, this is not the case for **umbrianite** and **hillesheimite**. The interstitial complex in **umbrianite** consists of three well-ordered K^+ ions coordinated by $O^{2-}_{10}Cl^-_2$, $O^{2-}_8Cl^-_2$ and $O^{2-}_8F^-Cl^-$, two sites containing K^+ that are too close to be both locally occupied but with coordinations $O^{2-}_8Cl^-_2$ (×2), one Na^+ ion coordinated by $O^{2-}_6F^-_2$, and one Ca^{2+} ion coordinated by $O^{2-}_5F^-$. The interstitial complex in **hillesheimite** consists of one K^+ ion coordinated by $O^{2-}_5(H_2O)_4$, one Mg^{2+} ion coordinated by $O^{2-}_5(H_2O)$, and four transformer (H_2O) groups.

Establishing the hierarchy within sheet silicates

In terms of the silicates as a whole, there is a decrease in the T:O ratio with increasing polymerisation, from TO_4 in neso-silicates to TO_2 in completely connected tecto-silicates. In this regard, it is logical to hierarchically arrange the sheet silicates in terms of decreasing T:O ratio, i.e. TO_x with decreasing x as an indicator of increasing connectivity. This is done in Table 11.

The range in x values for the reduced stoichiometry TO_x shown by sheet silicates varies from 3 to 2, i.e. from the maximum upper limit of x for chain silicates (TO_3) to the lower limit for framework silicates (TO_2). How is this possible? Consider the simple TO_3 graph shown in Fig. 59*a*; each vertex in this graph is 2-connected. The relation between tetrahedron connectivity and stoichiometry is shown in Fig. 60. A 3-connected tetrahedron (Fig. 60*a*) contributes $TO_{2.5}$ to the overall formula, a 2-connected tetrahedron (Fig. 60*b*) contributes TO_3 to the overall formula, and a 4-connected tetrahedron (Fig. 60*c*) contributes TO_2 to the overall formula. In Fig. 59*a*, each vertex is 2-connected and hence the stoichiometry of the corresponding chain of tetrahedra is TO_3. If we add another vertex to this graph, as in Fig. 59*b*, the connectivity of that vertex is 1, but this connectivity of the vertex to which it is linked becomes 3, and so there is no net change in the average tetrahedron connectivity and hence no change in the stoichiometry of the corresponding arrangement of tetrahedra. We may add vertices to the graph of Fig. 59*b* in such a way as to change the mean connectivity, as shown in Fig. 59*c*: an additional vertex is added to the graph of Fig. 59*b*, but two (not one) additional edges are added (i.e. the tetrahedra form a ring), the connectivity of the additional vertices is now 2, not 1 as in the graph of Fig. 59*b*. From this discussion, we may conclude that: (1) a chain silicate cannot have TO_x with $x > 3.0$; and (2) a sheet silicate cannot have TO_x with $x = 3.0$.

Inspection of Table 11 shows that **hyttsjöite** has a tetrahedron stoichiometry $[Si_{30}O_{90}] = [SiO_3]_{30}$. This does not seem possible according to the above argument; how does this happen? In the structure of **hyttsjöite** (Fig. 9; Tables 3, 11), there are two layers of tetrahedra. One layer is based on a 6^3 net into which pairs of 2-connected vertices are inserted in each edge to form a $(14^2)_8(14^3)_6$ net (Fig. 9*a*). The stoichiometry of the resultant sheet (Fig. 9*a*) arises as follows: the outline of the unit cell contains two 3-connected tetrahedra and six 2-connected tetrahedra for a T:O ratio of 8:2.5 x 2 + 3.0 x 6 = 8:23. The other layer of tetrahedra in the structure is discontinuous in terms of its linkage of tetrahedra (Fig. 9*b*), although it is continuous in terms of its strong bonds, as short Pb^{2+}–O^{2-} bonds link the tetrahedra into a sheet of strong bonds. In Fig. 9*b*, the 3-connected tetrahedra are orange-brown,

Table 10. Minerals with multi-layer sheets.

Mineral	Nets	u–d configurations	Formula	T:O ratio	Fig. No.	Ref.
Günterblassite	$[(4.8^2)]_4$ $[(4.8^2)]_4$	$(u^3d)(u^4du^2d)$ $(ud^3)(ud^4ud^2)$	$(K,Ca)_{3-x}Fe$**$[(Si,Al)_{13}O_{25}(OH,O)_4]$**$(H_2O)_7$	2.230	--	(1)
Hillesheimite	$[(4.8^2)]_4$ $[(4.8^2)]_4$	$(u^3d)(u^4du^2d)$ $(ud^3)(ud^4ud^2)$	$(K,Ca,\square)_2(Mg,Fe,Ca,\square)_2$**$[(Si,Al)_{13}O_{23}(OH)_6]$**$(OH)(H_2O)_8$	2.230	58	(2)
Umbrianite	$[(4.8^2)]_4$ $[(4.8^2)]_4$	$(u^3d)(u^4du^2d)$ $(ud^3)(ud^4ud^2)$	$K_7Na_2Ca_2$**$[Al_3Si_{10}O_{29}]$**F_2Cl_2	2.230	58	(3)

References: (1) Chukanov *et al.* (2012*a*); Rastsvataeva *et al.* (2012); (2) Chukanov *et al.* (2013); and (3) Sharygin *et al.* (2013).

https://doi.org/10.1180/mgm.2018.152 Published online by Cambridge University Press

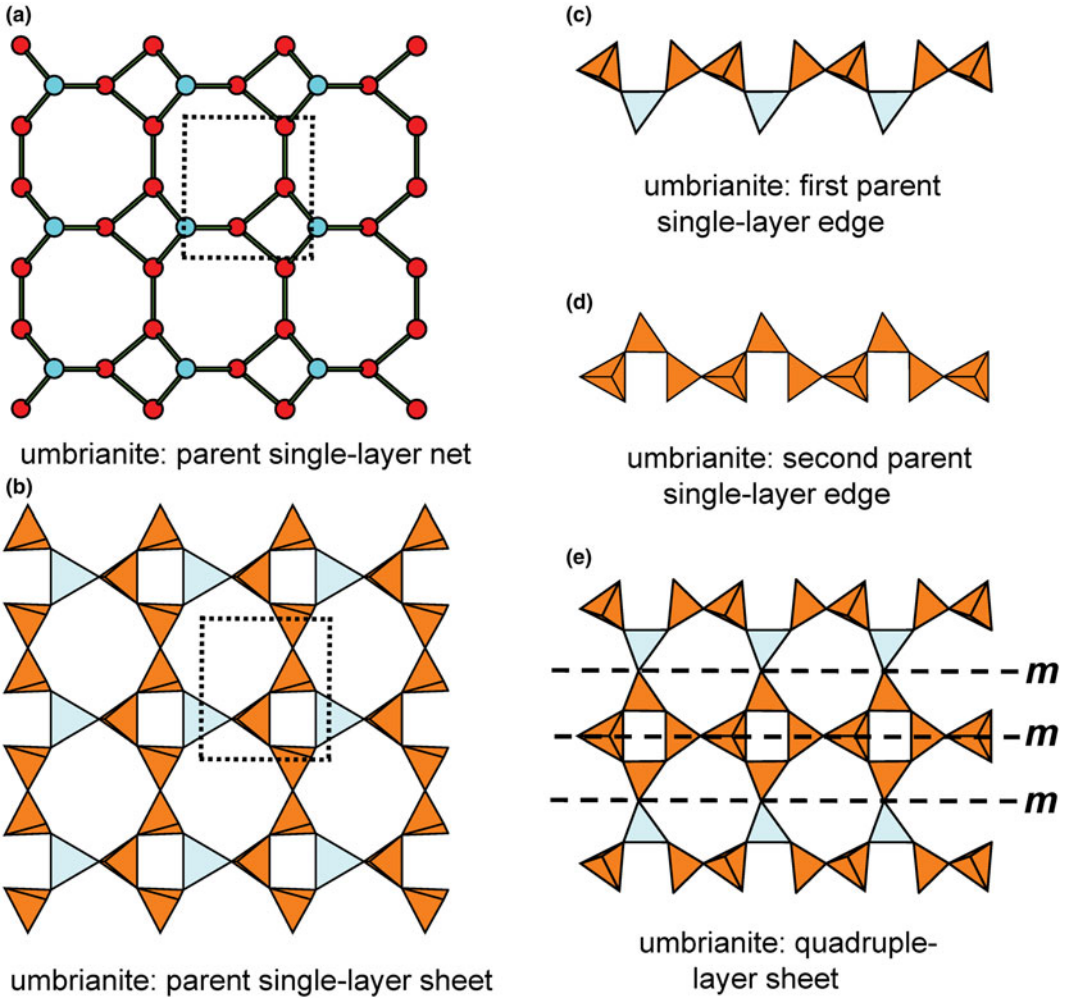

Fig. 58. Structures with multi-layer sheets: **umbrianite**. (*a*) The (4.8^2) net of the first parent single-layer sheet; (*b*) the first parent single-layer sheet; (*c*) the first parent single-layer sheet viewed "on edge"; (*d*) the second parent single-layer sheet viewed 'on edge'; and (*e*) the multi-layer sheet, showing the generating class-2 and class-3 oikodoméic mirror operations.

the 2-connected tetrahedra are yellow and the 1-connected tetrahedra are blue. The outline of the unit cell contains one 3-connected tetrahedra, three 2-connected tetrahedra and three 1-connected tetrahedra for a T:O ratio of 8:2.5 x 1 + 3.0 x 3 + 3.5 x 3 = 7:22. The aggregate formula is $T_{8+7}O_{23+22} = T_{15}O_{45}$ which, with T = Si and Z = 3, translates into $Si_{30}O_{90}$ in the formula (Tables 3, 11). Comparison of Figs 9*a* and 9*b* shows that lone-pair stereoactive Pb^{2+} has taken the place of a Si^{4+} ion in the lower layer of tetrahedra, changing the connectivity and hence the stoichiometry of the silicate component. Thus the **hyttsjöite** structure has a sheet-silicate unit and a silicate cluster, and it is the presence of this silicate cluster, with tetrahedra that are 1-connected, that allows the 'impossible' sheet stoichiometry of **hyttsjöite**. There is another example of a combination of different structural motifs in the sheet silicates. **Okenite** (Tables 5 and 11) has both a silicate sheet (Fig. 22*b*) and a silicate chain (Fig. 22*c*), and this has the effect of raising the TO_x value of okenite above the value of 2.5 that is characteristic of 3-connected nets.

At the other end of the scale, there are seven sheet-silicate minerals with a TO_x value of 2.0 (Table 11) that is the lowest possible value for 4-connected nets and framework silicates. This stoichiometry can be accommodated in a sheet by the linkage shown in Fig. 36 in which all the tetrahedra are 4-connected. Of course, for SiO_2, this would require the sheets to be held in a crystal structure by van Der Waals bonds, but this does not seem beyond the realm of possibility as there are several minerals in which such a mechanism is operative (e.g. **rutherfordine**; Finch *et al.*, 1999). More commonly, lower-valence cations partly substitute for Si^{4+}, requiring the presence of interstitial species that link the sheets into a structure, e.g. **dmisteinbergite**, Ca $[Al_2Si_2O_8]$ and **hexacelsian**, Ba$[Al_2Si_2O_8]$ (Fig. 36*a*; Table 7).

Broad compositional variations as a function of polymerisation

One of the advantages of establishing a hierarchy is that one is able to see at a glance the range in observed compositions shown by the major divisions in that hierarchy. This information is shown for the silicate minerals in Fig. 61. Compositions extend from TO_4, the composition of an isolated (TO_4) group, to TO_2, the composition of a completely connected $[TO_2]$ framework. Of more interest is the overlap in composition between the various major groups of connectivities. We have divided the structures into 0-dimensional **clusters**, 1-dimensional

https://doi.org/10.1180/mgm.2018.152 Published online by Cambridge University Press

Table 11. Structure hierarchy for sheet-silicate minerals.

Mineral	Formula	T:O ratio	Net*	P/F/ M*	*S/D/ M***	Fig. No.
Hyttsjöite	$Pb_{18}Ba_2Ca_5Mn^{2+}_2Fe^{3+}_2$**[$Si_{30}O_{90}$]**$Cl(H_2O)_6$	3.00	$[(14^2)_6(14^3)_2]_1$	P	*S*	9
Zeophyllite	Ca_{13}**[Si_5O_{14}]$_2$**$F_{10}(H_2O)_6$	2.80	$[(12^2)_3(12^3)_2]_1$	P	*S*	8*a*,*b*,*c*
Britvinite	$Pb_{15}Mg_9$**[$Si_{10}O_{28}$]**$(BO_3)_4(CO_3)_2(OH)_{12}O_2$	2.80	$[(12^2)_3(12^3)_2]_2$	P	*S*	"
Molybdophyllite	Pb_8Mg_9**[$Si_{10}O_{28}$]**$(OH)_8\|O_2\|(CO_3)_3(H_2O)$	2.80	$[(12^2)_3(12^3)_2]_2$	P	*S*	"
Tumchaite	$Na_2(Zr,Sn)$**[Si_4O_{11}]**$(H_2O)_2$	2.75	$[(10^2)_4(10^3)_4]_1$	1F	*S*	8*d*,*e*,*f*
Seidite-(Ce)	Na_4Ce_2Ti**[Si_8O_{22}]**$(OH)(H_2O)_5$	2.75	$[4.8^2]_8$	P	*D*	39
Kvanefjeldite	$Na_4(Ca,Mn)$**[Si_6O_{16}]**	2.67	$[(8^2)_4(8^3)_8]_1$	1F	*S*	8*h*,*I*,*j*
Ganophyllite	$[Ca_x(K, Na)_y(Mn_{6-z}Al_z)]_{\Sigma10}[Si_8(Al_{2x+y+z}Si_{2-2x-y-z})]$ $O_{24}(OH)_4(H_2O)_n$	~2.67	----	P	*D*	---
Eggletonite	$(Na,K,Ca)_{1.61}(Mn,Fe,Mg,Al)_8(Si,Al)_{12}O_{29}(OH)_7$ $(H_2O)_{8-9}$	~2.67	Iso ganophyllite	P	*D*	---
Tamaite	KMn_6**[Si_5AlO_{24}]**$(OH)_4(H_2O)_n$	2.67	$[(5.6^2)_6(5.6.7)_4(6^2.7)_{10}]_1$	P	*D*	43
Altisite	$Na_3K_6Ti_2$**[$Al_2Si_8O_{26}$]**Cl_3	2.60	$[(14^2)_8(14^3)_4]_1$	P	*D*	49*a*,*c*
Lemoynite	$(Na,K)CaZr_2$**[$Si_{10}O_{26}$]**$(H_2O)_{5-6}$	2.60	$[(14^2)_8(14^3)_4]_1$	P	*D*	49*b*
Natrolemoynite	Na_4Zr_2**[$Si_{10}O_{26}$]**$(H_2O)_9$	2.60	$[(14^2)_8(14^3)_4]_1$	P	*D*	49*b*
Okenite	Ca_{10}**[(Si_6O_{16})(Si_6O_{15})$_2$]**$(H_2O)_{18}$	2.56	$[(5^2.8)_2(5.8^2)_1]_2$	P	*S*	22*b*
Chlorite group	M_6**[T_4O_{10}]**$(OH)_8$	2.50	$[6^3]_2$	P	*S*	1*a*
Kaolinite subgroup	M_3**[T_2O_5]**$(OH)_4$	2.50	$[6^3]_2$	P	*S*	1*a*
Mica supergroup	AM_3**[T_4O_{10}]**$(OH)_2$	2.50	$[6^3]_2$	P	*S*	1*a*
Serpentine subgroup	M_3**[T_2O_5]**$(OH)_4$	2.50	$[6^3]_2$	P	*S*	1*a*
Talc group	M_3**[T_4O_{10}]**$(OH)_2$	2.50	$[6^3]_2$	P	*S*	1*a*
Chlorite group	M_6**[T_4O_{10}]**$(OH)_8$	2.50	$[6^3]_2$	P	*S*	1*a*
Clay minerals	M_6**[T_4O_{10}]**$(OH)_8$	2.50	$[6^3]_2$	P	*S*	1*a*
Hanjiangite	M_3**[T_2O_5]**$(OH)_4$	2.50	$[6^3]_2$	P	*S*	1*a*
Gyrolite	$NaCa_{16}$**[($Si_{23}Al$)O_{60}]** $(OH)_8(H_2O)_{14}$	2.50	$[6^3]_8$	P	*S*	11*a*
Ellingsenite	$Na_3Ca_4(NaCa)Si_{16}O_{36}(OH)_6(H_2O)_2$	2.50	$[6^3]_8$	P	*S*	11*b*
Martinite	$(Na,\square)_{13}Ca_4$**[$Si_{14}B_2O_{38}(OH)_2$]**$F_2(H_2O)_4$	2.50	$[6^3]_8$	P	*S*	11*c*
Cairncrossite	Sr_2Ca_7**[$Si_{16}O_{40}$]**$(OH)_2(H_2O)_{15}$	2.50	$[6^3]_8$	P	*S*	11*d*
Natrosilite	Na_2**[Si_2O_5]**	2.50	$[6^3]_4$	P	*S*	11*c*
Kanemite	Hna**[Si_2O_5]**$(H_2O)_3$	2.50	$[6^3]_4$	1F	*S*	12*a*
Sanbornite	Ba**[Si_2O_5]**	2.50	$[6^3]_4$	1F	*S*	12*a*
Makatite	Na_2**[Si_4 $O_8(OH)_2$]**$(H_2O)_4$	2.50	$[6^3]_4$	1F	*S*	12*b*
Pentagonite	$CaV^{4+}O$**[Si_4O_{10}]**$(H_2O)_4$	2.50	$[6^3]_8$	P	*S*	13*a*
Silinaite	$NaLi$**[Si_2O_5]**$(H_2O)_2$	2.50	$[6^3]_4$	P	*S*	13*b*
Plumbophyllite	Pb_2**[Si_4O_{10}]**(H_2O)	2.50	$[6^3]_8$	P	*S*	13*c*
Palygorskite	$MgAl$**[Si_4O_{10}]**$(OH)(H_2O)_4$	2.50	$[6^3]_8$	P	*S*	14*a*
Tuperssuatsiaite	$Na_{(2-x)}(Fe^{3+},Mn)_3$**[Si_8O_{20}]**$(OH)_2(H_2O)_4$	2.50	$[6^3]_8$	P	*S*	14*a*
Windhoekite	$Ca_2Fe^{3+}_{(3-x)}$**[($Si,Al)_8O_{20}$]**$(OH)_4(H_2O)_{10}$	2.50	$[6^3]_8$	P	*S*	14*a*
Yofortierite	$(Mn^{2+},Mg,Fe^{3+},\square)_5$**[$Si_8O_{20}$]**$(OH)_2(H_2O)_9$	2.50	$[6^3]_8$	P	*S*	14*a*
Raite	$Na_3Mn_3Ti_{0.25}$**[Si_2O_5]**$_4(OH)_2(H_2O)_{10}$	2.50	$[6^3]_8$	P	*S*	14*b*
Kalifersite	$(K,Na)_5Fe^{3+}_7$**[$Si_{20}O_{50}$]**$(OH)_6(H_2O)_{12}$	2.50	$[6^3]_{10}$	P	*S*	15*a*
Sepiolite	$(Mg,Fe,Al)_4$**[Si_2O_5]**$_3(O,OH)_2(H_2O)_4$	2.50	$[6^3]_{12}$	P	*S*	15*b*
Loughlinite	Na_2Mg_3**[Si_6O_{15}]**$O(H_2O)$	2.50	$[6^3]_{12}$	P	*S*	15*b*
Antigorite	Mg_{48}**[Si_4O_{10}]**$_{8.5}(OH)_{62}$	2.50	$[6^3]_{28}$	P	*S*	15*c*
Datolite	Ca**[$BSiO_4(OH)$]**	2.50	$[4.8^2]_8$	P	*S*	16*b*
Gadolinite-(Ce)	Ce_2Fe^{2+}**[$Be_2Si_2O_{10}$]**	2.50	$[4.8^2]_8$	P	*S*	16*b*
Gadolinite-(Y)	Y_2Fe^{2+}**[$Be_2Si_2O_{10}$]**	2.50	$[4.8^2]_8$	P	*S*	16*b*
Hingganite-(Ce)	$Ce_2\square$**[$Be_2Si_2O_8(OH)_2$]**	2.50	$[4.8^2]_8$	P	*S*	16*b*
Hingganite-(Y)	$Yb_2\square$**[$Be_2Si_2O_8(OH)_2$]**	2.50	$[4.8^2]_8$	P	*S*	16*b*
'Hingganite-(Yb)'	$Y_2\square$**[$Be_2Si_2O_8(OH)_2$]**	2.50	$[4.8^2]_8$	P	*S*	16*b*
'Calcybeborosilite'	$CaY\square$**[$BeBSi_2O_8(OH)_2$]**	2.50	$[4.8^2]_8$	P	*S*	16*b*
Homilite	Ca_2Fe^{2+}**[$B_2Si_2O_{10}$]**	2.50	$[4.8^2]_8$	P	*S*	16*b*
Minasgeraisite-(Y)	CaY_2**[$Be_2Si_2O_{10}$]**	2.50	$[4.8^2]_8$	P	*S*	16*b*
Apophyllite-(KF)	KCa_4**[Si_4O_{10}]**$_2F(H_2O)_8$	2.50	$[4.8^2]_8$	P	*S*	17*a*
Apophyllite-(KOH)	KCa_4**[Si_4O_{10}]**$_2(OH)(H_2O)_8$	2.50	$[4.8^2]_8$	P	*S*	17*a*
Apophyllite-(NaF)	$NaCa_4$**[Si_4O_{10}]**$_2F(H_2O)_8$	2.50	$[4.8^2]_8$	P	*S*	17*a*
Cavansite	CaV**[Si_4O_{10}]**$O(H_2O)_4$	2.50	$[4.8^2]_4$	P	*S*	17*b*
Cryptophyllite	K_2Ca**[Si_4O_{10}]**$(H_2O)_5$	2.50	$[4.8^2]_4$	P	*S*	18*a*
Mountainite	KNa_2Ca_2**[$Si_8O_{19}(OH)$]**$(H_2O)_6$	2.50	$[4.8^2]_4$	P	*S*	18*c*
Shlykovite	KCa**[$Si_4O_9(OH)$]**$(H_2O)_3$	2.50	$[4.8^2]_4$	P	*S*	18*b*
Cuprorivaite	$CaCu$**[Si_4O_{10}]**	2.50	$[4.8^2]_8$	2F	*S*	19*a*
Effenbergerite	$BaCu$**[Si_4O_{10}]**	2.50	$[4.8^2]_8$	2F	*S*	19*a*
Gillespite	$BaFe$**[Si_4O_{10}]**	2.50	$[4.8^2]_8$	2F	*S*	19*a*
Wesselsite	$SrCu$**[Si_4O_{10}]**	2.50	$[4.8^2]_8$	2F	*S*	19*a*
Arapovite	$U^{4+}(CaNa)K$**[Si_4O_{10}]**$_2$	2.50	$[4.8^2]_8$	2F	*S*	19*b*
Ekanite	$ThCa_2$**[Si_4O_{10}]**$_2$	2.50	$[4.8^2]_8$	2F	*S*	19*b*
Iraqite-(La)	$LaCa_2K$**[Si_4O_{10}]**$_2$	2.50	$[4.8^2]_8$	2F	*S*	19*b*
Steacyite	$Th(CaNa)K$**[Si_4O_{10}]**$_2$	2.50	$[4.8^2]_8$	2F	*S*	19*b*
Turkestanite	$Th(CaNa)K$**[Si_4O_{10}]**$_2$	2.50	$[4.8^2]_8$	2F	*S*	19*b*

(*Continued*)

https://doi.org/10.1180/mgm.2018.152 Published online by Cambridge University Press

Table 11. (*Continued.*)

Mineral	Formula	T:O ratio	Net*	P/F/M*	*S/D/M***	Fig. No.
Pyrosmalite-(Fe)	Fe_8^{2+}**[Si_6O_{15}]**$(OH,Cl)_{10}$	2.50	$[4.6.12]_{12}$	P	*S*	20
Pyrosmalite-(Mn)	Mn_8^{2+}**[Si_6O_{15}]**$(OH,Cl)_{10}$	2.50	$[4.6.12]_{12}$	P	*S*	20
Schallerite	$Mn_{16}^{2+}As_3^{3+}O_6$**[$Si_{12}O_{30}$]**$(OH)_{17}$	2.50	$[4.6.12]_{12}$	P	*S*	20
Friedelite	Mn_8**[Si_6O_{15}]**$(OH)_{10}$	2.50	$[4.6.12]_{12}$	P	*S*	20
Mcgillite	Mn_8**[Si_6O_{15}]**$(OH)_8Cl_2$	2.50	$[4.6.12]_{12}$	P	*S*	20
Nelenite	$Mn_{16}As_3^{3+}O_6$**[$Si_{12}O_{30}$]**$(OH)_{17}$	2.50	$[4.6.12]_{12}$	P	*S*	20
Armstrongite	$CaZr$**[Si_6O_{15}]**$(H_2O)_{2.5}$	2.50	$[(4.6.8)_2(6.8^2)_1]_2$	1F	*S*	21*a*
Dalyite	K_2Zr**[Si_6O_{15}]**	2.50	$[(4.6.8)_2(6.8^2)_1]_2$	1F	*S*	21*b*
Davanite	K_2Ti**[Si_6O_{15}]**	2.50	$[(4.6.8)_2(6.8^2)_1]_2$	1F	*S*	21*b*
Sazhinite-(Ce)	HNa_2Ce**[Si_6O_{15}]**$(H_2O)_n$	2.50	$[(4.6.8)_2(6.8^2)_1]_4$	1F	*S*	21*c*
Sazhinite-(La)	HNa_2La**[Si_6O_{15}]**$(H_2O)_n$	2.50	$[(4.6.8)_2(6.8^2)_1]_4$	1F	*S*	21*c*
Nekoite	Ca_3**[Si_6O_{15}]**$(H_2O)_7$	2.50	$[(5^2.8)_2(5.8^2)_1]_2$	P	*S*	22*a*
Zeravshanite	$Cs_4Na_2Zr_3$**[$Si_{18}O_{45}$]**$(H_2O)_2$	2.50	$[(5^2.8)_2(5.8^2)_1]_6$	1F	*S*	22*c*
Varennesite	$Na_8Mn_2^{2+}$**[$Si_{10}O_{25}$]**$(OH)_2(H_2O)_{12}$	2.50	$[(4.6.10)_4(6^2.10)_1]_4$	M	*S*	23*a*
Bementite	Mn_7^{2+}**[Si_6O_{15}]**$(OH)_8$	2.50	$[(5.6.7)_4(5.7^2)_1(6^2.7)_1]_4$	M	*S*	23*b*
Intersilite	$Na_6Mn^{2+}Ti$**[$Si_{10}O_{25}$]**$(OH)_2(H_2O)_4$	2.50	$[(5^2.8)_1(5.6^2)_1(5.6.8)_2(6^2.8)_1]_4$	M	*S*	23*c*
Yakovenchukite-(Y)	K_3NaCaY_2**[$Si_{12}O_{30}$]**$(H_2O)_4$	2.50	$[(4^2.14)_{12}(4.6.14)_8(6.14^2)_4]_1$	M	*S*	24
Diegogattaite	Na_2CaCu_2**[Si_8O_{20}]**(H_2O)	2.50	$[(6.14)_2(6.14^2)_4(14^2)_2]_1$	P	*D*	51
Leucosphenite	$BaNa_4Ti_2$**[$B_2Si_{10}O_{30}$]**	2.50	$[(14^2)_8(14^3)_4]_1$	P	*D*	48
Amstallite	$CaAl(OH)_2$**[$AlSi_3O_8(OH)_2$]**(H_2O)	2.50	$[(4.8)_2(4.8^3)_2]_2$	P	*S*	25
Prehnite	Ca_2Al**[Si_3AlO_{10}]**$(OH)_2$	2.50	$[(6^2)_2(6^4)_2]_1$	P	*S*	26
Minehillite	$K_2Ca_{28}Al_4$**[$Zn_5\square Si_{40}O_{112}$]**$(OH)_{16}$	2.49	$[6^3]_8[(9^2)_3(6.9^2)_6]_1$	P	*S/D*	54,56
Wickenburgite	Pb_3CaAl**[$AlSi_{10}O_{27}$]**$(H_2O)_4$	2.46	$[6^3]_6$	P	*D*	52
Armbrusterite	$Na_6K_5Mn^{3+}Mn_{14}^{2+}$**[$(Si_9O_{22})_4$]**$(OH)_{10}(H_2O)_4$	2.44	$[(5^2.7)_8(5.6.7)_8(6.7^2)_4(5.6.8)_8(5.7.8)_8]_1$	P	*D*	41*b*
Ferronordite-(Ce)	Na_3SrCe**[$Fe^{2+}Si_6O_{17}$]**	2.43	$[(4.5.8)_8(5^2.8)_4(5.8.5.8)_2]_2$	P	*S*	31
Ferronordite-(La)	Na_3SrLa**[$Fe^{2+}Si_6O_{17}$]**	2.43	$[(4.5.8)_8(5^2.8)_4(5.8.5.8)_2]_2$	P	*S*	31
Manganonordite-(Ce)	Na_3SrCe**[$Mn^{2+}Si_6O_{17}$]**	2.43	$[(4.5.8)_8(5^2.8)_4(5.8.5.8)_2]_2$	P	*S*	31
Bussyite-(Ce)	$(Ce,Ca)_3(Na,H_2O)_6Mn$**[$Si_9Be_5(O,OH)_{30}(F,OH)_4$]**	2.43	$[(4.5.8)_{16}(5.8.5.8)_4(5^2.8)_8]_2$	P	*S*	33*b*
Reyerite	$(Na,K)_2Ca_{14}$**[$Al_2Si_{22}O_{58}$]**$(OH)_8(H_2O)_6$	2.42	$[6^3]_8$	P	*S/D*	53,55
Samfowlerite	$Ca_{14}Mn_{23}$**[$(Be_7Zn)Zn_2Si_{14}O_{52}(OH)_6$]**	2.42	$[(4.5^2)_8(4.8^2)_4(4.5.8)_{12}(5^2.8)_{20}(5^2.8^2)_4]_1$	P	*S*	34*b*
Ciprianiite	$Ca_4(Th,U,Ca)Al(Be_{0.5}\square_{1.5})$**[$Si_4B_4O_{22}(OH)_2$]**	2.40	$[(4.5.8)_2(4.5^2.8)_2(5^3)_2(5^2.8)_4]_1$	P	*S*	30*a*
Hellandite-(Ce)	$Ca_4(REE)Ce_2Al$**[$\square_2Si_4B_4O_{22}(OH)_2$]**	2.40	$[(4.5.8)_2(4.5^2.8)_2(5^3)_2(5^2.8)_4]_1$	P	*S*	30*a*
Hellandite-(Y)	$Ca_4(REE)Y_2Al$**[$\square_2Si_4B_4O_{22}(OH)_2$]**	2.40	$[(4.5.8)_2(4.5^2.8)_2(5^3)_2(5^2.8)_4]_1$	P	*S*	30*a*
Mottanaite-(Ce)	$Ca_4Ce_2Al(Be_{1.5}\square_{0.5})$**[$Si_4B_4O_{22}O_2$]**	2.40	$[(4.5.8)_2(4.5^2.8)_2(5^3)_2(5^2.8)_4]_1$	P	*S*	30*a*
Tadzhikite-(Ce)	$Ca_4Ce_2Ti^{4+}$**[$\square_2Si_4B_4O_{22}(OH)_2$]**	2.40	$[(4.5.8)_2(4.5^2.8)_2(5^3)_2(5^2.8)_4]_1$	P	*S*	30*a*
Semenovite-(Ce)	$(Ca,Na)_8Na_{0-2}REE_2(Fe,Ti)$**[$(Si,Be)_{10}(O,F)_{24}$]**$_2$	2.40	$[(4.5^2)_1(4.5.8.5)_1(5^2.8)_3]_4$	P	*S*	32*a*
Harstigite	Ca_6Mn^{2+}**[$Be_4Si_6O_{22}(OH)_2$]**	2.40	$[(4.5^2)_1(4.5.8.5)_1(5^2.8)_3]_4$	P	*S*	32*b*
Perettiite	$Y_2Mn_4^{2+}Fe^{2+}$**[$Si_2B_8O_{24}$]**	2.40	$[(4.5^2)_1(4.5.8.5)_1(5^2.8)_3]_4$	P	*S*	32*c*
Aminoffite	Ca_2**[$Be_2Si_3O_{10}(OH)_2$]**	2.40	$[(6^4)_1(4.6^2)_4]_1$	P	*S*	33*a*
Vladykinite	Na_3Sr_4**[$(Fe^{2+}Fe^{3+})Si_8O_{24}$]**	2.40	$[(5^3)_4(5^2.8)_4(4.5.8)_8(5^3.8)_4]_1$	P	*S*	34*a*
Fedorite	$Na_3(Ca_4Na_3)$**[$Si_{16}O_{38}$]**$F_2(H_2O)_{3.5}$	2.38	$[6^3]_8$	P	*D*	37*a*
Lalondeite	$(Na,Ca)_6(Ca,Na)_3$**[$Si_{16}O_{38}$]**$F_2(H_2O)$	2.38	$[6^3]_8$	P	*D*	37*a*
Macdonaldite	$BaCa_4$**[$Si_{16}O_{36}(OH)_2$]**$(H_2O)_{10}$	2.38	$[4.8^2]_4$	P	*D*	38*a*
Monteregianite	KNa_2Y**[Si_8O_{19}]**$(H_2O)_5$	2.38	$[4.8^2]_4$	P	*D*	38*a*
Rhodesite	$HKCa_2$**[Si_8O_{19}]**$(H_2O)_5$	2.38	$[4.8^2]_4$	P	*D*	38*a*
Delhayelite	K_4Ca_2**[$AlSi_7O_{17}(OH)_2$]**$(OH)_2Cl$	2.38	$[4.8^2]_4$	P	*D*	38*b*
Fivegite	K_4Ca_2**[$AlSi_7O_{17}O_2$]**$(H_2O)_2Cl$	2.38	$[4.8^2]_4$	P	*D*	38*b*
Bannisterite	$(K,Ca)Mn_{10}$**[$(Si,Al)_{16}O_{38}$]**$(OH)_8(H_2O)_4$	2.38	$[(5.6^2)_8(5.6.7)_8(5.7^2)_4(6^2.7)_{12}]_1$	P	*D*	42*b*
Ajoite	$K_3Cu_{20}^{2+}$**[$Al_5Si_{29}O_{76}$]**$(OH)_{16}(H_2O)_8$	2.38	$[(5.6^2)_2(5.6.7)_4(5.7^2)_2(6^2.7)_6]_1$	P	*D*	41*a*
Piergorite-(Ce)	$Ca_8Ce_2(Al,Fe^{3+})[(\square$**,Li,Be$)_2$[$Si_6B_8O_{36}(OH)_2$]**	2.38	$[(4.5.8)_2(4.5^2.8)_2(5^3)_6(5^2.8)_4(5^4)_2]_1$	P	*S*	30*b*
Stilpnomelane	$(K,Ca)Mn_{10}$**[$(Si,Al)_{16}O_{38}$]**$(OH)_8(H_2O)_4$	2.33	$[(5.6^2)_6(6^3)_6(5.6.8)_{24}]_1$	P	*D*	42*a*
Franklinphilite	$((K,Na)_x(Mn^{2+},Mg,Zn)_8$**[$(Si,Al)_{12}O_{28}$]**$(OH)_8(H_2O)$	2.33	Iso stilpnomelane	P	*D*	42*a*
Lennilenapeite	$K_x(Mg,Mn^{2+},Fe^{2+},Zn)_8$**[$(Si,Al)_{12}O_{28}$]**$(OH)_8(H_2O)_{2.7}$	2.33	Iso stilpnomelane	P	*D*	42*a*
Chiappinoite-(Y)	Y_2Mn**[Si_3O_7]**$_4$	2.33	$[(4.6.8)_8(6^2.8)_8]_1$	P	*D*	40
Searlesite	Na**[$BSi_2O_5(OH)_2$]**	2.33	$[(5^2)_2(5^4)_4]_1$	P	*S*	27
Åkermanite	Ca_2**[$Mg(Si_2O_7)$]**	2.33	$[(5^3)_2(5^4)_1]_2$	P	*S*	29*a*
Alumoåkermanite	$(CaNa)$**[$Al(Si_2O_7)$]**	2.33	$[(5^3)_2(5^4)_1]_2$	P	*S*	29*a*
'Ferri-gehlenite'	Ca_2**[$Fe^{3+}(AlSiO_7)$]**	2.33	$[(5^3)_2(5^4)_1]_2$	P	*S*	29*a*
Gehlenite	Ca_2**[$Al(AlSiO_7)$]**	2.33	$[(5^3)_2(5^4)_1]_2$	P	*S*	29*a*
Gugiaite	Ca_2**[$Be(Si_2O_7)$]**	2.33	$[(5^3)_2(5^4)_1]_2$	P	*S*	29*a*
Hardystonite	Ca_2**[$Zn(Si_2O_7)$]**	2.33	$[(5^3)_2(5^4)_1]_2$	P	*S*	29*a*
Okayamalite	Ca_2**[$B(BsiO_7)$]**	2.33	$(5^3)_2(5^4)_1]_2$	P	*S*	29*a*
Leucophanite	$(NaCa)$**[$Be(Si_2O_6F)$]**	2.33	$[(5^3)_2(5^4)_1]_2$	P	*S*	29*b*
Meliphanite	$(Na,Ca)_4Ca_4$**[$Be_4AlSi_7O_{24}(F,O)_4$]**	2.33	$[(5^3)_2(5^4)_1]_4$	P	*S*	29*c*
Jeffreyite	$(Ca,Na)_2$**[$(Be,Al)Si_2(O,OH)_7$]**	2.33	$[(5^3)_2(5^4)_1]_n$	P	*S*	---
Chiappinoite-(Y)	Y_2Mn**[Si_3O_7]**$_4$	2.33	$[(4.6.8)_8(6^2.8)_8]_1$	P	*D*	40
Zussmanite	KFe_{13}^{2+}**[$AlSi_{17}O_{42}$]**$(OH)_{14}$	2.33	$[(3.8^2)_6(6.8^2)_6]_1$	P	*D*	44

(*Continued*)

https://doi.org/10.1180/mgm.2018.152 Published online by Cambridge University Press

Table 11. (*Continued.*)

Mineral	Formula	T:O ratio	Net*	P/F/M*	S/D/M**	Fig. No.
Coombsite	KMn^{2+}_{13}**[AlSi$_{17}$O$_{42}$]**$(OH)_{14}$	2.33	Iso zussmanite	P	*D*	44
Jagoite	$Pb^{2+}_{22}Fe^{3+}_{4}$**[Al$_{10}$Si$_{26}$O$_{82}$]**Cl_6	2.28	$[(12^2)_3(12^3)_2]_1$	P	*S/D*	54,55
Carletonite	KNa_4Ca_4**[Si$_8$O$_{18}$]**$(CO_3)_4(OH,F)(H_2O)$	2.25	$[4.8^2]_{16}$	P	*D*	38*c*
Sørensenite	Na_4Sn^{4+}**[Be$_2$Si$_6$O$_{18}$]**$(H_2O)_2$	2.25	-----	P	*D*	50
Günterblassite	$(K,Ca)_{3-x}Fe$**[(Si,Al)$_{13}$O$_{25}$(OH,O)$_4$]**$(H_2O)_7$	2.23	$[4.8^2]_4$	P	*M*	–--
Hillesheimite	$(K,Ca,\square)_2(Mg,Fe,Ca,\square)_2$**[(Si,Al)$_{13}O_{23}(OH)_6$]**$(OH)(H_2O)_8$	2.23	$[4.8^2]_4$	P	*M*	56
Umbrianite	$K_7Na_2Ca_2$**[Al$_3$Si$_{10}$O$_{29}$]**F_2Cl_2	2.23	$[4.8^2]_4$	P	*M*	56
Tuscanite	$KCa_{5.5}$**[(Si$_6$Al$_4$)O$_{22}$]**$(SO_4)_2(H_2O)$	2.20	$[(8^2)_1(6^2.8)_2(6.8^2)_2]_1$	M	*D*	46*a*
Latiumite	KCa_3**[Si$_2$Al$_3$)O$_{11}$]**$(SO_4)(CO_3)$	2.20	$[(8^2)_1(6^2.8)_2(6.8^2)_2]_1$	M	*D*	46*b*
Naujakasite	Na_6Fe^{2+}**[Al$_4$Si$_8$O$_{26}$]**	2.17	$[6^3]_{12}$	P	*D*	37*b*
Manganonaujakasite	Na_6Mn^{2+}**[Al$_4$Si$_8$O$_{26}$]**	2.17	$[6^3]_{12}$	P	*D*	37*b*
Esquireite	Ba**[Si$_6$O$_{13}$]**$(H_2O)_7$	2.17	$[(8^2)_2(8^3)_4]_1$	P	*D*	45
Magadiite	Na_2**[Si$_{14}$O$_{29}$]**$(H_2O)_{11}$	2.07	$[(5^4)_8(5^2.6^2)_4]_1$	P	*S*	35
Parsettensite	$K_{7.5}Mn_{49}$**[(Si,Al)$_{82}$O$_{168}$]**$(OH)_{50}$	2.05	$[(4.5.12)_{24}(5.6^2)_{12}(6^3)_{12}(5.6.12)_{24}]_1$	M	*D*	42*c*
Cymrite	Ba**[Al$_2$Si$_2$O$_8$]**(H_2O)	2.00	$[6^3]_2$	P	*D*	36*a*
Dmisteinbergite	Ca**[Al$_2$Si$_2$O$_8$]**	2.00	$[6^3]_2$	P	*D*	36*a*
Hexacelsian	Ba**[Al$_2$Si$_2$O$_8$]**	2.00	$[6^3]_2$	P	*D*	36*a*
Kampfite	$Ba_{12}(Si_{13}Al_3)O_{32}(CO_3)_8Cl_5$	2.00	$[6^3]_4$	P	*D*	36*c*
Burckhardtite	$Pb_2(Fe^{3+}Te^{6+})$**[AlSi$_3$O$_8$]**O_6	2.00	$[6^3]_2$	P	*D*	36*b*
Asbecasite	Ca_3Ti^{4+}**[Be$_2$Si$_2$As$^{3+}_6$O$_{20}$]**	2.00	$[(12^2)_3(12^3)_2]_1$	P	*D*	47*b*

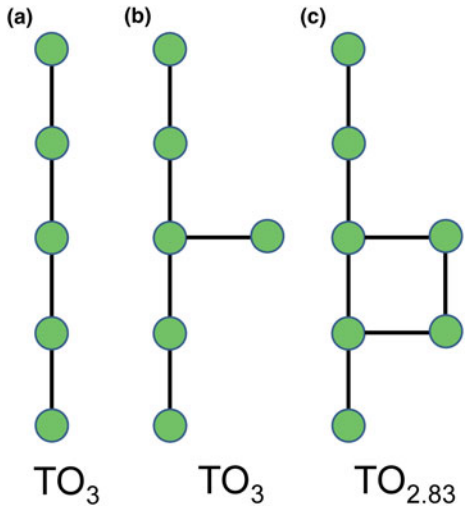

Fig. 59. Graphs of various connectivities: (*a*) simple TO_3 graph; (*b*) the graph in (*a*) with one added vertex and one added edge; the stoichiometry is still TO_3; and (*c*) the graph in (*a*) with two added vertices and two added edges; the stoichiometry is $TO_{2.83}$. Green circles: vertices; black lines: edges.

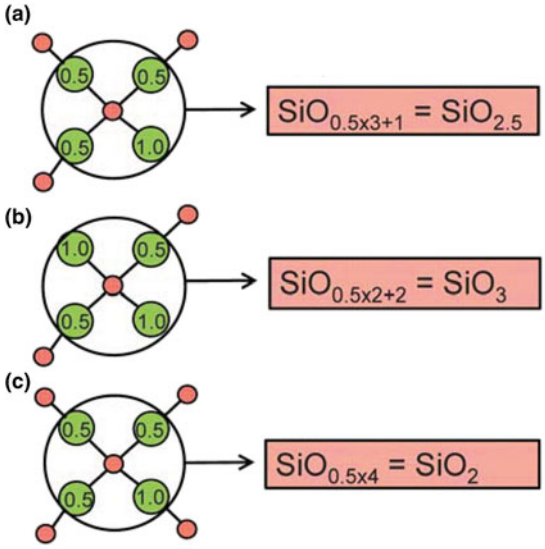

Fig. 60. The relation between tetrahedron connectivity and stoichiometry; (*a*) a 3-connected tetrahedron (i.e. three 2-connected and one 1-connected anions); (*b*) a 2-connected tetrahedron (i.e. two 2-connected anions and two 1-connected anions); and (*c*) a 4-connected tetrahedron (i.e. four 2-connected anions). Red circles: T cations; green circles: O anions; each anion shared between two T cations counts as one-half and each apical anion counts as one. From Hawthorne (2015*a*).

chains-ribbons-tubes, 2-dimensional **sheets**, and 3-dimensional **frameworks**. The cluster structures cover the largest range, but much of this range is not occupied by minerals. The sheet structures cover the largest observed range and overlap strongly with the chain-ribbon-tube structures and completely with the framework structures. The range of the framework structures is dashed in Fig. 61 as we have not looked in detail at these as yet and are uncertain as to the compositional limits of partly connected frameworks. We have not marked the transitional structures on these figures, i.e. the structures that contain silicate polymers from more than one group. These may lie within the range of the principal type of polymerisation of the structure, e.g. **okenite** (Fig. 22*b*; Table 5) which contains both sheets and chains, or outside that range, e.g. **hyttsjöite** (Fig. 9; Table 3). Prior to setting up this hierarchy, we were unaware of the broad overlap of

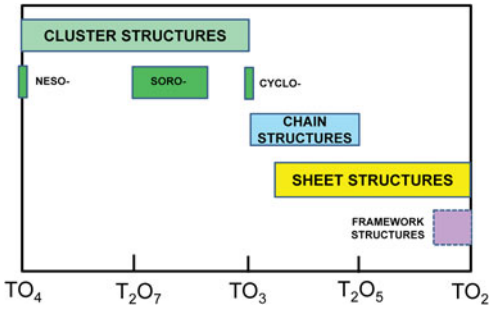

Fig. 61. The ranges of silicate stoichiometries in silicate minerals *sensu late* as a function of dimensionality of polymerisation, expressed as TO_x on the abscissa.

https://doi.org/10.1180/mgm.2018.152 Published online by Cambridge University Press

Table 12. Plane nets and their associated structures.

Single Nets	Minerals
6^3	antigorite, chlorite, kalifersite, kanemite, kaolinite, lizardite, pyrosmalite, mica, nontronite, palygorskite, raite, sanbornite, sepiolite, serpentines, hanjiangite, talc, gyrolite, ellingsenite, martinite, cairncrossite, natrosilite, kanemite, sanbornite, makatite, pentagonite, silinaite, plumbophyllite, palygorskite, tuperssuatsiaite, windhoekite, yofortierite, raite, kalifersite, sepiolite, loughlinite, antigorite
4.8^2	datolite, gadolinite-(Ce), gadolinite-(Y), hingganite-(Ce), hingganite-(Y), 'hingganite-(Yb)', 'calcybeborosilite', homilite, minasgeraisite-(Y), fluorapophyllite-(K), fluorapophyllite-(Na), hydroxyapophyllite-(K), cavansite, cryptophyllite, shlykovite, mountainite, cuprorivaite, effenbergite, gillespite, wesselsite, arapovite, ekanite, iraqite-(La), steacyite, turkestanite
3.12^2	---
$(4.6.8)_2(6.8^2)_1$	armstrongite, dalyite, davanite, sazhinite-(Ce), sazhinite-(La)
$(5^2.8)_1(5.8^2)_1$	nekoite, okenite, zeravshanite
$(4.6.10)_4(6^2.10)_1$	varennesite
4.6.12	pyrosmalite-(Fe), pyrosmalite-(Mn), schallerite, friedelite, mcgillite, nelenite
$(3.\ 8^2)_1(6.8^2)_1$	zussmanite
$(5^2.8)_1(5.6^2)_1(5.6.8)_2(6^2.8)_1$	intersilite
$(5.6.7)_4(5.7^2)_1(6^2.7)_1$	bementite
$(4^2.14)_{12}(4.6.14)_8(6.14^2)_4$	yakovenchukite
$8^3_2.8^2_1$	kvanefjeldite
$10^2_1 10^3_1$	tumchaite
$12^2_3 12^3_2$	zeophyllite, britvinite, molybdophyllite
$14^2_8 14^3_6$	hyttsjöite
$(4.8)_4(4.8^3)_4$	amstallite
$6^2_2 6^4_2$	prehnite
$5^2_2 5^4$	searlesite
$5^3_2 5^4_1$	åkermanite, alumoåkermanite, 'ferri-gehlenite', gehlenite, gugiaite, hardystonite, okayamalite
$(5^3_2 5^4_1)_n$	leucophanite, meliphanite, jeffreyite
$(4.5.8)_2(4.5^2.8)_2(5^3)_2(5^2.8)_4$	ciprianiite, hellandite-(Ce), hellandite-(Y), mottanaite-Ce), tadzhikite-(Ce)
$(4.5.8)_2(4.5^2.8)_2(5^3)_6(5^2.8)_4(5^4)_2$	piergorite-(Ce)
$(4.5.8)_8(5^2.8)_4(5.8.5.8)_2$	ferronordite-(Ce), ferronordite-(La), manganogordite-(Ce)
$[(4.5^2)_1(4.5.8.5)_1(5^2.8)_3]_4$	semenovite, harstigite, perettiite-(Y)
$(6^4)_2(4.6^2)_8$	aminoffite
$(4.5.8)_{16}(5.8.5.8)_4(5^2.8)_8$	bussyite-(Ce)
$(5^3)_4(5^2.8)_4(4.5.8)_8(5^2.8)_4$	vladykinite
$[(4.5^2)_8(4.8^2)_4(4.5.8)_{12}(5^2.8)_{20}\ (5^2.8^2)_4]_1$	samfowlerite
$(5^4)_8(5^2.6^2)_4$	magadiite

chain-ribbon-tubes, sheets and frameworks in terms of silicate connectivity. The relation of minerals with the same connectivity but different dimension of polymerisation remains to be understood.

The distribution of mineral structures over the plane nets

Casual inspection of Tables 3-10 shows that some nets are far more common than others as the basis of the silicate part of the structure. This aspect of structure is shown more quantitatively in Table 12 which lists the minerals and some mineral groups as a function of their fundamental nets; multiple-layer structures are listed under the type of their parent net. It is apparent immediately that 6^3 is by far the most common net, followed by 4.8^2, both for single-layer structures and multiple-layer structures. Some other nets have up to eight minerals, but these tend to be isostructural members of a group and do not show the diversity of structures found for 6^3 and 4.8^2 nets. These are the least topologically complex of the nets listed in Table 12, and this suggests (together with preliminary work on the other groups of silicate minerals) that structural units with the lowest complexity (the lowest Shannon entropy) tend to form (1) the most minerals in general, (2) the most common rock-forming minerals, and (3) mineral groups that show the largest range of solid solution and the largest number of mineral species. These issues will be investigated in more detail elsewhere.

Coda

Assembling, digesting and organising such a large body of information suggests a lot of very interesting and often novel questions that are not visible when one is fighting with the structure and chemical composition of an individual recalcitrant mineral. Below is a list of some of these questions that have surfaced during this work and surely deserve attention in the future; indeed, this is one of the reasons for expending this amount of effort. Let it be understood that each of these questions below is addressed to the sheet-silicate minerals:

[1] Why is the 6^3 net so dominant a motif?
[2] Why is the net 3.12^2 not represented in mineral structures?
[3] All 3-connected nets have the stoichiometry $[T_2O_5]$; what factors dictate which net is used for a specific mineral?
[4] Why do lower-valent tetrahedrally coordinated cations prefer 4-connected tetrahedra?
[5] Note that u^6 and d^6 rings of tetrahedra tend to occur in minerals with sheets of edge-sharing octahedrally coordinated (usually divalent) cations. Hawthorne (2012*b*) showed that where two parts of an atomic arrangement join, there must be a one-to-one mapping of the apical anions of the sheet of tetrahedra onto the anions of the interstitial complex. This may occur where a 6^3 sheet of tetrahedra links to an O-sheet of octahedra, accounting for the occurrence of u^6 and d^6 rings of tetrahedra in minerals with sheets of edge-

https://doi.org/10.1180/mgm.2018.152 Published online by Cambridge University Press

sharing octahedra. Mixed rings of tetrahedra are associated with interstitial cations of coordinations > [6]. The one-to-one mapping argument of Hawthorne (2012*b*) must hold, and it will be of considerable interest to relate the u–d character of the rings of silicate tetrahedra to the arrangements of the linking interstitial species.

[6] Why are many double-layer silicates based on parent nets that do not occur in single-layer structures?

[7] What is the relation between minerals with the same connectivity but different dimensions of polymerisation?

The next significant step involving the sheet-silicate minerals is to examine their occurrence in detail and see if there are general correlations between connectivity and paragenesis. Bowen's reaction series (Bowen, 1928) indicates that there are broad associations between silicate stoichiometry, paragenesis and degree of fractionation; is this broad correlation part of a more detailed correlation between silicate structure and both intensive thermodynamic variables and paragenesis? This is an important avenue of investigation that falls within the recently developed area of *mineral ecology* (e.g. Hazen *et al.*, 2015*a*,*b*; Grew *et al.*, 2016) and will hopefully be pursued in the future, particularly as the development and use of large datasets becomes more common in the Earth Sciences. There are significant and systematic variations in complexity of these sheet-silicate polymerisations; these will be addressed in a forthcoming paper.

Acknowledgements. This work was funded by a Discovery Grant from the Natural Sciences and Engineering Research Council of Canada. We thank the reviewers and Associate Editor for their comments on this paper.

References

Alberti A.A. and Galli E. (1983) The structure of nekoite, $Ca_3Si_6O_{15}·7H_2O$, a new type of sheet silicate. *American Mineralogist*, **65**, 1270–1276.

Annehed H., Fälth L. and Lincoln F.J. (1982) Crystal structure of synthetic makatite $Na_2Si_4O_8(OH)_2·4H_2O$. *Zeitschrift für Kristallographie*, **159**, 203–210.

Armbruster T., Röthlisberger F. and Seifert F. (1990) Layer topology, stacking variation, and site distortion in melilite-related compounds in the system $CaO–ZnO–GeO_2–SiO_2$. *American Mineralogist*, **75**, 847–858.

Artioli G. and Galli E. (1994) The crystal structures of orthorhombic and monoclinic palygorskite. *Materials Science Forum*, **166–169**, 647–652.

Bačik P., Fridrichová J., Uher P., Pršek J. and Ondrejka M. (2014) The crystal chemistry of gadolinite-datolite group silicates. *The Canadian Mineralogist*, **52**, 625–642.

Bačík P., Miyawaki R., Atencio D., Cámara F. and Fridrichová J., (2017) Nomenclature of the gadolinite supergroup. *European Journal of Mineralogy*, **29**(6), 1067–1082.

Bailey S.W. (editor) (1988) *Hydrous Phyllosilicates (Exclusive of Micas)*. Reviews in Mineralogy, **19**. Mineralogical Society of America, Washington, DC.

Bakakin V.V., Belov N.V., Borisov S.V. and Solovyeva L.P. (1970) The crystal structure of nordite and its relationship to melilite and datolite-gadolinite. *American Mineralogist*, **55**, 1167–1181.

Bartl H. and Pfeifer G. (1976) Neutronenbeugungsanalyse des Apophyllit $KCa_4(Si_4O_{10})_2(F/OH)(H_2O)_8$. *Neues Jahrbuch für Mineralogie – Monatshefte*, **1976**, 58–65.

Basciano L.C. and Groat L.A. (2007) The crystal structure of kampfite. *The Canadian Mineralogist*, **45**, 935–943.

Basso R., Dal Negro A., Della Giusta A. and Ungaretti L. (1975) The crystal structure of naujakasite, a double sheet silicate. *Bulletin Grønlands Geologiske Indersøgelse*, **116**, 11–24.

Baur W.H., Joswig W., Kassner D. and Hofmeister W. (1990) Prehnite: structural similarity of the monoclinic and orthorhombic polymorphs and their Si/Al ordering. *Journal of Solid State Chemistry*, **86**, 330–333.

Belov N.V. (1958) Essays on structural mineralogy IX. *Mineralogicheskiy Sbornik L'vovskogo Obshchestva*, **12**, 15–42 [in Russian].

Belov N.V. (1961) *Crystal Chemistry of Silicates with Large Cations*. Akademia Nauk SSSR, Moscow.

Bensch W. and Schur M. (1995) Crystal structure of calcium copper phyllodecaoxotetrasilicate, $CaCuSi_4O_{10}$. *Zeitschrift für Kristallographie*, **210**, 530–530.

Biedl A. and Preisinger A. (1962) Die Struktur des Loughlinit (Natrium-Sepiolith). *Fortschritte der Mineralogie*, **40**, 50–51.

Bindi L., Czank M., Röthlisberger F. and Bonazzi P. (2001) Hardystonite from Franklin, New Jersey: a natural modulated melilite. *American Mineralogist*, **86**, 747–751.

Blinov V.A., Voronkov A.A., Ilyukhin V.V. and Belov N.V. (1975) Crystal structure of lemoynite with a new type of mixed framework. *Soviet Physics Doklady*, **19**, 397–398.

Boiocchi M., Callegari A. and Ottolini L. (2006) The crystal structure of piergorite-(Ce), $Ca_8Ce_2(Al_{0.5}Fe^{3+}_{0.5})_{\Sigma1}(\square,Li,Be)_2Si_6B_8O_{36}(OH,F)_2$: A new borosilicate from Vetralla, Italy, with a modified hellandite-type chain. *American Mineralogist*, **91**, 1170–1177.

Bolotina N.B., Rastsvetaeva R.K. and Kashaev A.A. (2010) Refinement of the twinned structure of cymrite from the Ruby Creek Deposit (Alaska). *Crystallography Reports*, **55**, 569–574.

Bowen N.L. (1928) *Evolution of Igneous Rocks*. Princeton University Press, New Jersey, USA.

Bragg W.L. (1930) The structure of silicates. *Zeitschrift für Kristallographie*, **74**, 237–305.

Brese N.E. and O'Keeffe M.O. (1991) Bond-valence parameters for solids. *Acta Crystallographica*, **B47**, 192–197.

Brigatti M.F. and Guggenheim S. (2002) Mica crystal chemistry and the influence of pressure, temperature, and solid solution on atomistic models. Pp. 1–97 in: *Micas: Crystal Chemistry & Metamorphic Petrology* (A. Mottana, F.P. Sassi, J.B. Thompson Jr. and S. Guggenheim, editors). Reviews in Mineralogy and Geochemistry, **46**. Mineralogical Society of America, Washington, DC.

Brigatti M.F. and Poppi L. (1993) Crystal chemistry of Ba-rich trioctahedral micas-1M. *European Journal of Mineralogy*, **5**, 857–871.

Brigatti M.F., Guggenheim S. and Poppi M. (2003) Crystal chemistry of the 1M mica polytype: The octahedral sheet. *American Mineralogist*, **88**, 667–675.

Burns P.C. (1999) The crystal chemistry of uranium. Pp. 23–90 in: *Uranium: Mineralogy, Geochemistry, and the Environment* (P.C. Burns and R. Finch, editors). Reviews in Mineralogy, **38**. Mineralogical Society of America, Washington, DC.

Burns P.C. (2005) U^{6+} minerals and inorganic compounds: insights into an expanded structural hierarchy of crystal structures. *The Canadian Mineralogist*, **43**, 1839–1894.

Burns P.C., Grice J.D. and Hawthorne F.C. (1995) Borate minerals. I. Polyhedral clusters and fundamental building blocks. *The Canadian Mineralogist*, **33**, 1131–1151.

Burns P.C., Miller M.L. and Ewing R.C. (1996) U^{6+} minerals and inorganic phases: a comparison and hierarchy of structures. *The Canadian Mineralogist*, **34**, 845–880.

Cámara F., Garvie L.A.J., Devouard B., Groy T.L. and Buseck P.R. (2002) The structure of Mn-rich tuperssuatsiaite: a palygorskite-related mineral. *American Mineralogist*, **87**, 1458–1463.

Cámara F., Ottolini L., Devouard B., Garvie L.A.J. and Hawthorne F.C. (2006) Sazhinite-(La), $Na_3LaSi_6O_{15}(H_2O)_2$, a new mineral from the Aris phonolite, Namibia: Description and crystal structure. *Mineralogical Magazine*, **70**, 405–418.

Cámara F., Oberti R., Ottolini L., Della Ventura G. and Bellatreccia F. (2008) The crystal chemistry of Li in gadolinite. *American Mineralogist*, **93**, 996–1004.

Cannillo E., Giuseppetti G. and Tazzoli V. (1967) The crystal structure of leucophanite. *Acta Crystallographica*, **23**, 255–259.

Cannillo E., Rossi G. and Ungaretti L. (1968) The crystal structure of macdonaldite. *Atti Della Accademia Nazionale dei Lincei, Classe di Scienze Fisiche, Matematiche e Naturali*, **45**, 399–414.

Cannillo E., Giuseppetti G. and Tadini C. (1969) Crystal structure of asbecasite. *Atti Della Accademia Nazionale dei Lincei, Classe di Scienze Fisiche, Matematiche e Naturali*, **46**, 457–467.

https://doi.org/10.1180/mgm.2018.152 Published online by Cambridge University Press

Cannillo E., Dal Negro A. and Rossi G. (1973) The crystal structure of latiumite, a new type of sheet silicate. *American Mineralogist*, **58**, 466–470.

Cannillo E., Giuseppetti G., Mazzi F. and Tazzoli V. (1992) The crystal structure of a rare earth bearing leucophanite: $(Ca,RE)CaNa_2Be_2Si_4O_{12}(F,O)_2$. *Zeitschrift für Kristallographie*, **202**, 71–79.

Capitani G.C. and Mellini M. (2006) The crystal structure of a second antigorite polysome ($m = 16$), by single-crystal synchrotron diffraction. *American Mineralogist*, **91**, 394–399.

Chakhmouradian A.R., Cooper N.A., Ball N.A., Reguir E.P., Medici L., Abdu Y.A. and Antonov A.A. (2014) Vladykinite, $Na_3Sr_4(Fe^{2+}Fe^{3+})Si_8O_{24}$: A new complex sheet silicate from peralkaline rocks of the Murun complex, eastern Siberia, Russia. *American Mineralogist*, **99**, 235–241.

Chakoumakos B.C., Fernandez-Baca J.A. and Boatner L.A. (1993) Refinement of the structures of the layer silicates $MCuSi_4O_{10}$ (M = Ca, Sr, Ba) by Rietveld analysis of neutron powder diffraction data. *Journal of Solid State Chemistry*, **103**, 105–113.

Chao G.Y. (1972) The crystal structure of carletonite, $KNa_4Ca_4Si_8O_{18}(CO_3)_4(F,OH)\cdot H_2O$. *American Mineralogist*, **57**, 765–778.

Chesnokov B.V., Lotova E.V., Nigmatullina E.N., Pavlutchenko V.S. and Bushmakin A.F. (1990) Dmisteinbergite, $CaAl_2Si_2O_8$, (hexagonal), a new mineral. *Zapiski Vsesoyuznogo Mineralogicheskogo Obshchestva*, **119**(5), 43–46.

Chiari G., Giustetto R. and Ricchiardi G. (2003) Crystal structure refinements of palygorskite and Maya Blue from molecular, modeling and powder synchrotron diffraction. *European Journal of Mineralogy*, **15**, 21–33.

Christy A.G., Kampf A.R., Mills S.J., Housley R.M. and Thorne B. (2014) Crystal structure and revised chemical formula for burckhardtite, $Pb_2(Fe^{3+}Te^{6+})[AlSi_3O_8]O_6$: a double-sheet silicate with intercalated phyllotellurate layers. *Mineralogical Magazine*, **78**, 1763–1773.

Christy A.G., Mills S.J. and Kampf A.R. (2016) A review of the structural architecture of tellurium oxycompounds. *Mineralogical Magazine*, **80**, 415–545.

Chukanov N.V., Yakubovich O.V., Pekov I.V., Belakovsky D.I. and Massa W. (2008) Britvinite, $Pb_{15}Mg_9(Si_{10}O_{28})(BO_3)4(CO_3)_2(OH)_{12}O_2$, a new mineral species from Långban, Sweden. *Geology of Ore Deposits*, **50**, 713–719.

Chukanov N.V., Rastsvetaeva R.K., Aksenov S.M., Pekov I.V., Zubkova N.V., Britvin S.N., Belakovskiy D.I., Schüller W. and Ternes B. (2012*a*) Günterblassite, $(K,Ca)_{3-x}Fe$ $[(Si,Al)_{13}O_{25}(OH,O)_4]\cdot 7H_2O$, a new mineral: the first phyllosilicate with triple tetrahedral layer. *Geology of Ore Deposits*, **54**, 656–662.

Chukanov N.V., Britvin S.N., Blass G., Belakovskiy D.I. and Van K.V. (2012*b*) Windhoekite, $Ca_2Fe^{3+}_{3-x}(Si_8O_{20})(OH)_4\cdot 10H_2O$, a new palygorskite-group mineral from the Aris phonolite, Namibia. *European Journal of Mineralogy*, **24**, 171–179.

Chukanov N.V., Zubkova N.V., Pekov I.V., Belakovskiy D.I., Schüller W., Ternese B., Blass G. and Pushcharovsky D.Yu. (2013) Hillesheimite, $(K,Ca,\square)_2(Mg,Fe,Ca,\square)_2[(Si,Al)_{13}O_{23}(OH)_6](OH).8H_2O$, a New Phyllosilicate Mineral of the Günterblassite Group. *Geology of Ore Deposits*, **55**, 549–557.

Cooper M.A. and Hawthorne F.C. (2017) Cation order in the crystal structure of minasgeraisite-(Y). *Mineralogical Magazine*, **82**(2), 301–312.

Dai Y., Post J.E. and Appleman D.E. (1995) Crystal structure of minehillite: Twinning and structural relationships to reyerite. *American Mineralogist*, **80**, 173–178.

Dal Negro A., Rossi G. and Ungaretti L. (1967) The crystal structure of melilphanite. *Acta Crystallographica*, **23**, 260–264.

Danisi R.M., Armbruster T., Libowitzky E., Wang H.A.O., Gunther D., Nagashima M., Reusser E. and Bieri W. (2015) Perettiite-(Y), $Y^{3+}_2Mn^{2+}_4Fe^{2+}[Si_2B_8O_{24}]$, a new mineral from Momeik, Myanmar. *European Journal of Mineralogy*, **27**, 793–803.

Della Ventura G., Bonazzi P., Oberti R. and Ottolini L. (2002) Ciprianiite and mottanaite-(Ce), two new minerals of the hellandite group from Latium (Italy). *American Mineralogist*, **87**, 739–744.

Demartin F., Pilati T., Diella V., Gentile P. and Gramaccioli C.M. (1993) A crystal-chemical investigation of alpine gadolinite. *The Canadian Mineralogist*, **30**, 127–136.

Demartin F., Minaglia A. and Gramaccioli C.M. (2001) Characterization of gadolinite-group minerals using crystallographic data only: the case of hingganite-(Y) from Cuasso al Monte, Italy. *The Canadian Mineralogist*, **39**, 1105–1114.

Dódony I., Pósfai M. and Buseck P.R. (2002) Revised structure models for antigorite: an HRTEM study. *American Mineralogist*, **87**, 1443–1457.

Dondi M., Ercolani G., Fabbri B. and Marsigli M. (1999) Chemical composition of melilite formed during the firing of carbonate-rich and iron-containing ceramic bodies. *Journal of the American Ceramic Society*, **82**, 465–468.

Drits V.A., Kasahev A.A. and Sokolova G.V. (1975) Crystal structure of cymrite. *Soviet Physics – Crystallography*, **20**(2), 171–175.

Dunn P.J. and Peacor D.R. (1984) Nelenite, a manganese arsenosilicate of the friedelite group, polymorphous with schallerite, from Franklin, New Jersey. *Mineralogical Magazine*, **48**, 271–275.

Dunn P.J., Rouse R.C., Norberg J.A. and Peacor D.R. (1978) Hydroxyapophyllite, a new mineral, and a redefinition of the apophyllite group I. Description, occurrences, and nomenclature II. Crystal structure. *American Mineralogist*, **63**, 196–202.

Dunn P.J., Peacor D.R. and Simmons W.B. (1984) Lennilenapeite, the Mg-analogue of stilpnomelane, and chemical data on other stilpnomelane species from Franklin, New Jersey. *The Canadian Mineralogist*, **22**, 259–263.

Dunn P.J., Peacor D.R. and Su S.C. (1992) Franklinphilite, the manganese analog of stilpnomelane, from Franklin, New Jersey. *Mineralogical Record*, **23**, 465–468.

Eggleton R.A. (1972) The crystal structure of stilpnomelane. Part II. The full cell. *Mineralogical Magazine*, **38**, 693–711.

Eggleton R.A. and Chappell B.W. (1978) The crystal structure of stilpnomelane. Part III. Chemistry and physical properties. *Mineralogical Magazine*, **42**, 361–368.

Eggleton R.A. and Guggenheim S. (1986) The use of electron optical methods to determine the crystal structure of a modulated phyllosilicate: Parsettensite. *American Mineralogist*, **79**, 426–437.

Es'kova E.M., Semenov E.I., Khomyakov A.P., Kazakova M.E. and Shumyatskaya N.G. (1974) Sazhinite, a new silicate of sodium and rare earths. *Zapiski Vsesoyuznogo Mineralogicheskogo Obshchestva*, **103**, 338–341 [in Russian].

Evans Jr. H.T. (1973) The crystal structures of cavansite and pentagonite. *American Mineralogist*, **58**, 412–424.

Evans Jr. H.T. and Hughes J.M. (1990) Crystal chemistry of the natural vanadium bronzes. *American Mineralogist*, **75**, 508–521.

Fahey J.J., Ross M. and Axelrod J.M. (1960) Loughlinite, a new hydrous sodium magnesium silicate. *American Mineralogist*, **45**, 270–281.

Fang J.H., Robinson P.D. and Ohya Y. (1972) Redetermination of the crystal structure of eudidymite and its dimorphic relationship to epididymite. *American Mineralogist*, **57**, 1345–1354.

Ferraris G., Ivaldi G. and Khomyakov A.P. (1995) Altisite $Na_3K_6Ti_2[Al_2Si_8O_{26}]Cl_3$, a new hyperalkaline aluminosilicate from Kola Peninsula (Russia) related to lemoynite: crystal structure and thermal evolution. *European Journal of Mineralogy*, **7**, 537–546.

Ferraris G., Khomyakov A.P., Belluso E. and Soboleva S.V. (1998) Kalifersite, a new alkaline silicate from Kola Peninsula (Russia) based on a palygorskite-sepiolte poysomatic series. *European Journal of Mineralogy*, **10**, 865–874.

Ferraris G., Belluso E., Gula A., Soboleva S.V. and Khomyakov A.P. (2003) The crystal structure of seidite-(Ce), $Na_4(Ce,Sr)_2\{Ti(OH)_2(Si_8O_{18})\}(O,OH,F)_4\cdot 5H_2O$, a modular microporous titanosilicate of the rhodesite group. *The Canadian Mineralogist*, **41**, 1183–1192.

Filatov S.K., Semenova T.F. and Vergasova L.P. (1992) Types of polymerization of $[OCu_4]^{6+}$ tetrahedra in compounds with 'additional' oxygen atoms. *Proceedings of the USSR Academy of Sciences*, **322**, 536–539 [in Russian].

Finch R.J., Cooper M.A., Hawthorne F.C. and Ewing R.C. (1999) Refinement of the crystal structure of rutherfordine. *The Canadian Mineralogist*, **37**, 929–938.

Fleet S.G. (1965) The crystal structure of dalyite. *Zeitschrift für Kristallographie*, **121**, 349–368.

Foit F.F., Phillips M.W. and Gibbs G.V. (1973) A refinement of the crystal structure of datolite, $CaBSiO_4(OH)$. *American Mineralogist*, **58**, 909–914.

Foord E.E., Gaines R.V., Crock J.G., Simmons Jr. W.B. and Barbosa C.P. (1986) Minasgeraisite, a new member of the gadolinite group from Minas Gerais, Brazil. *American Mineralogist*, **71**, 603–607.

https://doi.org/10.1180/mgm.2018.152 Published online by Cambridge University Press

Gagné O. and Hawthorne F.C. (2015) Comprehensive derivation of bond-valence parameters for ion pairs involving oxygen. *Acta Crystallographica*, **B71**, 562–578.

Gagné O. and Hawthorne F.C. (2016) Bond-length distributions for ions bonded to oxygen: alkali and alkaline-earth metals. *Acta Crystallographica*, **B72**, 602–625.

Galuskina I.O, Galuskin E.V., Vapnik Y., Prusik K., Stasiak M., Dzierżanowski P., Murashko M. and Krivovichev S.V. (2017) Gurimite, $Ba_3(VO_4)_2$ and hexacelsian, $BaAl_2Si_2O_8$ – two new minerals from schorlomite-rich paralava of the Hatrurim Complex, Negev Desert, Israel. *Mineralogical Magazine*, **81**, 1009–1019.

Garcés J.M., Rocke S.C., Crowder C.E. and Hasha D.L. (1988) Hypothetical structures of magadiite and sodium octosilicate and structural relationships between the layered alkali metal silicates and the mordenite- and pentasil-group zeolites. *Clays and Clay Minerals*, **36**, 409–418.

Garvie L.A.J., Devouard B., Groy T.L., Cámara F. and Buseck P.R. (1999) Crystal structure of kanemite, $NaHSi_2O_5.3(H_2O)$, from the Aris phonolite, Namibia. *American Mineralogist*, **84**, 1170–1175.

Gatta G.D., Rotiroti N., McIntyre G.J., Guastoni A. and Nestola F. (2008) New insights into the crystal chemistry of epididymite and eudidymite from Malosa, Malawi: A single-crystal neutron diffraction study. *American Mineralogist*, **93**, 1158–1165.

Gebert W., Medenbach O. and Flörke O.W. (1983) Darstellung und kristallographie von $K_2TiSi_6O_{15}$ – isotyp mit dalyit $K_2ZrSi_6O_{15}$. *Tschermaks Mineralogische und Petrographische Mitteilungen*, **31**, 69–79.

Ghose S. and Wan C. (1976) Structural chemistry of borosilicates, part II: Searlesite, $NaBSi_2O_5(OH)$: Absolute configuration, hydrogen locations, and refinement of the structure. *American Mineralogist*, **61**, 123–129.

Ghose S., Sen Gupta P.K. and Campana C.F. (1987) Symmetry and crystal structure of montregianite, $Na_4K_2Y_2Si_{16}O_{38}{\cdot}10H_2O$, a new double-sheet silicate with zeolitic properties. *American Mineralogist*, **72**, 365–374.

Giester G. and Rieck B. (1994) Effenbergerite, $BaCu[Si_4O_{10}]$, a new mineral from the Kalahari manganese field, South Africa: description and crystal structure. *Mineralogical Magazine*, **58**, 663–670.

Giester G. and Rieck B. (1996) Wesselsite, $SrCu[Si_4O_{10}]$, a further new gillespite-group mineral from the Kalahari Manganese Field, South Africa. *Mineralogical Magazine*, **60**, 795–798.

Giester G., Lengauer C.L., Pristacz H., Rieck B., Topa D. and von Bezing K.-L. (2016) Cairncrossite, a new Ca-Sr (-Na) phyllosilicate from the Wessels Mine, Kalahari Manganese Field, South Africa. *European Journal of Mineralogy*, **28**, 495–505.

Giustetto R. and Chiari G. (2004) Crystal structure refinement of palygorskite from neutron powder diffraction. *European Journal of Mineralogy*, **16**, 521–532.

Grew E.S., Peacor D.R., Rouse R.C., Yates M.G., Su S.-C. and Marquez N. (1996) Hyttsjöite, a new, complex layered plumbosilicate with unique tetrahedral sheets from Långban, Sweden. *American Mineralogist*, **81**, 743–753.

Grew E.S., Krivovichev S.V., Hazen R.M. and Hystad G. (2016) Evolution of structural complexity in boron minerals. *The Canadian Mineralogist*, **54**, 125–143.

Grice J.D. (1991) The crystal structure of silinaite, $NaLiSi_2O_5.2H_2O$. *The Canadian Mineralogist*, **29**, 363–367.

Grice J.D. and Gault R.A. (1995) Varennesite, a new species of hydrated Na-Mn silicate with a unique monophyllosilicate structure. *The Canadian Mineralogist*, **33**, 1073–1081.

Grice J.D. and Hawthorne F.C. (1989) Refinement of the crystal structure of leucophanite. *The Canadian Mineralogist*, **27**, 193–197.

Grice J.D. and Hawthorne F.C. (2002) New data on meliphanite, $Ca_4(Na,Ca)_4Be_4AlSi_7O_{24}(F,O)_4$. *The Canadian Mineralogist*, **40**, 971–980.

Grice J.D. and Robinson G.W. (1984) Jeffreyite, $(Ca,Na)_2(Be,Al)Si_2(O,OH)_7$, a new mineral species and its relation to the melilite group. *The Canadian Mineralogist*, **22**, 443–446.

Grice J.D., Burns P.C. and Hawthorne F.C. (1999) Borate minerals II. A hierarchy of structures based on the borate fundamental building block. *The Canadian Mineralogist*, **37**, 731–762.

Grice J.D., Rowe R., Poirier G., Pratt A. and Francis J. (2009) Bussyite-(Ce), a new beryllium silicate mineral species from Mont Saint-Hilaire, Quebec. *The Canadian Mineralogist*, **47**, 193–204.

Guggenheim S. and Eggleton R.A. (1994) a comparison of the structures and geometric stabilities of stilpnomelane and parsettensite: a distance least-squares (DLS) study. *American Mineralogist*, **79**, 438–442.

Guggenheim S. and Eggleton R.A. (1998) Modulated crystal structures of greenalite and caryopilite: a system with long-range, in-plane structural disorder in the tetrahedra sheet. *The Canadian Mineralogist*, **36**, 163–179.

Hamberg A. (1890) Uber Ganophyllite, ein manganzeolith von Harstigen. *Geologiska Föreningens I Stockholm Förhandlungenar*, **12**, 586–598.

Hawthorne F.C. (1984) The crystal structure of stenonite and the classification of the alumino fluoride minerals. *The Canadian Mineralogist*, **22**, 245–251.

Hawthorne F.C. (1987) The crystal chemistry of the benitoite group minerals and structural relations in (Si_3O_9) ring structures. *Neues Jahrbuch für Mineralogie – Monatshefte*, **1987**, 16–30.

Hawthorne F.C. (1992) The role of OH and H_2O in oxide and oxysalt minerals. *Zeitschrift für Kristallographie*, **201**, 183–206.

Hawthorne F.C. (1998) Structure and chemistry of phosphate minerals. *Mineralogical Magazine*, **62**, 141–164.

Hawthorne F.C. (2002) The use of end-member charge-arrangements in defining new mineral species and heterovalent substitutions in complex minerals. *The Canadian Mineralogist*, **40**, 699–710.

Hawthorne F.C. (2012*a*) A bond-topological approach to theoretical mineralogy: crystal structure, chemical composition and chemical reactions. *Physics and Chemistry of Minerals*, **39**, 841–874.

Hawthorne F.C. (2012*b*) Bond topology and structure-generating functions: Graph-theoretic prediction of chemical composition and structure in polysomatic T-O-T (biopyribole) and H-O-H structures. *Mineralogical Magazine*, **76**, 1053–1080.

Hawthorne F.C. (2014) The Structure Hierarchy Hypothesis. *Mineralogical Magazine*, **78**, 957–1027.

Hawthorne F.C. (2015*a*) Generating functions for stoichiometry and structure of single- and double-layer sheet-silicates. *Mineralogical Magazine*, **79**, 1675–1709.

Hawthorne F.C. (2015*b*) Toward theoretical mineralogy: a bond-topological approach. *American Mineralogist*, **100**, 696–713.

Hawthorne F.C. and Schindler M. (2008) Understanding the weakly bonded constituents in oxysalt minerals. *Zeitschrift für Kristallographie*, **223**, 41–68.

Hawthorne F.C. and Smith J.V. (1986*a*) Enumeration of 4-connected 3-dimensional nets and classification of framework silicates. 3D nets based on insertion of 2-connected vertices onto 3-connected plane nets. *Zeitschrift für Kristallographie*, **175**, 15–30.

Hawthorne F.C. and Smith J.V. (1986*b*) Enumeration of 4-connected 3-dimensional nets and classification of framework silicates. Body-centred cubic nets based on the rhombicuboctahedron. *The Canadian Mineralogist*, **24**, 643–648.

Hawthorne F.C. and Smith J.V. (1988) Enumeration of 4-connected 3-dimensional nets and classification of framework silicates. Combination of zigzag and saw chains with 6^3, 3.12^2, 4.8^2, 4.6.12 and $(5^2.8)_2(5.8^2)_1$ nets. *Zeitschrift für Kristallographie*, **183**, 213–231.

Hawthorne F.C. and Sokolova E. (2012) The role of H_2O in controlling bond topology: The $^{[6]}Mg(SO_4)(H_2O)_n$ ($n = 0$–6) structures. *Zeitschrift für Kristallographie*, **227**, 594–603.

Hawthorne F.C., Burns P.C. and Grice J.D. (1996) The crystal chemistry of boron. Pp. 41–115 in: *Boron: Mineralogy, Petrology, and Geochemistry* (L.M. Anovitz and E.S. Grew, editors). Reviews in Mineralogy, **33**. Mineralogical Society of America, Washington, DC.

Hawthorne F.C., Cooper M.A and Taylor M.C. (1998) Refinement of the crystal structure of tadzhikite. *The Canadian Mineralogist*, **36**, 817–822.

Hawthorne F.C., Krivovichev S.V. and Burns P.C. (2000) The crystal chemistry of sulfate minerals. Pp. 1–112 in: *Sulfate Minerals: Crystallography, Geochemistry, and Environmental Significance* (C.N. Alpers, J.L. Jambor, and D.K. Nordstrom, editors). Reviews in Mineralogy and Geochemistry, **40**. Mineralogical Society of America, Washington, DC.

Hawthorne F.C., Abdu Y.A., Tait K.T. and Back M.E. (2013) The crystal structure of yofortierite. *The Canadian Mineralogist*, **51**, 243–251.

Hayase K., Dristas J.A., Tsutsumi S., Otsuka R., Tanabe S., Sudo T. and Nishiyama T. (1978) Surite, a new Pb-rich layer silicate mineral. *American Mineralogist*, **63**, 1175–1181.

https://doi.org/10.1180/mgm.2018.152 Published online by Cambridge University Press

Hazen R.M. and Finger L.W. (1983) High-pressure and high-temperature crystallographic study of the gillespite I-II phase transition. *American Mineralogist*, **68**, 595–603.

Hazen R.M., Grew E.S., Downs R.T., Golden J.J. and Hystad G. (2015*a*) Mineral ecology: chance and necessity in the mineral diversity of terrestrial planets. *The Canadian Mineralogist*, **53**, 295–324.

Hazen R.M., Hystad G., Downs R.T., Golden J.J., Pires A.J. and Grew E.S. (2015*b*) Earth's "missing" minerals. *American Mineralogist*, **100**, 2344–2347.

Heaney P.J. and Post J.E. (1992) The crystal structure of bannisterite. *Clays and Clay Minerals*, **40**, 129–144.

Heinrich A.R., Eggleton R.A. and Guggenheim S. (1994) Structure and polytypism of bementite, a modulated layer silicate. *American Mineralogist*, **79**, 91–106.

Hesse K.-F. and Liebau F. (1980) Crystal chemistry of silica-rich barium silicates. III. Refinement of the crystal structures of the layer silicates $Ba_2[Si_4O_{10}]$ (I) sanbornite, and $Ba_2[Si_4O_{10}]$ (h). *Zeitschrift für Kristallographie*, **153**, 33–51.

Hesse K.F. and Stümpel G. (1986) Crystal structure of harstigite, $MnCa_6Be_4[SiO_4]_2[Si_2O_7]_2(OH)_2$. *Zeitschrift für Kristallographie*, **177**, 143–148.

Hesse K.-F., Liebau F. and Merlino S. (1992) Crystal structure of rhodesite, $HK_{1-x}Na_{x+2y}Ca_{2-y}\{lB,3,2^2_\infty\}[Si_8O_{19}]\cdot(6-z)H_2O$, from three localities and its relation to other silicates with dreier double layers. *Zeitschrift für Kristallographie*, **199**, 25–48.

Hughes J.M., Rakovan J., Bracco R. and Gunter M.E. (2003) The atomic arrangement of the ganophyllite-group modulated layer silicates as determined from the orthorhombic dimorph of tamaite, with the elusive 16.8 Å ganophyllite-group superstructure revealed. *American Mineralogist*, **88**, 1324–1330.

Huminicki D.M.C. and Hawthorne F.C. (2002*a*) The crystal chemistry of the phosphate minerals. Pp. 123–253 in: *Phosphates* (M.L. Kohn, J. Rakovan and J.M. Hughes, editors). Reviews in Mineralogy and Geochemistry, **48**. Mineralogical Society of America, Washington, DC.

Huminicki D.M.C. and Hawthorne F.C. (2002*b*) Refinement of the crystal structure of aminoffite. *The Canadian Mineralogist*, **40**, 915–922.

Johnsen O., Leonardsen E.S., Fälth L. and Annehed H. (1983) Crystal structure of kvanefjeldite: The introduction of $^2_\infty[Si_3O_7OH]$ layers with eight-membered rings. *Neues Jahrbuch für Mineralogie – Monatshefte*, **11**, 505–512.

Kabalov Yu.K., Sokolova E.V., Pautov L.A. and Schneider Yu. (1998) Crystal structure of a new mineral, turkestanite, a Ca analogue of steacyite. *Kristallographiya*, **43**, 632–636.

Kahlenberg V. and Krueger H. (2004) $LaAlSiO_5$ and apatite-type $La_{9.71}(Si_{0.81}Al_{0.19}O_4)_6O_2$ – the crystal structures of two synthetic lanthanum alumosilicates. *Solid State Sciences*, **6**, 553–560.

Kampf A.R., Jackson L.L., Sidder G.B., Foord E.E. and Adams P.M. (1992) Ferrisurite, the Fe (super 3+) analogue of surite, from Inyo County, California. *American Mineralogist*, **77**, 1107–1111.

Kampf A.R. and Housley R.M. (2014) Chiappinoite-(Y), $Y_2Mn(Si_3O_7)_4$, a new layer silicate found in peralkaline syenitic ejecta from the Água de Pau volcano, Azores. *European Journal of Mineralogy*, **27**, 91–97.

Kampf A.R., Rossman G.R. and Housley R.M. (2009) Plumbophyllite, a new species from the Blue Bell claims near Baker, San Bernardino County, California. *American Mineralogist*, **94**, 1198–1204.

Kampf A.R., Housley R.M., Dunning G.E. and Walstrom R.E. (2015) Esquireite, $BaSi_6O_{13}\cdot7H_2O$, a new layer silicate from the barium silicate deposits of California. *The Canadian Mineralogist*, **53**, 3–11.

Kasahev A.A. and Sapozhnikov A.N. (1978) Crystal structure of armstrongite. *Soviet Physics Crystallography*, **23**(5), 539–542.

Kato T. and Takéuchi Y. (1983) The pyrosmalite group of minerals. I. Structure refinement of manganpyrosmalite. *The Canadian Mineralogist*, **21**, 1–6.

Kato T. and Watanabe I. (1992) The crystal structures of schallerite and friedelite. *Yamaguchi University, College of Arts Bulletin*, **26**, 51–63.

Khomyakov A.P., Nechelyustov G.N., Ferraris G. and Ivaldi G. (1994) Altisite $Na_3K_6Ti_2Al_2Si_8O_{26}Cl_3$ – a new mineral. *Zapiski Vserossijskogo Mineralogicheskogo Obshchestva*, **123**(6), 82–86.

Khomyakov A.P., Ferraris G., Belluso E., Britvin S.N., Nechelyustov G.N. and Soboleva S.V. (1998) Seidite-(Ce), $Na_4SrCeTiSi_8O_{22}F\cdot5H_2O$, a new mineral with zeolitic properties. *Zapiski Vserossijskogo Mineralogicheskogo Obshchestva*, **127**(4), 94–100.

Khomyakov A.P., Nechelystov G.N., Ferraris G. and Ivaldi G. (2000) Manganonaujakasite, $Na_6(Mn,Fe)Al_4Si_8O_{26}$, a new mineral from the Lovozero alkaline massif, Kola Peninsula. *Zapiski Vserossijskogo Mineralogicheskogo Obshchestva*, **129**(4), 48–53.

Kimata M. (1981) The crystal structure of synthetic akermanite, $Ca_2MgSi_2O_7$. *Neues Jahrbuch für Mineralogie – Abhandlungen*, **144**, 1–10.

Kimata M. (1983) The crystal structure and stability of Co-akermanite, $Ca_2CoSi_2O_7$, compared with the mineralogical behavior of Mg cation. *Neues Jahrbuch für Mineralogie – Abhandlungen*, **146**, 221–241.

Kimata M. (1985) Crystallo-chemical evolution of a crystal structure due to cationic substitution after the example of melilite. *Naturwissenschaften*, **72**, 372–373.

Kimata M. (1988) Crystallo-chemical evolution of melilite due to cationic substitution. *Neues Jahrbuch für Mineralogie – Abhandlungen*, **159**, 181–197.

Kimata M. and Li N. (1982) The structural property of synthetic gehlenite, $Ca_2Al_2SiO_7$. *Neues Jahrbuch für Mineralogie – Abhandlungen*, **144**, 254–267.

Kimata M. and Ohashi H. (1982) The crystal structure of synthetic gugiaite, $Ca_2BeSi_2O_7$. *Neues Jahrbuch für Mineralogie – Abhandlungen*, **143**, 210–222.

Knight K.S., Henderson C.M.B. and Clark S.M. (2010) Structural variations in the wesselsite–effenbergerite ($Sr_{1-x}Ba_xCuSi_4O_{10}$) solid solution. *European Journal of Mineralogy*, **22**, 411–423.

Kolitsch U., Merlino S. and Holstam D. (2012) Molybdophyllite: crystal chemistry, crystal structure, OD character and modular relationships with britvinite. *Mineralogical Magazine*, **76**, 493–516.

Kostov I. and Breskovska V. (1989) *Phosphate, Arsenate and Vanadate Minerals. Crystal Chemistry and Classification*. Kliment Ohridski University Press, Sofia, Bulgaria.

Krivovichev S.V. (2008) *Structural Crystallography of Inorganic Oxysalts*. International Union of Crystallography Monographs on Crystallography 22, Oxford University Press, UK.

Krivovichev S.V. (2009) *Structural Mineralogy and Inorganic Crystal Chemistry*. St. Petersburg University Press, Moscow, 398 pp.

Krivovichev S.V. and Burns P.C. (2003) Combinatorial topology of uranyl molybdate sheets: syntheses and crystal structures of $(C_6H_{14}N_2)_3[(UO_2)_5(MoO_4)_8](H_2O)_4$ and $(C_2H_{10}N_2)[(UO_2)(MoO_4)_2]$. *Journal of Solid State Chemistry*, **170**, 106–117.

Krivovichev S.V. and Filatov S.K. (1999*a*) Structural principles for minerals and inorganic compounds containing anion-centered tetrahedra. *American Mineralogist*, **84**, 1099–1106.

Krivovichev S.V. and Filatov S.K. (1999*b*) Metal arrays in structural units based on anion-centered metal tetrahedra. *Acta Crystallographica*, **B55**, 664–676.

Krivovichev S.V., Filatov S.K. and Semenova T.F. (1998) Types of cationic complexes on the base of oxocentered tetrahedra $[OM_4]$ in crystal structures of inorganic compounds. *Russian Chemical Reviews*, **67**, 137–155.

Krivovichev S.V., Pakhomovsky Y.A., Ivanyuk G.Y., Mikhailova J.A., Men'shikov Y.P., Armbruster T., Selivanova E.A. and Meisser N. (2007) Yakovenchukite-(Y), $K_3NaCaY_2(Si_{12}O_{30})(H_2O)_4$, a new mineral from the Khibiny massif, Kola Peninsula, Russia: a novel type of octahedral-tetrahedral open-framework structure. *American Mineralogist*, **92**, 1525–1530.

Krivovichev S.V., Mentré O., Siidra O.I., Colmont M. and Filatov S.K. (2013) Anion-centered tetrahedra in inorganic compounds. *Chemical Reviews*, **113**, 6459–6535.

Lam A.E., Groat L.A., Cooper M.A. and Hawthorne F.C. (1994) The crystal structure of wickenburgite, $Pb_3CaAl[AlSi_{10}O_{27}](H_2O)_3$, a sheet structure. *The Canadian Mineralogist*, **32**, 525–532.

Lazebnik K.A., Lazebnik Y.D. and Makhotko V.J. (1984) Davanite, $K_2TiSi_6O_{15}$, a new alkali titanosilicate. *Zapiski Vsesoyuznogo Mineralogicheskogo Obshchestva*, **113**(1), 95–97.

Le Page Y. and Perrault G. (1976) Structure crystalline de la lemoynite, $(Na,K)_2CaZr_2Si_{10}O_{26}\cdot5\text{-}6H_2O$. *The Canadian Mineralogist*, **14**, 132–138.

Liebau F. (1985) *Structural Chemistry of Silicates: Structure, Bonding and Classification*. Springer-Verlag, Berlin.

Lin H.C., Liao F.L. and Wang S.L. (1992) Structure of $BaCuSi_4O_{10}$. *Acta Crystallographica*, **C48**, 1297–1299.

https://doi.org/10.1180/mgm.2018.152 Published online by Cambridge University Press

Liu J.J., Li G., Mao Q., Wu S., Liu Z., Su S., Xiong M. and Yu X. (2012) Hanjiangite, a new barium-vanadium phyllosilicate carbonate mineral from the Shiti barium deposit in the Dabashan region, China. *American Mineralogist*, **97**, 281–290.

Livingstone A., Atkin D. and Hutchison D. (1976) Iraqite, a new rare-earth mineral of the ekanite group. *Mineralogical Magazine*, **40**, 441–445.

Lopes-Vieira A. and Zussman J. (1969) Further detail on the crystal structure of zussmanite. *Mineralogical Magazine*, **37**, 49–60.

Louisnathan S.J. (1969) Refinement of the crystal structure of hardystonite $Ca_2ZnSi_2O_7$. *Zeitschrift für Kristallographie*, **130**, 427–437.

Louisnathan S.J. (1970) The crystal structure of synthetic soda melilite, $CaNaAlSi_2O_7$. *Zeitschrift für Kristallographie*, **131**, 314–321.

Louisnathan S.J. (1971) Refinement of the crystal structure of a natural gehlenite, $Ca_2Al(Al,Si)_2O_7$. *The Canadian Mineralogist*, **10**, 822–837.

Majzlan J., Drahota P. and Filippi M. (2014) Paragenesis and crystal chemistry of arsenic minerals. Pp. 17–184 in: *Arsenic: Environmental Geochemistry, Mineralogy, and Microbiology* (R.J. Bowell, C.N. Alpers, H.E. Jamieson, D.K. Nordstrom and J. Majzlan, editors). Reviews in Mineralogy and Geochemistry, **79**. Mineralogical Society of America, Washington, DC.

Maksimova N.V., Ilyukhin V.V. and Belov N.V. (1974) Crystal structure of sørensenite. *Soviet Physics – Doklady*, **18**, 681–682.

Malinovskii Y.A., Yamnova N.A. and Belov N.V. (1981) The refined crystal structure of the leucosphenite. *Doklady Akademii Nauk SSSR*, **257**, 1128–1132.

Matchatski F. (1928) Zur Frage der Struktur und Konstitution der Feldspate. *Zentralblatt für Mineralogie Abhandlungen A*, **1928**, 97–104.

Matsubara S., Miyawaki R., Kato A., Yokoyama K. and Okamoto A. (1998) Okayamalite, $Ca_2B_2SiO_7$, a new mineral, boron analogue of gehlenite. *Mineralogical Magazine*, **62**, 703–706.

Matsueda H., Miura Y., Rucklidge J. and Kato T. (1981) Natroapophyllite, a new orthorhombic sodium analog of apophyllite. *American Mineralogist*, **66**, 410–423.

Mazzi F., Ungaretti L., Dal Negro A., Petersen O.V. and Rönsbo J.G. (1979) The crystal structure of semenovite. *American Mineralogist*, **64**, 202–210.

McDonald A.M. and Chao G.Y. (2001) Natrolemoynite, a new hydrated sodium zirconosilicate from Mont Saint-Hilaire, Quebec: Description and structure determination. *The Canadian Mineralogist*, **39**, 1295–1306.

McDonald A.M. and Chao G.Y. (2007) Martinite, a new hydrated sodium calcium fluorborosilicate species from Mont Saint-Hilaire, Quebec: Description, structure determination and genetic implications. *The Canadian Mineralogist*, **45**, 1281–1292.

McDonald A.M. and Chao G.Y. (2009) Lalondeite, a new hydrated Na–Ca fluorosilicate species from Mont Saint-Hilaire, Quebec: Description and crystal structure. *The Canadian Mineralogist*, **47**, 181–191.

Mellini M. and Merlino S. (1977) Hellandite: a new type of silicoborate chain. *American Mineralogist*, **62**, 89–99.

Mellini M. and Merlino S. (1981) The crystal structure of jagoite. *American Mineralogist*, **66**, 852–858.

Mellini M., Merlino S. and Rossi G. (1977) The crystal structure of tuscanite. *American Mineralogist*, **62**, 1114–1120.

Merlino S. (1972) The crystal structure of zeophyllite. *Acta Crystallographica*, **B28**, 2726–2732.

Merlino S. (1983) Okenite, $Ca_{10}Si_{18}O_{46}{\cdot}18H_2O$: the first example of a chain and sheet silicate. *American Mineralogist*, **68**, 614–622.

Merlino S. (1988*a*) Gyrolite: its crystal structure and crystal chemistry. *Mineralogical Magazine*, **52**, 377–387.

Merlino S. (1988*b*) The structure of reyerite, $(Na,K)_2Ca_{14}Si_{22}Al_2O_{58}(OH)_8]{\cdot}6H_2O$. *Mineralogical Magazine*, **52**, 247–256.

Merlino S. (2014) Polytypism in hanjiangite, sheet silicate-carbonate-fluoride of calcium, aluminium, vanadium and barium. *Atti della Società Toscana di Scienze Naturali, Memorie, Serie A*, **121**, 71–77.

Metcalf-Johansen J. and Hazell R.G. (1976) The crystal structure of sørensenite, $Na_4SnBe_2(Si_3O_9)_2.2H_2O$. *Acta Crystallographica*, **B32**, 2553–2556.

Mitchell R.H. and Burns P.C. (2001) The structure of fedorite: a re-appraisal. *The Canadian Mineralogist*, **39**, 769–777.

Miyawaki R., Nakai I. and Nagashima K. (1985) Structure of homilite, $Ca_{2.00}(Fe_{0.90}Mn_{0.03})B_{2.00}Si_{2.00}O_{9.86}(OH)_{0.14}$. *Acta Crystallographica*, **C41**, 13–15.

Miyawaki R., Matsubara S., Yokoyama K. and Okamoto A. (2007) Hingganite-(Ce) and hingganite-(Y) from Tahara, Hirukawa-mura, Gifu Prefecture, Japan: The description on a new mineral species of the Ce-analogue of hingannite-(Y) with a refinement of the crystal structure of hingganite-(Y). *Journal of Mineralogical and Petrological Sciences*, **102**, 1–7.

Miyawaki R., Momma K., Yokoyama K., Shigeoka M., Matsubara S., Ito M., Nakai I. and Kristiansen R. (2015) Mn-bearing hellandite-(Y) from the Heftetjern pegmatite, Toerdal, Norway. *The Canadian Mineralogist*, **53**, 345–356.

Noe D.C. and Veblen D.R. (1999) Incommensurate modulation and the crystal structure of ganophyllite. *American Mineralogist*, **84**, 1088–1098.

Oberti R., Ottolini L., Camara F. and Della Ventura G. (1999) Crystal structure of non-metamict Th-rich hellandite-(Ce) from Latium (Italy) and crystal chemistry of the hellandite-group minerals. *American Mineralogist*, **84**, 913–921.

Oberti R., Della Ventura G., Ottolini L., Hawthorne F.C. and Bonazzi P. (2002) Re-definition, nomenclature and crystal-chemistry of the hellandite group. *American Mineralogist*, **87**, 745–752.

Oberti R., Langone A., Boiocchi M., Hawthorne F.C. and Bernabé E. (2018) Ferri-mottanaite-(Ce), IMA 2017-087a. CNMNC Newsletter No. 46, December 2018, page 1189. *European Journal of Mineralogy*, **30**, 1181–1189.

Ozawa T., Takéuchi Y., Takahata T., Donnay G. and Donnay D.H. (1983) The pyrosmalite group of minerals. *II. The layer structure of mcgillite and friedelite.* The Canadian Mineralogist, **21**, 7–17.

Pabst A. (1943) The crystal structure of gillespite, $BaFeSi_4O_{10}$. *American Mineralogist*, **28**, 372–390.

Pant A.K. (1968) A reconsideration of the crystal structure of beta $Na_2Si_2O_5$. *Acta Crystallographica*, **B24**, 1077–1083.

Papike J.J. and Zoltai T. (1967) Ordering of tetrahedral aluminum in prehnite, $Ca_2(Al,Fe^{3+})[Si_3AlO_{10}](OH)_2$. *American Mineralogist*, **52**, 974–984.

Pasero M., (2019) *The New IMA List of Minerals*. http://nrmima.nrm.se/

Peacor D.R., Dunn P.J. and Simmons W.B. (1984) Eggletonite, the Na analogue of ganophyllite. *Mineralogical Magazine*, **48**, 93–96.

Pekov I.V., Chukanov N.V., Kononkova N.N., Belakovsky D.I., Pushcharovsky D.Y. and Vinogradova S.A. (1998) Ferronordite-(Ce) $Na_3SrFeSi_6O_{17}$ and manganonordite-(Ce) $Na_3SrMnSi_6O_{17}$ – the new minerals from Lovozero massif, Kola Peninsula. *Zapiski Vserossijskogo Mineralogicheskogo Obshchestva*, **127**(1), 32–41.

Pekov I.V., Chukanov N.V., Turchkova A.G. and Grishin V.G. (2001) Ferronordorite-(La), $Na_3Sr(La,Ce)FeSi_6O_{17}$, a new mineral of the nordite group from Lovozero Massif, Kola Peninsula. *Zapiski Vserossijskogo Mineralogicheskogo Obshchestva*, **130**(2), 53–58.

Pekov I.V., Zubkova N.V., Chukanov N.V., Zadov A.E. and Pushcharovsky D.Yu. (2011) Fivegite $K_4Ca_2[AlSi_7O_{17}(O_{2-x}OH_x)][(H_2O)_{2-x}OH]Cl$: A New Mineral Species from the Khibiny Alkaline Pluton of the Kola Peninsula in Russia. *Geology of Ore Deposits*, **53**, 591–603.

Perrault G. and Szymański J.T. (1982) Steacyite, a new name, and re-evaluation of the nomenclature of "ekanite"-group minerals. *The Canadian Mineralogist*, **20**, 59–63.

Petersen O.V., Johnsen O., Leonardsen E.S. and Rønsbo J.G. (1984) Kvanefjeldite, a new mineral species from the Ilímaussaq Alkaline Complex, southwest Greenland. *The Canadian Mineralogist*, **22**, 465–467.

Pluth J.J. and Smith J.V. (2002) Arizona porphyry copper/hydrothermal deposits II: Crystal structure of ajoite, $(K+Na)_3Cu_{20}Al_3Si_{29}O_7(OH)_{16}{\sim}8H_2O$. *Proceedings of the National Academy of Sciences*, **99**, 11002–11005.

Pluth J.J., Smith J.V., Pushcharovsky D.Yu., Semenov Eu.I., Bram A., Riekel C., Weber H.-P. and Broach R.W. (1997) Third-generation synchrotron x-ray diffraction of 6-μm crystal of raite, ≈ $Na_3Mn_3Ti_{0.25}Si_8O_{20}(OH)_2{\cdot}10H_2O$, opens up new chemistry and physics of low-temperature minerals. *Proceedings of the National Academy of Sciences*, **94**, 12263–12267.

Post J.E. and Heaney P.J. (2008) Synchrotron powder X-ray diffraction study of the structure and dehydration behavior of palygorskite. *American Mineralogist*, **93**, 667–675.

Post J.E., Bish D.L. and Heaney P.J. (2007) Synchrotron powder X-ray diffraction study of the structure and dehydration behavior of sepiolite. *American Mineralogist*, **92**, 91–97.

Pushcharovskii D.Y., Pekov I.V., Pluth J.J., Smith J.V., Ferraris G., Vinogradova S.A., Arakcheeva A.V., Soboleva S.V. and Semenov E.I.

https://doi.org/10.1180/mgm.2018.152 Published online by Cambridge University Press

(1999) Raite, manganonordite-(Ce), and ferronordite-(Ce) from the Lovozero massif: Crystal structures and mineralogical geochemistry. *Crystallography Reports*, **44**, 565–574.

Quint R. (1987) Description and crystal structure of amstallite, CaAl$(OH)_2[Al_{0.8}Si_{3.2}O_8(OH)_2]\cdot[(H_2O)_{0.8}Cl_{0.2}]$, a new mineral from Amstall, Austria. *Neues Jahrbuch für Mineralogie – Monatshefte*, **1987**, 253–262.

Rao C., Hatert F., Wang R.C., Gu X.P., Dal Bo F. and Dong C.W. (2015) Minjiangite, $BaBe_2(PO_4)_2$, a new mineral from Nanping No. 31 pegmatite, Fujian Province, southeastern China. *Mineralogical Magazine*, **79**, 1195–1202.

Rastsvetaeva R.K., Pushcharovskii D. Yu., Pekov I.V. and Voloshin A.V. (1996) Crystal structure of calcybeborosilite and its place in the datolite–gadolinite isomorphous series. *Kristallografiya*, 41, 235–239 [in Russian].

Rastsvetaeva R.K., Aksenov S.M. and Chukanov N.V. (2012) Crystal structure of günterblassite, a new mineral with a triple tetrahedral layer. *Doklady Chemistry*, **442**, 766–770.

Rinaldi R., Gatta G.D. and Angel R.J. (2010) Crystal chemistry and low-temperature behavior of datolite: a single-crystal X-ray diffraction study. *American Mineralogist*, **95**, 1413–1421.

Robinson P.D. and Fang J.H. (1970) The crystal structure of epididymite. *American Mineralogist*, **55**, 1541–1549.

Rouse R.C., Peacor D.R., Dunn P.J., Su S., Chi P.H. and Yeates H. (1994) Samfowlerite, a new Ca Mn Zn beryllosilicate mineral from Franklin, New Jersey: Its characterization and crystal structure. *The Canadian Mineralogist*, **32**, 43–53.

Rumsey M.S., Welch M.D., Kampf A.R. and Spratt J. (2013) Diegogattaite, $Na_2CaCu_2Si_8O_{20}\cdot H_2O$: a new nanoporous copper sheet silicate from Wessels Mine, Kalahari Manganese Fields, Republic of South Africa. *Mineralogical Magazine*, **77**, 3155–3162.

Sabelli C. and Trosti-Ferroni T. (1985) A structural classification of sulfate minerals. *Periodico di Mineralogia*, **54**, 1–46.

Saburov S.P., Britvin S.N., Bekenova G.K., Sergieva M.N., Kotelnikov P.E., Chukanov N.V. and Yagovkina M.A. (2005) Niksergievite, $[Ba_{1.33}Ca_{0.67}Al(CO_3)(OH)_4]$ $[Al_2(AlSi_3O_{10})(OH)_2]\cdot nH_2O$, a new phyllosilicate related to the surite-ferrisurite series, *American Mineralogist*, **90**, 1163–1166.

Sacerdoti M., Parodi G.C., Mottana A., Maras A. and Della Ventura G. (1993) Asbecasite: Crystal structure refinement and crystal chemistry. *Mineralogical Magazine*, **57**, 315–322.

Sahama Th.G. and Kai Hytönen M.A. (1959) Delhayelite, a new silicate from the Belgian Congo. *Mineralogical Magazine*, **32**, 6–9.

Sameshima T. and Kawachi Y. (1991) Coombsite, Mn analogue of zussmanite, and associated Mn-silicates, parsettensite and caryopilite, from southeast Otago, New Zealand. *New Zealand Journal of Geology and Geophysics*, **34**, 329–335.

Sandomirski P.A. and Belov N.V. (1984) *Crystal Chemistry of Mixed Anionic Radicals*. Nauka, Moscow [in Russian].

Schindler M. and Hawthorne F.C. (2001*a*) A bond-valence approach to the structure, chemistry and paragenesis of hydroxy-hydrated oxysalt minerals: I Theory. *The Canadian Mineralogist*, **39**, 1225–1242.

Schindler M. and Hawthorne F.C. (2001*b*) A bond-valence approach to the structure, chemistry and paragenesis of hydroxy-hydrated oxysalt minerals: II. Crystal structure and chemical composition of borate minerals. *The Canadian Mineralogist*, **39**, 1243–1256.

Schindler M. and Hawthorne F.C. (2001*c*) A bond-valence approach to the structure, chemistry and paragenesis of hydroxy-hydrated oxysalt minerals: III. Paragenesis of borate minerals. *The Canadian Mineralogist*, **39**, 1257–1274.

Schindler M. and Hawthorne F.C. (2004) A bond-valence approach to the uranyl-oxide hydroxy-hydrate minerals: Chemical composition and occurrence. *The Canadian Mineralogist*, **42**, 1601–1627.

Schindler M. and Hawthorne F.C. (2008) The stereochemistry and chemical composition of interstitial complexes in uranyl-oxysalt minerals. *The Canadian Mineralogist*, **46**, 467–501.

Schindler M.C., Hawthorne F.C. and Baur W.H. (2000) A crystal-chemical approach to the composition and occurrence of vanadium minerals. *The Canadian Mineralogist*, **38**, 1443–1456.

Schindler M., Huminicki D.M.C. and Hawthorne F.C. (2006) Sulfate minerals: I. Bond topology and chemical composition. *The Canadian Mineralogist*, **44**, 1403–1429.

Scott J.D. (1976) Crystal structure of miserite, a Zoltai type 5 structure. *The Canadian Mineralogist*, **14**, 515–528.

Segalstad T.V. and Larsen A.O. (1978) Gadolinite-(Ce) from Skien, south-western Oslo region, Norway. *American Mineralogist*, **63**, 188–195.

Sharygin V.V., Pekov I.V., Zubkova N.V., Khomyakov A.P., Stoppa F. and Pushcharovsky D.Yu. (2013) Umbrianite, $K_7Na_2Ca_2[Al_3Si_{10}O_{29}]F_2Cl_2$, a new mineral species from melilitolite of the Pian di Celle volcano, Umbria, Italy. *European Journal of Mineralogy*, **25**, 655–669.

Shumyatsaya N.G., Voronkov A.A. and Belov N.V. (1971) X-ray diffraction study of leucosphenite. *Soviet Physics – Crystallography*, **16**(3), 416–422.

Shumyatsaya N.G., Voronkov A.A. and Pyatenko Ya.A. (1980) Sazhinite, $Na_2Ce[Si_6O_{14}(OH)](H_2O)_n$, a new representative of the dalyite family in crystal chemistry. *Soviet Physics – Crystallography*, **25**(4), 419–423.

Smith J.V. (1977) Enumeration of 4-connected 3-dimensional nets and classification of framework silicates; I, Perpendicular linkage from simple hexagonal net. *American Mineralogist*, **62**, 703–709.

Smith J.V. (1978) Enumeration of 4-connected 3-dimensional nets and classification of framework silicates, II, Perpendicular and near-perpendicular linkages from 4.82, 3.122 and 4.6.12 nets. *American Mineralogist*, **63**, 960–969.

Smith J.V. (1988) Topochemistry of zeolites and related materials. I. Topology and geometry. *Chemical Reviews*, **188**, 149–182.

Ståhl K. (1993) A neutron powder diffraction study of partially dehydrated fluorapophyllite, $KCa_4Si_8O_{20}F_6\cdot 9H_2O$. *European Journal of Mineralogy*, **5**, 845–849.

Subbotin V.V., Merlino S., Pushcharovsky D.Yu., Pakhomovsky Ya.A., Ferro O., Bodanova A.N., Vloshin A.V., Sorokhtina N.V. and Zubkova N.V. (2000) Tumchaite $Na_2(Zr,Sn)Si_4O_{11}\cdot 2H_2O$ – a new mineral from carbonatites of the Vuoriyarvi alkali-ultrabasic massif, Murmansk region, Russia. *American Mineralogist*, **85**, 1516–1520.

Szymański J.T., Owens D.R., Roberts A.C., Ansell H.G. and Chao G.Y. (1982) A mineralogical study and crystal-structure determination of nonmetamict ekanite, $ThCa_2Si_8O_{20}$. *The Canadian Mineralogist*, **20**, 65–75.

Takéuchi Y. and Donnay G. (1959) The crystal structure of hexagonal $CaAl_2Si_2O_8$. *Acta Crystallographica*, **12**, 465–470.

Takéuchi Y., Kawada I., Irimaziri S. and Sadanaga R, (1969) The crystal structure and polytypism of manganpyrosmalite, *Mineralogical Journal*, **5**, 450–467.

Takéuchi Y., Ozawa T. and Takahata T. (1983) The pyrosmalite group of minerals III. *Derivation of polytypes*. The Canadian Mineralogist, **21**, 19–27.

Uehara M., Yamazaki A. and Tsutsumi S. (1997) Surite: its structure and properties. *American Mineralogist*, **82**, 416–422.

Uvarova Y.A., Sokolova E., Hawthorne F.C., Agakhanov A. and Pautov L.A. (2004*a*) The crystal structure of arapovite, $U^{4+}(Ca,Na)_2K_{1-x}\square_x)[Si_8O_{20}]$, $x \sim 0.5$, a new mineral of the steacyite group from the Dara-i-Pioz moraine, Tien-Shan Mountains, Tajikistan. *The Canadian Mineralogist*, **42**, 1005–1011.

Uvarova Y.A., Sokolova E., Hawthorne F.C., Pautov L.A. and Agakhanov A.A. (2004*b*) A novel $[Si_{18}O_{45}]^{18-}$ sheet in the crystal structure of zeravshanite, $Cs_4Na_2Zr_3[Si_{18}O_{45}](H_2O)_2$. *The Canadian Mineralogist*, **42**, 125–134.

Voronkov A.A., Zhdanova T.A. and Pyatenko Yu.A. (1974) Refinement of the structure of vlasovite $Na_2ZrSi_4O_{11}$ and some characteristics of the compositions and structure of the zirconosilicates. *Soviet Physics Crystallography*, **19**, 152–156.

Voronkov A.A., Ilyukhin V.V. and Belov N.V. (1975) Chemical crystallography of mixed frameworks; formation principals. *Soviet Physics Crystallography*, **20**, 340–345.

Vortmann S., Rius J., Marler B. and Gies H. (1999) structure solution from powder data of the hydrous layer silicate kanemite, a precursor of the industrial ion exchanger SKS-6. *European Journal of Mineralogy*, **11**, 125–134.

Welch M.D. and Rumsey M.S. (2013) A new naturally-occurring nanoporous copper sheet-silicate with 6^48^2 cages related to synthetic "CuSH" phases. *Journal of Solid State Chemistry*, **203**, 260–265.

Wells A.F. (1962) *Structural Inorganic Chemistry*. 3rd Ed. Oxford University Press, Oxford, UK.

Wells A.F. (1977) *Three-Dimensional Nets and Polyhedra*. Wiley, New York.

Wiedenmann D., Zaitsev A.N., Britvin S.N., Krivovichev S.V. and Keller J. (2009) Alumoåkermanite, (Ca,Na)2(Al,Mg,Fe2+)(Si2O7), a new mineral

https://doi.org/10.1180/mgm.2018.152 Published online by Cambridge University Press

from the active carbonatite-nephelinite-phonolite volcano Oldoinyo Lengai, northern Tanzania *Mineralogical Magazine*, **73**, 373–384.
Ximen L. and Peng Z. (1985) Crystal structure of hingganite. *Acta Mineralogica Sinica*, **5**, 289–293 [in Chinese].
Yakovenchuk V.N., Krivovichev S.V., Pakhomovsky Ya.A., Ivanyuk G.Yu., Selivanova E.A., Men'shikov Yu.P. and Britvin S.N. (2007) Armbrusterite, $K_5Na_6Mn^{3+}Mn^{2+}_{14}[Si_9O_{22}]_4{\cdot}4H_2O$, a new Mn hydrous heterophyllosilicate from the Khibiny alkaline massif, Kola Peninsula, Russia. *American Mineralogist*, **92**, 416–423.
Yakovenchuk V.N., Ivanyuk G.Yu., Pakhomovsky Y.A., Selivanova E.A. and Mikhailova J.A. (2011) Ellingsenite, $Na_5Ca_6Si_{18}O_{38}(OH)_{13}{\cdot}6H_2O$, a new martinite-related mineral species from phonolite of the Aris alkaline complex, Namibia. *The Canadian Mineralogist*, **49**, 1165–1173.
Yakubovich O.V., Matvienko E.N., Voloshin A.V. and Simonov M.A. (1983) The crystal structure of hingganite-(Yb), $(Y_{0.51}Ln_{0.36}Ca_{0.13})Fe_{0.065}Be(SiO_4)(OH)$. *Kristallografiya*, **28**, 457–460 [in Russian].
Yakubovich O.V., Massa W. and Chukanov N.V. (2008) Crystal structure of britvinite $[Pb_7(OH)_3F(BO_3)_2(CO_3)][Mg_{4.5}(OH)_3(Si_5O_{14})]$: a new layered silicate with an original type of silicon-oxygen networks. *Kristallografiya*, **53**, 233–242.
Yamnova N.A., Egorov-Tismenko Yu.K. and Khomyakov A.P. (1996) Crystal structure of a new natural (Na,Mn,Ti)-phyllosilicate. *Kristallografiya*, **41**, 257–262.
Yang Z., Fleck M., Pertlik F., Tillmanns E. and Tao K. (2001) The crystal structure of natural gugiaite, $Ca_2BeSi_2O_7$. *Neues Jahrbuch für Mineralogie – Monatshefte*, **2001**, 182–186.
Yang H., Downs R.T., Yang Y.W and Allen W.H. (2011) Pyrosmalite-(Fe), $Fe_8Si_6O_{15}(OH,Cl)_{10}$. *Acta Crystallographica*, **E68**, i7–i8.
Zoltai T. (1960) Classification of silicates and other minerals with tetrahedral structures. *American Mineralogist*, **45**, 960–973.
Zubkova N.V., Pekov I.V., Pushcharovsky D.Y. and Chukanov N.V. (2009) The crystal structure and refined formula of mountainite, $KNa_2Ca_2[Si_8O_{19}(OH)]{\cdot}6H_2O$. *Zeitschrift für Kristallographie*, **224**, 389–396.
Zubkova N.V., Filinchuk Y.E., Pekov I.V., Pushcharovsky D.Yu. and Gobechiya E.R. (2010) Crystal structures of shlykovite and cryptophyllite: comparative crystal chemistry of phyllosilicate minerals of the mountainite family. *European Journal of Mineralogy*, **22**, 547–555.

Table A1. Coordinates and site-occupancy factors (SOF) of atoms in the partial model of the structure of ellingsenite.

Atom	*x*	*y*	*z*	SOF
Na(1)	½	0	½	Na
Na(2)	0.8448(13)	−0.2128(13)	−0.7107(6)	$Na_{0.86(4)}$
Ca(1)	0.3564(6)	−0.2907(6)	−0.5025(3)	Ca
Ca(2)	0.0818(5)	−0.8582(5)	−0.5130(2)	Ca
Ca(3)	0.7756(8)	−0.4159(7)	−0.4942(3)	$Ca_{0.55(6)}Na_{0.45(6)}$
Si(1)	0.4595(8)	−0.4440(8)	−0.2301(4)	Si
Si(2)	0.8056(8)	−0.6630(7)	−0.3328(3)	Si
Si(3)	0.2987(8)	0.4577(8)	−0.3268(4)	Si
Si(4)	0.0501(7)	−0.0324(7)	−0.3309(3)	Si
Si(5)	0.9247(8)	−0.4153(8)	−0.3246(4)	Si
Si(6)	0.4183(8)	−0.1603(7)	−0.3312(3)	Si
Si(7)	0.5453(8)	0.0888(7)	−0.3254(3)	Si
Si(8)	0.7899(8)	−0.1100(8)	−0.2225(4)	Si
O(1)	0.085(2)	−0.0778(19)	−0.4272(9)	O
O(2)	0.930(3)	−0.365(3)	−0.4182(12)	O
O(3)	0.664(2)	0.067(2)	−0.4171(9)	O
O(4)	0.370(2)	0.479(2)	−0.4222(10)	O
O(5)	0.815(2)	−0.6616(19)	−0.4293(9)	O
O(6)	0.7816(19)	−0.1980(18)	−0.5624(9)	O
O(7)	0.392(2)	0.271(2)	−0.3022(10)	O
O(8)	0.757(3)	−0.091(3)	−0.1237(13)	O
O(9)	0.870(2)	−0.550(2)	−0.3030(10)	O
O(10)	0.932(2)	−0.841(2)	−0.3092(9)	O
O(11)	0.638(2)	0.044(2)	−0.2506(9)	O
O(12)	0.109(2)	0.496(2)	−0.3075(10)	O
O(13)	0.495(2)	−0.231(2)	−0.4249(9)	O
O(14)	0.308(2)	−0.438(2)	−0.2593(10)	O
O(15)	0.963(2)	−0.121(2)	−0.2697(10)	O
O(16)	0.625(2)	−0.606(2)	−0.2730(10)	O
O(17)	0.454(2)	−0.018(2)	−0.3154(9)	O
O(18)	0.214(2)	−0.072(2)	−0.3035(10)	O
O(19)	0.482(2)	−0.291(2)	−0.2622(10)	O
O(20)	0.802(2)	−0.272(2)	−0.2505(10)	O
O(21)	0.421(3)	−0.440(3)	−0.1317(13)	O
O(22)	0.385(13)	0.084(13)	−0.187(6)	$H_2O_{0.25(5)}$
O(23)	0.915(5)	−0.222(4)	−0.857(2)	$H_2O_{0.73(5)}$

Appendix: Revised formulae for ellingsenite and kampfite

While doing this work, we realised that several structures have chemical formulae that are incompatible with their refined crystal-structures. In this Appendix, we consider these minerals and attempt to improve the compatibility between their formulae and their crystal structures.

Ellingsenite

Ellingsenite is a single-layer structure (Fig. 11*b*, Table 4) based on the 6^3 net (Fig. 1) described by Yakovenchuk *et al.* (2011) in the space group $P\bar{1}$ with Z = 1 and the ideal formula $Na_5Ca_6Si_{18}O_{38}(OH)_{13}(H_2O)_6$. The atom coordinates are shown in Table A1. There are several discrepancies between the assigned chemical formula and the crystal structure: (1) There are 8 *Si* general sites (with a multiplicity of 2) listed in Table A1, and thus there should be 16 Si^{4+} ions in the chemical formula; however, there are 18 Si^{4+} ions in the assigned formula. (2) The O(22) and O(23) sites are partly occupied by (H_2O) with a net amount of (H_2O) of 2 per formula unit (pfu), whereas the formula gives 6 (H_2O) pfu. (3) Table A1 has 46 [anions + (H_2O) groups] pfu, whereas the assigned formula has 57 [anions + (H_2O) groups] pfu. (4) Table A2 shows the bond-valence table for **ellingsenite**. The bond-valence sums at the anions show that the O(6), O(8) and O(21) sites are occupied by $(OH)^-$ groups and the remaining anions are O^{2-}. This gives a content of 6 (OH) groups pfu in the structure whereas the assigned formula gives 13 (OH) groups pfu.

The chemical formula of the structure may be derived from Tables A1 and A2 by counting the atoms in the refined structure. This procedure gives the following formula: $Na_{3.62}Ca_{5.10}Si_{16}O_{36}(OH)_6(H_2O)_{1.96}$ which has a sum of positive charges of 77.82^+ and a sum of negative charges of 78^-, with a difference of 0.18^- that is well within the uncertainty of the refined site-occupancies.

The next step is to derive the end-member formula. The charge on the oxyanion component of the structure, $Si_{16}O_{36}(OH)_6(H_2O)_{1.96}$, is 14^- and hence the charge on the cation component of the structure is 14^+. The *Na*(1) and *Na*(2) sites will be completely occupied by Na to give a sum of 3 Na pfu, and the *Ca*(1) and *Ca*(2) sites are completely occupied by Ca to give a sum of 4 Ca pfu, giving a charge of 11^+. Thus the charge at the *Ca*(3) site must be $14–11 = 3^+$. The *Ca*(3) site has occupancy 0.55(5) Ca + 0.45(5) Na which, with a site multiplicity of 2, gives a net charge of 3.1^+. Thus the end-member formula of the structure may be written as $\mathbf{Na_3Ca_4(NaCa)Si_{16}O_{36}(OH)_6(H_2O)_2}$, which has one site that is occupied by fixed amounts of two ions, as is allowed for an end-member composition (Hawthorne, 2002). We may also write the ideal chemical composition as $\mathbf{Na_4Ca_5Si_{16}O_{36}(OH)_6(H_2O)_2}$.

Kampfite

Kampfite is a double-layer structure (Fig. 36*c*, Table 7) based on the 6^3 net (Fig. 1) described by Basciano and Groat (2007) in the space group *Cc* with *Z* = 1 and the assigned ideal formula $Ba_{12}(Si_{11}Al_5)O_{31}(CO_3)_8Cl_5$. The atom coordinates are shown in Table A3 and the bond-valence table is shown as Table A4. From Table A4, we see that there are no monovalent anions in the structure except for Cl^-. For a T (= $Si^{4+} + Al^{3+}$) content of 16 cations (see assigned formula), the minimum number of anions bonded to T is 32, whereas the assigned formula has 31 anions bonded to T, which would require at least one T cation to be [3]-coordinated, which is not the case (Table A4). The T cations are all [4]-coordinated and each of their coordinating anions link to two T atoms for a stoichiometry of $T_{16}O_{32}$. For the (CO_3) groups, the O atoms of each group refine to occupancies of 6.71 / 8 = 0.84, which

https://doi.org/10.1180/mgm.2018.152 Published online by Cambridge University Press

Table A2. Bond-valence table* for ellingsenite.

	Na(1)	*Na*(2)	*Ca*(1)	*Ca*(2)	*Ca*(3)	*Si*(1)	*Si*(2)	*Si*(3)	*Si*(4)	*Si*(5)	*Si*(6)	*Si*(7)	*Si*(8)	Σ	
O(1)			0.28	0.27					1.12					1.99	
				0.30											
O(2)				0.37	0.24					1.13				1.88	
					0.14										
O(3)	0.11 x2↓		0.31	0.38								1.08		1.88	
O(4)			0.27		0.20			1.11						1.90	
			0.32												
O(5)			0.28	0.30	0.24		1.16							1.98	
O(6)	0.19 x2↓	0.18		0.41	0.29									1.07	OH
O(7)		0.11						0.99				1.03		2.13	
O(8)													1.12	1.12	OH
O(9)		0.10					0.96			1.05				2.11	
O(10)		0.12					1.02		1.04					2.18	
O(11)												1.04	1.02	2.06	
O(12)		0.12						1.03		1.00				2.15	
O(13)	0.16 x2↓		0.35		0.25						1.16			1.92	
O(14)						1.03		1.08						2.11	
O(15)									1.04				1.08	2.12	
O(16)						1.07	1.09							2.16	
O(17)	0.05 x2↓	0.11									1.03	1.01		2.15	
O(18)		0.12							1.07		0.95			2.14	
O(19)						1.02					1.02			2.04	
O(20)										0.99			1.09	2.08	
O(21)						1.17								1.17	OH
O(22)		0.06												0.06	
O(23)		0.19												0.19	
Σ	1.02	1.11	1.81	2.03	1.36	4.29	4.23	4.21	4.27	4.17	4.16	4.16	4.31		

*Bond valences in valence units, calculated using the parameters of Gagné and Hawthorne (2015).

Table A3. Final atom parameters for kampfite.

	x	*y*	*z*	e^-
Be(1)	0.39588(1)	0.2498(2)	0.05925(3)	56
Be(2)	0.61035(1)	0.2503(2)	0.27376(3)	56
Be(3)	0.00309(2)	0.2503(2)	0.33408(6)	51.1(2)
T(1)	0.19850(7)	0.1885(4)	0.5271(5)	14
T(2)	0.19884(8)	0.3121(3)	0.1973(3)	14
T(3)	0.30741(8)	0.3118(3)	0.3059(3)	14
T(4)	0.30768(7)	0.1888(4)	0.6361(2)	14
C(1)	0.0736(2)	0.2483(8)	0.0693(5)	7.98(9)
C(2)	0.4327(2)	0.2461(8)	0.4289(5)	7.98(9)
O(1)	0.4299(2)	0.033(1)	0.3556(9)	6.71(4)
O(2)	0.4320(2)	0.255(2)	0.5724(5)	6.71(4)
O(3)	0.4307(3)	0.464(1)	0.3545(9)	6.71(4)
O(4)	0.3272(2)	0.5988(9)	0.2758(5)	8
O(5)	0.3266(2)	0.0982(9)	0.2031(5)	8
O(6)	0.3288(1)	0.232(1)	0.4907(5)	8
O(7)	0.0763(3)	0.028(1)	0.002(9)	6.71(4)
O(8)	0.0757(2)	0.461(1)	−0.0003(9)	6.71(4)
O(9)	0.0741(2)	0.257(2)	0.2136(6)	6.71(4)
O(10)	0.1797(2)	0.0987(9)	0.0574(5)	8
O(11)	0.1793(2)	0.5999(9)	0.1262(6)	8
O(12)	0.1776(2)	0.232(1)	0.3395(5)	8
O(13)	0.2532(2)	0.1957(7)	0.5784(6)	8
O(14)	0.2532(2)	0.3114(7)	0.2557(7)	8
Cl(1)	0.5031(1)	0.2499(2)	0.1675(6)	17
Cl(2)	0.5030(6)	0.255(3)	0.500(1)	4.1(2)

Table A4. Bond-valence* arrangement in kampfite.

	Ba(1)	*Ba*(2)	*Ba*(3)	*T*(1)	*T*(2)	*T*(3)	*T*(4)	*C*(1)	*C*(1)	Sum
O(1)	0.25		0.25						1.31	2.04
	0.23									
O(2)	0.24		0.27						1.23	1.95
	0.21									
O(3)	0.24		0.25						1.21	1.92
	0.22									
O(4)	0.17					0.86	0.90			1.93
O(5)	0.17					0.86	0.90			1.93
O(6)	0.08					0.88	0.92			1.93
	0.05									
O(7)		0.25	0.25					1.21		1.93
		0.22								
O(8)		0.24	0.25					1.30		2.01
		0.22								
O(9)		0.24	0.27					1.25		1.97
		0.21								
O(10)		0.17		0.89	0.89					1.95
O(11)		0.17		0.93	0.85					1.92
O(12)		0.08		0.92	0.88					1.93
		0.05								
O(13)				0.97			0.99			1.96
O(14)					1.00	1.01				2.01
Cl(1)	0.25	0.25	0.37							1.60
			0.36							
			0.37							
Cl(2)			0.10							0.28
			0.09							
			0.09							
Sum	2.12	2.10	2.92	3.71	3.62	3.61	3.71	3.76	3.75	

* Calculated from the curves of Brese and O'Keeffe (1991) assuming fully occupied sites except for *Ba*(3) and *Cl*(2). Values are expressed in valence units.

suggests a total (CO_3) content of 0.84 x 8 = 6.72 pfu. On the other hand, the occupancies of the C atoms of each group refine to infeasible values of 7.98 / 6 = 1.33. Using a total (CO_3) content of 6.72 pfu derived from the refined occupancies of the O anions of the (CO_3) groups, we end up with the following formula: $Ba_{11.91}(Si_{16-x}Al_x)O_{32}(CO_3)_{6.72}Cl_{4.96}$. Solving for electroneutrality, we get $x = 5.42$, which is reasonably close to the Al content given by Basciano and Groat (2007) by electron microprobe analysis. Thus the more probable empirical formula for kampfite is as follows: $Ba_{11.91}(Si_{10.58}Al_{5.42})O_{32}(CO_3)_{6.72}Cl_{4.96}$. The Ba, ($CO_3$) and Cl contents of an end-member composition are 12, 8 and 5 species pfu, respectively. The constraint of electroneutrality gives the following end-member formula: $\mathbf{Ba_{12}(Si_{13}Al_3)O_{32}(CO_3)_8Cl_5}$.

https://doi.org/10.1180/mgm.2018.152 Published online by Cambridge University Press